WAMSI Biannual Progress Report to 30 June 2009 for

WAMSI Node 1 Project 1 (WAMSI Code 1.1): Southwest Australian Coastal Biogeochemistry

WAMSI project reference no: 1.1

Project title: Southwest Australian Coastal Biogeochemistry

Node Leader: John Keesing

Project Leader: John Keesing

Project duration: 1 July 2006 to 30 June 2011

Due date for current milestone report: 30 June 2009

Project Objectives: To better characterise the south west Australian marine coastal and shelf ecosystem structure and function, and enhance our shared capacity to understand, predict and assess ecosystem response to anthropogenic and natural pressures by producing:

1. Downscaled hydrodynamic models to explore influences on benthic habitat, and the cross-shore and longshore exchange of water, nutrients and particles between the lagoon and shelf regions.

2. Coupled hydrodynamic and biogeochemical models and a quantitative nutrient budget for coastal waters at shelf and lagoon scales.

3. Improved descriptions and conceptual biogeochemical models for shelf and lagoon waters incorporating seasonal and interannual variability and improved representation of benthic primary production and bentho-pelagic coupling

4. Simple models for assessing and predicting impacts of physical forcing factors, primarily nutrients, on key benthic functional groups/habitats informed by experiments and observations conducted across a range of naturally varying and anthropogenically altered gradients related to nutrient enrichment

WAMSI Node 1 Project 1 (WAMSI Code 1.1) Southwest Australian Coastal Biogeochemistry

Executive Summary

1.1 Downscaled hydrodynamic models to explore influences on benthic habitat, and the cross-shore and longshore exchange of water, nutrients and particles between the lagoon and shelf regions.

Large-scale dynamics

Data from two global hydrodynamic models and a global wave model are being used to assess potential travel distances of organisms such as larvae, at the Cape-to-Cape scale. The main applications are to urchins, in Project 1.2, and lobster larvae, in WAMSI Node 2. BRAN (the BLUElink ReANalysis) is the primary source of model data. BRAN currents have been compared with data from the Southern Surveyor cruise in 2007, WOCE moorings from 1995, and SRFME moorings from 2004/5. In general, BRAN underestimates currents along the shelf by a factor of 0.2 to 0.6, probably because its 10 km grid-size does not fully resolve the Leeuwin Current. BRAN predicts negligible cross-shelf currents. The addition of Stokes Drift, that is, transport of buoyant material by waves, enhances the potential for cross-shore flow. The inclusion of randomness into particle tracks, emulating realistic scales of turbulent behaviour, does not significantly affect conclusions about particle sources and destinations.

Lagoon-scale hydrodynamics

Between July 2007 and May 2008 we completed four periods of intensive measurement of waves, currents and water properties across the Marmion lagoon. The program incorporated over 40 mooring deployments and recoveries, and 10 CTD and nutrient surveys (about 300 stations). The measurements have been complemented by the development of a high-resolution (~50 m) coupled current and wave model of the lagoon. The measurement program was designed particularly to quantify currents inside the lagoon that are driven by waves breaking on the reef-line. Both the measurements and model show that, when waves are low, the currents inside the lagoon are principally driven by longshore winds, at approximately 3% of the wind speed. When waves at the reef are larger than 1.5 m, water flows into the lagoon across the reef, and out of the lagoon through the north and south, and through gaps in the reef. Agreement between the model and data is improved significantly with the introduction of wave forcing. Water temperature varies by about 8 °C over the year, with temperatures inside the lagoon about 2 °C warmer than outside the reef in summer, and 2 °C cooler in winter. The field data are presented in a separate data report.

Lagoon-scale biogeochemistry
Water-column nutrient levels tend to vary on time-scales right down to hours. Nutrient levels are highest in winter, and there is evidence that high nutrients are associated with large wave events. Waves may pump particulates, or nutrient-rich pore water, from the sediments. Nutrient concentrations increase from the shore out, with local maxima over the reefs. Meanwhile, there is a chlorophyll minimum over the reefs. It is possible that filter-feeders, resident on the reef, draw down the phytoplankton, thus reducing the uptake of nutrients. Chlorophyll levels are highest in late autumn, corresponding to the time of the shelf-wide maximum concentrations. Across the lagoon, chlorophyll is highest in the north, possibly due to a local nutrient source (groundwater or a sewage outfall).

<u>Specific milestones to be reported on in this period</u>

Milestone 1.1.7 Initiate connectivity modelling runs
This work continues to be well advanced with connectivity model runs moving well beyond initiation phase (see this section in full report). Connectivity runs are being applied to explore large-scale patterns of larval retention and dispersal and to better elucidate the source components of Leeuwin current waters. The modelling is also meeting the requirements of WAMSI Project 1.2 which is using population genetics to compare with physical dispersal modelling and is informing Node 2 work on lobster larvae movements.

Milestone 1.1.8 Evaluation of lagoon-scale model runs
The Regional Ocean Modelling System (ROMS) has been configured for Marmion Lagoon. ROMS is a free-surface, terrain-following, primitive-equation ocean model widely used by the scientific community for a diverse range of applications. It includes hydrodynamic, wave, sediment, and biogeochemical sub-models, very suitable for multidisciplinary studies in dynamic coastal environments like Marmion Lagoon, which is subject to forcing by tide, wind and waves. The model of Marmion Lagoon has a grid size of 60x120 with horizontal resolution of about 100m and 8 vertical levels. The 3D hydrodynamic simulations were conducted for two periods, from 1 January to 1 April 2008 and from 1 July to 1 September 2007, which correspond to the third and first deployments from the Lagoonal wave and current measurement program (see Milestone 1.1.5), respectively. Model results have confirmed the importance of wave forcing in Marmion Lagoon and the model is reproducing currents and tidal elevations. It has been found in previous observations at Two Rocks that longshore current near the coast is about 2.5%~3% of the longshore wind speed. Our model results are consistent with this relationship demonstrating a strong correlation between modelled surface longshore current and observed longshore wind component during times of low waves. Full details can be found in the detailed report.

Milestone 1.1.9 Data report on lagoon wave and current measurements

An extensive Data Report has been complied for this milestone and has been supplied to WAMSI in a separate report. It provides a full description of the field program and data including the CTD surveys, the instrument array and moorings.

Milestone 1.1.10 Complete 2009 Marmion biophysical sampling

Arguably this work is complete in that much of work planned was carried out during 2008 (see sections 1.1.6 and 1.1.10 of the full report) although completion of the assessment of the data still awaiting nutrient analyses to be completed. However given that this research revealed unexpected small scale spatial variability in nutrient distributions in Marmion lagoon especially around reefs and the emerging importance of the influence of waves on sediment nutrient resuspension we have extended this field work into the present winter. We are adding to the high frequency sampling targeting short lived storm events with instrument deployments extending over winter 2009. We have deployed a McLane remote access sampler to safely sample during periods of high physical forcing associated with winter storms. Such events are highly dynamic and short lived so sampling intervals are brief (12 hours) to adequately capture the temporal variation. In conjunction with the automated water sampler, we have deployed a mooring frame equipped with (i) a Seabird SBE19plus measuring temperature, salinity, PAR, fluorescence and oxygen; (ii) a Seabird SBE26 wave and tide gauge; (iii) a RDI Workhorse Sentinel ADCP with waves enabled; and (iv) TAPS measuring vertical distribution of suspended particles to get an accurate estimate of the state of the physical environment during sampling. Improved temporal nutrient data (particularly during storms) combined with accurate estimates of the magnitude of the forcing will allow us to test the hypothesis suggested by the historical sampling that nutrient resupply is enhanced by physical factors. These data are also an important means of testing and informing the biogeochemical models. We would thus like to revise this milestone to be completed by the end of 2009.

1.2. Coupled hydrodynamic and biogeochemical models and a quantitative nutrient budget for coastal waters at shelf and lagoon scales.

Primary production estimates, based on accumulated physical and biogeochemical data, suggest that the southwestern shelf region is largely self-sustaining. About 84% of primary production appears to be recycled on the shelf. Around half of the recycling happens in the sediments.

A simple steady-state model, in which production balances mortality, and production is governed by nutrient and light availability, appears to capture the cross-shelf structure of phytoplankton concentration. Analysis of over 450 light profiles, collected at water depths from 10 m to 500 m, indicates a relatively simple pattern of light availability over the shelf. Light attenuation is highest in shallow water, and decreases out to about 100 m water depth. As a consequence, light levels at the seabed are reasonably constant out to about 40 m water depth, and then diminish.

Nutrients recycled through the seabed must be reinjected back to the water column. There appears, from observation, to be a correlation between nutrient levels and waves (see Milestone 1.1.10). A 1-d (vertical) biogeochemical model, in which nutrient availability is parameterised with wave-height, reproduces the seasonal and interannual concentrations of chlorophyll, as observed by satellite. This modelling also shows that the surface chlorophyll concentration is sensitive to vertical mixing. With low vertical mixing, chlorophyll production will be restricted by the availability of nutrients to the lower part of the water column.

Benthic grazing has also been incorporated in the 1-d model. Concentrations of chlorophyll are low over the Marmion reefs, suggesting clearance by filter feeders (Milestone 1.1.10). This effect is reproduced, at least qualitatively, by the 1-d model.

Beyond the shelf break, the biogeochemical dynamics change, as deep nutrients become potentially available. A deeper-water application of the 1-d model shows how the early winter bloom at the shelf-edge may be due to increased mixing, resulting from both the increase in speed of the Leeuwin Current, and overturning from surface cooling.

These relatively simple model applications are designed to demonstrate the processes controlling primary production over the shelf. An application of a 3-d model (Milestone 1.2.2) demonstrated the apparent importance of coastal sources (e.g. groundwater, surface water, outfalls) to the regional nutrient balance. It also supported the conclusion that the shelf is largely isolated from deeper water. These results are currently being analysed to provide a model-based budget for the shelf.

The 3-d ROMS model, presently being run at the lagoonal scale (Milestone 1.1.8), and in WAMSI Node 2, is also being implemented, with a coupled biogeochemical model, at the shelf scale. It will be used to extend the biogeochemical process understanding from 1 to 3 dimensions.

Specific milestones to be reported on in this period

Milestone 1.2.4 Begin incorporating lagoon and shelf scale C& N flux into BGC models

Several approaches to incorporating carbon and nitrogen data as well as proxies for these parameters into models have been made:

1. Mass balance model of nitrogen budget on the continental shelf

A nitrogen budget has been established using a mass balance model that identifies the major fluxes of nitrogen on the West Australian continental shelf. The total nitrogen requirement for the primary production on the continental shelf off the west coast of WA is estimated to be 14.8 gN $m^{-2}y^{-1}$ in the water column, and 2.0 gN $m^{-2}y^{-1}$ in the benthic community, which equates to a total primary production of 111.3 gC $m^{-2}y^{-1}$, or 1.1×10^{7} tonne C y^{-1} over the whole shelf. Preliminary estimates indicate that, of the new nitrogen required to support this annual production, 8% is derived from advection by the LC and its eddy field, and 7% from seasonal upwelling. Terrestrial and atmospheric contribution of nitrogen to the shelf accounts for less than 1% of the primary production. Although the direct offshore nutrient inputs may be small, they may still be important in driving the annual cycles in the marine ecosystem on the shelf. It is estimated that 84% of the primary production is recycled on the shelf, both within the pelagic system and through the pelagic-benthic coupling. Thus, despite the uncertainties in the offshore input estimates, the continental shelf off the west coast of WA must be primarily a recycling system, more typical of wider shelf regions. Improved quantification of benthic-pelagic coupling on the shelf will lead to a better understanding of the marine ecosystem. This work is to be published as follows: Feng, M & K. Wild-Allen (in press). Productivity and nitrogen fluxes along the downwelling coast off Western Australia. In: *Carbon and Nutrient Fluxes in Continental Margins: A Global Synthesis*. Editors: Kon-Kee Liu, L. Atkinson, R. Quinones, L. Talaue-McManus.

2. 3D Biogeochemical Modelling of the WA Shelf

Using a range of data sources from this WAMSI project, the 3D biogeochemical model developed during the SRFME program is being used to quantify a modelled nutrient budget for the region. The model has a 10km spatial resolution and simulates the cycling of carbon and nitrogen through organic and inorganic dissolved and particulate phases including phytoplankton, zooplankton, detritus, nutrient and benthic macrophyte pools. The model simulates a coupled pelagic and benthic system including deposition, remineralisation and resuspension of material. To compute a modelled nutrient budget for the WA shelf, fluxes of all nutrient components of the biogeochemical model are computed along sections parallel to the shelf break. As the shelf has a convoluted shape this is a non-trivial task and requires the estimation of fluxes along a multitude of short east-west and north-south sections which are then summed to produce a net budget. The budget sums are repeated for each day of simulation and summed for seasonal and annual budget descriptions. Initial results show the cross shelf fluxes to be considerably smaller than along shelf water movements. This suggests the shelf waters are hydrodynamically isolated from offshore waters with cross-shelf exchange dominated by event scale Leeuwin Current meanders and eddy transport. These findings are supportive of the earlier estimates of cross-shelf transport, and the general accumulative knowledge of the system dynamics. Work is ongoing to finalise the modelled budget calculations by the end of June and complete a manuscript for publication. For consistency with the lagoonal modelling (Milestone 1.1.8), and with modelling in other Nodes of WAMSI, we are also implementing the coupled ROMS hydrodynamics and biogeochemistry at shelf scale. This will have up to 5 times higher resolution than the SRFME model.

3. Incorporating seasonal chlorophyll a dynamics into a BGC model

   The phytoplankton pigment, chlorophyll a, is a good proxy for phytoplankton carbon (and nitrogen) content, and relatively easy to measure. It is therefore an important quantity to include in BGC models. The dynamics of the seasonal evolution of chlorophyll a at the continental shelf break around 32 degrees south has been investigated using a numerical BGC model. The results show that a combination of vertical mixing associated with the Leeuwin Current and surface cooling during the winter months is responsible for the wintertime increase in chlorophyll a concentration. Variation in the timing and magnitude of the winter increase is shown to relate to the strength of the Leeuwin Current. The findings have been published as: Greenwood, J. & K Soetaert (2008) Interannual variability in the seasonal cycle of chlorophyll within the Leeuwin Current off the southwest Western Australian coast. Journal of Marine Research, 66 (3), pp. 373-390

4. Incorporating regional chlorophyll a dynamics into a BGC model

   The regional distribution of chlorophyll on the continental shelf has been investigated using a steady-state phytoplankton growth model. Using the model, chlorophyll a concentration is calculated for any location on the continental shelf by assuming a balance between growth (which is assumed to be light and nitrogen limited) and mortality (which is assumed to be constant). In a depth integrated sense the model is able to predict the cross shelf variation that is observed in chlorophyll a on the SW WA continental shelf.

5. Incorporating benthic nitrogen fluxes into a BGC model

   The estimate, reported above, that approximately 40% of the nitrogen production on the shelf could be recycled via the sediment has important implications for the modelling tasks in this project. As a minimum, it requires that some detail of the sediment biogeochemistry must be included in any realistic simulation of the shelf. Coupling between marine sediments and overlying water can be added to a BGC model in different ways. To help make an informed choice of how best to represent the sediment biogeochemistry for the lagoon and shelf scale models, a number of simplified numerical experiments have been conducted to examine likely interactions between the water column and the sediment. The response of pelagic production to changes in the sediment nutrient flux has been investigated using a coupled pelagic-benthic model configured at different water depths. Model results have shown that variations in this flux within the range of field measurements can account for observed seasonal variations in surface chlorophyll. This flux could be affected by hydrodynamics. As an example of this, the benthic nitrogen flux has been linked to the surface wave field in a 1-D BGC model (following the completion of milestone 1.2.3). The model is able to provide a good simulation of chlorophyll a biomass for at least six years of observations at a 40m station on the inner shelf. The results have been written up as a manuscript: Greenwood (2009), Seasonal variability in near-shore chlorophyll biomass on the Western Australian continental shelf: Evidence of a wave-driven mechanism.

6. Incorporating underwater light dynamics into a BGC model

The fixation of atmospheric carbon by autotrophic plankton is a major flux of carbon in biogeochemical ocean models, and is critically dependent on available sunlight. The attenuation of light with water depth is therefore an important parameterisation in BGC models, and warrants separate attention. This is especially true when benthic production is important, since the sea bed often receives very small amounts of light. Moreover, modelling underwater light can often be problematic in near-shore and shelf environments, where both inorganic and organic constituents can strongly affect the transparency of the water column. In preparation for this challenge, of the underwater light field along the Western Australian coast has been analysed and modelled. Over 450 light profiles, collected from shelf depths between 10 and 500 m, have been compared with a light-attenuation model to determine the rate of attenuation of the downward component of light. The result is that light attenuation decreases exponentially with increasing shelf depth until it reaches a minimum of approximately 0.06 m^{-1} around the 100-150 depth contour. The increase in attenuation toward the coast appears to offset the effect of a shallowing seabed, so that there is little difference between the amount of light that reaches the seafloor inside the coastal lagoon and the amount that reaches the seafloor at mid-shelf depths

Greater detail on the results from each of these approaches is given in the full report.

1.3. Improved descriptions and conceptual biogeochemical models for shelf and lagoon waters incorporating seasonal and interannual variability and improved representation of benthic primary production and bentho-pelagic coupling

During this reporting period much of the effort towards this output focussed on further analyses of results from the May 2007 Southern Surveyor voyage and completing milestone 1.3.5 which was to draw together all the ecological data collected at the continental shelf and lagoon scale into a single data report. These data include biomass and abundance of key functional groups, production of kelp, growth of mussels, measurements of sources of production with stable isotopes, measurements of grazing and predation, measurements of filter feeder grazing rates and will form an important part of the modelling work which will be undertaken once primary productivity measurements (milestone 1.3.6) are completed. Much of this work, as with many other components of the project, continues to be hampered by delays in getting nutrient analyses completed. However while a significant backlog of nutrient samples remains a good plan to deal with the backlog has been implemented and extra effort is being applied in both Floreat and Hobart to clear the backlog and make the nutrient data available for work

A significant update to the analyses of zooplankton and phytoplankton dynamics has been added to the analysis of data collected on the May 2007 Southern Surveyor cruise. Among the findings of this newest work are results showing that coastal waters, the Leeuwin Current and eddies forming from the Leeuwin Current favour increased growth rates and secondary production of zooplankton relative to oceanic water and that there is a strong correlation between phytoplankton and zooplankton biomass indicating that zooplankton were feeding directly on phytoplankton or indirectly by consumption of protozoa that were feeding on phytoplankton. These results are assumed in our biogeochemical models and field data supporting this is encouraging.

Specific milestones to be reported on in this period

1.3.5 Data report on shelf and lagoon biomass & ecological sampling

A data report that contains summaries of data that has been collected as part of the shelf and lagoon benthic ecology research (see milestones 1.3.1 – 1.3.4 including biomass and abundance of key functional groups, production of kelp, growth of mussels, measurements of sources of production with stable isotopes, measurements of grazing and predation, measurements of filter feeder grazing rates) has been completed and is provided separate to this Biannual Report. The Summary of that report is as follows:

As part of CSIRO Marine & Atmospheric Research's research in WAMSI Node 1, efforts are focussed on characterising benthic ecosystems from shallow lagoon ecosystems to deep (100 m or so) mid-shelf ecosystems. This program provides observations required to understand ecosystem dynamics from the coastal lagoon to mid-shelf depths off the central to southwest coast of WA.

Benthic biomass and habitat characterisation of the shelf region near Perth was investigated during the 2007 *Southern Surveyor* "autumn bloom cruise." The voyage was conducted in three legs, with the first (May) focusing on characterising the variation in benthic communities with depth; it is this data which is presented here. Sampling across the domain included swath mapping, towed video, benthic sleds, sediment grabs and cores and CTD profiles at stations between 30-150m depth across two transects in the Perth area. Densities and biomasses of animal groups and biomasses of macroalgae and seagrass obtained by benthic sled dredge sampling and benthic habitat classifications and proportions of reef and sand bottom types as determined by towed videos are presented.

Benthic biomass and ecological process characterisation was focussed at widely-separated locations, Marmion Lagoon, Rottnest Island and Jurien Bay. The biomass of key benthic fauna functional groups was investigated by measuring patterns of abundance of key fauna at different habitats (reef and seagrass). Fish, macro-invertebrates and western rock lobster were surveyed by visual census along transects. The data presented in this report include the biomass of these key taxa at each of the sites within these three regions.

Additionally, a series of measurements of key ecological processes were undertaken. These experiments attempted to investigate any trends regarding primary production, secondary production, predation, grazing and filtration rates of benthic filter feeders across the shelf, with inshore, midshore and offshore sites investigated. Water column nutrients, light and temperature were also measured across the shelf at Marmion as part of the primary productivity experiments. Predation was measured by measuring mortality of caged and uncaged mussels and herbivory was measured by consumption of tethered kelp. Filtering and retention rates were measured by quantifying removal of particulate organic matter and selectivity by abundant ascidians and sponges of reef habitat. The data presented here include sponge and ascidian filtration rates, morphometric data relevant to filtration to allow for future community filtration rate estimates and nutrient levels next to and away from filter feeders to assess their impact on nutrient dynamics.

1.4. Simple models for assessing and predicting impacts of physical forcing factors, primarily nutrients, on key benthic functional groups/habitats informed by experiments and observations conducted across a range of naturally varying and anthropogenically altered gradients related to nutrient enrichment

The milestones for this output are mostly not due until the end of 2010, however modelling component of this output continues to make good progress drawing on results from other parts of the project (eg. 1.2.4). For example results from simple models developed so far have shown that variations in the benthic nutrient flux can account for observed seasonal variations in pelagic chlorophyll, and this can theoretically be linked to wave forcing. Also our modelling shows that benthic production dominates over pelagic production when the system is closed (i.e. no external nutrient sources). This pelagic-benthic balance has been shown to be sensitive to changes in water column mixing rate, but also benthic grazing. In addition because an understanding of productivity and growth rates is essential for modelling the impact of environmental forcing, we have derived seasonal estimates of benthic primary productivity for benthic microalgae and a number of macroalgal species. We also have direct measurements of kelp growth across gradients of wave energy, depth, light, temperature, nutrients. Estimates of secondary productivity (from mussel growth) have been made across gradients in depth and sources of nutrition.

This empirical work towards milestones for this output has two components. Firstly, we are carrying out a comparison of environmental and biotic attributes of pre-existing sediment nutrient gradients at a range of sites with a gradient of anthropogenic impacts. We can use these measurements to develop simple models which estimate ecosystem to increased sediment nutrient load. Following discussions with DEC we have added Northern Harbour in Cockburn Sound and the Whitfords sewage outfall site to an expanded set of 29 sites for this work. This milestone report provides an extensive description of the results of these field studies to date (see section 1.4.2 in full Biannual Report) Secondly we have planned to follow up the above pilot experiment (see milestone 1.4.1 above) with a more extensive manipulative experiment which would look at the seasonal response of reef and soft sediment habitats to artificially induced nutrient enrichment. We have decided to suspend this latter component of the work for reasons outlined in the second of the two sections below.

Specific milestones to be reported on in this period

1.4.1 Complete Nutrient enrichment pilot study

This milestone is complete and has been reported on in previous milestone (Biannual) reports. We conducted a pilot study to test a system for the delivery of nutrients to primary producer communities in reef and seagrass meadow habitats which will be used to investigate the effects of elevated nutrient concentrations on these communities. Sachets of slow release fertiliser (or clean gravel for the controls) were anchored in nine places to form a grid over a 2 m x 2 m plot in reef and seagrass habitat. Photosynthetic efficiency (quantum yield and electron transport rates) of 4 algal and 3 seagrass species found in both plots were monitored over a 2 week period. Samples for bioassays (isotopic composition, soluble tissue nitrogen pools, TN, TP) were collected, along with samples for ambient seawater nutrient concentration.

There was some evidence that that the fertilisation treatment has had some influence on the plants (total nitrogen content in two macroalgal species was significantly higher in the experimental plot than the control plot for example) but the results were somewhat ambiguous (there was a concurrent reduction in the tissue nitrogen content of both the control and experimental plants over the course of the experiment). As such, it is not possible to definitively isolate differences in tissue nitrogen content between treatments from variations in the effect of the temporal decrease in the background levels. While the nutrient delivery system has shown promise, questions still remain its efficiency. In particular, the temperature dependence of the release rates of different types of "slow release" fertiliser will need to be carefully considered before commencing the main trial. A full analysis of the results from the pilot experiment are given in section 1.4.2 of the full Biannual Report while an explanation for the reasons for not proceeding with the full enrichment experiment are given in section 1.4.2.

Research Activity: Listed below by milestone within each project objective.

1. Downscaled hydrodynamic models to explore influences on benthic habitat, and the cross-shore and longshore exchange of water, nutrients and particles between the lagoon and shelf regions.

Milestone 1.1.1: Appoint hydrodynamic modeller

Original Forecast Finish Date: 20/12/06

Revised Forecast Finish Date: 19/5/08

This section unchanged from previous Biannual Report

Summary of Activities Undertaken, Outputs Produced:

As described in the June 07 progress report, the hydrodynamic modelling position was offered to Dr Mingshun Jiang of Massachusetts University. He accepted the position on 21 June, but then informed us on 4 September that he would be unable to take up the appointment, citing real estate issues as his main consideration.

We subsequently brought out the second candidate, Dr Liejun Zhong, of the University of Maryland, to Perth for interview in the week of 12-16 November, as soon as he was able to obtain a visitor visa. He was offered the position shortly after his visit, and took up his appointment on 19 May 2008.

Salary savings from the late appointment have been used to engage alternative staff on milestone 1.2.1 and to increase effort or bring forward other relevant activities towards milestones 1.1.5, 1.1.6, 1.3.1, 1.3.3, 1.3.4 and 1.4.2.

Milestone 1.1.2: Lagoon hydrodynamic field program commenced, hydrodynamic model assessment

Original Forecast Finish Date: 30/06/07

Revised Forecast Finish Date: 30/06/08

This section unchanged from previous Biannual Report

Summary of Activities Undertaken, Outputs Produced:

The lagoon hydrodynamic field program commenced in July, 2007 and progress to date is reported under milestone 1.1.5.

A preliminary review of hydrodynamic models suitable for modelling wave-driven flows over reefs has been completed. The two presently favoured hydrodynamic models are our in-house model SHOC, and the open-source model ROMS. SHOC has the advantage, for us, of familiarity and versatility, but does not presently incorporate wave-forcing. ROMS is a very well supported model with wave interactions recently incorporated. Progress on development of hydrodynamic models is discussed under milestone 1.1.4 however further work on model assessment has been tasked to the new hydrodynamic modeller whose appointment is discussed in detail under milestone 1.1.1. Due to the delays in making this appointment the task of completing model assessment has not yet been completed.

Milestone 1.1.3: Integrate IMOS sampling into WAMSI Node 1 program

Original Forecast Finish Date: 30/06/07

Revised Forecast Finish Date: 30/06/07

This section unchanged from previous Biannual Report

Summary of Activities Undertaken, Outputs Produced:

Ming Feng has been closely involved in IMOS planning to ensure compatibility between IMOS and WAMSI measurement programs.

IMOS WA Node has recognised that the scientific interest along the West Australian continental shelf includes the variability in Leeuwin Current and continental shelf currents, both in terms of alongshore and cross-shore variability, as well as processes within the Perth canyon. These regions have been the focus many research groups including the CSIRO, Department of Fisheries (WA) and the universities. Thus, time-series monitoring of physical and biological parameters in this region would augment the past and current (WAMSI) research activity. In view of this, it is proposed to deploy 10 moorings in the region between Shark Bay and Perth Canyon as follows:

- 1 mooring (ADCP, CTD, fluorescence and a thermistor chain) on the 'Two Rocks transect' at 200m depth.
- 1 mooring (ADCP, CTD, fluorescence and a thermistor chain) at the head of Perth canyon in 150m depth.
- thermistor chains on the Two Rocks transect at 100 and 50 m
- 2 thermistor chains within Perth canyon at about 500 m
- 5 thermistor chains on the 200m contour between Two Rocks and Shark Bay.

All thermistor chains will include two pressure sensors at mid-depth to correct the mooring movements. Some of the thermistor chains will also be quipped with bottom pressure sensors to derive the alongshore and cross-shore pressure gradient and geostrophic currents. The thermistor moorings will be serviced at 6 monthly intervals using the Department of Fisheries (WA) research vessel *Naturaliste* and the ADCP and multisensor moorings will be serviced every 6 months by the CSIRO research vessel *Linnaeus*.

In WA IMOS proposal, a Slocum glider (surface to 200 m) will be released off Two Rocks and will travel along the SRFME transect and return via the Perth Canyon. It is expected that one deployment over 30 days will be able to cover two cycles - which will provide fortnightly transects across the Two Rocks and Perth canyon transects. It is proposed that CSIRO provide in-kind support to deploy and retrieve the Slocum glider on the monthly basis using research vessel *Linnaeus*.

Two Seagliders (has a maximum depth of 1000 m and endurance of up to 4500 km) are proposed in WA IMOS. The Sea gliders will be deployed from Dampier and then traverse across the Leeuwin Current along the shelf and slope southwards. A high spatial resolution of transects is proposed along the southern end of the track to coincide with WAMSI Node 1 research region, as well the region covered by the CODAR HF Radar system and shelf moorings, and the gliders will then be recovered off Rottnest Island. As the Seaglider has a 6-month endurance, it is proposed to release gliders at 3-monthly intervals (i.e. release one and 3 months later release the second one), resulting in two Seagliders in the water - so that we get 3-monthly transects off the west coast.

In WA IMOS, two different radar systems (long-range CODAR and medium range WERA) are proposed. These systems are scheduled to be deployed in January 2008 for one year and are being requested to be extended to 2009/2010. The radars will cover the WAMSI Node 1 research region and provide hourly surface currents at 6 km resolution in the Leeuwin Current system, as well as surface wave measurements north of Rottnest.

In WAMSI Node 1, the IMOS mooring, glider, and Radar data, will be used to improve the numerical simulations of the ocean circulation, and seasonal and interannual variations of primary production in both pelagic and benthic ecosystems. These understanding will help quantify the climate impacts on the marine ecosystem of WA.

Milestone 1.1.4: Establish nested shelf/lagoon hydrodynamic model grids

Original Forecast Finish Date: 30/06/08

Revised Forecast Finish Date: 30/06/08

This section unchanged from previous Biannual Report

Summary of Activities Undertaken, Outputs Produced:

Final establishment of the model grids will occur with the arrival of the new hydrodynamic modeller (see objective 1.1.1). In the meantime, we have experimented with new grid configurations.

SRFME modelling was done on a model grid with 10 km resolution, corresponding to the 10 km grid used for the CSIRO global model archive, called "BRAN" (see objective 2.3.2). We have also implemented a 100 m grid for the Marmion lagoon. A potential connecting polar grid, with a resolution range from about 200 m inshore to 5 km offshore, is shown in Figure 1

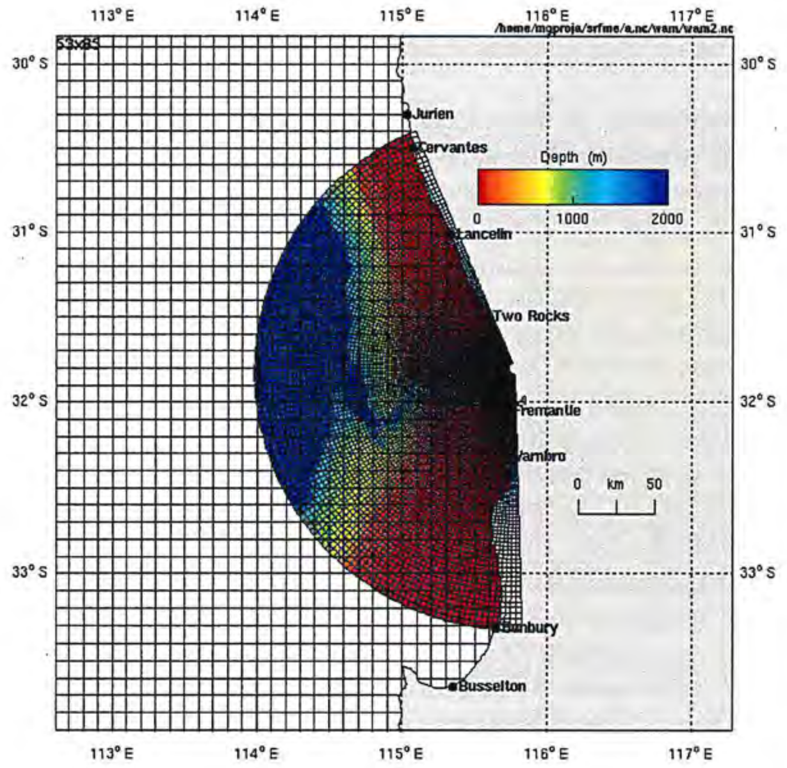

Figure 1. Polar model grid overlaid on the10 km SRFME model grid.

The fine-scale Marmion domain is shown in Figure 2, overlaid on the inshore region of the polar grid.

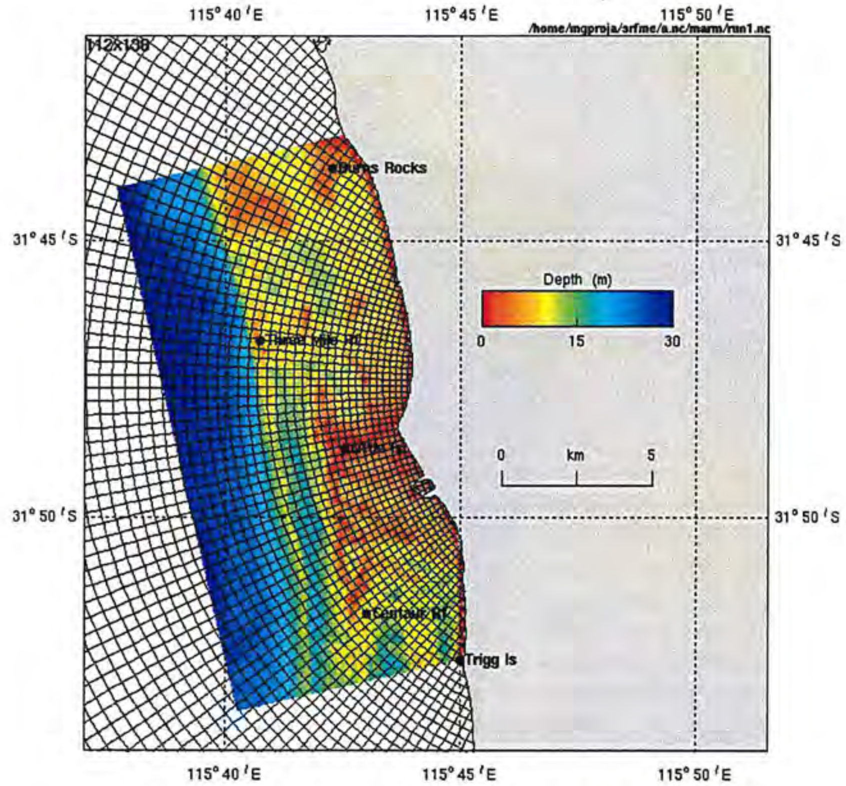

Figure 2. Marmion model domain inset on the polar grid.

A 3-D hydrodynamic model (SHOC) has been set up and tested against measurements in Marmion Lagoon (Figure 3) on the fine-scale grid. The horizontal resolution of the model is ~100m (87x182 grid cells). In the vertical direction, the modelling domain was represented by 11 levels with the refined resolution at the sea surface. The simulation period covered July-August 2007. The model time step was 30 sec. The run time ratio of the model was 30.25 (e.g. to simulate 2 months takes ~2 days).

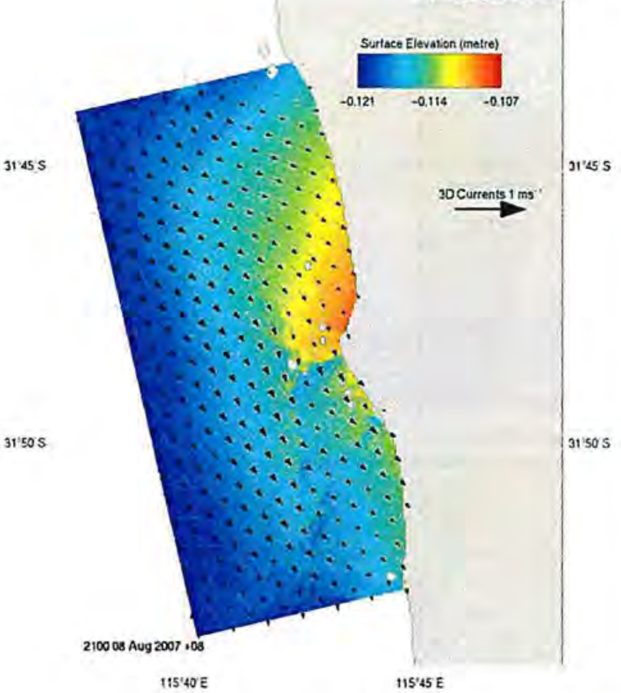

Figure 3. Snapshot of the simulated surface elevation and velocities in Marmion Lagoon.

The model was driven by hourly winds as measured at Ocean Reef. At the west open-sea boundary, the surface elevation was driven by tides derived from Admiralty tables. At the north and south boundaries, the surface elevation was adjusted to allow surface gravity waves to leave the modelling domain. Temperature and salinity fields during the simulations were uniform throughout the modelling domain. A sponge layer of 5 cells' thickness was specified at all sea boundaries to suppress numerical instabilities associated with the open boundaries.

A number of parameters and processes, including the horizontal diffusion coefficient, vertical background diffusion, boundary conditions for the gravity waves, number of cells in the sponge layers, and the model time step, have been altered and tested to produce a stable model run. The pilot model (see last Progress Report) produced reasonable agreement with the surface elevation data, but overestimated tidal currents in the region. To improve the model performance additional model runs has been carried out with varying specifications of the boundary conditions and the model parameters.

The model was tested against surface elevation and current measurements at ADV1, ADV2, ADV3, and AQ1 sites (see Section 1.1.4). An agreement between the model and near-bottom currents measured at ADV1, ADV2 and ADV3 sites was poor (not shown here). The discrepancies between model and data were attributed to potentially large variability of the near bottom currents associated with the small-scale topographical features not resolved by the model, and to high variability of vertical profiles in this region. The model reproduces observed surface elevation at all measurement sites reasonably well. Figure 4 illustrates the data model comparison at ADV2 site.

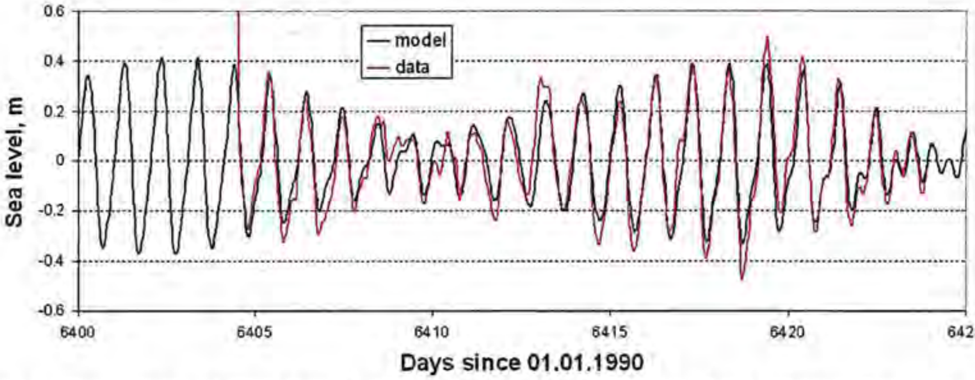

Figure 4. Preliminary comparison of sea-level from the model and field program from the ADV2 measurement site.

Figure 5 shows the simulated and measured depth-integrated velocities at AQ1 site. The calibration runs involved scenarios having varying specifications of the boundary conditions, the bottom roughness and the wind drag-force parameters. The best agreement between model and data has been achieved for the scenario having boundary-elevation prescribed at the west and north boundaries, and the bottom roughness increased from 0.1 to 10 cm. Typical values for the bottom roughness in coastal waters vary considerably. On the Scotian Shelf Li and Amos (1998) reported the bottom roughness over the rippled sea-bed under combined waves and currents varying from 0.1 to 10 cm, with the median values being less than 1 cm. Xu and Wright (1994) reported the bottom roughness varying from 0.11 to 0.7 cm on the inner shelf of the Middle Atlantic Bight. Gross and Werner (1994) presented bottom roughness data for various shallow-shelf environments ranging from 0.25 to 4 cm, with the highest values estimated for the areas having occasional rock outcrops, such as reef platforms. The value used in our study (10 cm) is at the higher end of published values, suggesting strong attenuation of currents in Marmion Lagoon. One may speculate that this attenuation can be driven by either interaction with topographic features (large bedforms or reef platforms) or by the turbulent wave bottom boundary layer. However additional research is needed to clarify this issue. Finally, it should be mentioned that the model does not reproduce small-scale, likely wind-driven, variability of currents.

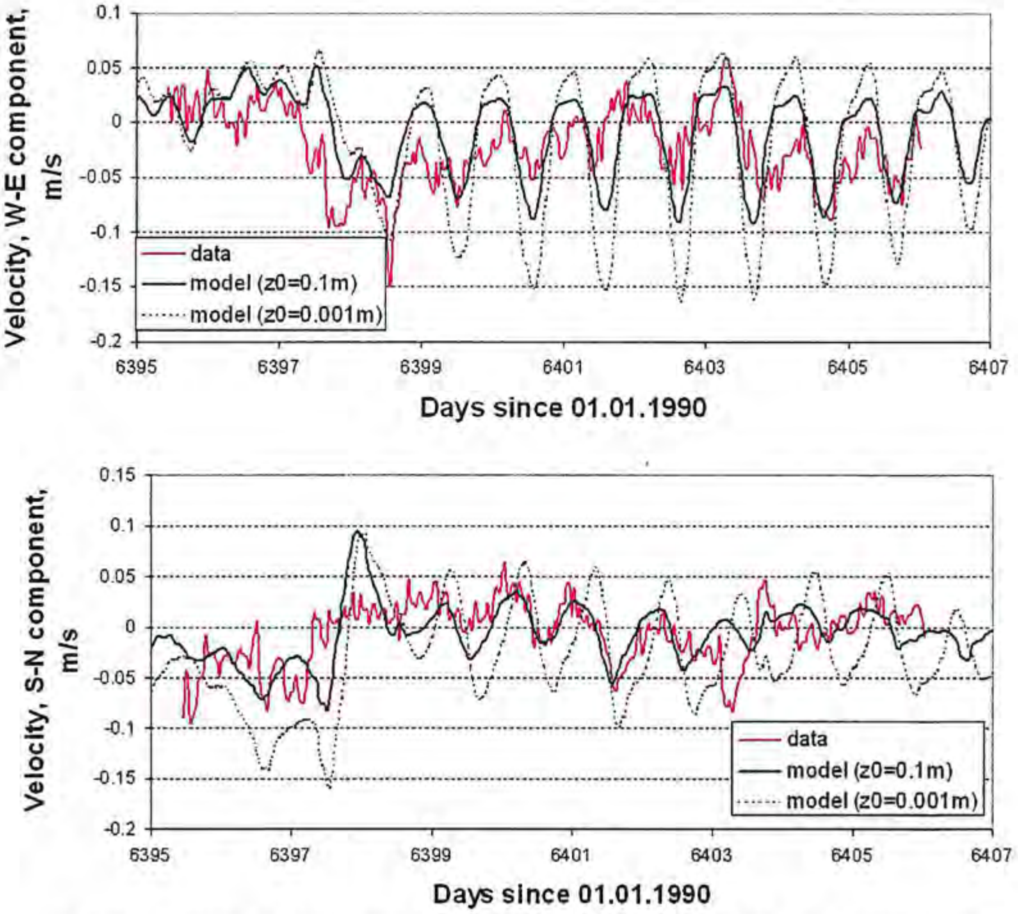

Figure 5. Modelled depth integrated currents vs measurements at AQ1 site. The modelling results represent scenarios having varying roughness parameter (z0).

A pilot sediment model for Marmion Lagoon was reported on in the previous Biannual Report.

References

Gross T., Werner F. (1994) Residual circulation due to bottom roughness variability under Tidal flows. *J. Phys. Oceanogr.* 24: 1494-1502.

Li M., Amos C. (1998) Predicting ripple geometry and bottom roughness under combined waves and currents in a continental shelf environment. *Continental Shelf Research* 18: 941-970.

Xu J., Wright L. (1995) Test of bed roughness models using field data from the Middle Atlantic Bight. *Continental Shelf Research* 15 (11/12): 1409-1434.

Milestone 1.1.5: Complete lagoonal wave and current measurements for model cal/val

Original Forecast Finish Date: 30/06/08

Revised Forecast Finish Date: 30/06/08

This section unchanged from previous Biannual Report

Summary of Activities Undertaken, Outputs Produced:

The lagoon hydrodynamic measurement program was completed with recovery of the instrument array during the third week of May. Details of the instrument array and sampling schedule were reported in the Biannual report for December 2007. The locations and site names of the instrument array are shown in Figure 6 and the actual deployment times by site are summarised in Table 1. During the first deployment a number of instruments were buried in sand to varying degrees, though only one (ADV4) was completely buried and was eventually recovered in February. On the second and subsequent deployments we chose sites on reef or seagrass beds to avoid burial, as close as possible to the original locations. In the third and fourth deployments the current meter at site ADV1 was deployed at site ADV4 to fill the data gap resulting from the burial during deployment 1. In spite of the burial of some instruments during the first deployment and some instrument failure in subsequent deployments the data return has been good. Detailed analysis of these data will be undertaken in the coming months. As part of the lagoon measurement program we also completed monthly CTD surveys using a grid of stations over the region shown in Figure 6 These data provide temperature, salinity and nutrient distributions and are reported under milestone 1.1.6. Times of the CTD surveys are shown in Table 1.

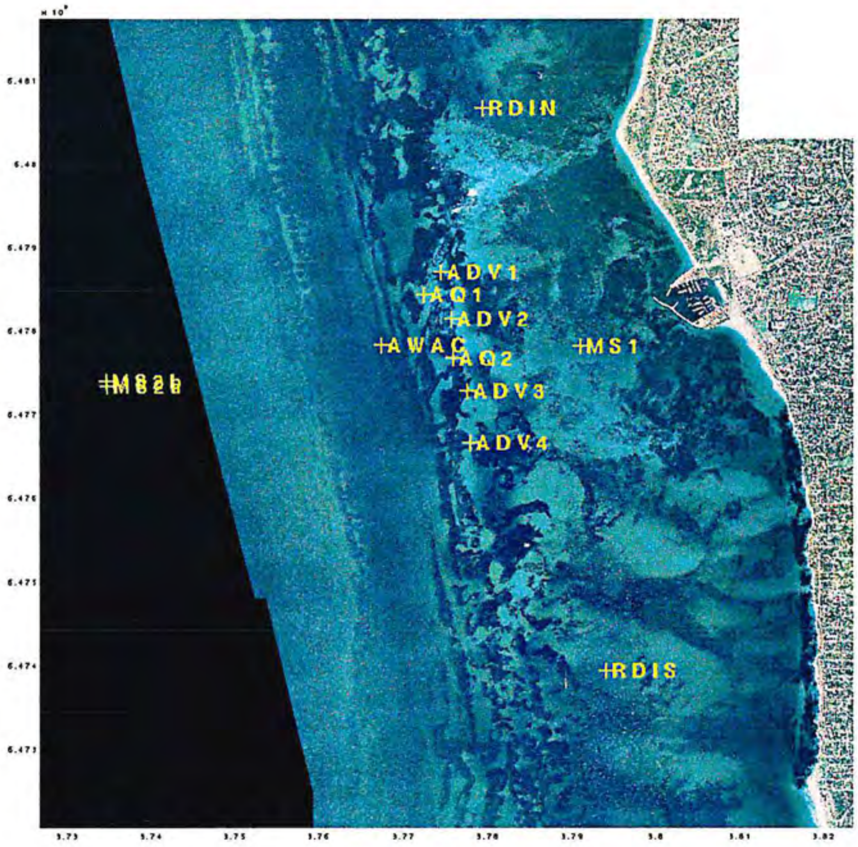

Figure 6. Instrument array for first deployment, adjusted slightly in subsequent deployments.

Table 1. Deployment dates by site and CTD survey times. Parameters u, v, and w are velocity components east, north and up respectively; P mean pressure; Pw wave resolving pressure; T temperature; C Conductivity; S salinty; eta sea surface elevation; P Phosphorous; NH4 ammonium; Si silcate; NOX total nitrogen.

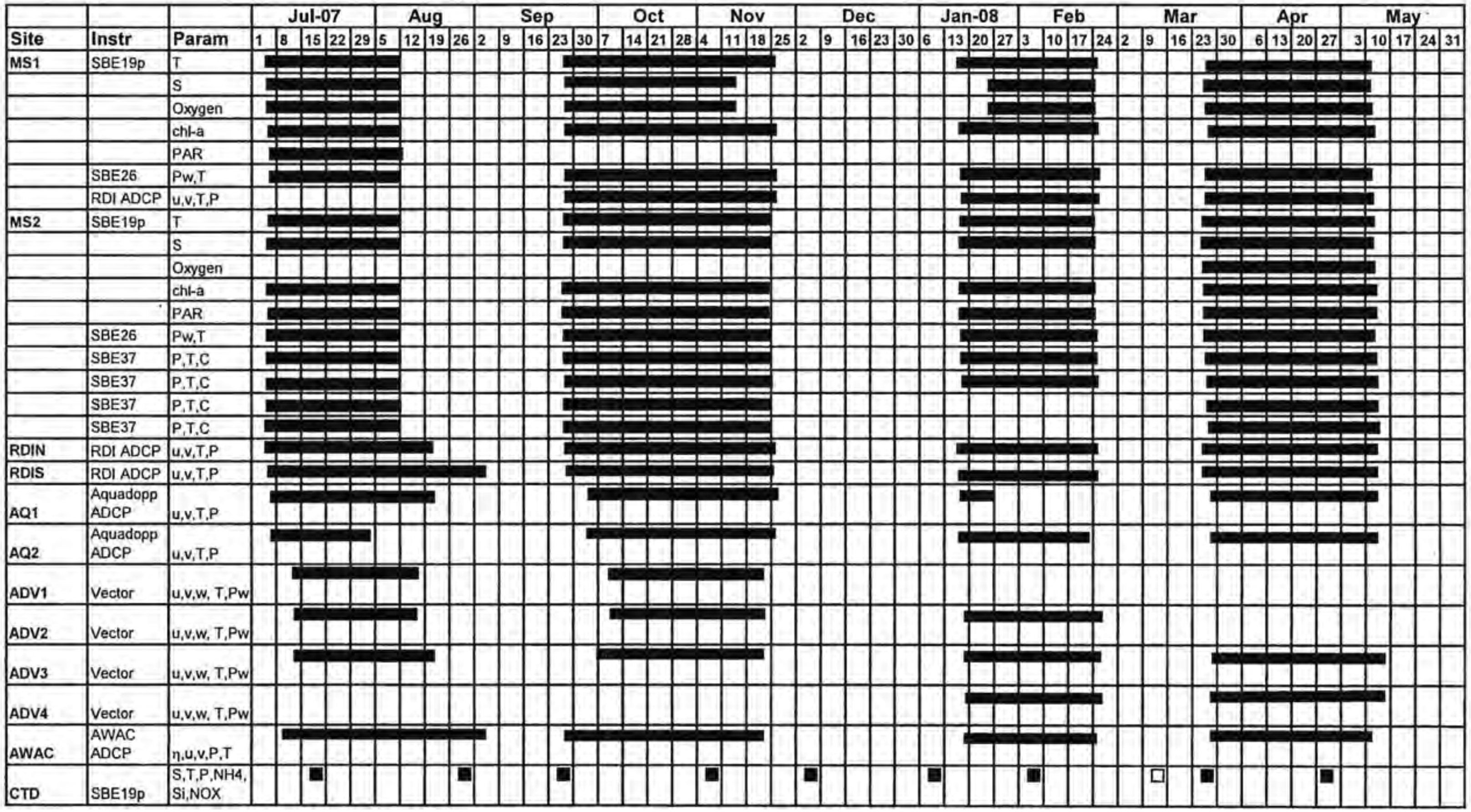

Site	Instr	Param
MS1	SBE19p	T
		S
		Oxygen
		chl-a
		PAR
	SBE26	Pw,T
	RDI ADCP	u,v,T,P
MS2	SBE19p	T
		S
		Oxygen
		chl-a
		PAR
	SBE26	Pw,T
	SBE37	P,T,C
	SBE37	P,T,C
	SBE37	P,T,C
	SBE37	P,T,C
RDIN	RDI ADCP	u,v,T,P
RDIS	RDI ADCP	u,v,T,P
AQ1	Aquadopp ADCP	u,v,T,P
AQ2	Aquadopp ADCP	u,v,T,P
ADV1	Vector	u,v,w, T,Pw
ADV2	Vector	u,v,w, T,Pw
ADV3	Vector	u,v,w, T,Pw
ADV4	Vector	u,v,w, T,Pw
AWAC	AWAC ADCP	η,u,v,P,T
CTD	SBE19p	S,T,P,NH4, Si,NOX

Milestone 1.1.6: Complete 2008 Marmion biophysical sampling

Original Forecast Finish Date: 30/06/08

Revised Forecast Finish Date: 30/06/08

This section updated from previous Biannual Report

Summary of Activities Undertaken, Outputs Produced:

Marmion Lagoon's physical nature (it is a shallow and semi-enclosed water body) and location (urban) make it susceptible to anthropogenic nutrient stress (waste water discharge, ground water discharge and riverine input). We need to understand the temporal and spatial nutrient distribution and important nutrient processes within the lagoon to asses the possible impact and threats posed by changing effluent patterns. We have now completed twelve quasi-monthly surveys investigating spatial variations in nutrient concentration at 30 sampling stations distributed along six east – west transects across Marmion Lagoon. Elevated levels of nitrate, phosphate, silicate and ammonium over the limestone reefs bordering the lagoon suggest these reef systems are a source of pelagic nutrients (Figure 7). Preliminary results suggest that this nutrient source is spatially and temporally variable. For example, surface nitrate concentrations were highest at Station 23 in both the July 18 (2.6 μM) and August 31 (2.5 μM) sampling (Figure 8). Station 23 is located in a particularly shallow reef area. In contrast nitrate concentrations were elevated over reef at stations 14 (1.6 μM) and 18 (1.4 μM) in July but not obviously so in August (Figure 8). While the high concentrations measured at station 4 (1.4 μM) in August, were not evident at that station in July. In addition to the general trend of elevated nutrient concentrations over the reef systems, There was also a single elevated nutrient pool (0.9 μM) was measured inshore at station 11 during August.

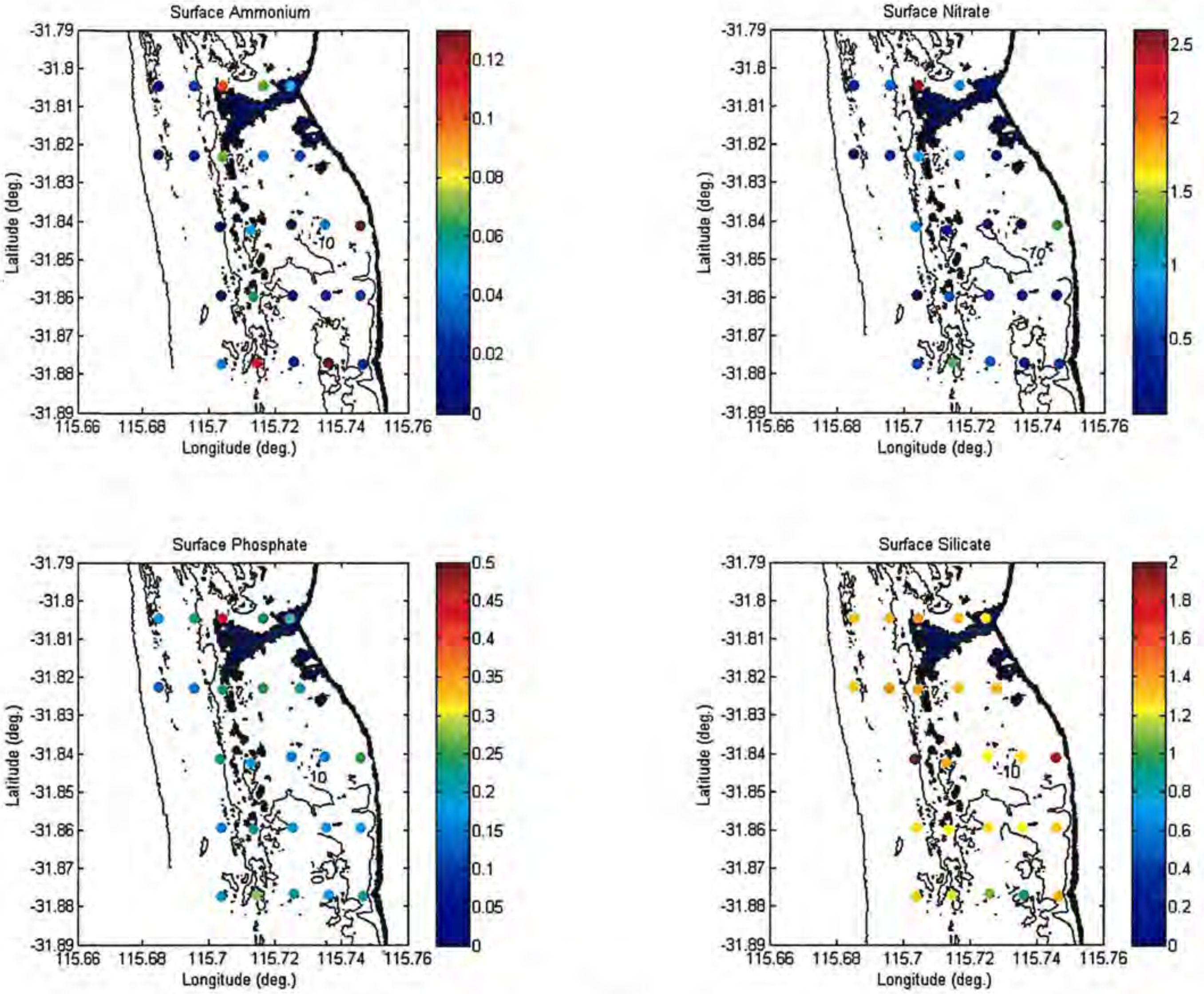

Figure 7. Surface nutrient concentrations (μM) in Marmion Lagoon measured on the 31st of August 2007. The blue shaded area is where the bathymetry is less than 4m.

The true nature of this spatial and temporal variability is difficult to determine. Marmion Lagoon is a complex and energetic environment and conditions likely vary considerably between the stations on our survey grid and between the monthly sampling trips. Two endeavours will help address this situation. Firstly, we have modified a nutrient autoanalyser for underway operation in Marmion lagoon and which will be deployed during the 2008 – 2009 sampling season. Secondly, we have deployed a 48 sample remote access autosampler to investigate variations in nutrient concentration on a range of time scales varying from hourly to 12 houly at low nutrient lagoon and higher nutrient reef stations. Samples collected from the autosampler deployments are yet to be analysed.

The mechanisms that generate the high nutrient concentrations over reefs are presently uncertain but may include excretion by sessile filter feeders, erosion and/or remineralisation of macroalgae thali, influx of groundwater from the limestone or efficient resupply from surrounding (shallow) sediments. Our improved understanding of the spatial and temporal variability of nutrient concentrations (plus salinity and temperature) as well as other biophysical measurements (nutrients, chlorophyll a, primary production, phytoplankton pigment concentrations, particulate organic carbon, suspended solids and zooplankton biomass) that are being collected will help identify the reasons for the present nutrient distribution.

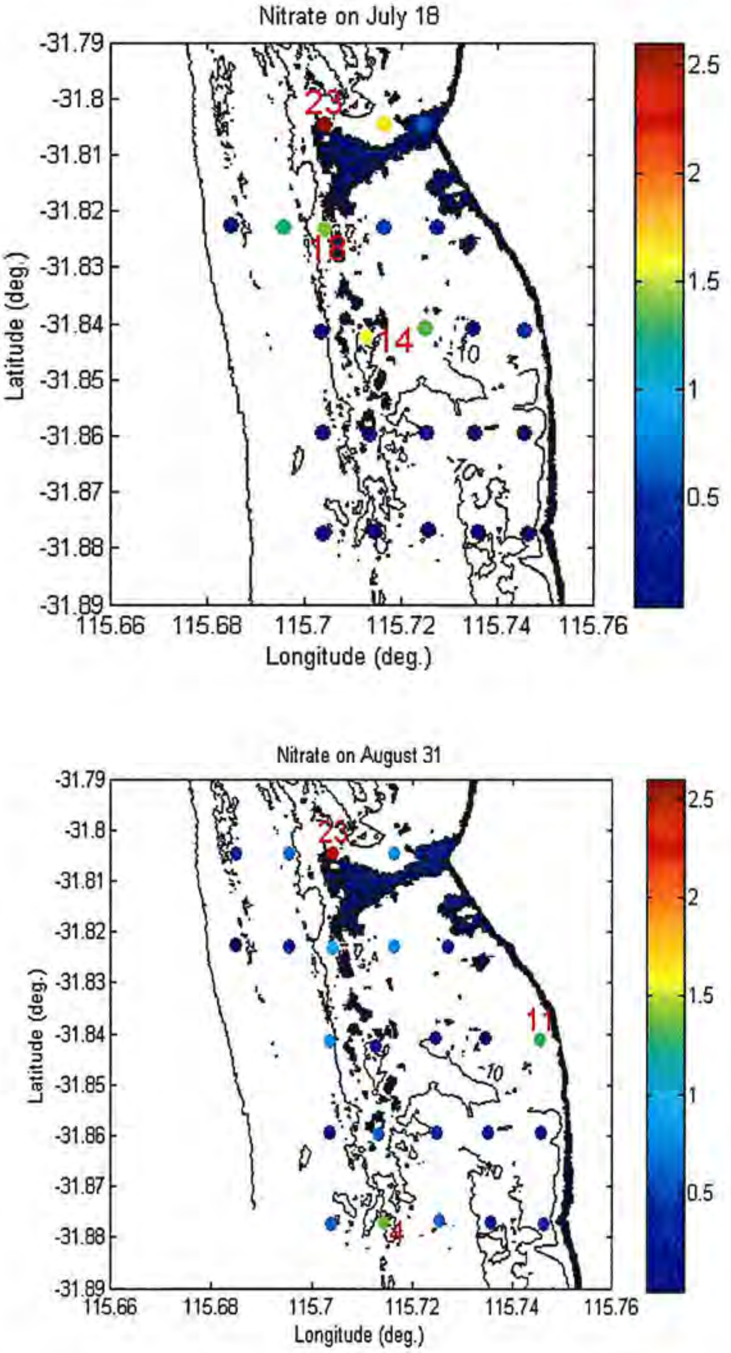

Figure 8. Surface nitrate concentrations (μM) measured in Marmion Lagoon on the 18th of July and 31st of August 2007. The Blue shaded area is <4m deep. Some stations are labelled in red.

Summer sampling of zooplankton in Marmion Lagoon was repeated in August 2007 in three offshore and three inshore stations to obtain winter data. Size fractionated samples were collected for secondary production and artificial cohort analysis. To better understand temporal pattern of zooplankton in Marmion Lagoon we decided to supplement winter and summer sampling by more frequent collections. Two moorings housing multisensors were chosen as additional zooplankton sampling stations. In addition, after analysing nutrient data a third station in the vicinity of AWAC mooring was included. Consequently in August and November zooplankton was collected using replicate tows. Microzooplankton from surface and chlorophyll max layer was sampled using Niskin's.

Three offshore and three inshore stations in Marmion Lagoon were sampled in May 2008. Size fractionated samples were collected for secondary production and artificial cohort analysis. In addition, experiments to determine grazing rates of copepods on natural phytoplankton and microzooplankton communities using 24 hours incubations were carried out. Experiments were design to compare the plankton community evolution with and without added grazers. Modified Frost equations (Strzelecki and Koslow, in SRFME final Report eds. Keesing, J. et al, December 2006, vol 2 p. 95) will be used to determine microzooplankton grazing on phytoplankton, mesozooplankton grazing on phytoplankton and predation on microzooplankton. This method will also detect possible trophic cascade effects. It is recognized that small phytoplankton that dominates oligotrophic waters such as off Western Australia is mainly grazed by microzooplankton and they in turn, along with the larger phytoplankton, are the main food of the mesozooplankton. As a result trophic cascades are observed when increased mesozooplankton biomass leads to increase in phytoplankton because increased predation on microzooplankton releases grazing pressure on phytoplankton. These measurements will add to understanding of plankton dynamics and trophic links in Marmion Lagoon.

The experiments were carried out in 3 L bottles maintained at ambient sea surface temperature and light. Design consisted of treatments without mesozooplankton containing small (< 5 µm) phytoplankton, total phytoplankton (<20 µm) and total phytoplankton and microzooplankton (<200 µm), and treatments with three concentration levels of mesozooplankton added to water containing total phytoplankton and microzooplankton. There were three replicates per treatment. At the end of incubations samples for size fractionated phytoplankton biomass, phytoplankton, microzooplankton and mesozooplankton species composition were collected from all treatments. Sea water was also filtered at the beginning of incubations and a subsample was taken to assess phytoplankton and microzooplankton biomass at the start of incubations. We hypothesized that in treatments with added mesozooplankton small phytoplankton will increase due to trophic cascade and addition of nutrients from sloppy feeding and excretion from mesozooplankton and microzooplankton and large phytoplankton and microzooplankton will decrease because of grazing by mesozooplankton.

In addition to offshore inshore stations mesozooplankton and microzooplankton was sampled next to multisensory (MS1 and MS2) and AWAC moorings in January, March and April. March samples were analysed for fatty acid composition. This is a newly forged collaboration between CSIRO and Chemistry Centre WA with Shao Fang Wang, senior chemist and research officer leading the project at the Centre side. The aim is to determine the seasonal fatty acid composition of mesozooplankton from Marmion lagoon and spatial composition of mesozooplankton fatty acids from samples collected on Southern Surveyor voyage from parallel 34 to 22ºS. The biochemical composition of plankton off Western Australia has not been investigated before. Fatty acids are used as biomarkers of trophic relations and changes in plankton composition are associated with behaviour, diet and seasonal and spatial plankton productivity.

This first set of results indicated that strictly herbivorous zooplankton was absent at that time of the year in Marmion Lagoon (lack of 20:1 (n-9) and 22:1 (n-11) markers (Table 1). Relatively high proportion of saturated fatty acids (14:0 and 16:0) and proportion of short-chain saturates versus long-chain monounsaturates also corroborates omnivorous and carnivorous feeding. Zooplankton from all three locations and all size fractions had a high ratio of 16 : 0 (palmitic acid) to 16 : 1 (palmitoleic acid). They both originate from phytoplankton diet and indicate preferential feeding on flagellates comparing to diatoms since diatoms are rich in 16:1 relative to 16:0 and flagellates are the opposite. Low ratios of 18:1 (n-9) to 18:1 n-7 and EPA to DHA suggested that omnivory was more important than carnivory.

Table 2. Fatty Acid composition in size fractionated mixed zooplankton samples.

	Site name	**MS1**	**MS1**	**MS1**	**MS1**	**MS2**	**MS2**	**MS2**	**MS2**	**AWAC**	**AWAC**	**AWAC**	**AWAC**
	Size fraction (µm)	**1000 to 355**	**355 to 250**	**250 to 150**	**150 to 100**	**1000 to 355**	**355 to 250**	**250 to 150**	**150 to 100**	**1000 to 355**	**355 to 250**	**250 to 150**	**150 to 100**
Saturated		%	%	%	%	%	%	%	%	%	%	%	%
Myristic	C14:0	6.6	6.0	4.1	**6.8**	**15.5**	6.1	5.3	2.9	3.3	**12.5**	6.1	**7.7**
Pentanoic	C15:0	1.1	0.7	0.6	1.0	2.3	0.8	0.7	0.9	0.6	1.1	0.6	0.8
Palmitic	C16:0	**17.5**	**17.5**	**18.0**	**29.8**	**29.9**	**17.1**	**15.1**	**8.0**	**15.4**	**31.0**	**17.7**	**24.0**
Margaric	C17:0	1.3	0.9	0.3	0	1.8	0.9	1.1	1.6	1.2	1.5	1.0	1.3
Stearic	C18:0	6.2	5.7	7.3	**10.3**	**8.8**	5.5	6.8	3.7	7.1	**10.0**	6.3	**7.9**
Nonadecanoic	C19:0	0.2	0.2	1.9	2.2	0.2	0.2	0.2	0.2	0.2	0.2	0.2	0.2
Arachidic	C20:0	0.3	0.4	0.4	0.0	0.0	0.3	0.2	0.1	0.4	0.5	0.3	0.4
Heneicosanoic	C21:0	0.2	0.2	0.0	0.0	0.3	0.1	0.1	1.0	0.1	0.0	0.2	0.1
Behenic	C22:0	0.5	0.8	0.3	0.0	0.2	0.9	0.9	0.4	0.2	0.3	0.8	0.0
Tricosanoic	C23:0	0.0	0.1	0.0	0.0	0.2	0.2	0.1	0.3	0.1	0.0	0.1	0.0
Lignoceric	C24:0	0.9	1.2	1.4	1.8	0.0	1.1	1.5	0.8	1.2	0.3	1.2	0.8
Cerotic	C26:0	0.0	0.0	0.3	0.0	0.0	0.2	0.0	0.0	0.0	0.0	0.0	0.0
Heptacosanoic	C27:0	0.0	0.1	0.0	0.0	0.5	0.1	0.2	0.0	0.0	0.0	0.1	0.1
Triacontanoic	C30:0	0.1	0.0	0.0	0.0	0.3	0.0	0.0	0.0	0.0	0.0	0.0	0.0
	sum	**34.9**	**33.8**	**34.7**	**52.0**	**60.1**	**33.5**	**32.2**	**19.9**	**29.8**	**57.5**	**34.5**	**43.4**
Branched	i-C15:0	0.6	0.4	0.3	0.0	0.8	0.2	0.2	0.2	0.2	0.4	0.2	0.4
	i-C16:0	0.5	0.2	0.3	0.0	0.2	0.0	0.0	1.0	0.2	0.0	0.1	0.1
	i-C17:0	0.6	0.5	0.5	0.0	0.7	0.4	0.4	0.2	0.3	0.6	0.4	0.4
	sum	**1.6**	**1.0**	**1.1**	**0.0**	**1.7**	**0.6**	**0.6**	**1.4**	**0.8**	**1.0**	**0.7**	**1.0**
Monounsaturated													
Palmitelaidic	C16:1n-7t	0.3	0.4	0.0	0.0	0.4	0.3	0.3	0.2	0.1	0.5	0.3	0.4
Palmitoleic	C16:1n-7c	3.7	6.9	4.6	**8.3**	5.1	5.8	2.8	1.7	2.7	**10.8**	4.2	5.1
	c16.1	0.8	0.2	0.0	0.0	2.6	0.3	0.3	0.1	0.2	0.3	0.2	0.3
Heptadecenoic	C17:1n-7c	0.6	0.2	0.0	0.0	0.5	0.2	0.1	0.2	0.6	0.2	0.4	0.6
Petroselaidic	C18.1 t-6	0.1	0.1	0.0	0.0	0.0	0.1	0.1	0.0	0.1	0.0	0.1	0.3

Petroselenic	C18:1 c-6	0.0	0.2	0.0	0.0	0.0	0.2	0.0	0.0	0.0	0.0	0.2	0.1
Oleic	C18:1n-9c	4.8	3.1	3.6	5.8	**12.7**	3.6	3.9	2.1	5.0	5.7	4.1	6.0
Vaccenic	C18:1n-7c	3.0	1.4	1.9	3.5	3.9	1.1	1.1	0.9	2.4	2.2	1.2	1.7
Gadoleic	C20:1n-10c	0.0	0.0	0.8	0.9	0.2	0.0	0.4	0.3	0.5	0.3	0.3	0.8
Gondoic	C20:1n-8c	0.5	0.2	0.4	1.9	0.3	0.5	0.0	2.1	0.5	0.4	0.0	0.6
Eicosenoic	C20:1n-6c	0.1	0.6	0.3	0.0	0.0	0.3	0.1	0.2	0.1	0.5	0.3	0.1
Brassidic	C22:1n-9t	0.1	0.0	0.0	1.4	0.0	0.1	0.1	0.0	0.2	0.2	0.1	0.2
Erucic	C22:1n-9c	0.0	0.1	0.3	0.0	0.5	0.0	0.0	0.0	0.0	0.0	0.1	0.1
Nervonic	C24:1n-7c	0.3	0.4	0.0	0.0	0.3	0.9	0.2	**26.9**	0.5	0.4	0.3	0.3
	sum	**14.0**	**13.4**	**11.9**	**21.8**	**26.1**	**12.4**	**9.3**	**7.9**	**12.6**	**21.1**	**11.5**	**16.4**
Poluunsaturated													
Linoleic	C18:2n-6c	3.1	1.8	0.0	0.0	3.8	2.3	2.3	1.1	2.0	1.6	2.0	2.2
Linolenelaidic	C18:3n-3t	0.2	0.2	0.0	0.0	0.0	0.2	0.2	0.0	0.1	0.0	0.2	0.2
	C18.3 t9,t12,c15	0.3	0.3	0.3	0.0	0.2	0.3	0.2	0.0	0.3	0.0	0.2	0.3
Linolenic	C18:3n-3c	2.5	1.4	2.4	3.3	0.0	1.5	1.5	1.1	1.0	0.7	1.3	1.5
gamma-Linolenic	C1:3n-6c,	0.0	0.0	0.0	0.0	0.7	0.0	0.0	0.0	0.0	0.0	0.0	0.0
Stearidonic	C18:4n-3c	1.2	1.6	1.4	0.0	0.3	2.3	2.1	1.0	1.1	0.8	2.0	1.8
Eicosadienoic	C20:2n-6c	0.4	0.2	0.5	0.0	0.4	0.2	0.4	0.3	0.6	0.2	0.4	0.5
Arachidonic	C20:4n-6c, AA	3.5	2.3	3.0	2.8	0.5	2.1	1.7	1.3	3.7	1.2	2.0	2.4
Eicosatrienoic	C20:3n-3c	0.2	0.1	0	0.0	0.0	0.1	0.15	0.2	0.16	0	0.1	0.2
Eicosatetraenoic	C20:4n-8c	0.2	0.3	0.0	0.0	0.0	0.2	0.1	0.0	0.0	0.0	0.2	0.3
Eicosapentanoic	C20:5n-3, EPA	**15.1**	**13.6**	**12.8**	5.9	1.4	**12.7**	**12.0**	5.5	**14.8**	4.8	**12.3**	**8.0**
Docostetraenoic	C22:4n-6c	0.0	0.0	0.0	1.3	0.4	0.0	0.0	1.1	0.1	0.0	0.0	0.2
Docasapentenoic	C22:5n-3c	0.8	0.9	1.0	0.0	0.0	0.8	0.8	0.6	1.0	0.3	0.8	1.0
Docosahexenoic	C22:6n-3, DHA	**18.3**	**25.7**	**26.4**	**8.0**	0.8	**24.1**	**32.8**	**14.0**	**27.9**	**7.3**	**28.3**	**14.8**
	sum	**45.8**	**48.3**	**47.9**	**21.2**	**8.4**	**46.7**	**54.4**	**26.4**	**52.8**	**16.9**	**49.7**	**33.4**
	Sum n-3	23.5	30.2	31.6	11.3	1.3	29.2	37.8	17.0	31.6	9.0	33.0	19.8
	sum n-6	7.1	5.1	3.8	4.0	5.7	5.1	4.6	4.1	6.5	3.6	4.7	5.6
	n-3:n-6	3.3	5.9	8.2	2.8	0.2	5.7	8.2	4.1	4.8	2.5	7.0	3.5

Zooplankton in Marmion lagoon was sampled in October 2008 in three offshore and inshore stations. Size fractionated samples were collected for secondary production measurements and artificial cohort incubations. Grazing experiments following May 2008 design were conducted to reveal grazing patterns in Winter/Spring. Laboratory processing of the samples from Marmion Lagoon has commenced.

Measurements of zooplankton biomass indicate that the biomass was comparable to inshore waters sampled during SS0407 cruise and there was no significant difference (t = 0.42) between inshore and offshore of the reef line (Figure 9).

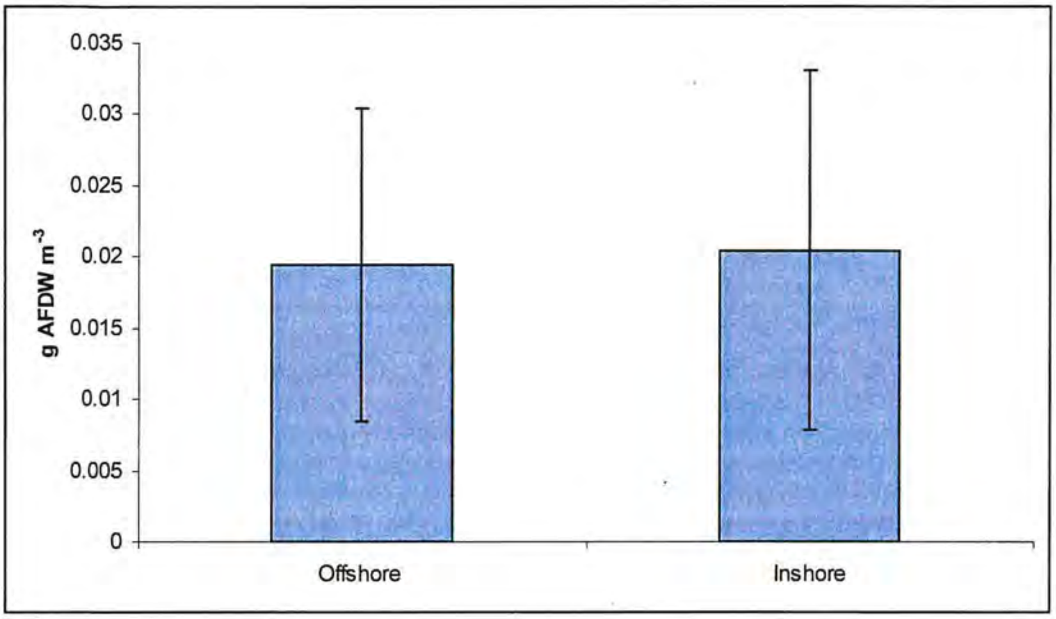

Figure 9
Biomass of zooplankton offshore and inshore of the reefs

Measurements at three additional stations: MS1, MS2 and AWAC (see Figure 6 for stations' positions) revealed no difference in zooplankton biomass among stations (Figure 10).

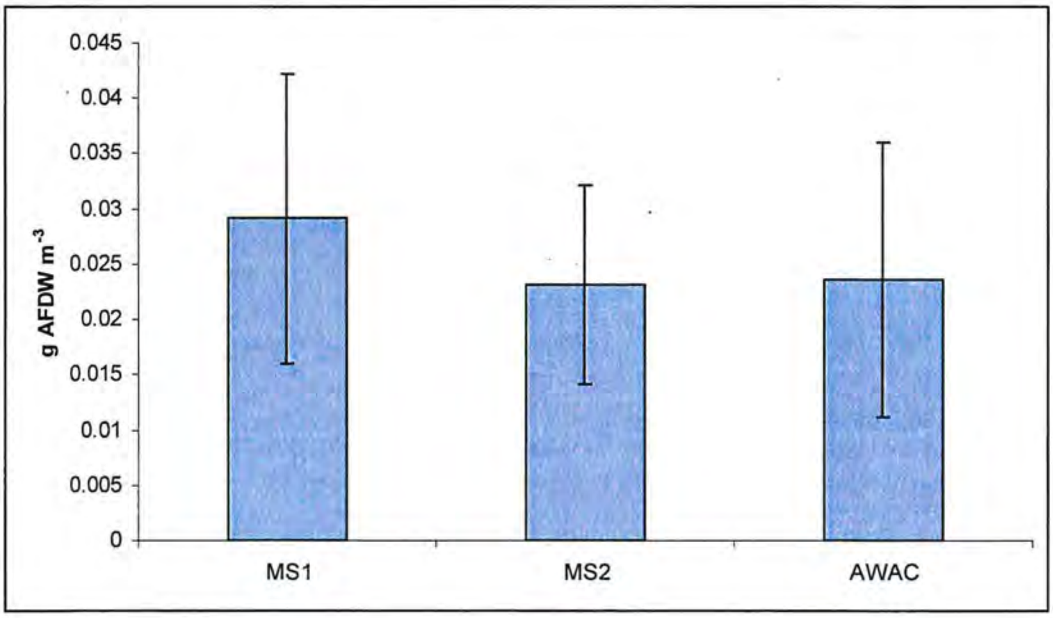

Figure 10
Biomass of total zooplankton at MS1, MS2 and AWAC

There was large variability of biomass among all stations. There was no temporal pattern in plankton biomass and again variability among seasons was high (Figure 11)

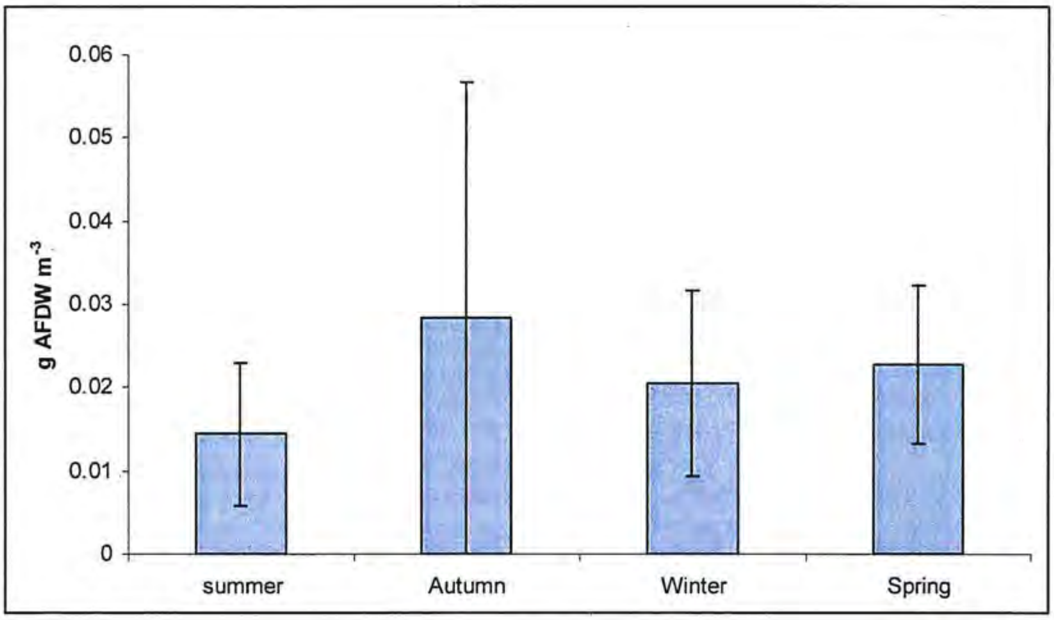

Figure 11
Biomass of zooplankton (all stations combined)

355 µm biomass dominated size fraction in both inshore and offshore stations except for August 2007 when small organisms dominated in one inshore station. Small size fractions were also important in one station in April (Figure 12 and Figure 13).

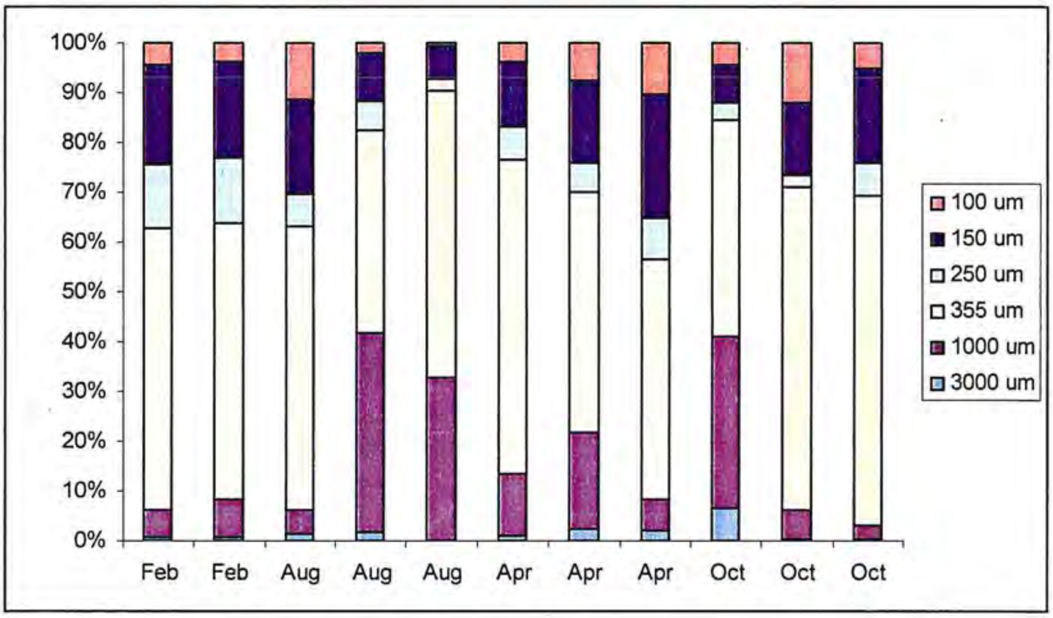

Figure 12
Size structure of zooplankton sampled offshore of reefs.

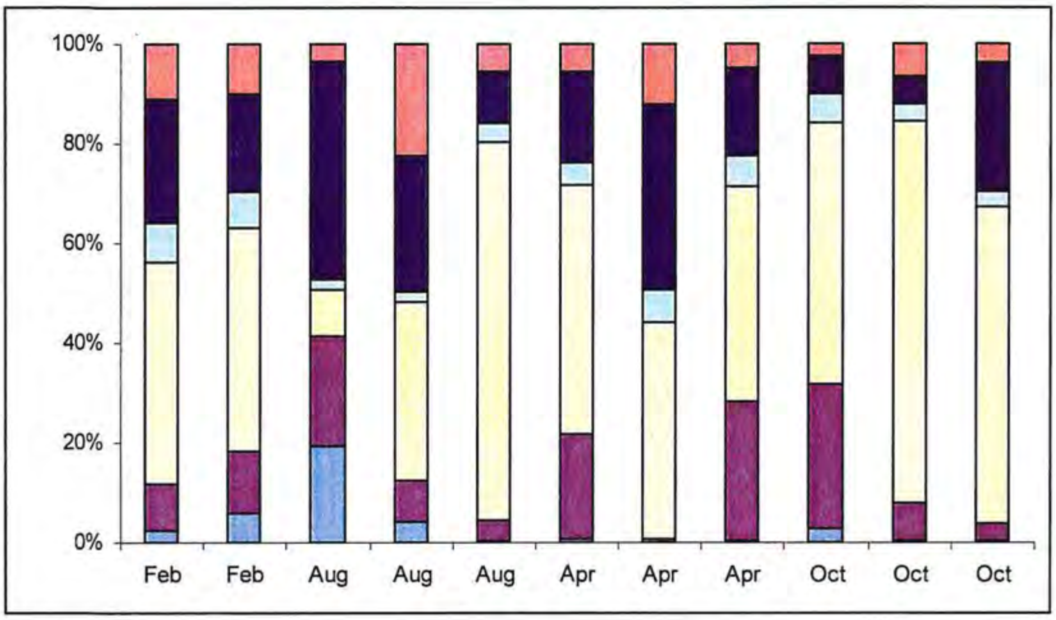

Figure 13
Size structure of zooplankton sampled inshore of reefs.

Large size structure dominated also MS1, MS2 and AWAC stations (Figure 14.) at all sampling times except one MS1 station in winter (Figure 14.).

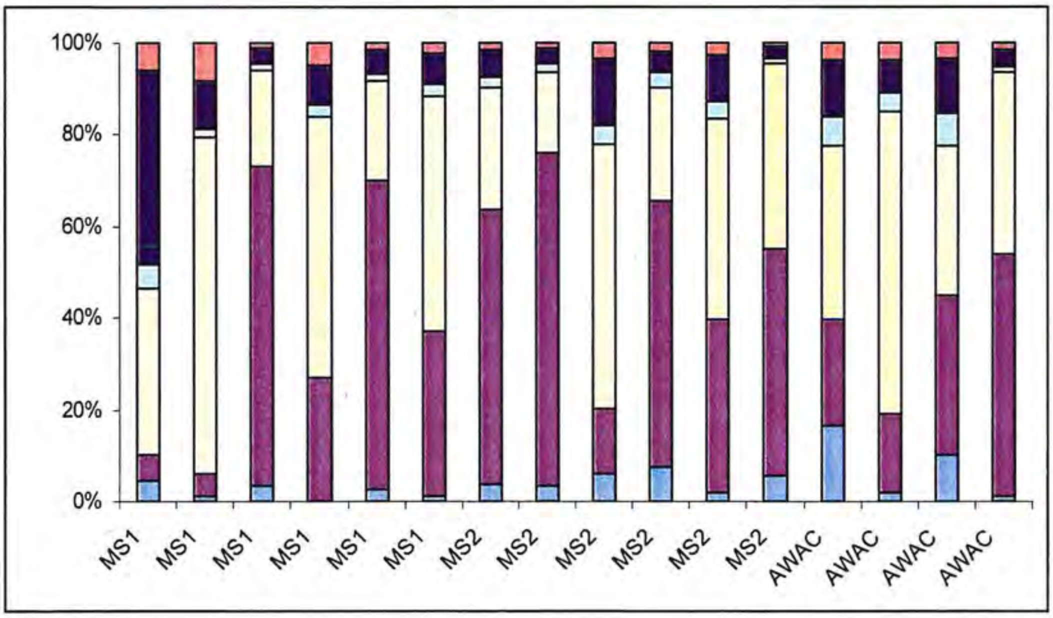

Figure 14.
Size structure of zooplankton sampled at MS1, MS2 and AWAC

Broadly the biomass of zooplankton in Marmion Lagoon was comparable to the biomass of inshore stations sampled along the coast of Western Australia during SS0407 cruise. The biomass data in Marmion was variable both spatially and temporarily. The mechanisms leading to variability of zooplankton biomass in

Marmion lagoon are unclear at the moment. Relationships with biotic (phytoplankton) and physics (hydrodynamics) and chemistry (nutrients) will be explored.

Milestone 1.1.7: Initiate connectivity model runs

Original Forecast Finish Date: 30/06/09

Revised Forecast Finish Date: 30/06/09

This section updated from previous Biannual Report

Particle tracking was initiated under WAMSI Project 1.2 milestone 2.3.2, "Identification of potential connectivity patterns between Shark Bay and the Capes based on particle track modelling", completed in December 2007. Milestone 1.1.7 continues the connectivity studies.

Data preparation

BRAN outputs
Bluelink ReANalysis, or BRAN, is based on a global ocean model, OFAM (Ocean Forecasting Australia Model), developed as part of the BLUElink partnership between CSIRO, the Bureau of Meteorology, and the Royal Australian Navy (Schiller et al., 2008). BRAN assimilates (is corrected by) satellite (including altimeter) and in-situ data as it runs (Oke et al., 2008), and has been used to create a 1993-2008 archive of daily values of ocean properties including ocean currents, salinity and temperature in 3 dimensions, resolved at 10 km horizontally and 10 m vertically (in the upper ocean) in the Australian region.

HYCOM outputs
HYCOM is the Hybrid Coordinate Ocean Model, with a vertical coordinate that is isopycnal in the open, stratified ocean, but smoothly reverts to a terrain-following coordinate in shallow coastal regions, and to z-level coordinates in the mixed layer and/or unstratified seas (Bleck and Boudra 1981; Bleck and Benjamin 1993). The HYCOM hindcast system is configured for the global ocean with HYCOM 2.2 as the dynamical model. Computations are carried out on a mercator grid between 78°S and 47°N (1/12° equatorial resolution). Daily output from the model is downloaded from (http://hycom.rsmas.miami.edu/hycom-model/overview.html).

WW3
Significant wave height, wave period and direction from Wave Watch 3 model (WW3) data (http://polar.ncep.noaa.gov/waves/wavewatch.shtml; Tolman et al. 2002) were used to derive Stokes Drift velocity for the particle tracking. Eight-hourly global WW3 data at 1-degree longitude by 1.25-degree latitude resolution from 1997 to present were downloaded. The WW3 data are converted to daily means, and then interpolated onto the ~10km x ~10km BRAN velocity grid between 90E – 130E and 1N – 61S.

QuikScat
QuikScat (http://winds.jpl.nasa.gov/missions/quikscat/index.cfm) satellite derived wind data are also used in the particle tracking. The twice daily global data at ¼ degree by ¼ degree resolution from 1999 to present were downloaded. The data

are averaged into daily values, and then interpolated onto the BRAN ~10km by ~10km velocity grid.

Validation of model outputs

Monthly climatology of horizontal currents from BRAN is consistent with observations in the southeast Indian Ocean region (Figure 15). The seasonal cycles of the Indonesian Throughflow, South Equatorial Current, and the Leeuwin Current are well reproduced by BRAN. Similar climatology can be derived from HYCOM (not shown).

In the following, BRAN and HYCOM simulated currents off the west coast are compared against shipboard and mooring observations, to validate the model performance in the region.

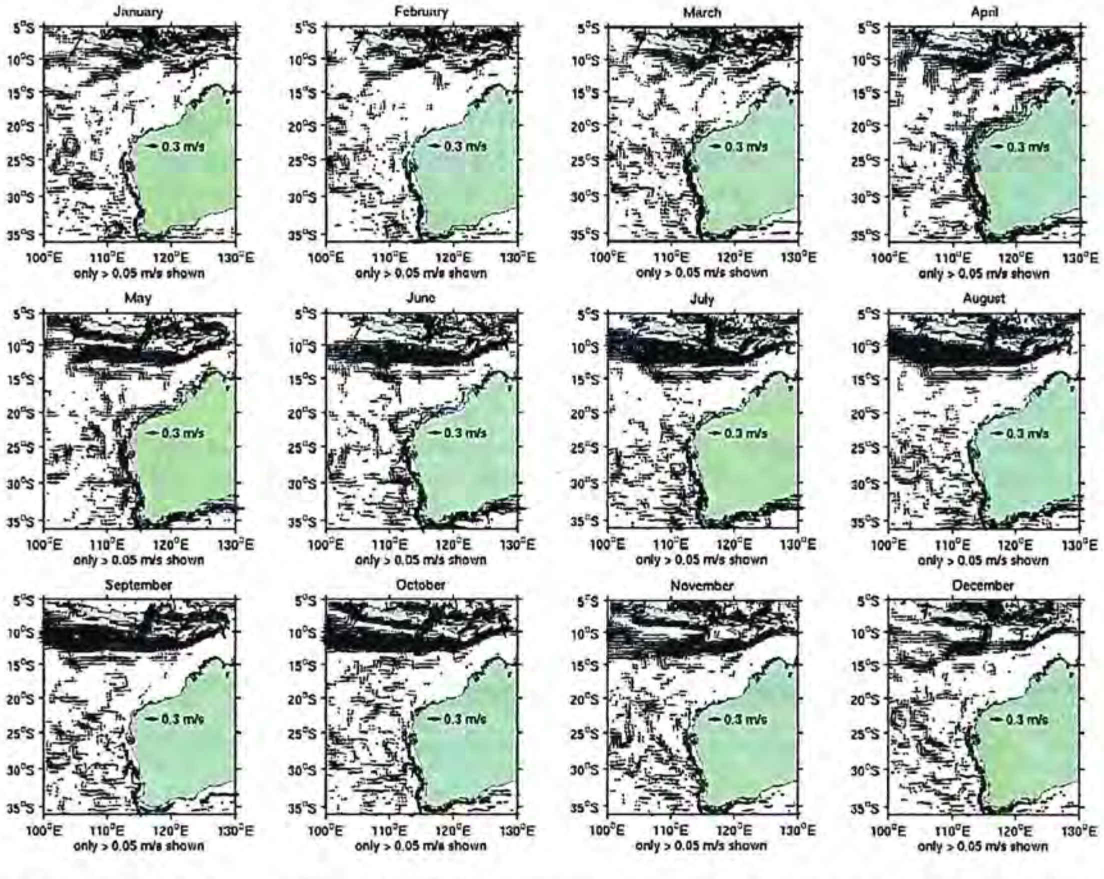

Figure 15. Monthly climatology of horizontal currents, averaged over the top 150 m, from BRAN.

Comparison of BRAN and HYCOM near-surface ocean current velocities measured with ADCP from Southern Surveyor cruise SS200704 in May-June 2007 shows that visually there are agreements in broad-scale features of the Leeuwin Current and eddies off the west coast, though the model outputs tend to lack of some of the sub-mesoscale variability in the observation (Figure 16).

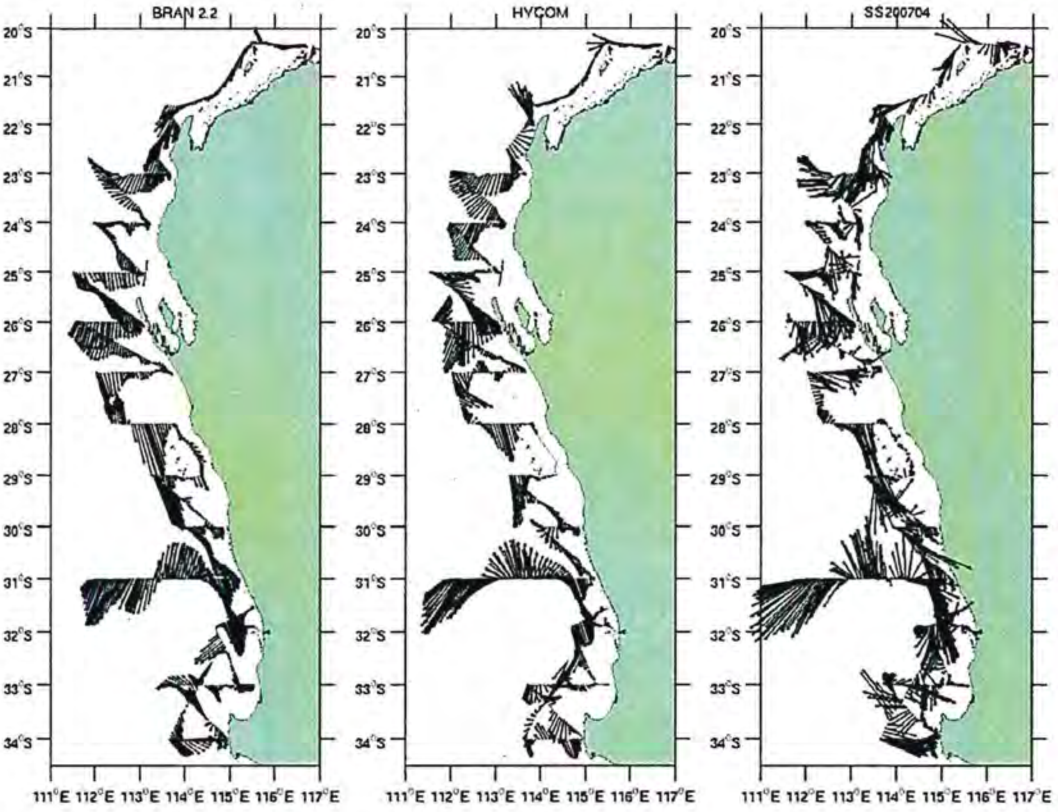

Figure 16. Comparison of near-surface current velocities derived from BRAN, HYCOM outputs and SS200704 shipboard measurements at 95 metres depth.

The eastward and northward components of current velocity can be approximately regarded as cross-shelf and alongshore off the west coast. Figure 17 below shows the comparisons of the two components of the velocity fields from models and observations during the SS200704 cruise. As shown in Figure 16, the cross-shelf velocities in both BRAN and HYCOM have noticeably underestimated the observations. This is quantified in the linear regression between the cruise data and the BRAN data (interpolated to the cruise data locations and times). The overall correlation is 0.6-0.7.

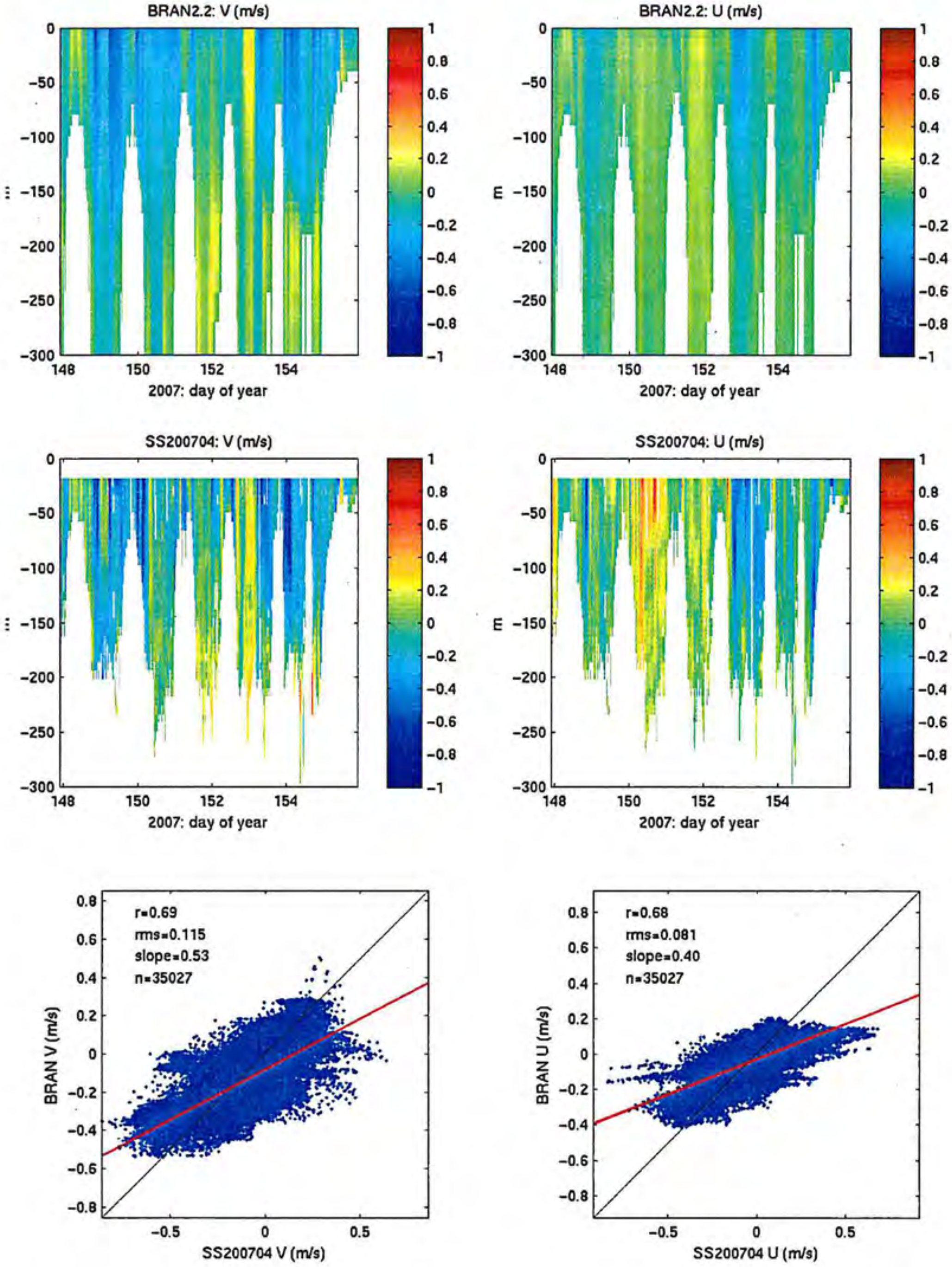
BRAN2.2: V (m/s)
BRAN2.2: U (m/s)
SS200704: V (m/s)
SS200704: U (m/s)
m
0
-50
-100
-150
-200
-250
-300
148
150
152
154
2007: day of year
1
0.8
0.6
0.4
0.2
0
-0.2
-0.4
-0.6
-0.8
-1
r=0.69
rms=0.115
slope=0.53
n=35027
BRAN V (m/s)
SS200704 V (m/s)
r=0.68
rms=0.081
slope=0.40
n=35027
BRAN U (m/s)
SS200704 U (m/s)
-0.5
0
0.5

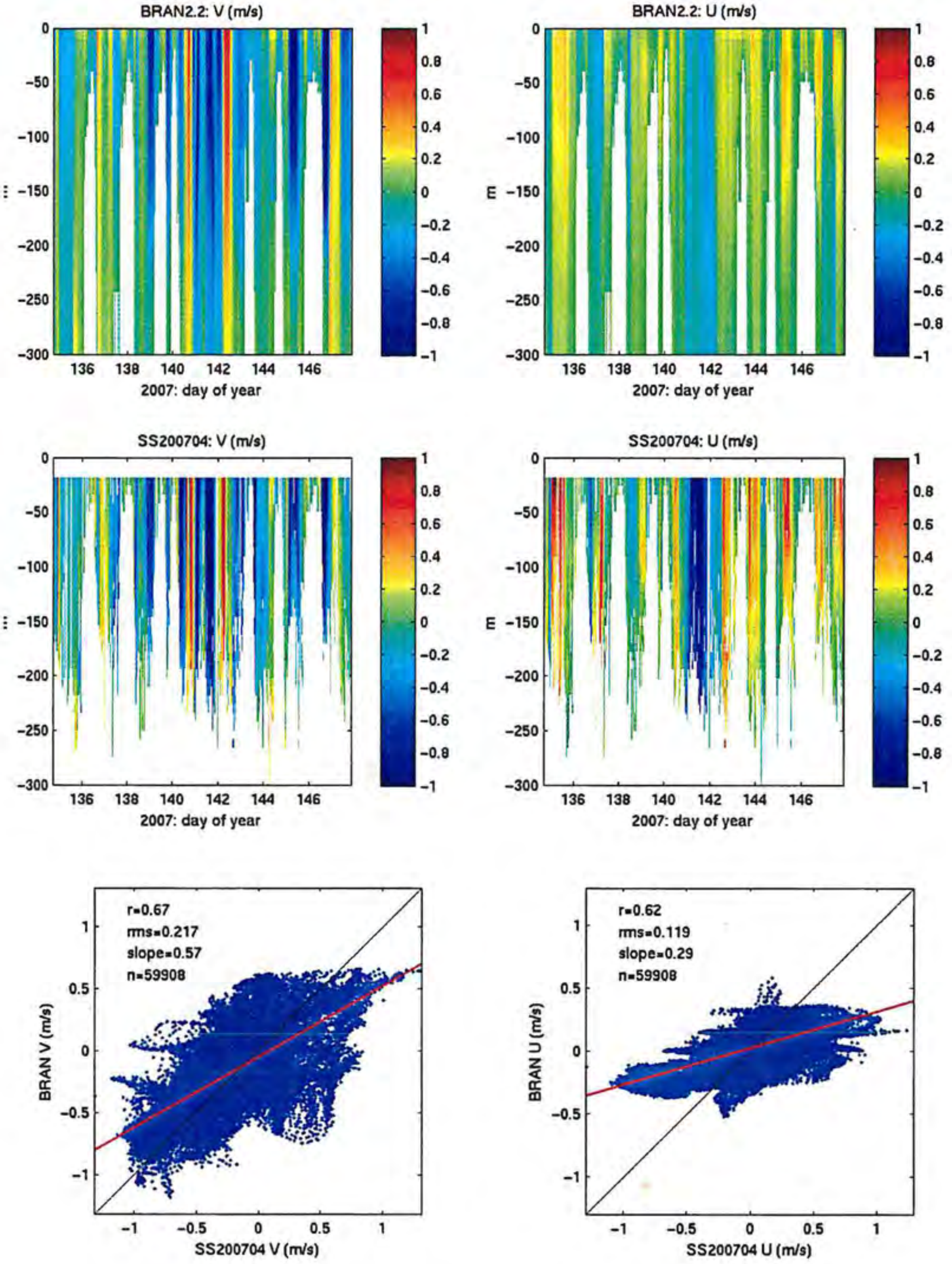

Figure 17. Cruise track comparison of eastward and northward velocity components and BRAN data.

Binning of SS200704 CTD data (temperature and salinity) into daily means for comparison with BRAN data resulted in very high data matching with values of 'r' being greater than 0.9. Figure 18 shows the comparison and linear regression. Salinities above 35psu tended to be underestimated in BRAN, values below 35psu tended to be overestimated. The comparison with HYCOM is similar although the underestimate of salinity was greater than that of BRAN (Figure 19).

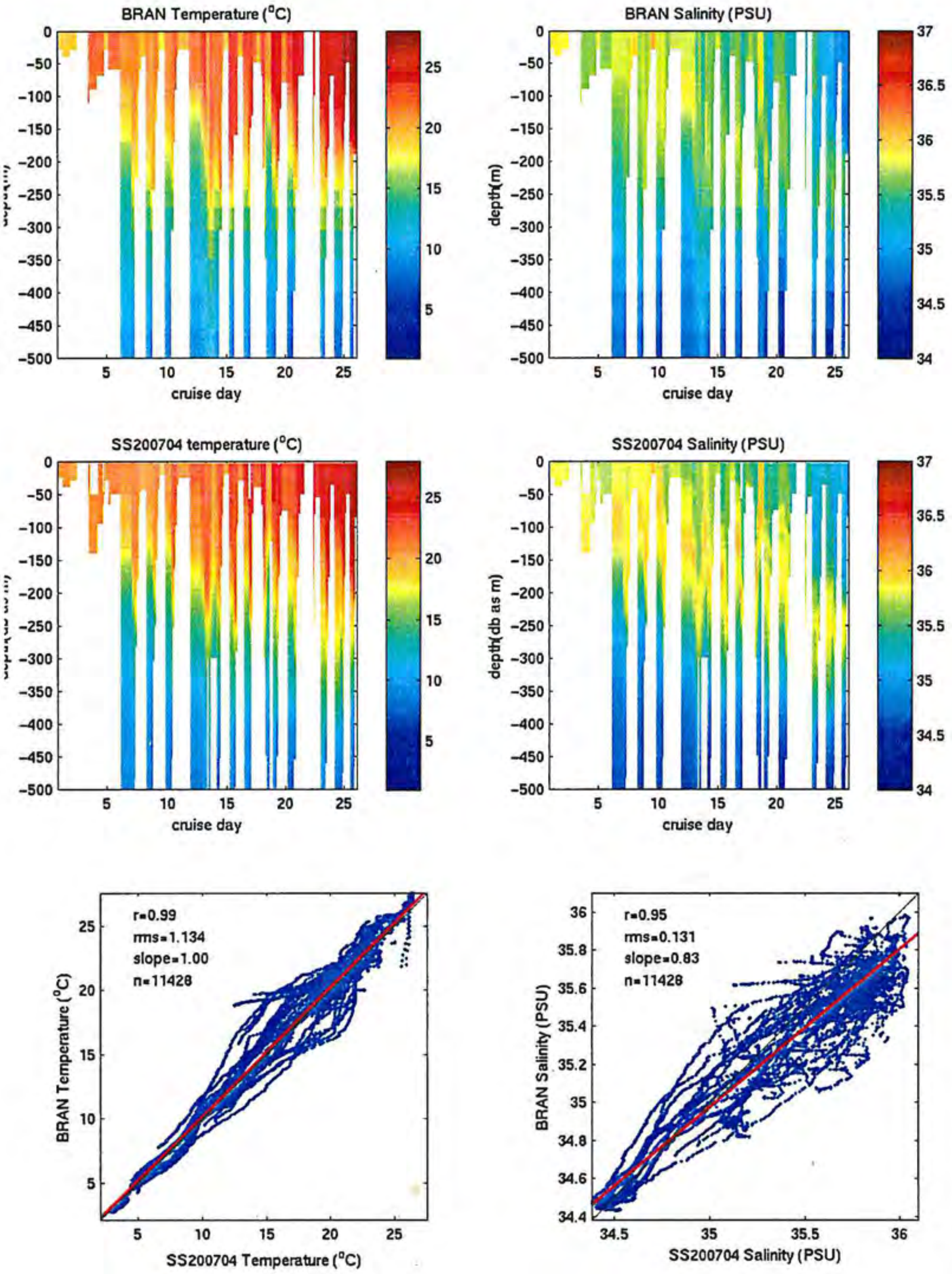

Figure 18. Daily binned cruise temperatures and salinities compared with BRAN data.

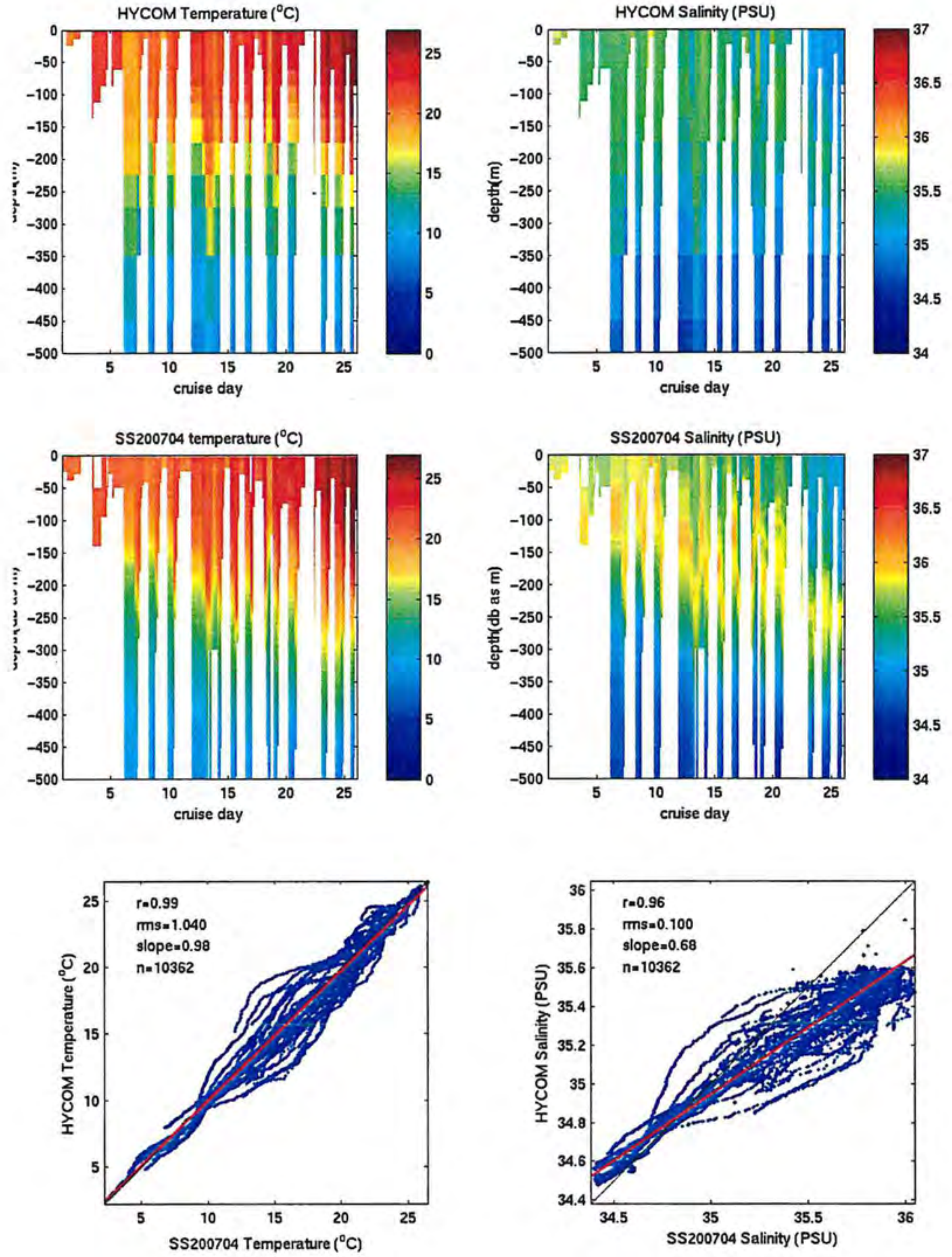

Figure 19. Daily binned cruise temperatures and salinities compared with HYCOM data.

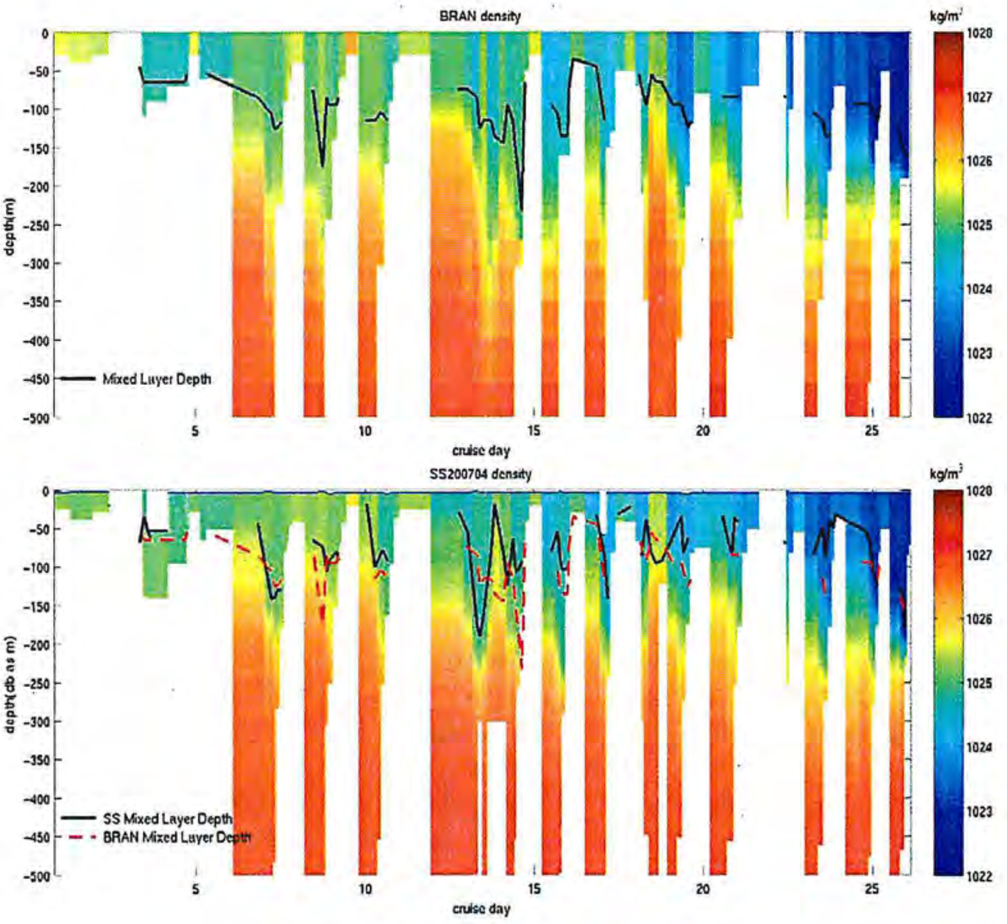

Figure 20. Mixed layer depth and potential density.

Using the temperature and salinity from the cruise data and the BRAN data, the mixed-layer depths were calculated using the criterion of a 0.125 kg/m^3 of the density change from the sea surface (10m). Figure 20 shows the calculated mixed-layer depths and potential density profiles. The comparison is visually reasonable while the correlation is only 0.34.

BRAN data off Ningaloo Reef are compared with current metre data collected as part of the WOCE program in 1995 and 1996. Figure 21 below shows the locations of the moorings near Ningaloo Reef (Domingues et al. CSIRO technical report). Only moorings m61 (1995/1996), m62 (1995/1996) and m63 (1995) had data that were suitable for comparison.

As with the cruise data, the comparison of the alongshore current is much better than that of the cross-shore. This confirms that BRAN underestimates cross-shore currents near the shelf break.

Overall the correlation in the meridional flow is around 0.6 or better if extremes are removed. Figure 22, Figure 23 and Figure 24 below show the comparisons in more detail. One can see a "bimodal" shape to some of the data especially in 1995. The separation of the modes appears to be related to the timing of events, which implies a seasonal variation of the model performance off the Western Australian coast.

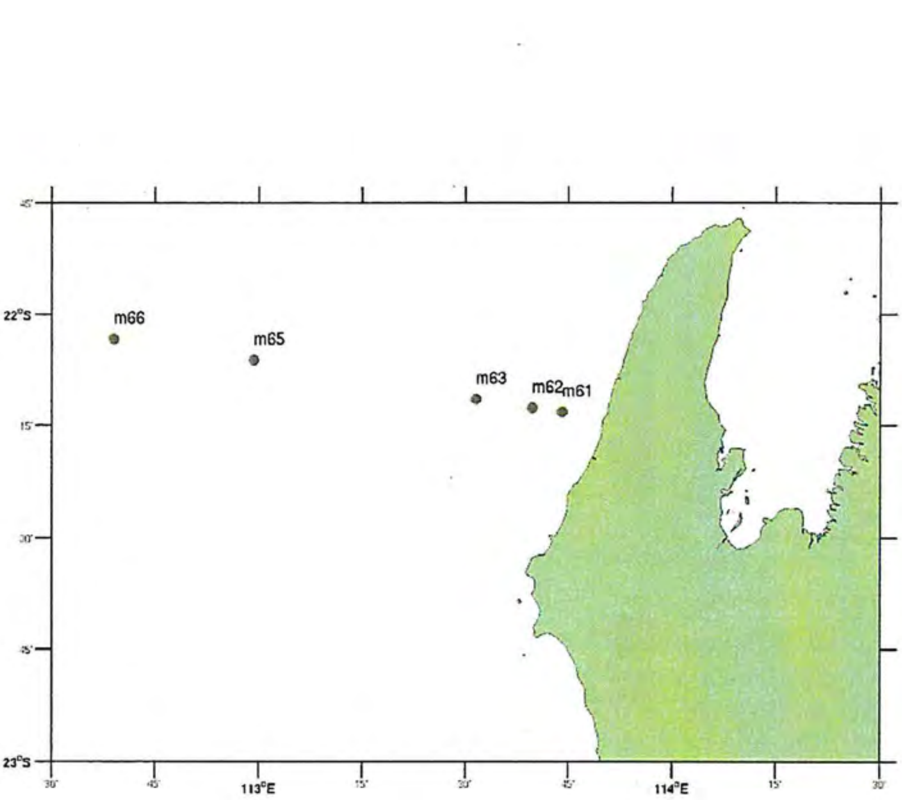

Figure 21. WOCE mooring locations.

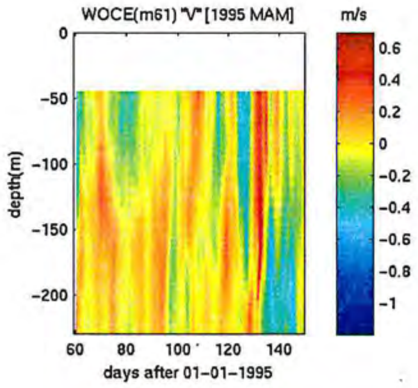
WOCE(m61) "V" [1995 MAM]
m/s
0
-50
-100
-150
-200
depth(m)
60
80
100
120
140
days after 01-01-1995
0.6
0.4
0.2
0
-0.2
-0.4
-0.6
-0.8
-1

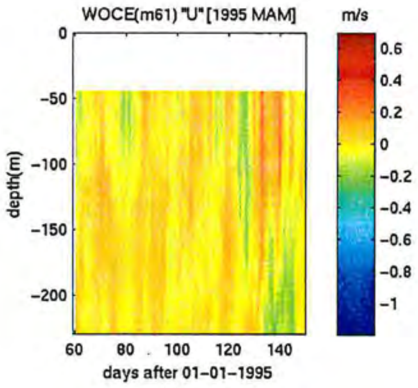
WOCE(m61) "U" [1995 MAM]
m/s
0
-50
-100
-150
-200
depth(m)
60
80
100
120
140
days after 01-01-1995
0.6
0.4
0.2
0
-0.2
-0.4
-0.6
-0.8
-1

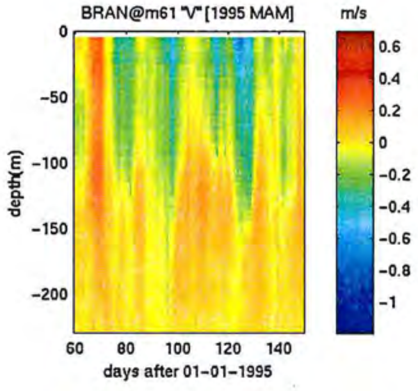
BRAN@m61 "V" [1995 MAM]
m/s
0
-50
-100
-150
-200
depth(m)
60
80
100
120
140
days after 01-01-1995
0.6
0.4
0.2
0
-0.2
-0.4
-0.6
-0.8
-1

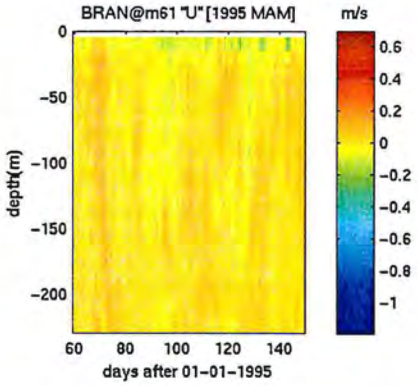
BRAN@m61 "U" [1995 MAM]
m/s
0
-50
-100
-150
-200
depth(m)
60
80
100
120
140
days after 01-01-1995
0.6
0.4
0.2
0
-0.2
-0.4
-0.6
-0.8
-1

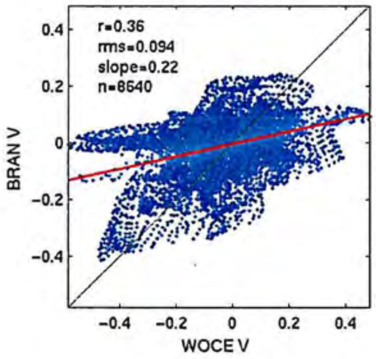
r=0.36
rms=0.094
slope=0.22
n=8640
0.4
0.2
0
-0.2
-0.4
BRAN V
-0.4
-0.2
0
0.2
0.4
WOCE V

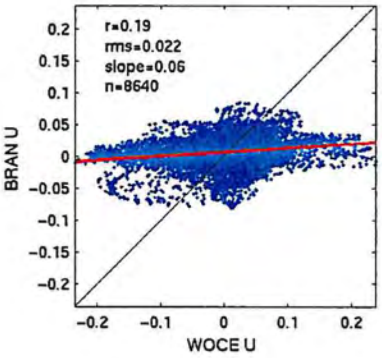
r=0.19
rms=0.022
slope=0.06
n=8640
0.2
0.15
0.1
0.05
0
-0.05
-0.1
-0.15
-0.2
BRAN U
-0.2
-0.1
0
0.1
0.2
WOCE U

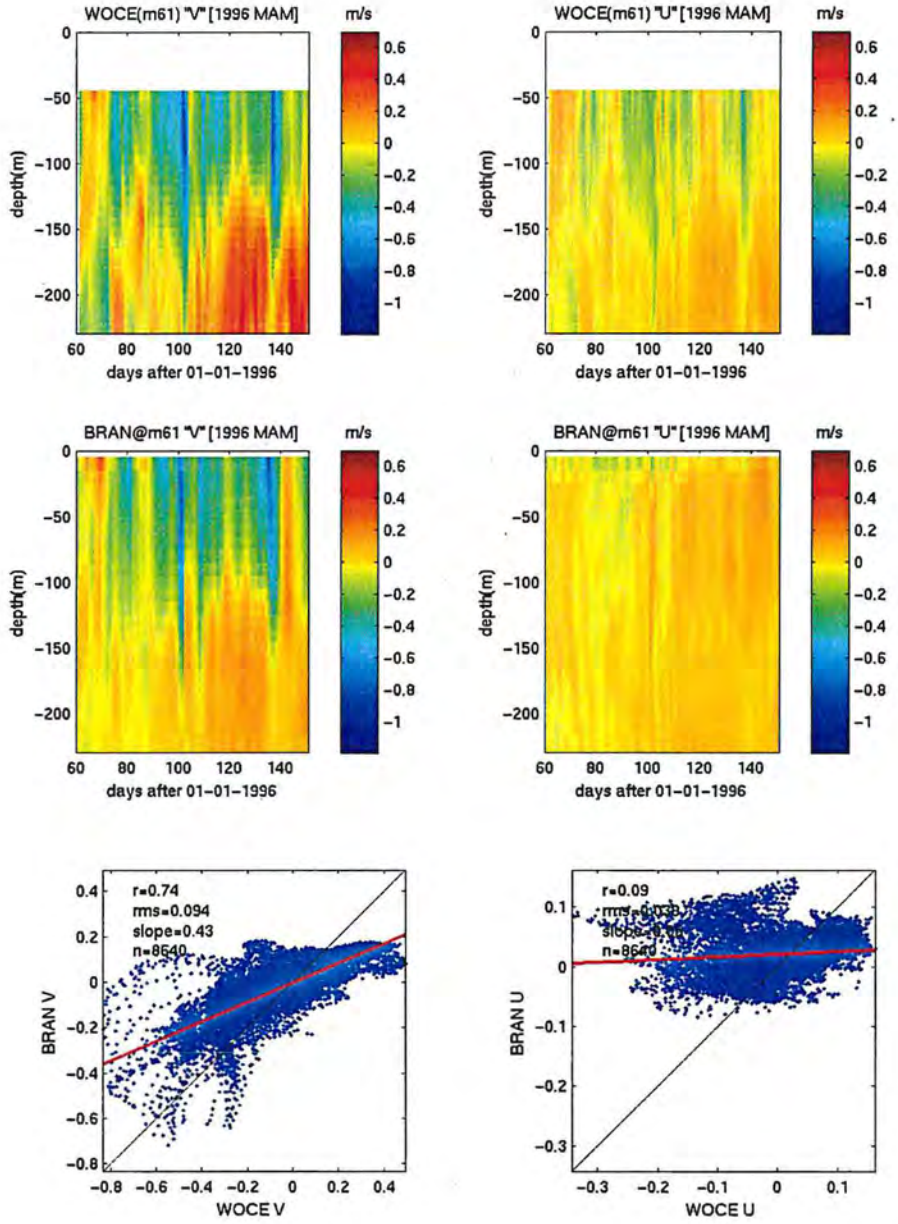

Figure 22. WOCE mooring m61 compared with BRAN

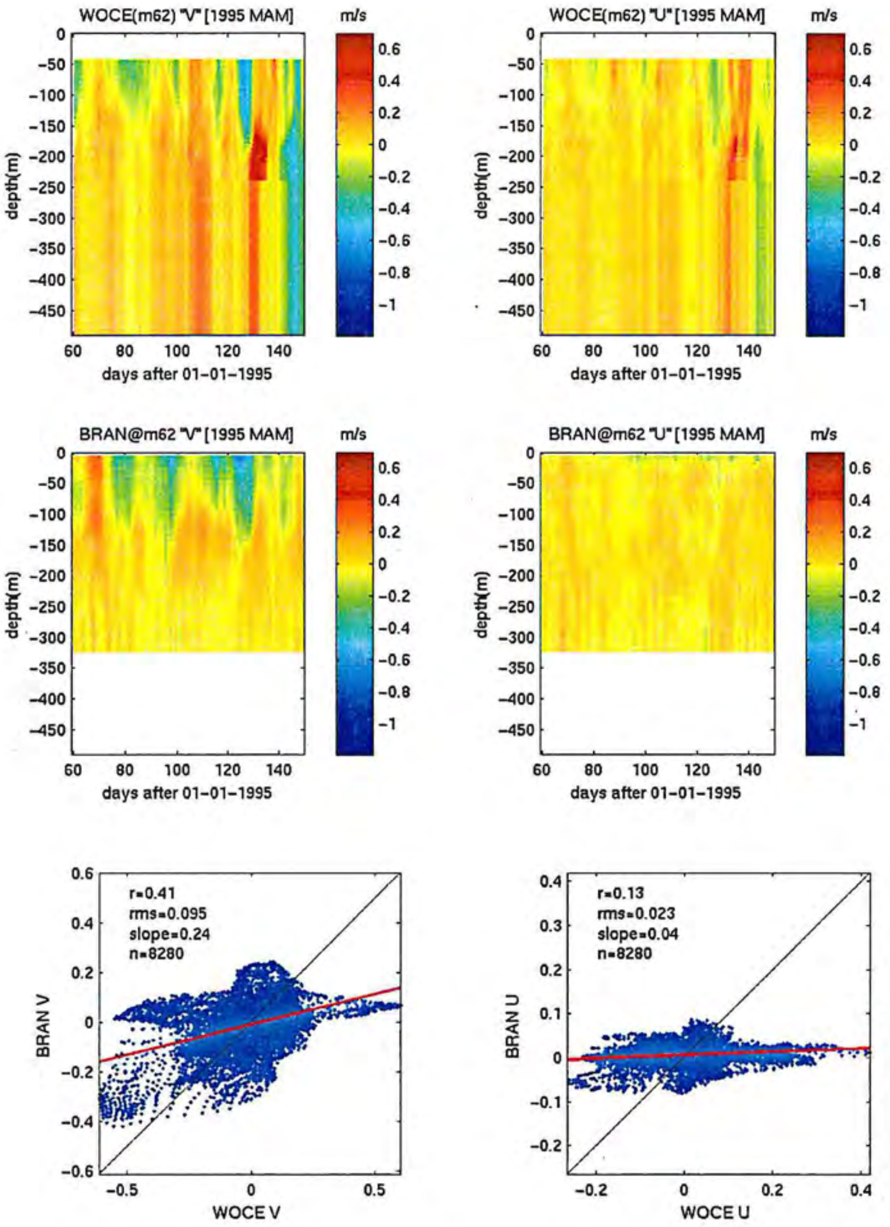
WOCE(m62) "V" [1995 MAM]
WOCE(m62) "U" [1995 MAM]
BRAN@m62 "V" [1995 MAM]
BRAN@m62 "U" [1995 MAM]
m/s
depth(m)
days after 01-01-1995
0
-50
-100
-150
-200
-250
-300
-350
-400
-450
60
80
100
120
140
0.6
0.4
0.2
0
-0.2
-0.4
-0.6
-0.8
-1
r=0.41
rms=0.095
slope=0.24
n=8280
BRAN V
WOCE V
r=0.13
rms=0.023
slope=0.04
n=8280
BRAN U
WOCE U
-0.5
0.5
-0.6
0.3
0.1
-0.1

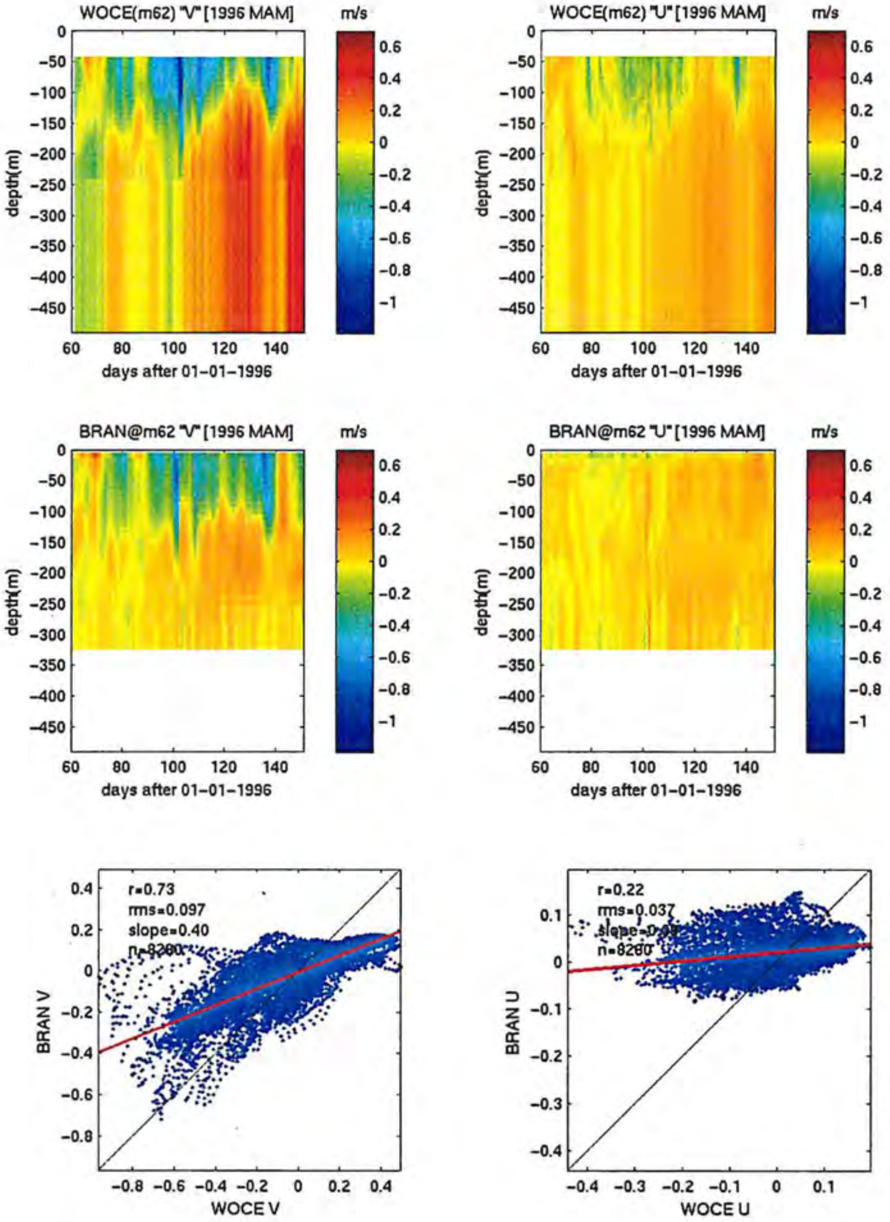

Figure 23. WOCE mooring m62 compared with BRAN

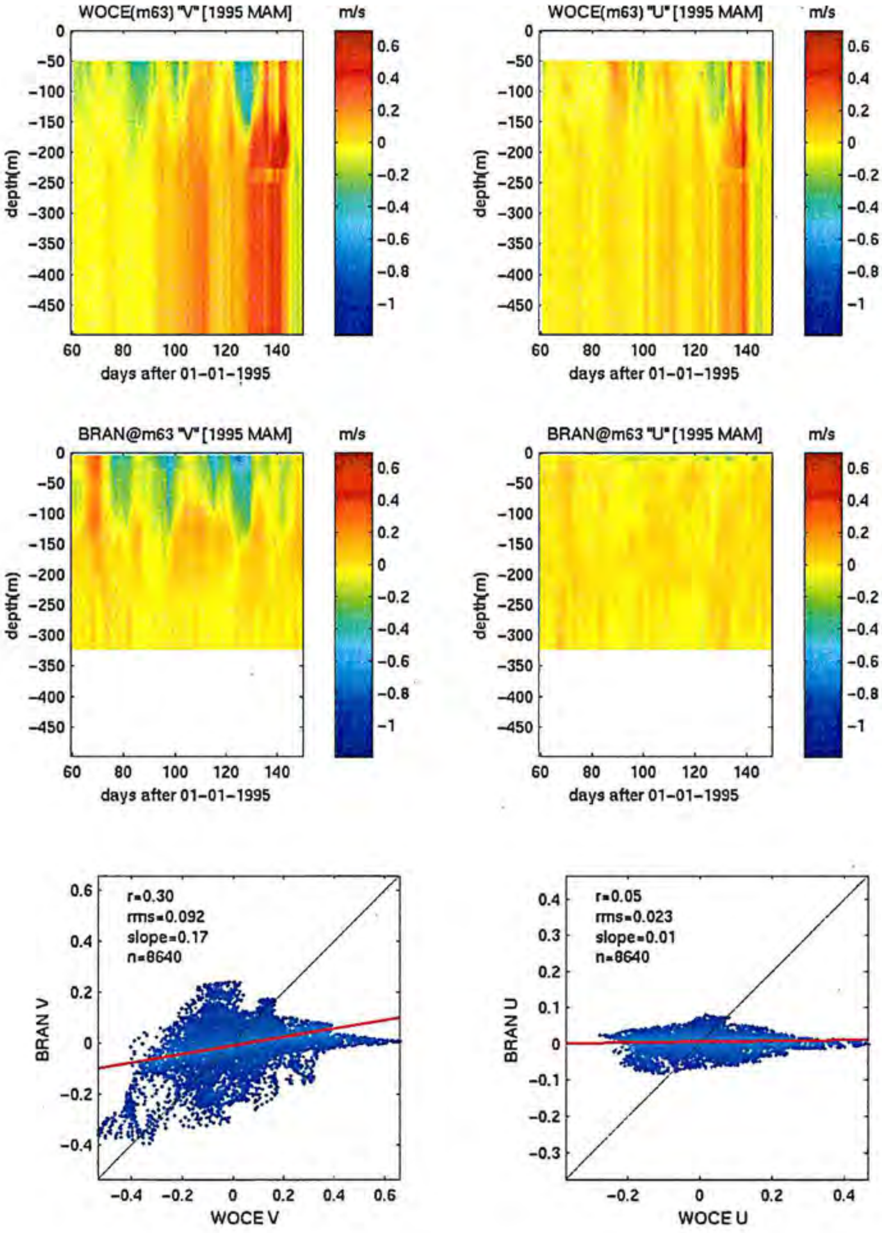

Figure 24. WOCE mooring m63 compared with BRAN

The SRFME current measurements off Two Rocks in 2004-2005 are being used to assess how realistically the output from BRAN simulates the current system along the lower west Western Australian continental shelf (Pearce et al. 2009). Full-column ADCP current meters were deployed for a year (with gaps) at SRFME sites A (20m) and C (100m), while a single-point current meter was used at mid-depth at Site B for part of 2005 (Fandry *et al.* 2006). Temperature was also measured at fixed depths at all 3 sites for varying periods. The original current records were at 15-minute intervals and Fandry *et al.* (2006) derived hourly current components using 5-point moving averages. Because the temporal resolution of the BRAN model is daily in 10 m depth layers, daily vector-averaged currents have been derived from the ADCP measurements in 10 m depth bins for this analysis and monthly current statistics have been calculated. In this note, only the surface layer currents and temperatures at sites A and C are discussed.

At the shallow inshore site A, the BRAN daily alongshore components closely matched the measured currents in the surface layer (Figure 25, upper) -- both the average current velocity and the daily variability were very similar, with a correlation coefficient of 0.61 over the year-long period. Agreement was not as good for the cross-shelf flow (Figure 25, lower) where the observed currents were much lower than the modelled values (especially in the first half of the record); the correlation coefficient was only 0.21. The isolated southward/offshore "spike" in the measured currents (>50 cm/s) in August 2004 was not reproduced by the model. For the deeper layer (not shown here), the alongshore correlation between the model and the observations was 0.68, while the cross-shelf correlation of 0.30 was also higher than that near the surface.

For the 3 successful deployment periods at site C, the BRAN near-surface alongshore currents were generally weaker than the observed flow (Figure 26 upper), particularly during the 2nd deployment in summer 2005 although the few-day variability matched reasonably well. The correlation coefficient was 0.56 (over 107 days). Again, the cross-shelf agreement was poorer (Figure 26 lower) with a correlation of -0.22. Down the water column, the alongshore correlations decreased marginally to 0.49, but the cross-shelf correlations improved substantially to +0.44 near the seabed.

The modelled 10 m temperatures at site A agreed moderately well with the measurements during the summer period, but were too high (by 2 to 3 °C) in winter (Figure 27 upper). Nevertheless, because of the strong seasonal signal, the correlation was overall quite high at 0.84. As would be expected in such shallow water, the correlation at 20 m was similar at 0.85.

Further offshore at site C, the comparison between the modelled and observed temperatures was better than at site A (correlation of 0.91 near the surface – Figure 27 lower), but dropped to 0.74 in the deepest layer).

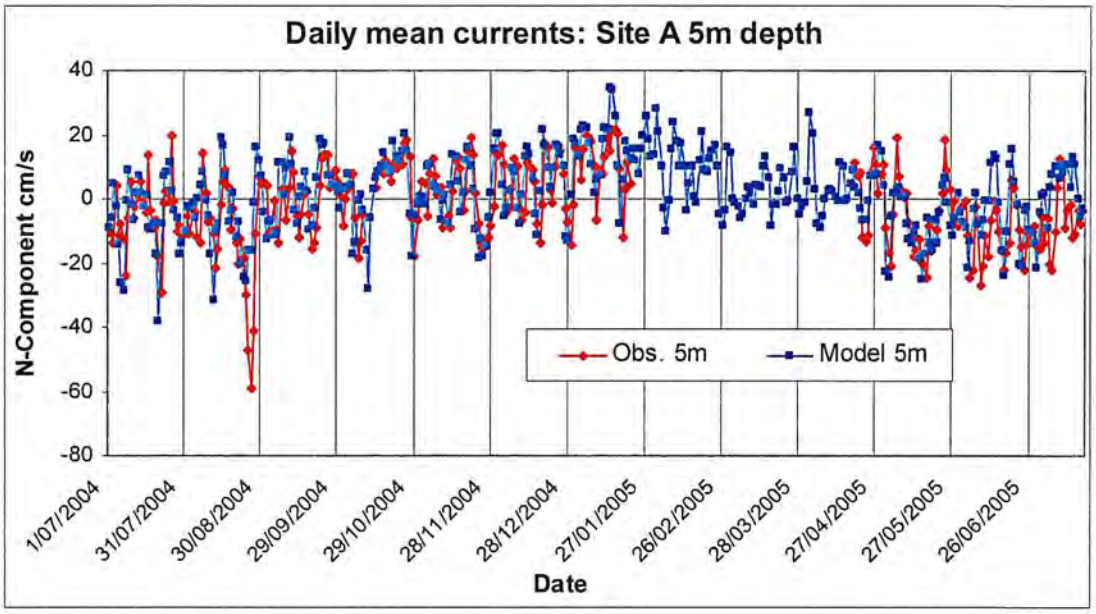

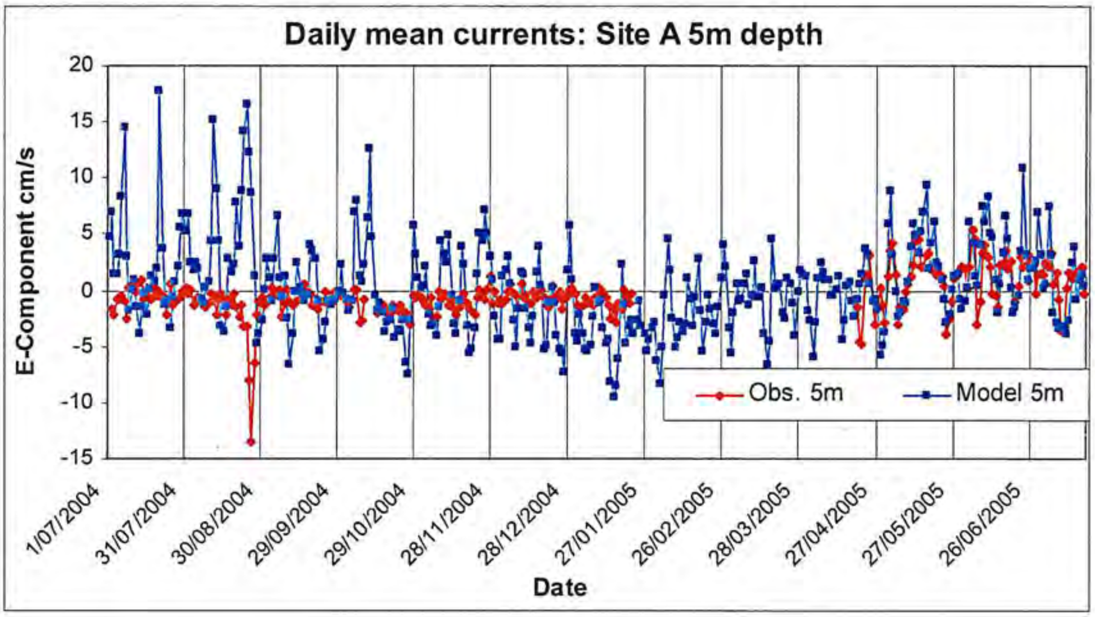

Figure 25. Daily alongshore (upper) and cross-shelf (lower) current components at 5 m depth at Two Rocks Transect site A in 2004/2005; red represents the observed ADCP currents and blue the BRAN simulation.

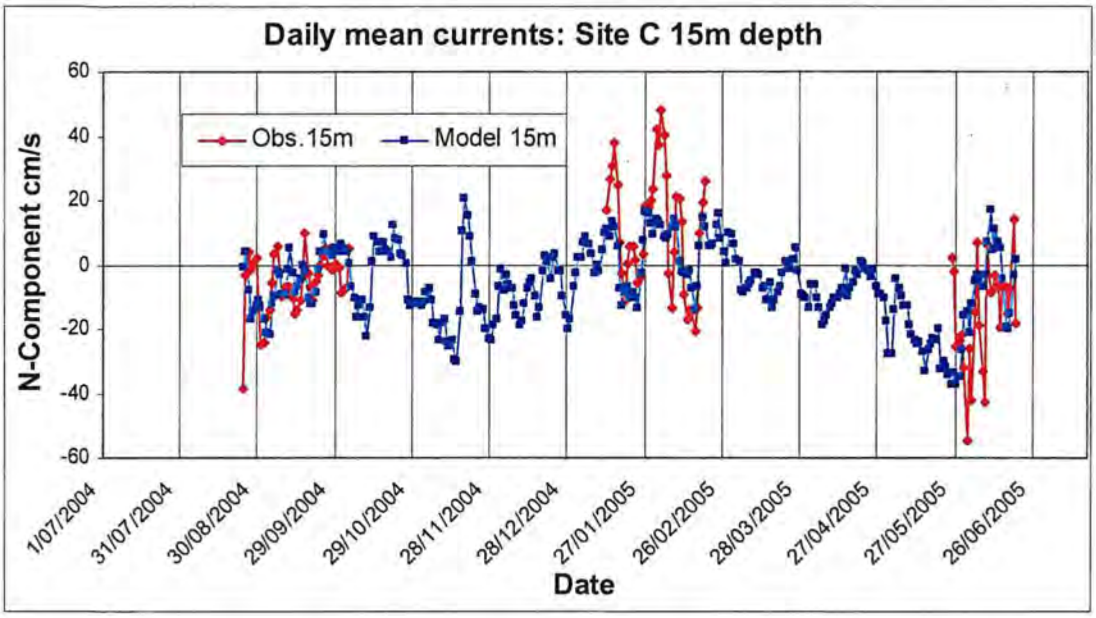

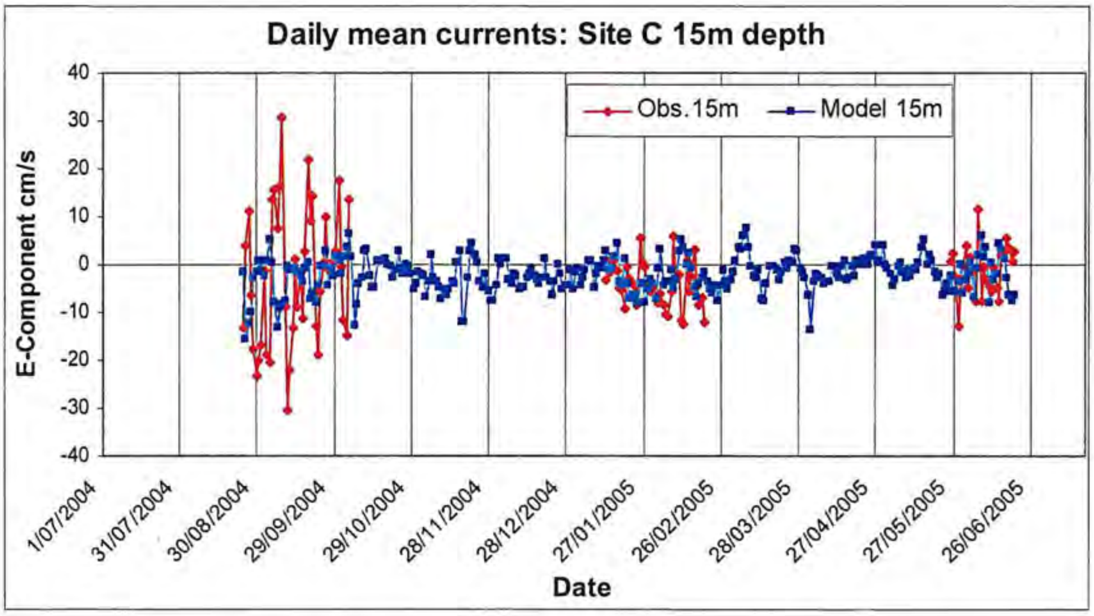

Figure 26. Daily alongshore (upper) and cross-shelf (lower) current components at 15 m depth at Two Rocks Transect site C in 2004/2005; red represents the observed ADCP currents and blue the BRAN simulation.

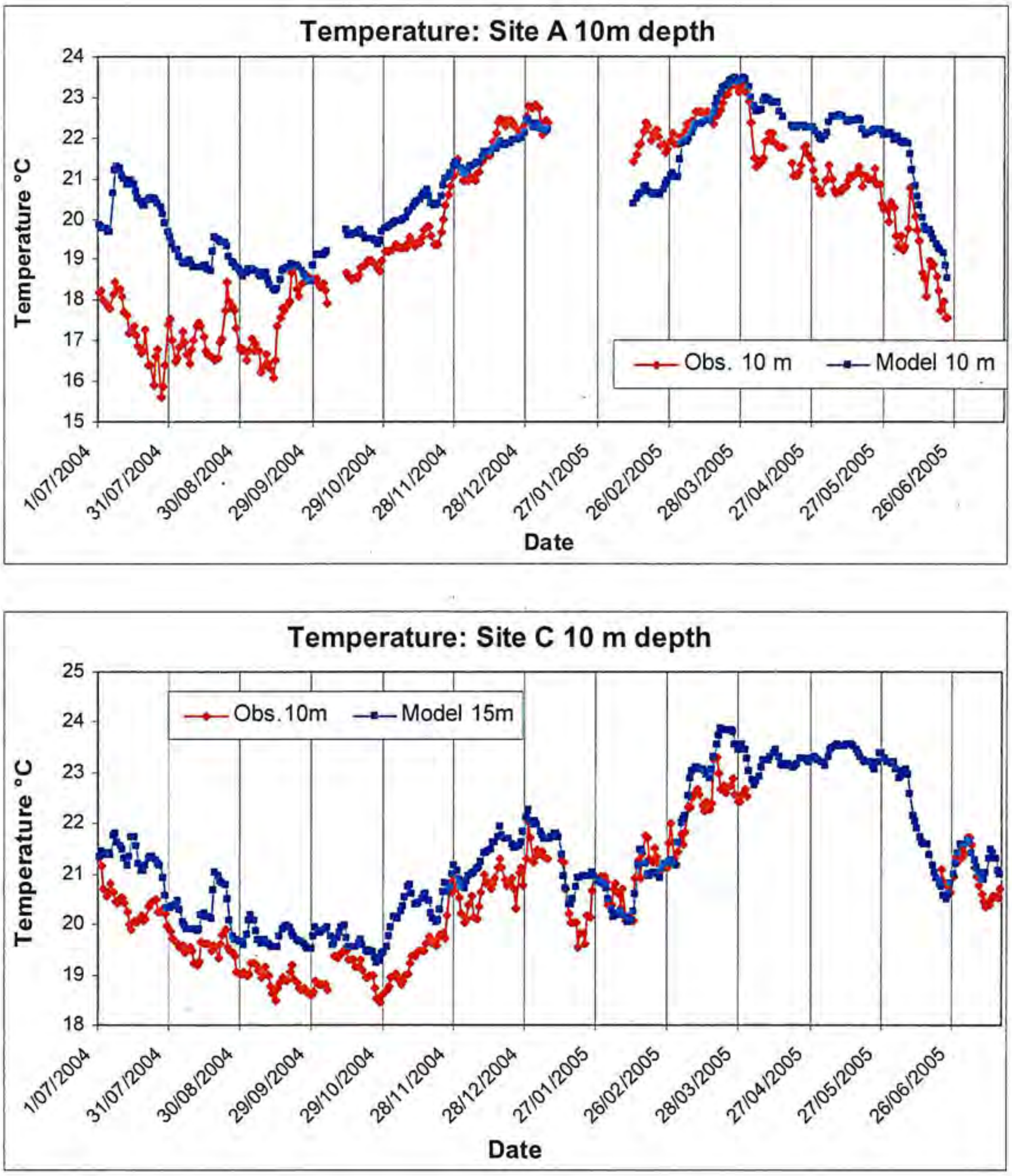

Figure 27. Daily mean near-surface temperatures from observations (red) and BRAN (blue) at site A (upper) and site C (lower) in 2004/2005.

Particle tracking model

A marine-connectivity model, based on a Lagrangian particle tracking method, is being used to investigate the sources and destinations of planktonic larvae in the marine system of the WA region. The advection scheme is 4th-order Runge-Kutta, in which the position of a particle at time step *n+1* in one direction, x_{n+1}, is given by

$$x_{n+1} = x_n + u_{n+1/2}\Delta t + R\left[2r^{-1}K_m\Delta t\right]^{1/2},$$

where x_n is the position of the particle at the previous time step, Δt is the time step, and $u_{n+1/2}$ is velocity at the predicted position at time $n+½\,\Delta t$. The third term on the right-hand side represents sub-grid scale processes unresolved by the BRAN data. It is a model of diffusion by random-walk, with R a random number having zero mean and variance of 1, and K_m the horizontal diffusivity.

The selection of K_m is dependent on the length and time scales of the unresolved processes. This is usually achieved by comparing the statistics of surface drifters and modelled particles. Most studies suggest that the source-sink relationship of particles is not strongly related to the choice of K_m, and commonly used K_m values range from 0 to100 m^2/s (Table 3).

Table 3: Summary of diffusivity used in different particle tracking models.

Hydrodynamic Model Grid Size	*Diffusivity (m^2/s)*	*"Ocean Scape"*	*Reference*
Analytical domain	*10, 100*	*Coastal*	*Parslow and Gabric 1989*
0.5 km x 0.5 km	*10, 50*	*Shelf/Open Ocean*	*Hannah* et al. *1998*
500 m x 500 m	*10*	*Coastal*	*Ommundsen 2002*
0.25° x 0.25°	*100*	*Shelf/Open Ocean*	*Thorpe* et al. *2004*
0.25° x 0.25°	*0*	*Shelf/Open Ocean*	*Murphy* et al. *2004*
1.4 to 47.3 km (non-uniform grid)	*60*	*Shelf*	*Ribergaard* et al. *2004*
3 m to 4 km (non-uniform grid)	*1, 10*	*Coastal*	*Bilgili* et al. *2005*
2.5° x 2.5°	*100*	*Shelf/Coastal*	*Marinone 2006*
3 km to 5 km (curvilinear grid)	*20, 200, 400*	*Shelf/Open Ocean*	*Xue* et al. *2008*
4 km x 4 km	*~33*	*Shelf/Coastal*	*Mitarai* et al. *2008*

Here we show results to test K_m selections in the particle tracking based on BRAN off the WA coast Figure 28 and Figure 29). Particles were released in the surface layer in a 50 by 50 km box about 300 km offshore of the Abrolhos Islands on 1 January and 1 July 2000, and were followed for 30 days. The particles were advected by the horizontal current at the sea-surface. Results show that the particles experience long-distance excursions during the 30 days from their release site, mostly due to the mean current and eddy activity. By comparing the simulations using different K_m, it is confirmed that the random walk plays only a minor role in the spatial dispersion of the particles and the dispersion patterns are not sensitive to the K_m selection in the range of 10 – 50 m^2/s.

We emphasize that it is important to seed a large number of particles for tracking, to properly represent the flow variability and range of possible outcomes, and thus achieve correct statistics.

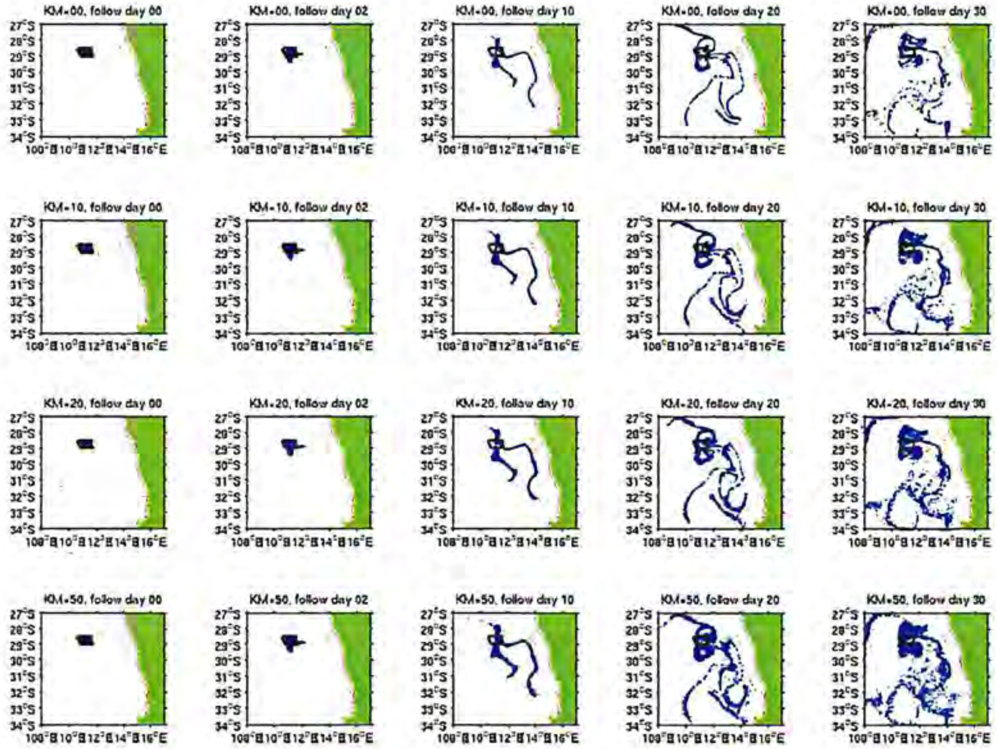

Figure 28. Distribution patterns of 4997 particles released on 01 January 2000. The particles were advected for one month using the BRAN velocity field. Particle locations at 0, 2, 10, 20 and 30 days after release are shown. Each row represents a realization using a different diffusivity coefficient (K_m) of 0, 10, 20 and 50 m^2/s, respectively.

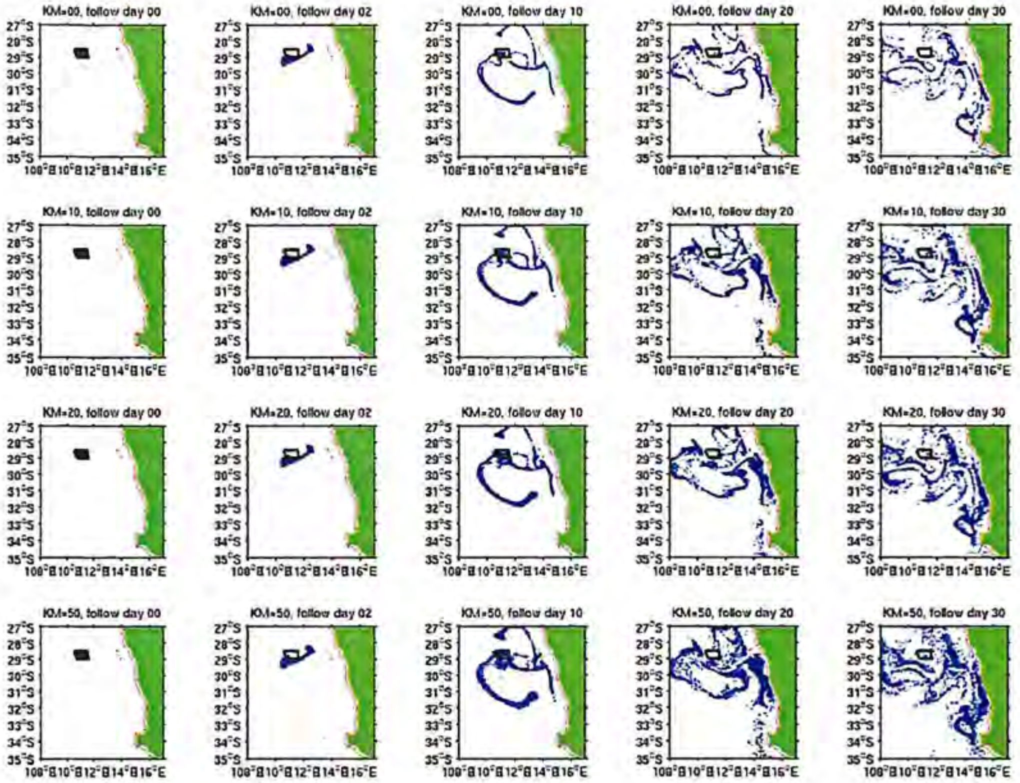

Figure 29. same as Figure 1 except for particles released on 01 July 2000.

A reflection scheme, based on geometric intersections of boundaries, was added to the 2D particle tracking code to prevent particles from stranding onto land. For the 3D case, the scheme is inefficient in its current form and so has not been implemented in the model. For the 2D case the scheme works well except when a particle travels further than the length of a boundary segment. An iterative approach has been tested to correct this situation. Future 2D model runs will use this approach.

Stokes Drift

The Stokes drift velocity in the direction of wave propagation can be calculated as

$$U_s = \frac{(ak)^2 C_P \cosh[2k(z+H)]}{2\sinh^2(kH)}$$

Here, $C_P = \sigma / k$, is the phase speed of the waves, $\sigma^2 = gk\tanh(kH)$, where a is the wave height, k is the wavenumber, z is the depth which is zero at sea surface and positive upward, and H is the water depth. Using the WW2 data, $a = H_S / 2$, and $\sigma = 2\pi / T_S$, where H_S is the significant wave height, and T_S is the significant wave period (Monismith and Fong 2004).

An alternative way to calculate the Stokes Drift is using 2-3% of the wind speed, 20-30 degrees to the left of wind direction in the southern hemisphere (Jenkins 1987).

We tend to use the calculation from wind speed on the shelf when the WW3 may not accurately capture the wave height or direction.

Particles trapped in the surface layer are sensitive to the Stokes Drift. Initial test results based on comparing modelled particle distributions with observed distributions of costal larvae species indicate that the inclusion of a Stokes Drift model more realistically represents the conditions that larvae would experience, e.g. some are "pushed" closer to shore than just the velocity field would allow. To this stage, the results are only preliminary.

Source of the Leeuwin Current waters

Particle tracking is also being used to identify the source and fate of Leeuwin Current waters. Particles were seeded in the upper 200 m along 22 °S, offshore of the Ningaloo Reef, in the region generally regarded as the start of the Leeuwin Current. From there, the particles were back-tracked using the 3-dimensional BRAN velocity field. Over the 10-year period, 1997 – 2006, about 500 particles were released on the 1st of each month, and then back-tracked for 6 months. The back-tracking uses only advection, with no random walk component.

The modelled seasonal variations of the source regions of the LC seem to be consistent with those identified in earlier studies (e.g. Domingues *et al.*, 2007): in spring and summer the LC waters tend to have a western source, while in autumn and winter they seem to have a more northern source (Figure 30). Most of the particles arrive from the region between 15-25 °S off the northwest Australia.

These are preliminary results from ongoing studies that will be extended to include a random walk component, and longer back-tracking

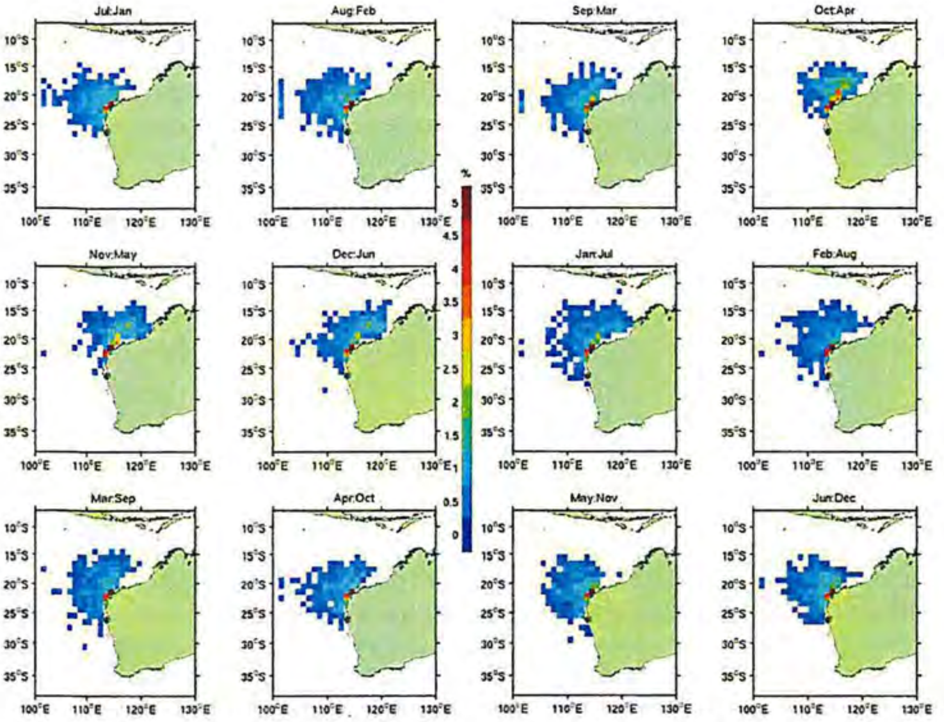

Figure 30. Average distributions of back tracked particles released at 22 °S in the Leeuwin Current for 1997 – 2006. The particles are back tracked for 6 months.

References:

Bilgili, A., Jeffrey A. Proehl, Daniel R. Lynch, Keston W. Smith, M. Robinson Swift (2005), Estuary/ocean exchange and tidal mixing in a Gulf of Maine Estuary: A Lagrangian modeling study, Estuarine, Coastal and Shelf Science 65, 607-624.

Bleck, R., and D. Boudra, 1981: Initial testing of a numerical ncean circulation model using a hybrid (quasi-isopycnic) vertical coordinate. *J. Phys. Oceanogr.*, 11, 755-770.

Bleck, R., and S. Benjamin, 1993: Regional weather prediction with a model combining terrain-following and isentropic coordinates. Part I: Model description. *Mon. Wea. Rev.*, 121, 1770-1785.

Domingues, C.M., M.E. Maltrud, S.E. Wijffels, J.A. Church, M. Tomczak (2007). Simulated Lagrangian pathways between the Leeuwin Current system and the upper-ocean circulation of the southeast Indian Ocean, Deep-Sea Research II, 54, 797-817.

Fandry,C.B., D.Slawinski & L.Pender (2006). Two-Rocks moorings data report. CSIRO Marine and Atmospheric Research Paper 005, January 2006, 26pp.

Hannah, C. G., C. E. Naimie, J. W. Loder and F. E. Werner (1998), Upper-ocean transport mechanisms from the Gulf of Maine to Georges Bank, with implications for Calanus supply, Continental Shelf Research 17, 1887-1911.

Jenkins, A. D. (1987), A Lagrangian model for wind- and wave-induced near-surface currents, Coastal Engineering, 11, 513-526.

Marinone, S. G. (2006), A numerical simulation of the two- and three-dimensional Lagrangian circulation in the northern Gulf of California, Estuarine, Coastal and Shelf Science 68, 93-100.

Mitarai, S., D.A. Siegel, K.B. Winters (2008): A numerical study of stochastic larval settlement in the California Current system, Journal of Marine Systems 69, 295–309.

Monismith S. G. and D. A. Fong (2004): A note on the potential transport of scalars and organisms by surface waves, Limnology and Oceanography 49, 1214-1217.

Murphy, E. J., S.E. Thorpe, J.L. Watkins, R. Hewitt (2004), Modeling the krill transport pathways in the Scotia Sea: spatial and environmental connections generating the seasonal distribution of krill, Deep-Sea Research II 51, 1435–1456.

Ommundsen, A. (2002), Models of cross shelf transport introduced by the Lofoten Maelstrom, Continental Shelf Research 22, 93–113.

Oke, P. R., G. B. Brassington, D. A. Griffin and A. Schiller, 2008: The Bluelink Ocean Data Assimilation System (BODAS). *Ocean Modelling,* 20, 46-70, doi:10.1016/j.ocemod.2007.11.002.

Parslow J. S. and A. J. Gabric (1989), Advection, Dispersal and Plankton Patchiness on the Great Barrier Reef, Aust. J. Mar. Freshwater Res. 40, 403-19.
Pearce, A.F., M.Feng, D.Slawinski & B.Hutchins (2009, in prep). Modelling the transport of tropical fish larvae in the Leeuwin Current. To be submitted to Continental Shelf Research.

Ribergaard, M., Søren Anker Pedersen, Bjørn Adlandsvik, Nicolai Kliem (2004), Modelling the ocean circulation on the West Greenland shelf with special emphasis on northern shrimp recruitment, Continental Shelf Research 24, 1505–1519.

Schiller, A., P. R. Oke, G. B. Brassington, M. Entel, R. Fiedler, D. A. Griffin, and J. Mansbridge, 2008: Eddy-resolving ocean circulation in the Asian-Australian region inferred from an ocean reanalysis effort. *Progress in Oceanography,* doi:10.1016/j.pocean.2008.01.003.

Thorpe, S. E., Karen J. Heywood, David P. Stevens, Mark A. Brandon (2004), Tracking passive drifters in a high resolution ocean model: implications for interannual variability of larval krill transport to South Georgia, Deep-Sea Research I 51, 909–920.

Tolman, H. L., B. Balasubramaniyan, L. D. Burroughs, D. V. Chalikov, Y. Y. Chao, H. S. Chen, and V. M. Gerald (2002), Development and implementation of wind generated ocean surface wave models at NCEP. *Weather and Forecasting*, **17**, 311-333.

Xue, H., Lewis Incze, Danya Xu, Nicholas Wolff, Neal Pettigrew (2008), Connectivity of lobster populations in the coastal Gulf of Maine Part I: Circulation and larval transport potential, Ecological Modelling 210, 193-211.

Milestone 1.1.8: Evaluation of lagoon scale model runs

Original Forecast Finish Date: 30/06/09

Revised Forecast Finish Date: 30/06/09

This section updated from previous Biannual Report

Summary of Activities Undertaken, Outputs Produced:

The Regional Ocean Modelling System (ROMS) has been configured for Marmion Lagoon. ROMS is a free-surface, terrain-following, primitive-equation ocean model widely used by the scientific community for a diverse range of applications. It includes hydrodynamic, wave, sediment, and biogeochemical sub-models, very suitable for multidisciplinary studies in dynamic coastal environments like Marmion Lagoon, which is subject to forcing by tide, wind and waves.

The model of Marmion Lagoon has a grid size of 60x120 with horizontal resolution of about 100m and 8 vertical levels. The model is driven by tides at the open boundaries and momentum, heat and fresh water fluxes at the sea surface. Tidal elevation at the open boundaries consists of 8 major tidal constituents, K1, O1, P1, Q1, M2, S2, N2 and K2, whose harmonic constants were derived from the Oregon State University global inverse tidal model TPXO6. Surface fluxes of momentum, heat and fresh water were calculated internally in ROMS using standard bulk parameterizations of the ocean-atmosphere boundary layer, and modelled sea-surface temperature and meteorological observations. Cloud correction was applied to the calculations of both shortwave and long-wave radiation fluxes. The required meteorological data, including wind, relative humidity, air temperature, air pressure, precipitation and cloud fraction, were collected from the measurements at stations of Ocean Reef, Swanbourne, Rottnest Island and Perth Airport.

The 3D hydrodynamic simulations were conducted for two periods, from 1 January to 1 April 2008 and from 1 July to 1 September 2007, which correspond to the third and first deployments from the Lagoonal wave and current measurement program (see Milestone 1.1.5), respectively. During the third deployment (summer), waves were relatively low and wind forcing associated with the sea-breeze cycle was dominant. During the first deployment (winter), the observed currents are likely forced by the combined effects of wind and waves, though wave forcing is not included in the model simulations. The model solutions were compared with measurements taken at a number of stations, AQ1, AQ2, ADV2, ADV3, ADV4, RDIN and RDIS, described under milestone 1.1.5. Our model results have confirmed the importance of wave forcing in Marmion Lagoon.

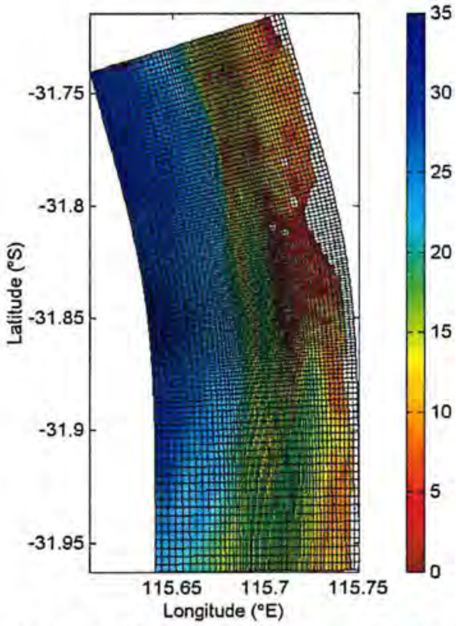

Figure 31. The model domain for the Marmion Lagoon and the horizontal curvilinear coordinate system.

The model reproduced tidal elevation reasonably well. An example of model-data comparison of sea-level is shown in Figure 32. The model-predicted sea-level has root-mean-square error 6.1 cm and correlation coefficient 0.95 for the deployment #3 simulation, and 3.5 cm and 0.98 for the deployment #1 simulation.

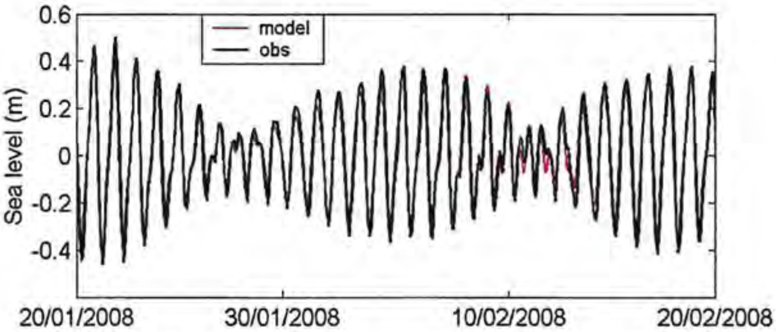

Figure 32. Time series comparison of the model predicted and observed sea-level elevation at ADV2 site in the deployment #3 period.

It has been found in previous observations at Two Rocks that longshore current near the coast is about 2.5%~3% of the longshore wind speed. Our model results are consistent with this relationship. Figure 33 demonstrates a strong correlation between modelled surface longshore current (averaged over the stations mentioned above) and observed longshore wind component. Correlation coefficients are 0.92 and 0.86 for deployment #3 and #1, respectively. Note the strong sea-breeze cycle during the first half of deployment #3.

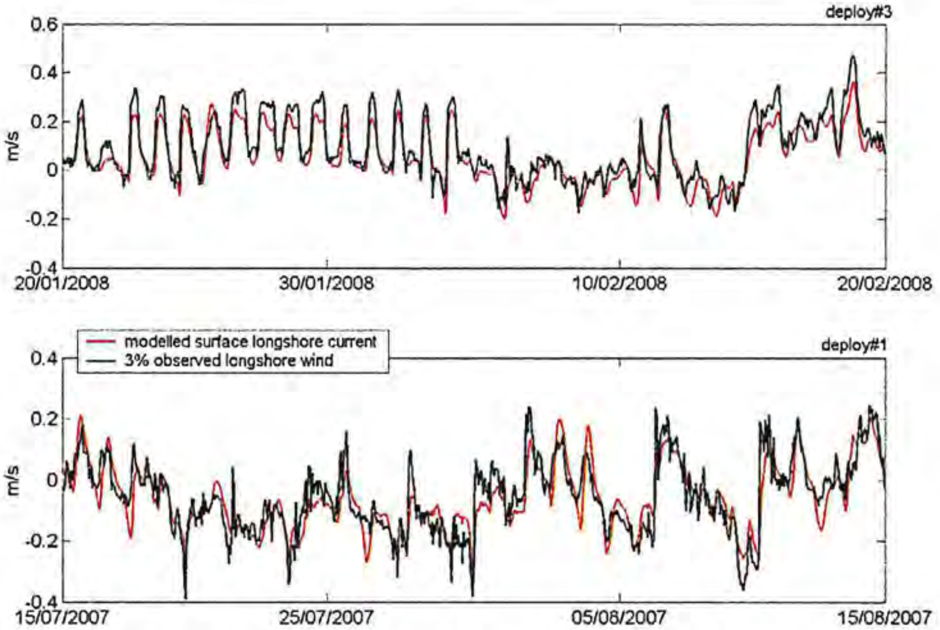

Figure 33. Modelled longshore surface current versus 3% of observed longshore wind speed in deployment #3 (upper panel) and deployment #1 (lower panel).

Deployment 3

Model-data comparison of depth-averaged currents at sites AQ1 and AQ2, and near-bottom currents at sites ADV1, ADV2, ADV3 and ADV4 are shown in Figure 34 and Figure 35, respectively. In general the modelled alongshore currents show better agreement with the observations than the cross-shore currents. This is also evident in the statistics shown in Table 2. The root-mean-square error between modelled and observed alongshore current is smaller, and the correlation higher, than for the corresponding cross-shore values.

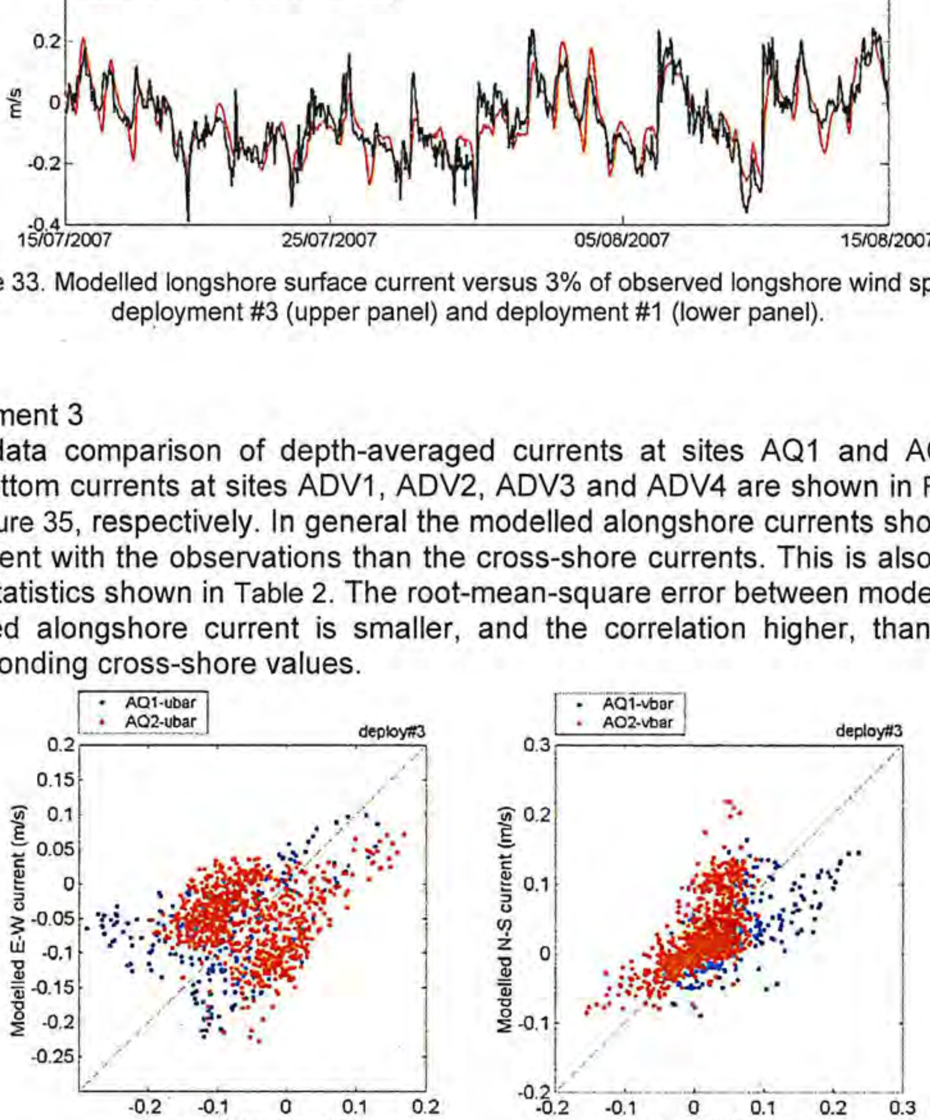

Figure 34. Observed depth-averaged currents versus model predictions at sites of AQ1 and AQ2 in deployment #3. Left panel is E-W velocity component and right panel N-S component.

Surprisingly there are very strong near-bottom onshore currents, up to 0.25 m/s, observed at ADV3 site (see Figure 35). The model not only failed to capture the strong current but also produced an offshore flow.

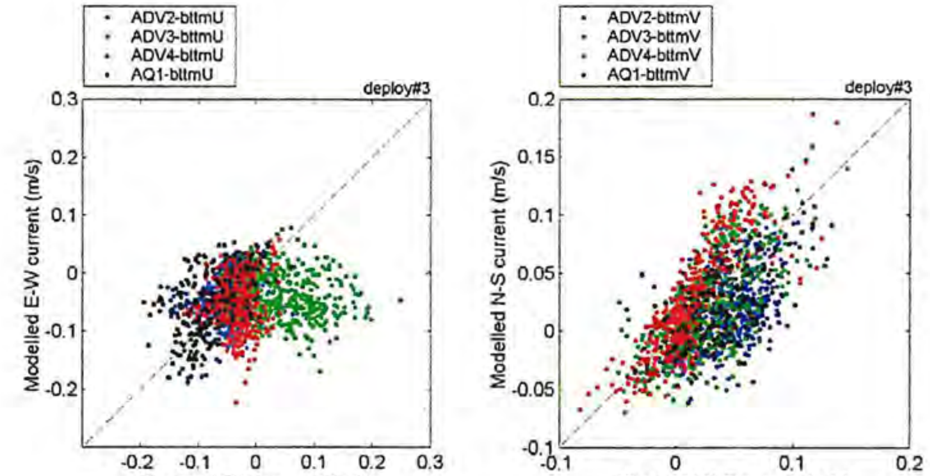

Figure 35. Observed near-bottom currents versus model predictions at sites of AQ1, ADV2, ADV3 and ADV4 in deployment #3. Left panel is E-W velocity component and right panel N-S component.

Figure 36 shows comparison of near-surface currents at site AQ2. The agreement between modelled and observed onshore current is slightly better than alongshore. The model over-predicted the alongshore currents and the reason is not clear yet.

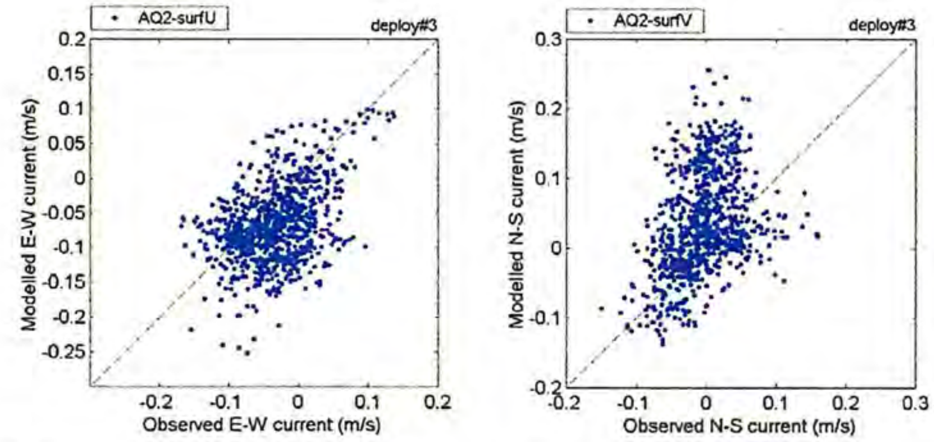

Figure 36. Observed near-surface currents versus model predictions at AQ2 in deployment #3. Left panel is E-W velocity component and right panel N-S component.

Table 4. Statistical analysis of the model predicted currents during the period of deployment #3. rms denotes the root-mean-square error in cm/s and cor the correlation coefficient.

deploy#3	depth-averaged		bottom				surface
	AQ1	AQ2	ADV2	ADV3	ADV4	AQ1	AQ2
rms-u	8.8	7.8	4.5	10.6	5.1	5.9	6.5
rms-v	5.7	4.3	3.8	3.0	2.9	3.5	7.8
cor-u	0.43	0.06	0.24	-0.12	0.16	0.55	0.42
cor-v	0.70	0.66	0.52	0.69	0.84	0.62	0.36

Deployment 1

After the model was calibrated for the period with weak wave forcing, we conducted a simulation for deployment #1, when measured wave forcing was the strongest, to assess the importance of wave forcing in Marmion Lagoon.

Good agreement is found only at AQ1 and RDIS sites (see Figure 37). The correlation coefficient between modelled and observed alongshore current is high (see **Error! Reference source not found.**) and comparable to the simulation in deployment #3 (cf, **Error! Reference source not found.**).

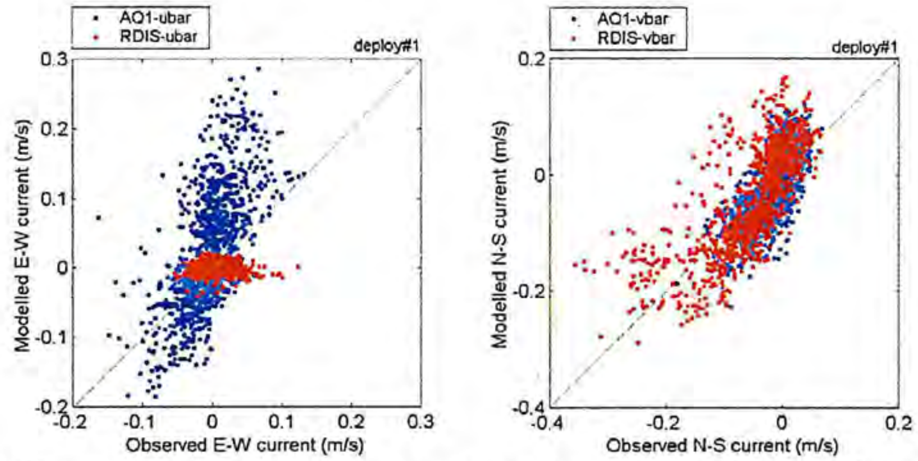

Figure 37. Observed depth-averaged currents versus model predictions at sites of AQ1 and RDIS in deployment #1. Left panel is E-W velocity component and right panel N-S component.

Model-data comparison in bottom currents at the ADV sites is slightly poorer (see Figure 38), compared to the previous simulation in deployment #3.

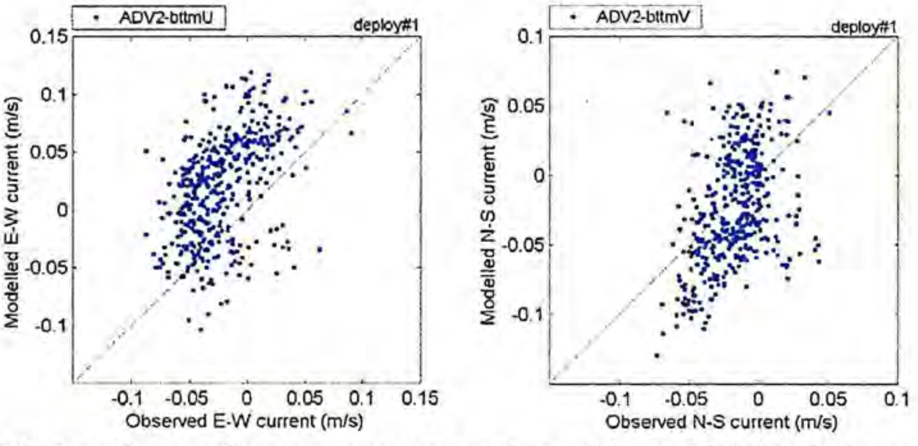

Figure 38. Observed near-bottom currents versus model predictions at ADV2 in deployment #1. Left panel is E-W velocity component and right panel N-S component.

The model-data comparison at sites AQ2 and RDIN are quite poor. As shown in Figure 39, strong offshore currents close to 0.6 m/s were observed at AQ2 but are completely missing in the model solution. For alongshore current, there are many periods when northward currents were observed at AQ2 and RDIN while the model predicts southward currents. Correlation coefficients at AQ2 and RDIN are much lower than that at AQ1 and RDIS (see Table 3).

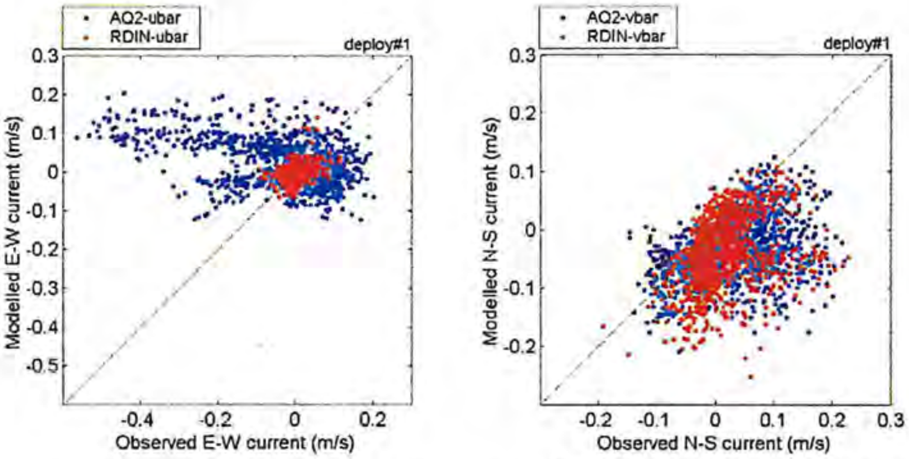

Figure 39. Observed depth-averaged currents versus model predictions at sites of AQ2 and RDIN in deployment #1. Left panel is E-W velocity component and right panel N-S component.

Table 5. Statistic analysis of the model predicted currents during the period of deployment #1. rms denotes the root-mean-square error in cm/s and cor the correlation coefficient.

deploy#1	depth-averaged				bottom
	AQ1	AQ2	RDIS	RDIN	ADV2
rms-u	7.5	19.3	2.2	2.7	5.8
rms-v	4.3	10.0	5.9	8.5	3.6
cor-u	0.64	-0.43	-0.09	0.30	0.47
cor-v	0.71	0.34	0.74	0.34	0.45

The difference between modelled and observed currents at selected sites is plotted against the observed significant wave height in Figure 40, where the difference is between onshore currents (in E-W direction) at AQ1 and AQ2 and alongshore currents (in N-S direction) at RDIS and RDIN. The selection of alongshore current at RDIS and RDIN is because these two sites are close to the shoreline and the flows are mainly in the alongshore direction. When the significant wave height exceeds about 1.5m the difference between model and data at sites AQ2 and RDIN appears to be correlated with the wave height. There is no obvious correlation at AQ1 and RDIS.

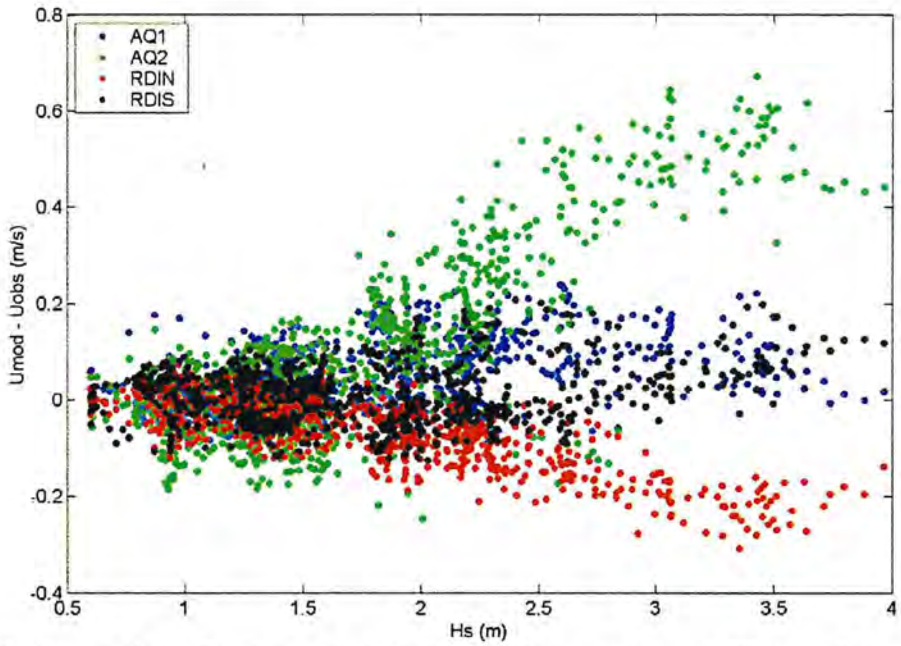

Figure 40. Observed significant wave-height at MS2 site versus current difference between model predictions and observations in deployment #1 at sites of AQ1, AQ2, RDIS and RDIN. The difference is between onshore currents at AQ1 and AQ2 and alongshore currents at RDIS and RDIN.

Wave-forcing of mean currents occurs through depth-dependent wave breaking, so necessarily requires the waves to be big enough to break over the offshore reefs. A general rule-of-thumb is that depth-induced wave breaking occurs when the ratio of wave height to depth is equal to 0.8. Figure 40 suggests this occurs for wave heights greater than about 1.5m. Wave-forcing has recently been added to ROMS and the following section describes its implementation for the Marmion Lagoon.

Coupled ROMS-SWAN model and its simulation in deployment 1

To examine the wave-driven circulation in the Marmion, a coupled hydrodynamic and wave model is used to simulate the circulation in the first deployment period, during which the measured wave height was the biggest among the four deployments.

ROMS has been recently coupled with the wave model Simulating Waves in the Nearshore (SWAN). We have implemented and configured the coupled ROMS-SWAN model for the Marmion Lagoon. To better represent the complex topography in the Marmion domain, we have doubled the grid size of previous model in both directions so that the model horizontal resolutions are refined to about 50m in the reef region. Now the model has a grid size of 120x240 with 8 vertical levels. As in the previous numerical studies, the hydrodynamic model (ROMS) is driven by tides at the open boundaries and momentum, heat and fresh water fluxes at the sea surface. Tidal forcing consists of 8 major tidal constituents, K1, O1, P1, Q1, M2, S2, N2 and K2. Surface fluxes of momentum, heat and fresh water are calculated internally in ROMS using standard bulk parameterizations of ocean-atmosphere boundary layer, and modelled sea-surface temperature and meteorological observations including wind, relative humidity, air temperature, air pressure, precipitation and cloud fraction.

SWAN is a wave-averaged model that solves transport equations for wave action density, and accounts for shoaling, refraction, diffraction, partial transmission and reflection. SWAN shares the same grid with ROMS. The wave parameters at the offshore open boundary are from the wave measurements at the site AWAC. The offshore site MS2 is much closer to the open boundary than AWAC; however, the observations at MS2 did not yield reliable parameters of wave period and direction. Meanwhile, significant wave heights are quite similar at MS2 and AWAC, therefore the wave parameters measured at AWAC are used as the boundary-forcing in SWAN.

When ROMS is coupled with SWAN, new terms, called radiation-stress due to the waves, are added to the momentum equations. Radiation-stress is calculated from wave properties such as wave length, energy, and direction etc. Meanwhile, SWAN takes account of currents and sea level changes provided by ROMS, so that currents (ROMS) and waves (SWAN) are two-way coupled. ROMS and SWAN run concurrently and they exchange information in every 10 minutes.

The wave-driven circulation in the Marmion lagoon can be illustrated in an idealised test with an offshore wave having constant significant height 3m, and without tidal and surface wind forcing. As shown in Figure 41, the circulation features onshore flows over the reefs and offshore flows in the deep channel (such as at AQ2 site) between the reefs. Onshore flows are driven by the onshore radiation stress gradient as a result of incident wave-breaking occurring over the shallow reefs. Wave-breaking also results in wave set-up inside the lagoon (see the colour in Figure 41), which produces return flow through the gap at AQ2 between the reefs. In addition, wave set-up inside the lagoon drives the northward (at the site RDIN) and southward (at the site RDIS) flows at both ends of the lagoon. The observations in the first deployment bear the circulation features in this idealised test.

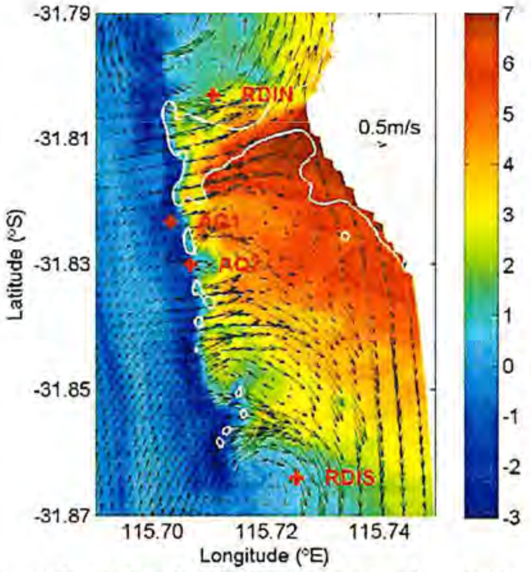

Figure 41. The wave-driven circulation (vector) and wave set-up (colour, in cm) produced in a coupled ROMS-SWAN model with the only forcing of constant offshore wave height. The white lines are 4m isobars and sites AQ1, AQ2, RDIN and RDIS are marked by plus signs.

The results from the coupled 3D ROMS and 2D SWAN model are presented and discussed in the following. To help understand the wave influences on the circulation, the results from a no-coupling model (ROMS is not coupled with SWAN and thus wave effect is not considered in ROMS) are also included in the model-data comparison. Note the no-coupling model has the same high resolution as the coupled model, and so it is different from the coarser-resolution model described above.

Time series of wave-driven currents

We first examine the wave-driven currents by looking the time series of wave and wind forcing, observed and modelled velocity at the site AQ2. As shown in Figure 42, there were four wave events (wave height exceeding 1.5m) from 18 July to 1 August 2007, during which offshore currents and northward longshore currents were observed at AQ2, while wind blew in the onshore and southward longshore directions. The no-coupling model generates wind-driven currents in the wind direction and could not reproduce the observed currents at AQ2 against the wind direction. When wave effects are considered, the coupled model reproduces the currents at AQ2 reasonably well. As explained in the idealised test, the wave set-up in the lagoon (see Figure 41) drives the strong offshore flows at AQ2. The northward flow at AQ2 is expected from theoretical consideration of wave-driven flow over shallow reefs (Symonds et al., 1995).

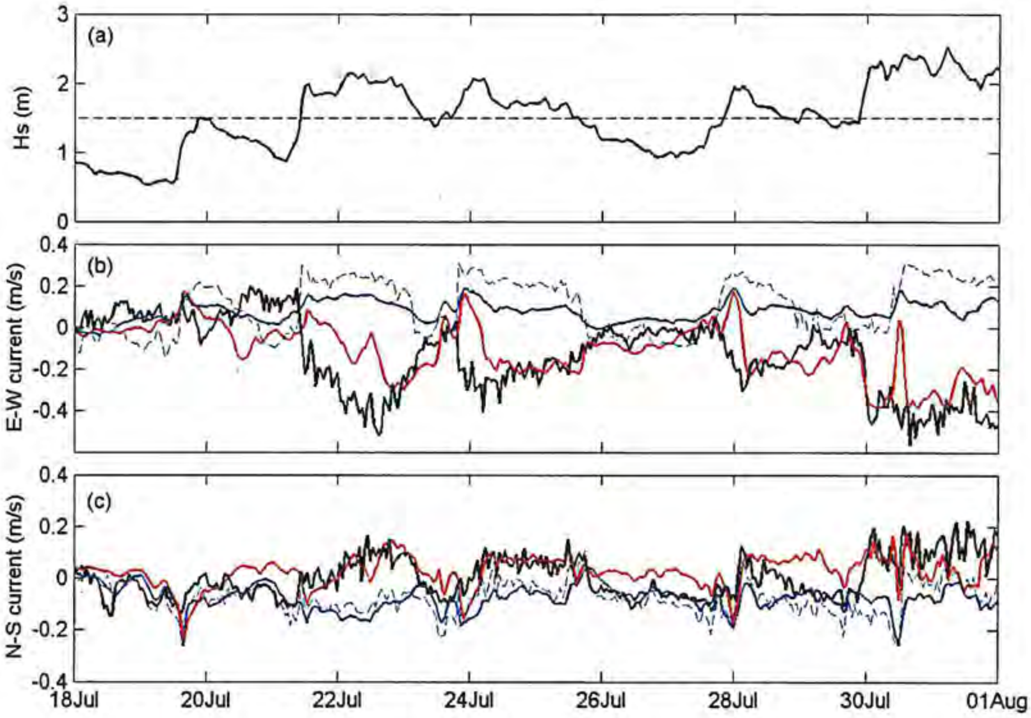

Figure 42. Time series of significant wave height at MS2 (a) and depth-averaged eastward (b) and northward (c) velocity components at AQ2. In (b) and (c), black, red and blue lines denote currents from the observation, the coupled ROMS-SWAN model and no-coupling model, respectively, while the dashed blue line is 2% of wind speed.

Wave height

Model-data comparison of significant wave height is shown in Figure 43. Although SWAN overestimates the wave height at the offshore site MS2, the model produces more accurate wave height at the inshore site MS1 and the site AWAC at the offshore edge of the reefs. The correlation coefficient is no less than 0.90 at all three sites (see Table 6). As indicated in Figure 43, there is not much attenuation as waves propagate from offshore to the offshore edge of the reefs. However from the reefs to inshore, wave height is significantly reduced by wave-breaking and bottom dissipation. A snapshot of wave field is shown in Figure 44.

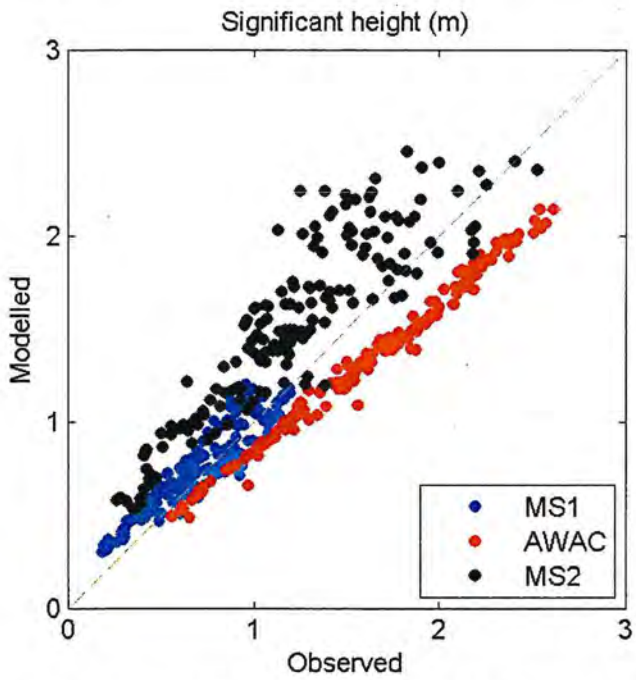

Figure 43. Observed significant wave heights versus the model predictions at MS1 (inshore), AWAC (offshore edge of the reefs) and MS2 (offshore).

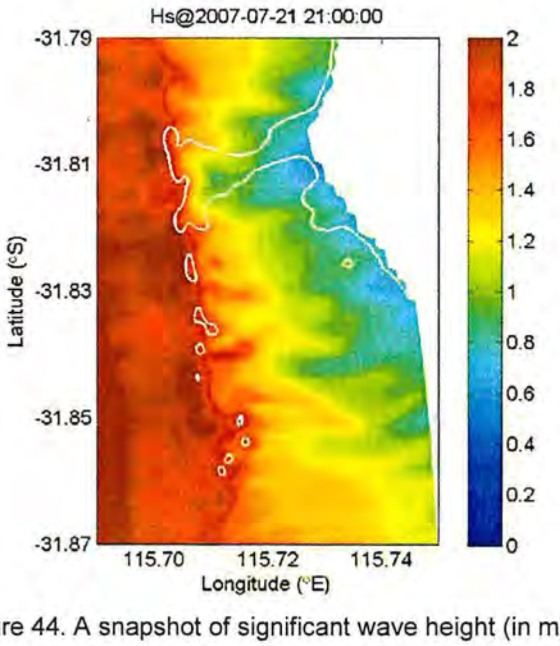

Figure 44. A snapshot of significant wave height (in m).

Table 6. Statistical analysis of the wave model predicted significant wave height. rms denotes the root-mean-square error and corr the correlation coefficient.

	MS2	AWAC	MS1
rms (m)	0.38	0.30	0.11
corr	0.90	0.99	0.92

Currents

Depth-averaged velocities are compared at four sites AQ1, AQ2, RDIN and RDIS (see Figure 41 for their location).

The currents measured at the site AQ1 were usually less than 0.1 m/s (see Figure 45). However, the model predicts much stronger currents no matter whether wave is considered in ROMS. The reason for the mismatch is not clear.

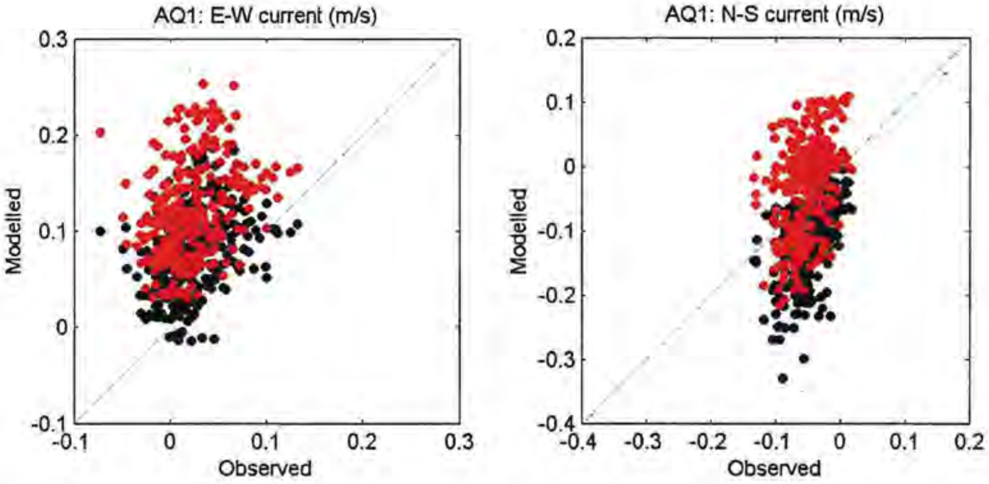

Figure 45. Observed depth-averaged currents versus the model predictions (red for the coupled model and black no-coupling model) at AQ1. Left panel is E-W velocity component and right panel N-S component.

We have shown in Figure 42 that the inclusion of wave effects in ROMS improves the model performance significantly at the site AQ2. As shown in Figure 46, strong offshore currents (up to -0.6 m/s) were observed at AQ2 in the big-wave events, but they are completely absent in the no-coupling model. In the coupled ROMS-SWAN model, the strong offshore currents are captured reasonably well. Meanwhile, the coupled model reproduces the observed northward longshore currents, that are against the longshore wind and absent in the no-coupling model.

The improved performance in the coupled model is clear in the statistical analysis. As seen in Table 7, the currents in the no-coupling model do not have positive correlation with the observations. In the coupled model, the correlation coefficients have increased to 0.55 and 0.40 for onshore and longshore currents, respectively, and root-mean-square errors are much reduced.

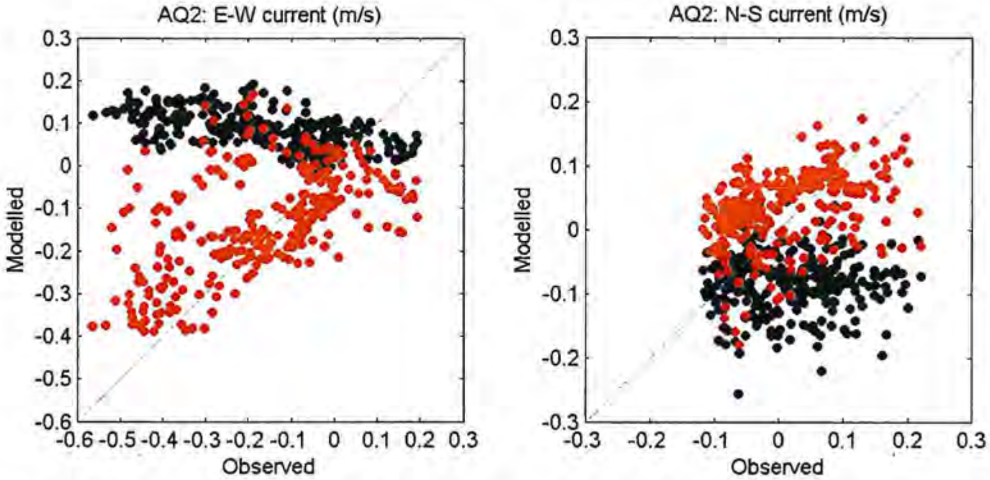

Figure 46. Observed depth-averaged currents versus the model predictions (red for the coupled model and black no-coupling model) at AQ2. Left panel is E-W velocity component and right panel N-S component

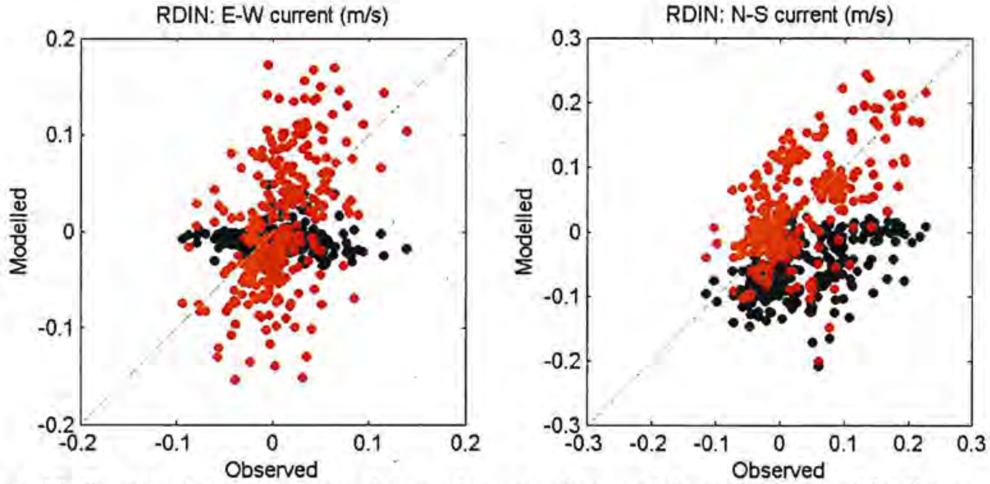

Figure 47. Observed depth-averaged currents versus the model predictions (red for the coupled model and black no-coupling model) at RDIN. Left panel is E-W velocity component and right panel N-S component

The velocities at RDIN and RDIS are dominated by longshore components since they are close to the coastline. At RDIN, the no-coupling model produces mainly southward (negative) wind-driven longshore currents (see black dots in right panel of Figure 47), which are in the opposite direction to the observed longshore current. As explained in the above idealised test, the wave set-up in the lagoon due to the depth-induced wave breaking in the reefs provides the driving force for the northward longshore current at RDIN. The longshore currents at RDIN, against the surface wind, have been captured in the wave-current coupled model. For the onshore velocity component, the coupled model has a much better correlation with the observations than the no-coupling model (see Table 7).

At RDIS on the southern end of lagoon, the observed longshore current is in the wind direction, that is, southward (negative). The southward longshore currents at RDIS are captured in the no-coupling model but obviously underestimated (see Figure 48). As discussed in the idealised test, the wave set-up in the lagoon due to wave-breaking on the reefs also produces a southward current at RDIS, that enhances the wind-driven southward flow. Thus the longshore current at RDIS from the coupled model is in better agreement with the observations than that from the no-coupling model, and it has smaller root-mean-square error and higher correlation coefficient (see Table 7). Similarly to the site RDIN, the onshore current at RDIS predicted in the coupled model is much better correlated with the observations than in the no-coupling model although its root-mean-square error is a little bigger (see Table 7).

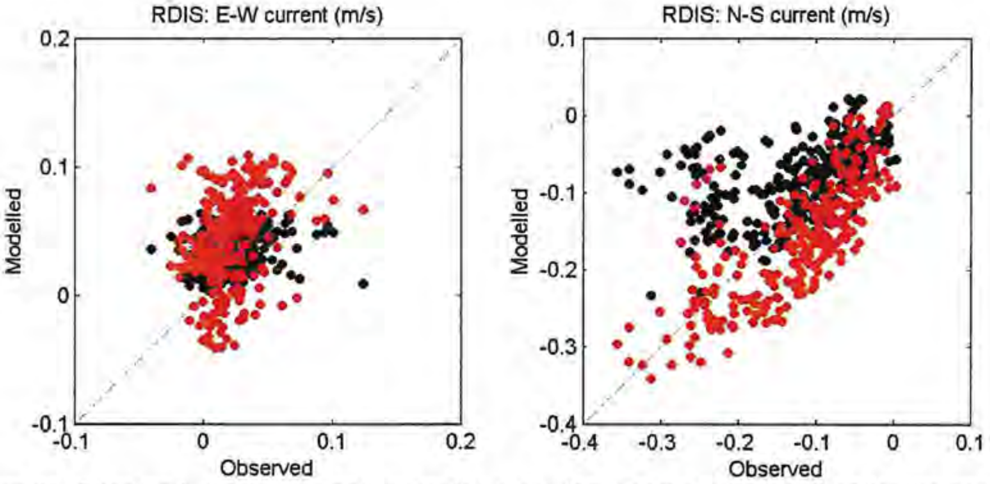

Figure 48. Observed depth-averaged currents versus the model predictions (red for the coupled model and black no-coupling model) at RDIS. Left panel is E-W velocity component and right panel N-S component

Table 7. Statistical analysis of the model predicted depth-averaged currents. u-rms and u-cor (v-rms and v-cor) denote the root-mean-square error in cm/s and correlation coefficient, respectively, of E-W (N-S) velocity component.

	AQ1	AQ2	RDIN	RDIS
u-rms	11.1 (7.0)	15.3 (32.5)	6.0 (4.1)	4.3 (2.7)
u-cor	0.34 (0.36)	0.55 (-0.58)	0.46 (-0.08)	0.36 (0.28)
v-rms	7.1 (8.2)	8.0 (13.0)	6.8 (10.4)	6.2 (7.9)
v-cor	0.41 (0.48)	0.40 (-0.03)	0.58 (0.48)	0.77 (0.50)

The coupled ROMS-SWAN model is capable of capturing the wave-driven circulation in the observations. To improve the quantitative agreement between the model and observations, even higher horizontal resolution of 20~30m is warranted to resolve the complex bathymetry in the reef region.

Milestone 1.1.9: Data report on lagoon wave and current measurements

Original Forecast Finish Date: 30/06/09

Revised Forecast Finish Date: 30/06/09

This section updated from previous Biannual Report

Summary of Activities Undertaken, Outputs Produced:

Between July 2007 and May 2008 we completed four periods of intensive measurement of waves, currents and water properties across the Marmion lagoon. During the course of the measurement program, we completed over 40 mooring deployments and recoveries and 10 CTD and nutrient surveys (about 300 stations). The locations and site names of the instrument array, and the actual deployment times, instruments and measured parameters at each site are shown under milestone 1.1.2. The wind and wave conditions experienced during the course of the measurement program are summarised in Figure 49. Root-mean-square wave heights at Rottnest, AWAC and MS1 are shown, together with the monthly mean Hs at Rottnest derived from 15 years of data in the top panel, and eastward (u_w) and northward(v_w) components of wind in the lower two panels.

The Rottnest wave buoy is off the western end of the island in 48m water depth. Between Rottnest and the AWAC, wave height is reduced mainly through refraction, while the reduction between the AWAC and MS1 is due to the combined effects of depth-induced breaking and bottom friction.

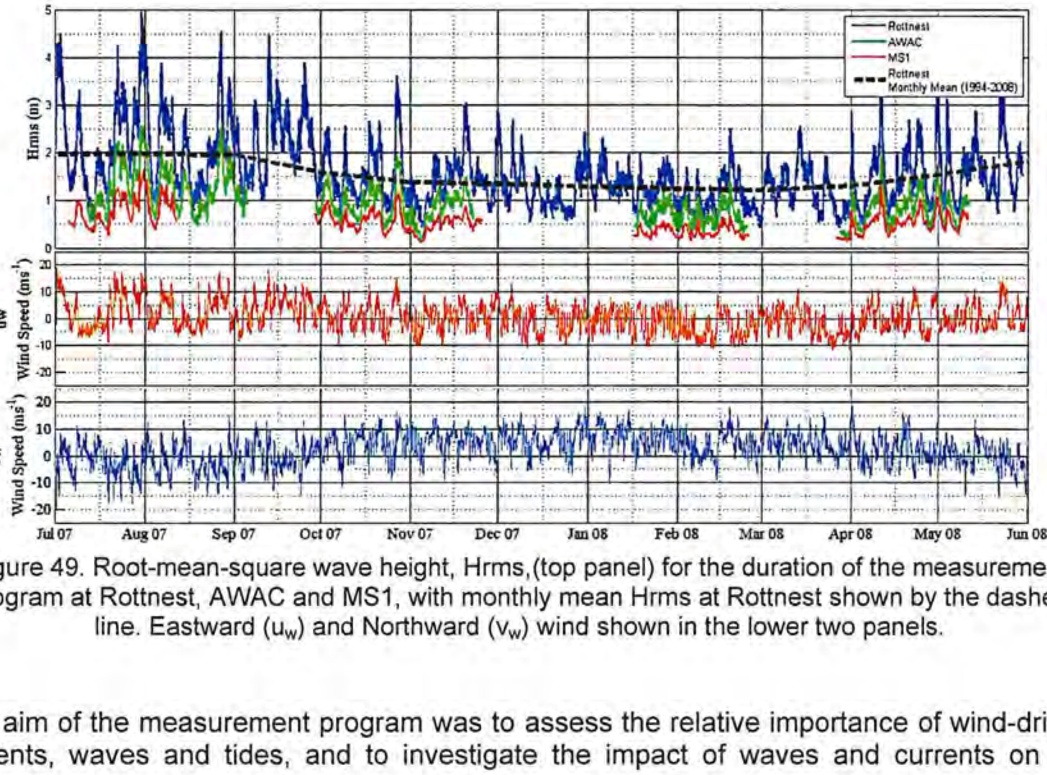

Figure 49. Root-mean-square wave height, Hrms,(top panel) for the duration of the measurement program at Rottnest, AWAC and MS1, with monthly mean Hrms at Rottnest shown by the dashed line. Eastward (u_w) and Northward (v_w) wind shown in the lower two panels.

The aim of the measurement program was to assess the relative importance of wind-driven currents, waves and tides, and to investigate the impact of waves and currents on the biogeochemistry and benthic habitat of the reef environments. Nortek Vector velocimeters were deployed at sites ADV1, ADV2, ADV3 and ADV4, located on the shoreward edge of reefs, and during storms were sometimes beneath breaking waves. Time-series of the observed currents at these sites are shown in Figure 50 where, during periods of high waves, both eastward (u) and northward(v) velocity components are positive, into the lagoon as expected from theoretical consideration of wave-driven flow over shallow reefs (Symonds *et al.*, 1995). During the first deployment, the Vectors were deployed on sand in slightly deeper water and, during the course of the deployment, sank into the sand such that the sensor head was very close to the bottom. Consequently, while the highest waves were observed during the first deployment, the currents are generally weaker than during subsequent deployments when the Vectors were moved onto reef and into shallower water. Strongest currents were generally observed at site ADV3.

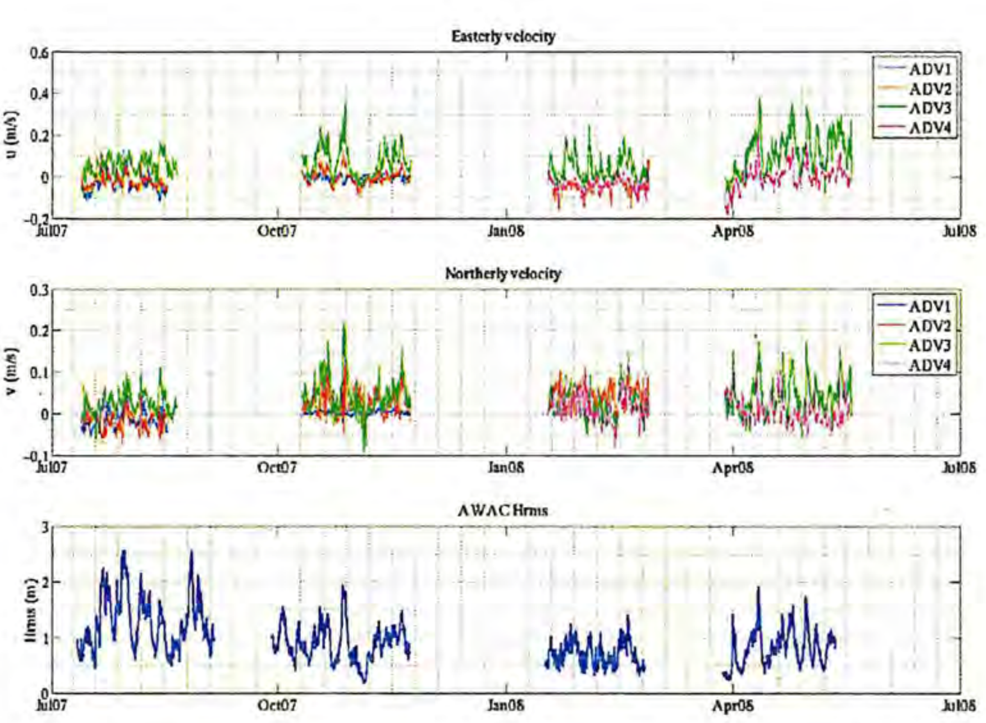

Figure 50. Time-series of eastward (u) and northward(v) velocity components at the ADV sites. Root-mean-square wave height at the AWAC shown in the bottom panel

Sites AQ1 and AQ2 were located in the channels between the reefs (see Figure 51), and both were shifted to more solid substrate after they sank into the sand during the first deployment. Time series of the depth averaged currents at AQ1 and AQ2 are shown in Figure 51. Contrary to the flows measured over the adjacent reefs, at sites AQ1 and AQ2 the eastward velocities are typically negative, particularly during the higher wave events, indicating flow out of the lagoon. For example at AQ2 during the first deployment strong westerly flow is associated with the first two events when the root mean square wave height exceeds 2m. This sensor clearly started to be affected by burial from about mid way through the deployment. During the same deployment AQ1 shows positive eastward velocity during the corresponding wave events. In subsequent deployments peaks in wave height are sometimes associated with westward flow at AQ1 though other periods of westward flow are not associated with wave events. In the lagoon at sites RDIN and RDIS the longshore flow during deployment 1 appears to be correlated with wave height as shown in Figure 52, with northward flow at RDIN and southward flow at RDIS. However, in subsequent deployments there is little correlation between longshore current and wave height.

The results presented here suggest wave forcing may be important in driving mean flows over the reefs into Marmion lagoon. At least some of this inflow appears to return offshore through the gaps between the reefs, and alongshore flow within the lagoon. However, peaks in wave height often occur with peaks in onshore wind speed so correlation between currents and waves might reflect wind forcing. During the first part of deployment 3, when the mean wave height was smallest, a persistent sea breeze cycle can be seen in the measured alongshore currents at ADV4.

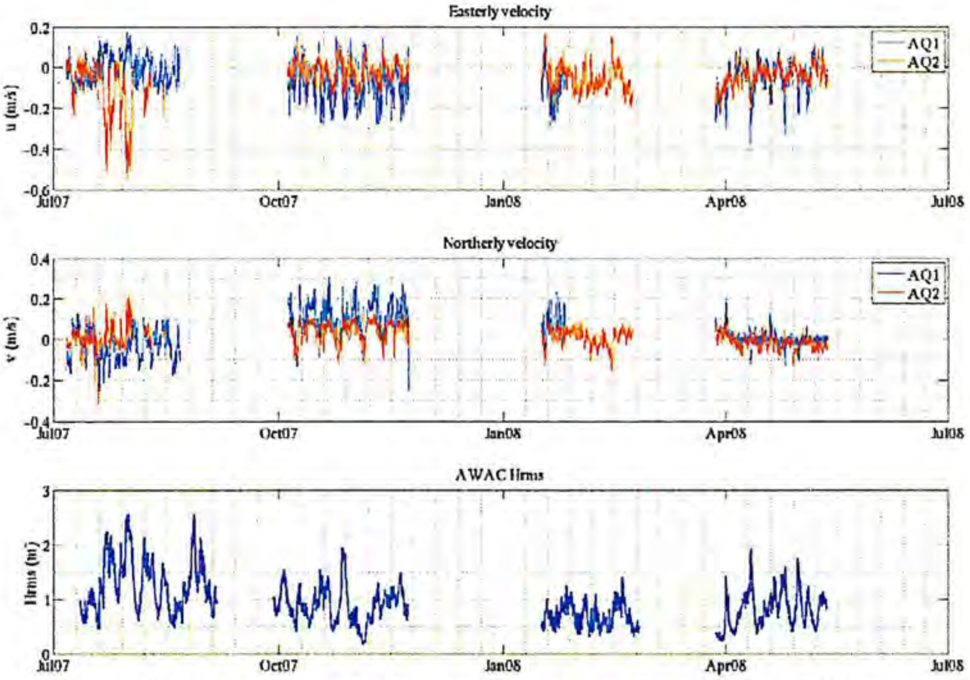

Figure 51. Time series of eastward (top) and northward (middle) velocities at AQ1 and AQ2 and Hrms at the AWAC (bottom).

Previous studies such as the Perth Coastal Waters Study and SRFME conclude that currents on the inner shelf are forced by the wind. In Fandry *et al.* (2006), the longshore current was shown to be predicted quite well using 3% of the alongshore wind speed, and we have found a similar relationship using a hydrodynamic model reported under milestone 1.1.8.

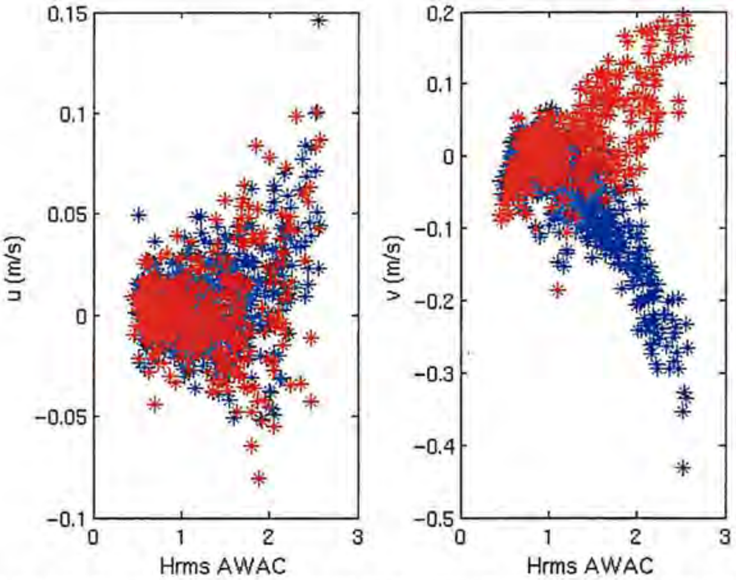

Figure 52. Eastward (left panel) and northward (right panel) currents at RDIS (blue) and RDIN (red) plotted against Hrms.

The data analysis is ongoing and will be presented in full as a data report in June 2009.

Time-series of temperature, salinity, chlorophyll, dissolved oxygen and underwater light were successfully recovered from the two multi-sensor moorings located at the sites MS1 and MS2 (see Milestone 1.1.5). The highest temporal variability at both sites was seen in temperature, chlorophyll and underwater light. Variations in dissolved oxygen and salinity were relatively small. Temperature varied throughout the year by more than 8^0C with lowest temperatures recorded during the first deployment and highest temperatures recorded during the third deployment (Figure 53). Highest chlorophyll concentrations were recorded during the two winter-time deployments (Figure 53).

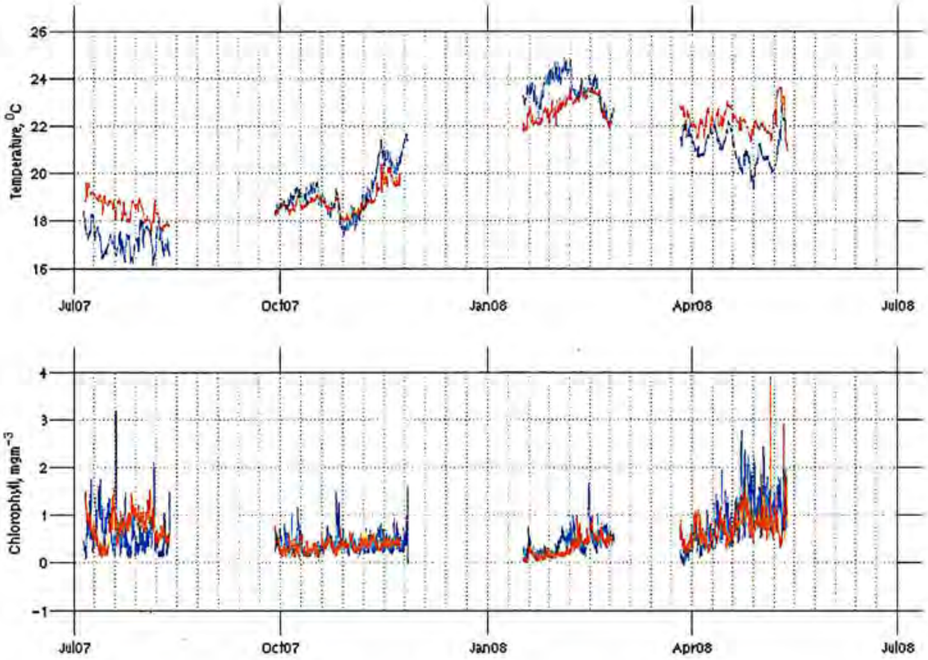

Figure 53. Temperature (upper panel) and chlorophyll (lower panel) measured at MS1 (blue) and MS2 (red) between July 2007 and June 2008.

Large temperature differences between the two moorings were also recorded, with temperatures inside the lagoon (MS1) as much as 2^0C lower during winter and 2^0C higher during summer compared with MS2 Chlorophyll concentration was also often quite different at the two sites especially during the two winter-time deployments

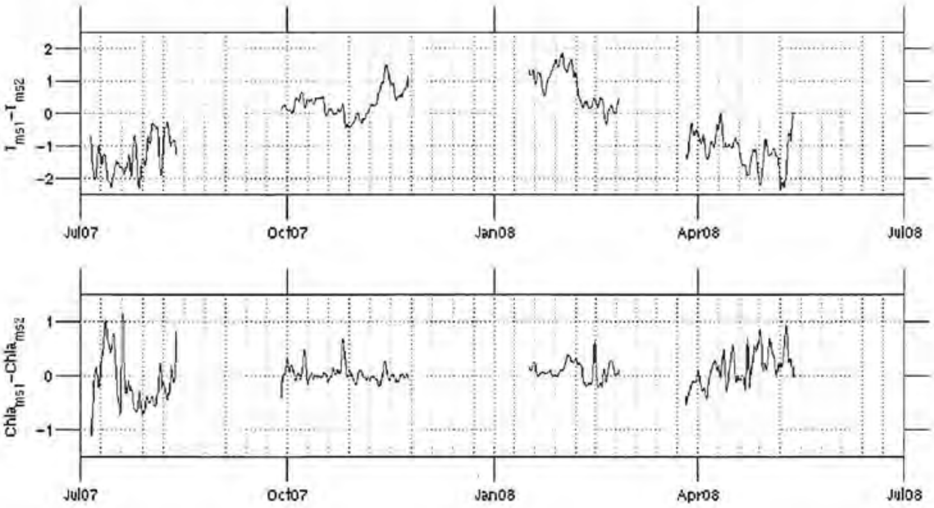

Figure 54. Numerical difference in temperature (^{0}C) (upper panel), and chlorophyll, (mg m^{-3}) (lower panel) between MS1 and MS2.

Importantly, the variability in chlorophyll observed at the multisensor sites cannot be easily explained by variations in waves, currents, temperature or salinity.

Comparison of underwater light with the chlorophyll measured at MS2 shows the strongest relationship between any two variables measured by the multi-sensors Figure 55. This result provides two pieces of information for the calibration of the biogeochemical model that is planned in the next phase of research. Firstly, the larger range in chlorophyll concentration at the lower light levels measured during deployments 1 and 4 indicates that the system is unlikely to be light limited during winter months. Secondly, the trend of decreasing light with increasing chlorophyll within each deployment (especially during deployment 3) is strongly suggestive of self- shading by the phytoplankton, which has important implications for how light attenuation is parameterised in the biogeochemical model.

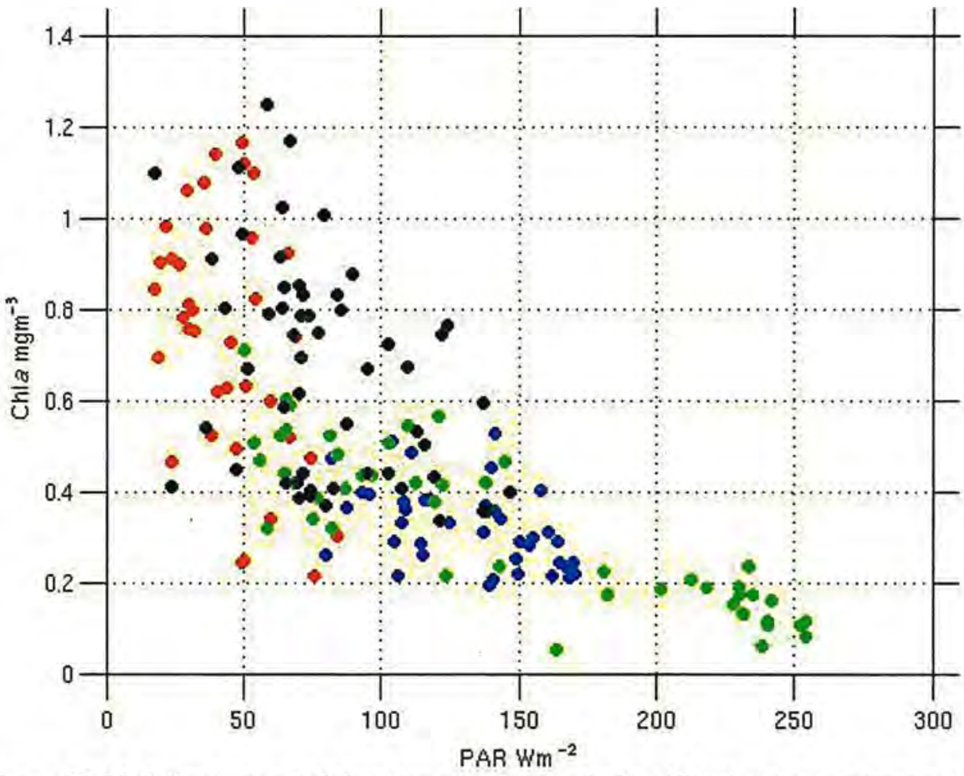

Figure 55. Variation in mean daily chlorophyll concentration (Chla) and mean daily underwater light (PAR), at MS2 during deployments 1 (red), 2 (green), 3(blue) and 4(black).

A full description of the field program and its results has been compiled in a separate data report provided to WAMSI.

Milestone 1.1.10: Complete 2009 Marmion biophysical sampling

Original Forecast Finish Date: 30/06/09

Revised Forecast Finish Date: 30/12/09

This section updated from previous Biannual Report

Arguably this work is complete in that much of work planned was carried out during 2008 (see also section 1.1.6) although completion of the assessment of the data still awaiting nutrient analyses to be completed. However given that this research revealed unexpected small scale spatial variability in nutrient distributions in Marmion lagoon especially around reefs and the emerging importance of the influence of waves on sediment nutrient resuspension we have extended this field work into the present winter. We are adding to the high frequency sampling targeting short lived storm events with instrument deployments extending over winter 2009. We have deployed a McLane remote access sampler to safely sample during periods of high physical forcing associated with winter storms. Such events are highly dynamic and short lived so sampling intervals are brief (12 hours) to adequately capture the temporal variation. In conjunction with the automated water sampler, we have deployed a mooring frame equipped with (i) a Seabird SBE19plus measuring temperature, salinity, PAR, fluorescence and oxygen; (ii) a Seabird SBE26 wave and tide gauge; (iii) a RDI Workhorse Sentinel ADCP with waves enabled; and (iv) TAPS measuring vertical distribution of suspended particles to get an accurate estimate of the state of the physical environment during sampling. Improved temporal nutrient data (particularly during storms) combined with accurate estimates of the magnitude of the forcing will allow us to test the hypothesis suggested by the historical sampling that nutrient resupply is enhanced by physical factors. These data are also an important means of testing and informing the biogeochemical models. We would thus like to revise this milestone to be completed by the end of 2009.

Research to date is reported in two sections below. The first section presents results from the analysis of historical data showing variability in nutrients associated with waves and storm events. This body of work has in part lead to the strong focus on making the high frequency measurements of biophysical and biogeochemical variables conducted in 2007 and 2008 in this study and the winter sampling program currently underway. These are described in the second section below.

Historical nitrate analysis.

Dissolved nutrient concentrations in the coastal waters off southwestern Australia are low and pelagic primary productivity appears to be nitrogen limited. In contrast, shelf waters support abundant seagrass and macroalgal communities. The source of the nutrients that supports benthic primary productivity is unclear, but it is possible that tight cycling between organic matter production (microalgae, macroalgae and seagrass) and remineralisation contributes. A recent shelf nutrient budget estimated that 84% of total primary production is recycled on the shelf (see milestone 1.2.4). We present historical surface water nitrate data collected at a range of temporal scales (weekly to hourly) with the aim of better understanding nutrient resupply mechanisms to Marmion Lagoon (Figure 56).

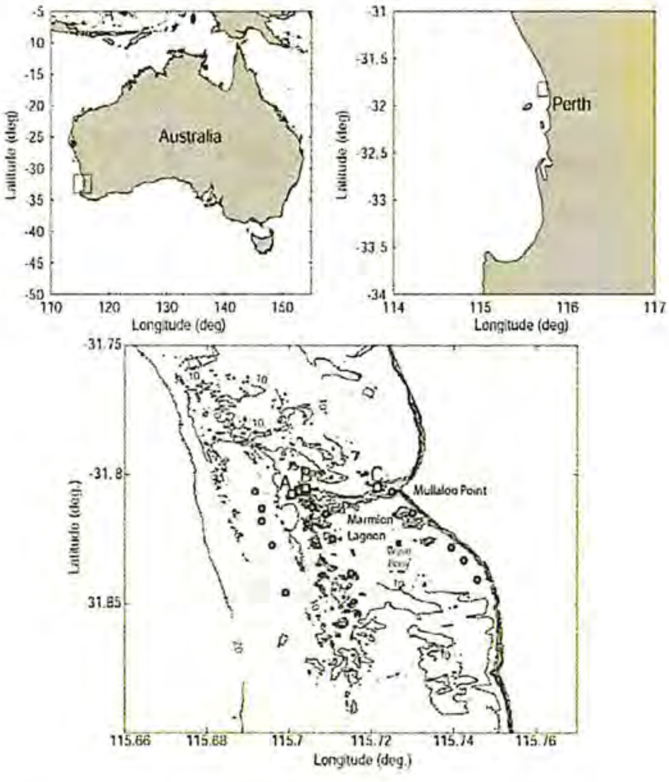

Figure 56. Map of the study area (bottom) showing its location relative to the Australian mainland (top right) and within South-Western Australia (top right). The three main stations, A, B and C are labelled (grey squares), as is the location of the wave rider buoy (black square). The grey circles are the three north-south transects occupied to examine spatial variations.

Nitrate concentrations varied considerably between weekly (Figure 57), daily Figure 58) and even hourly (Figure 59) sampling events. Not surprisingly, in an area such as this where the surface waters are strongly nitrogen limited, large nitrate increases between sampling trips were equally rapidly depleted. Although not necessarily "new" nitrogen, these nitrate pulses appear to make a considerable contribution to maintaining primary producers in Marmion Lagoon. Over the course of each of the daily sampling periods, nitrate accumulation during the periods where nitrate increased between sampling trips was 6.2 μM (average of 0.26 μM day^{-1} for the period) in September 1983 and 18.7 μM (an average 0.35 μM day^{-1} for the period) from June to August in 1984. Annually, the average of the two daily flux measurements would correspond to an effective flux of around 111.5 μM for the year or, in 7 m of water, 7.8 x 10^5 μM m^{-2} yr^{-1} (10.9 gN m^{-2} yr^{-1}).

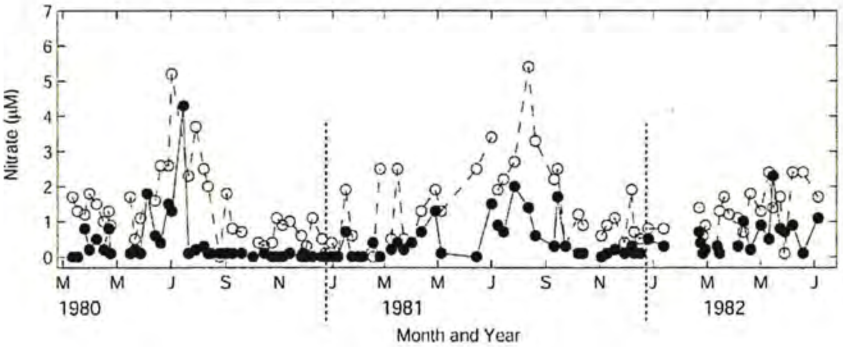

Figure 57. Mean weekly dissolved nitrate concentrations (µM) of station A, reef (open circles) and station C, shore (closed circles) sites.

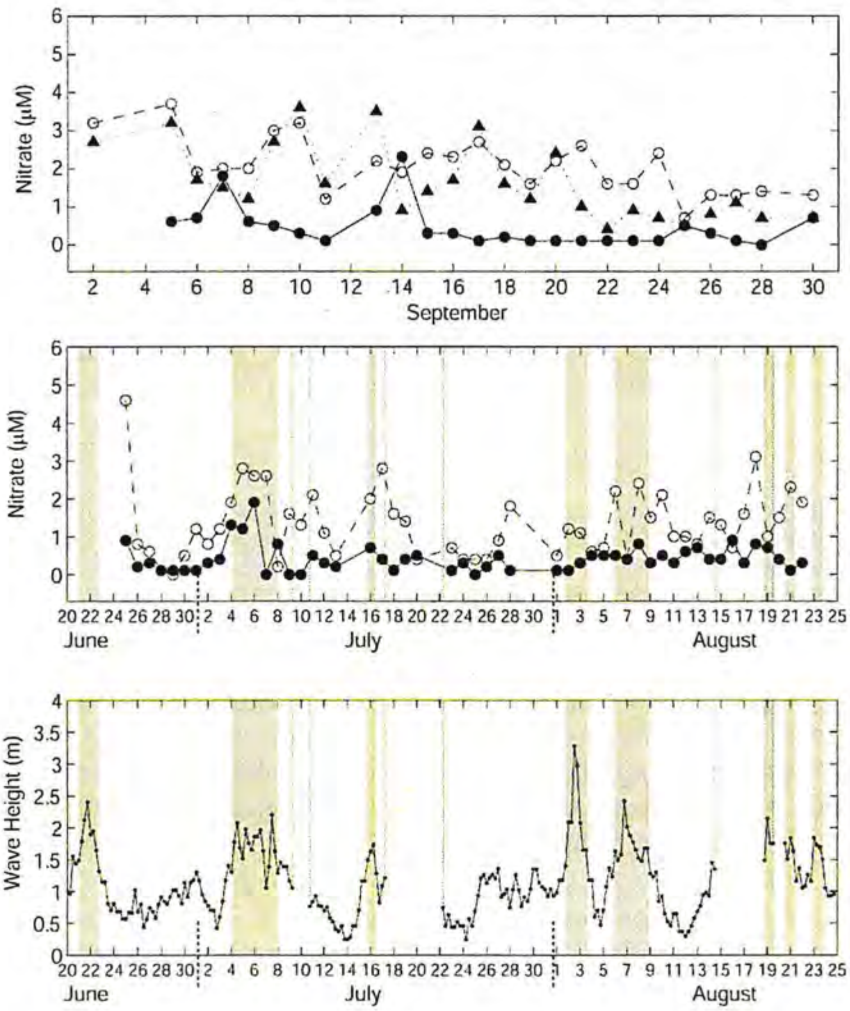

Figure 58. Top: Daily nitrate concentration (µM) in September 1983 taken at two reef sites (stations A located outside and B located inside, open circles and closed triangles, respectively) and the shore (station C, closed circles) site. Mid. Daily nitrate concentration (µM) from late June until late August (winter) 1984 at reef (station B, open circles) and shore (station C) sites. Bottom. Six-hourly average wave height in the Lagoon for the period from late June until late August (winter) 1984. The

shaded areas in both upper and lower plots are periods where measured wave heights are over 1.5m.

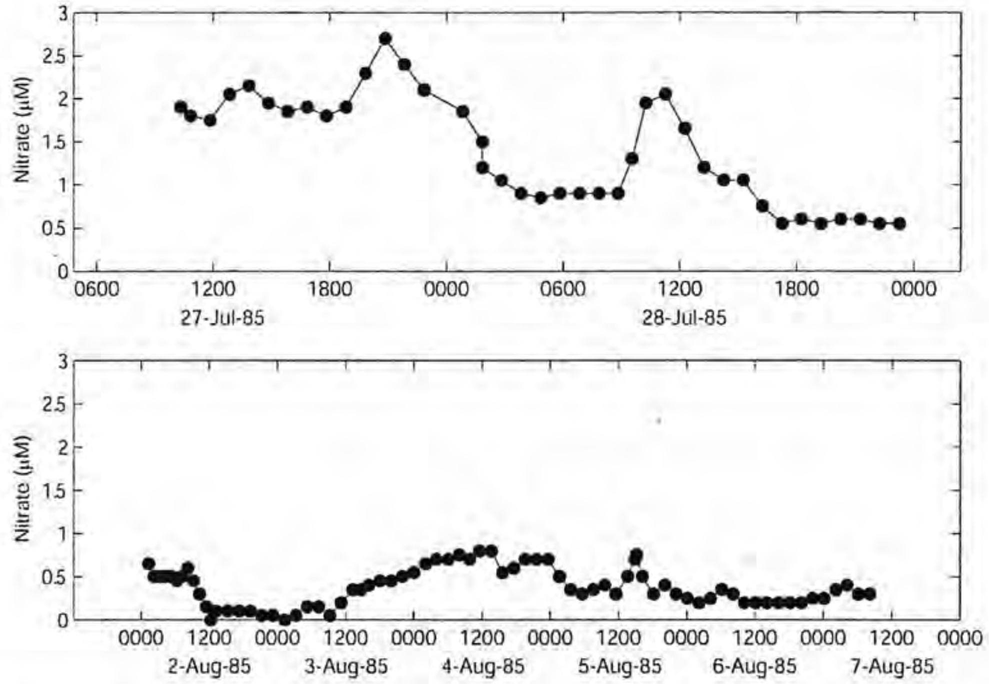

Figure 59. Four hourly means of nitrate concentration of hourly samples taken by ISCO automatic water samplers on two occasions.

This annualized nitrate flux is comparable with the estimated nitrate recycling flux required to balance the whole-of-shelf nutrient budget (6.2 gN m^{-2} yr^{-1}, see milestone 1.2.4) and our flux estimates are likely to be conservative as the calculations only consider the flux attributable to observable increases in nitrate and do not consider the depletion due to uptake by phytoplankton during and between the periods of accumulation. The observed flux calculated above combined with the unquantifed uptake during periods of accumulation suggest that on an areal basis, shallow areas such as Marmion Lagoon may make a particularly important contribution to the overall shelf nutrient budget.

Generally, ammonium is the direct product of the decomposition of organic material and nitrate such as measured here is derived from ammonium by bacterial nitrification. In this system, rapid ammonium consumption by autotrophs would leave little scope for conversion of significant amounts to nitrate. It is perhaps more likely that the remineralisation and nitrification processes that generate the nitrate observed here are isolated from the autotrophic biota. Porewaters trapped by surface sediment layers may provide the conditions required for nitrification of ammonium to nitrate.

The short lived pulses of nitrate suggest that the mechanism that generates them is dynamic. On average, nitrate concentrations were highest in winter (although there was considerable interannual variability in the timing and magnitude of the winter maxima) between June and August (Figure 60). Winter is the high wave energy period and physical processes may generate the nitrate pulses observed here and as such sustain primary production. Wave data coinciding with the collected nitrate data are limited and only coincide with daily samples collected between late June and August in 1984 (Figure 58). There is a general correlation between periods of increased wave activity and elevated nitrate concentration (see Figure 61) although the correlation between them is not statistically significant (p = 0.17).

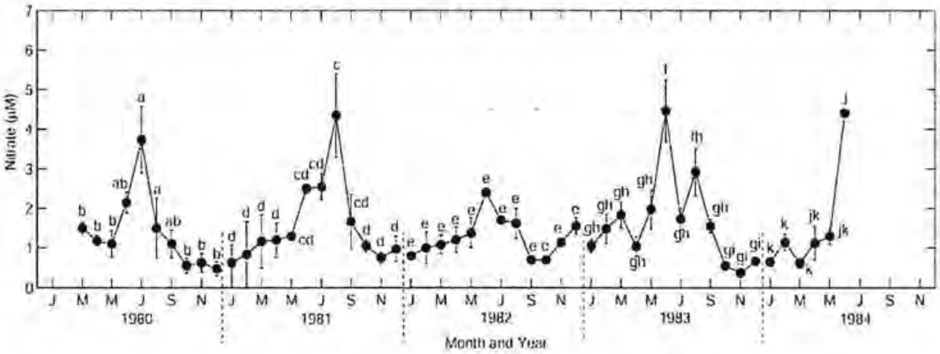

Figure 60. Mean monthly (upper) dissolved nitrate concentrations at the reef site (station A) for five years. The error bars are 1 standard error about the mean. The number of samples each month varies. Significant differences for individual comparisons within each year are denoted by letters. Months in any one year with differing letters are significantly different from one another.

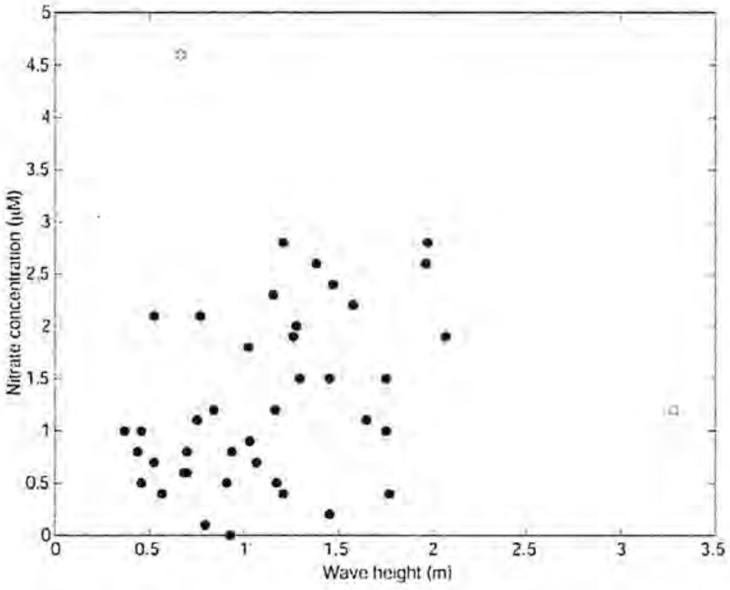

Figure 61. The relationship between nitrate concentrations (μM) measured daily between late June and late August (winter) in 1984 at reef station B, and the corresponding wave height (from six-hourly measurements). The open circles are outliers.

Physical processes may promote the remineralisation and release of nutrients bound up in organic carbon accumulated in rock crevices or between reefs, or large pieces of detritus lying on the bottom or fine grained material trapped within the surface sediments. Alternatively, the organic carbon could also be derived from living tissue, such as attached macroalgae and seagrass whose tips are physically abraded during storms. Finally it is possible that wave driven variations in pressure on uneven (ridges and troughs) permeable sediments enhances pore water circulation within the sediments and drives it across the sediment-water interface.

Nitrate concentrations measured outside the reef were significantly higher than those measured inside the reef which, in turn, were higher than those measured inshore (Figure 62). This is not particularly surprising as the Lagoon stations (B and C) are sheltered somewhat by a series of offshore reefs (Figure 56) which dissipate some of the wave energy encountered at the outer. It is possible that rates of macroalgal erosion or sediment resuspension are lower inside the reef due to the reduced physical forcing. The high concentrations at stations nearest the reef suggest that the reefs themselves may act as nutrient point sources. The reefs typically have a high biomass of macroalgae and abraded plant material and may be a more important source of labile biomass to surface waters. If most of the small organic matter decomposes on or near the reef or is incorporated into the sediments close by, then the reefs would appear to be a nutrient source. In contrast the inner station (the site with the lowest pelagic nitrate concentrations) is well removed from this abrading macro algae and could be limited by a reduced fresh detrital supply. However, the inshore site is very shallow, disturbance is omnipresent, the sediments are likely to be resuspended more often than in deeper areas and this continuous disturbance may not allow detritus to accumulate to an extent sufficient to generate the nitrate peaks observed further offshore.

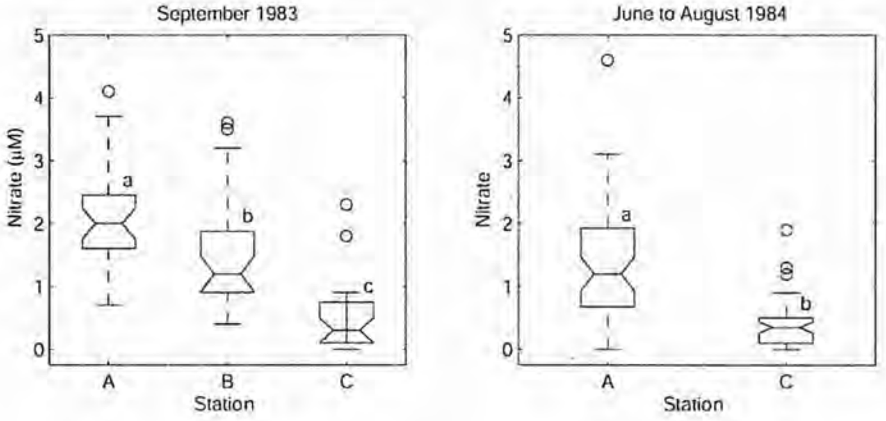

Figure 62. Box plots comparing the distribution of nitrate concentrations (µM), measured daily during September 1983 (left) and between late June and late August 1984 (right) at three positions across the Lagoon. Station A located outside the Lagoon near a reef, Station B located inside the Lagoon and station C located near shore in the Lagoon (see **Error! Reference source not found.**). The centre line is the median. The notched area is the uncertainty about the medians for box-to-box comparison (boxes whose notches do not overlap indicate that the medians of the two groups differ at the 5% significance level). Stations with differing letters are significantly different from one another. The top and bottom of the box represent the 25th and 75th percentiles (the distance between the upper and lower percentiles is the interquartile range). The error bars bound the rest of the data except for outliers (open circles which are data that are more than 1.5 times the interquartile range outside the 25th or 75th percentiles).

Marmion Biophysical Oceanography

The historical analysis above and measurements described under milestone 1.1.6 suggest that nutrient concentrations are highest near the reef and may vary in response to increased remineralisation stimulated by variations in wave energy. Results from a simple model (milestone 1.2.4) have shown that observed seasonal variations in pelagic chlorophyll can theoretically be linked to wave forcing, suggesting that wave enhanced remineralisation and release of nutrient benefits the pelagic community. Partitioning of productivity between benthic and pelagic plant communities is of considerable interest. Here we compare pelagic chlorophyll a biomass measurements with the nutrient distributions described earlier (milestone 1.1.6).

While nitrate concentrations were high near to the reef, extracted chlorophyll a concentrations tended to be low directly over the reef and highest in areas removed from the reef (Figure 63).

In contrast to our earlier hypothesis that the reefs appear to be nutrient sources, this decoupling of pelagic nutrient concentration and chlorophyll a concentration could indicate that variations in "top-down" processes (grazing) at least partly control pelagic nutrient concentrations. Substantial assemblages of filter feeding organisms are common on local reef systems which likely efficiently remove chlorophyll from the water column. Higher rates of grazing on reefs could result in nutrients accumulating over the reefs due to the reduced uptake by smaller phytoplankton community. Because of scant available nutrient data this spatial comparison of nutrients with biomass is extremely preliminary. The actual balance between nutrient supply and the control on uptake exerted by grazers will require more nutrient observations to fully decipher.

Seasonally, chlorophyll a concentrations were highest in our April and May sampling trips, principally in the north of our sampling domain (Figure 64). The late spring/early winter increase in chlorophyll biomass occurs in the period previously identified with the onset of a shelf-scale phytoplankton bloom (Lourey et al., 2006), and is consistent with what we would expect during the higher-energy winter period, based on results of the simple model that suggests variations in the benthic nutrient flux stimulated by variations in the magnitude of wave forcing can account for observed seasonal variations in pelagic chlorophyll. However, it is not clear that such a seasonal pattern of accumulation can necessarily be expected in the lagoon (Koslow et al., 2008). The high concentrations in the north of our domain during this period suggest that the accumulation (and mechanism driving such accumulation) are spatially patchy. There are several mechanisms that could explain this north south gradient of chlorophyll a concentration: firstly, higher benthic nutrient exchange in the shallower northern section of our domain; secondly, higher input from terrestrial sources (i.e. groundwater) to that particular area; finally, the influence of the sewage outfall located just to the north of the domain.

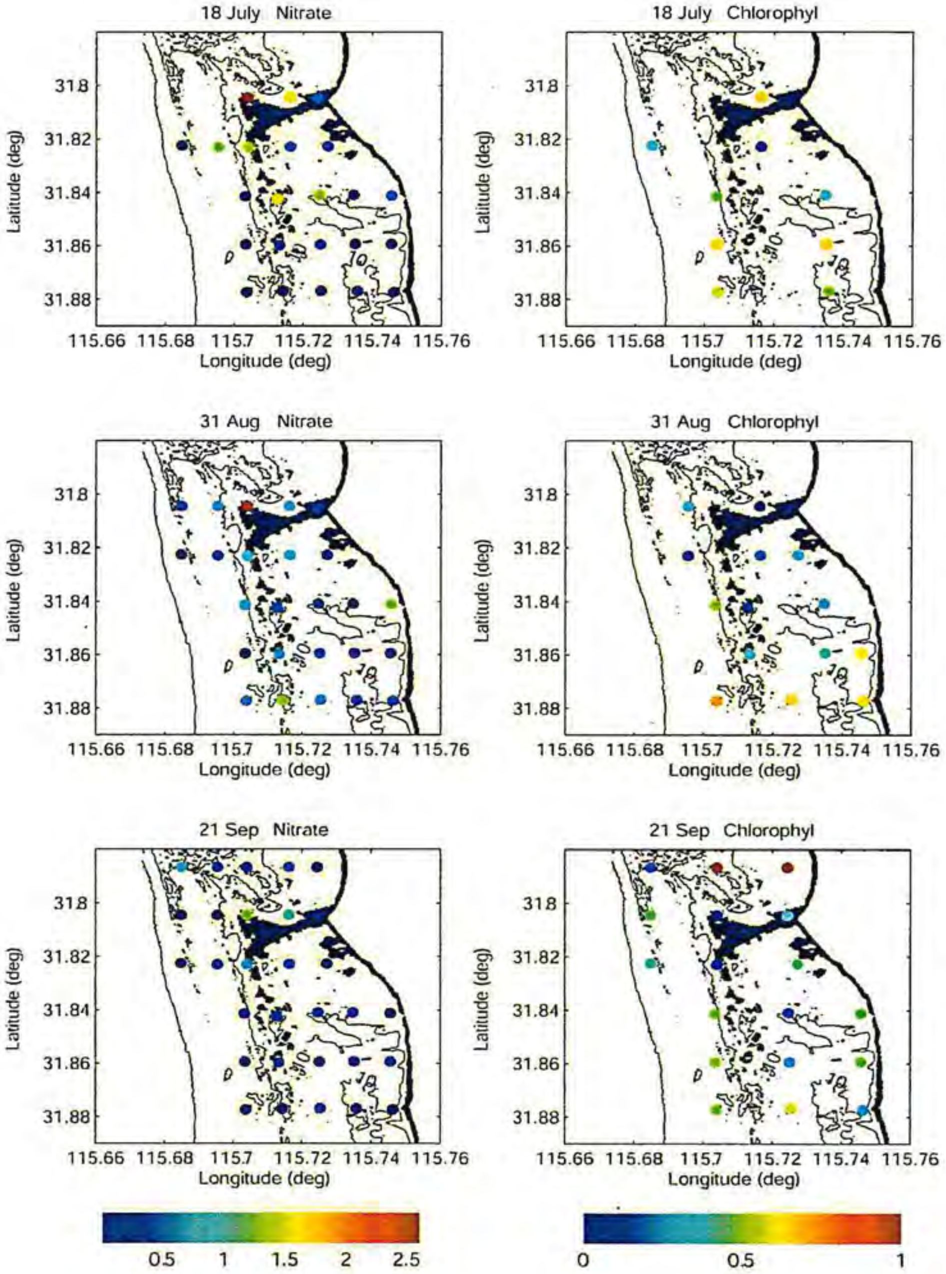

Figure 63. A comparison of available surface nitrate concentrations (μM, left) and extracted chlorophyll concentration (mg m^{-1}) for three sampling cruises conducted in 2008.

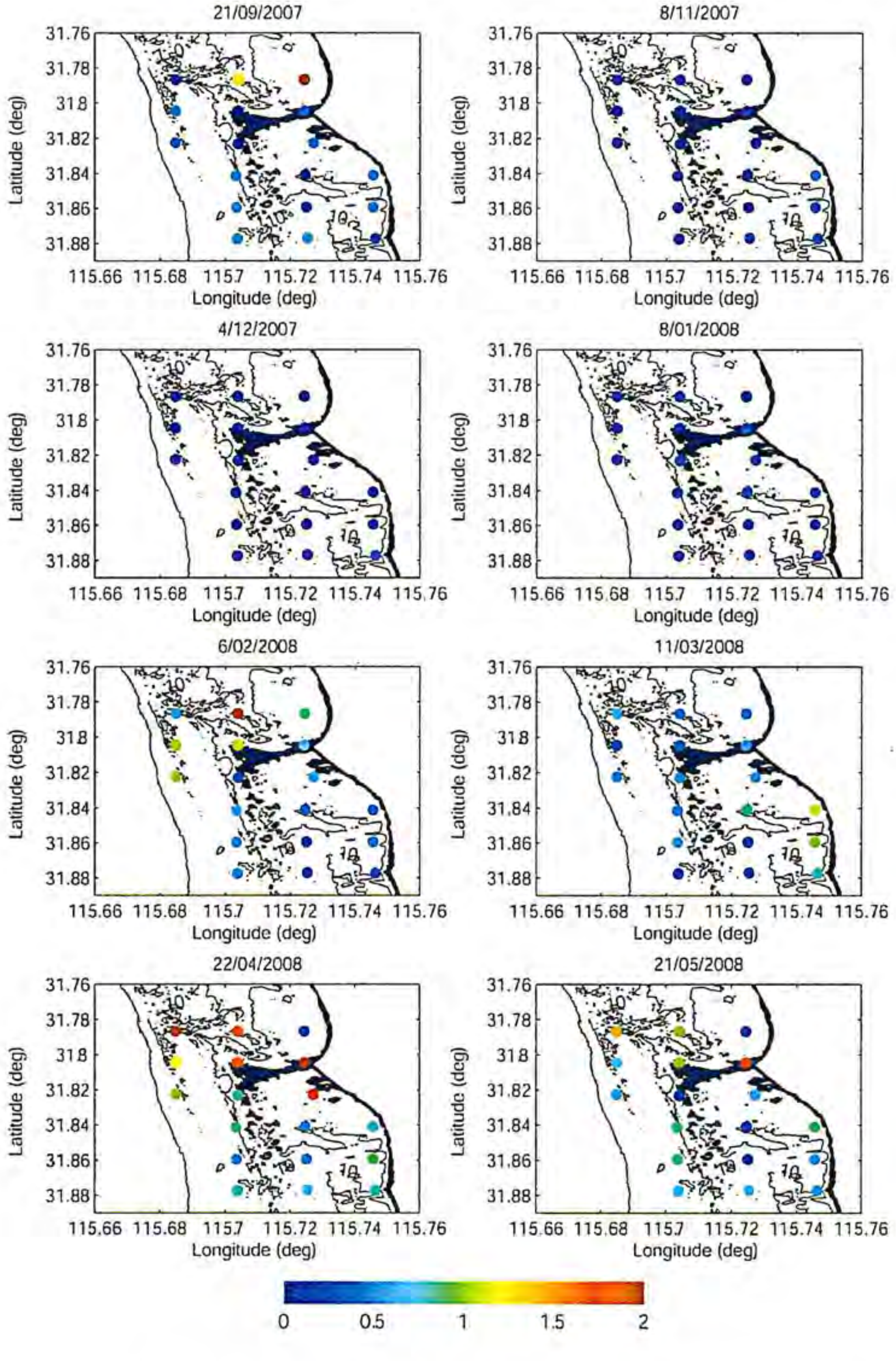

Figure 64. Temporal variations in chlorophyll a concentration (mg m^{-3}).

2. Coupled hydrodynamic and biogeochemical models and a quantitative nutrient budget for coastal waters at shelf and lagoon scales.

Milestone 1.2.1: Complete 'SynTSN' algorithm, incorporating nutrients in synthetic TS analysis

Original Forecast Finish Date: 30/06/07

Revised Forecast Finish Date: 30/06/07

This section unchanged from previous Biannual Report

Summary of Activities Undertaken, Outputs Produced:

Existing approaches for estimating sea-surface nitrate (SSN) determine expressions for SSN as a function of sea-surface temperature (SST) and chlorophyll and/or obtain a nitrate estimate from the difference between satellite SST and a climatological nitrate depletion temperature. We have developed a system for obtaining upper-ocean profiles of nitrate from surface altimetry, temperature, chlorophyll and climatology. This includes an improved estimate of the mixed-layer depth.

Two approaches have been developed.

SynTN

The surface values from satellite platforms, (SST and Chl) are used to infer NO3 profiles. The estimate is referenced to the local CARS climatology; that is, we use the surface observations to derive the NO3 anomalies. The vertical covariance structure is determined from the historical dataset (training set).

N (T) climatology

An alternative method uses a climatology of nitrate mapped on temperature levels. In many regions a good N(T) relation exists for some parts of the water column. In our region in near-surface waters the relationship appears to asymptote at high T - low N, although this might be partly due to poor data. Poor data definitely obscures the relation at low T - high N. However, in cases where we have an accurate T profile (not just SST) then this method has some skill.

Summary

These methods have demonstrated skill in deriving nitrate estimates from surface satellite observations. However, the overall the results were disappointing due to the following factors:

- absence of significant nitrate signals in the test region. The regions used in most other studies had large nitrate signals and strong relationships between these and other parameters. In our region there was very little real variability, and most of that was seasonal (much of which is captured by CARS), or of very short time and space scales (of the same order of measurement error, or perhaps due to measurement error).

- poor quality data. The majority of our "training set" data comes from CSIRO, with several defects:
    - large variability throughout the water column, for example, ~5 µM (~20% of total value) differences between adjacent casts at 5000 m. This is highly implausible and gives reason to doubt all the data.
    - clearly doubtful data prior to 1970 (all analyses had to be repeated with pre-1970 data excluded), but evidence that problems persist.
    - decadal differences in the determination or attribution of zero or very low values. This is of concern because most of the upper ocean and shelf values are very small (<.3 µM), and also because the concept of nitrate depletion temperature (NDT) could potentially have been useful for this study.
- sparsity of data (especially quality nitrate data collected during periods for which we have usable SST and ocean colour data) for calculating the inference coefficients and for withholding to validate the method. We are used to testing methods on oceanic T-S sections - but these are not easily found with NO3-Chl-a.

A more complete report is presented at www.marine.csiro.au/~dunn/synN/

Milestone 1.2.2: Test regional nutrient source scenarios with geochemical model

Original Forecast Finish Date: 30/06/08

Revised Forecast Finish Date: 30/06/08

This section unchanged from previous Biannual Report

Summary of Activities Undertaken, Outputs Produced:

Simulations with the regional 3D fully coupled biogeochemical model show that coastal nutrient sources are essential for realistic simulation of the seasonal shelf productivity (Figure 65). This is surprising as Feng & Wild-Allen (in press) estimated coastal loads to account for <1% of the shelf nitrogen supply as a whole. Model simulations support the growing consensus that cross-shelf exchange off WA is very small with the Leeuwin Current acting as a barrier to lateral advection. The shelf biogeochemistry appears to be largely isolated from the Indian Ocean with coastal nutrient loads and benthic-pelagic recycling on the shelf having significant impact on the shelf productivity.

This work was presented at the ASLO conference in Orlando, Florida as: Wild-Allen & Feng 'Nutrient Supply to the Western Australian Shelf'.
Work is ongoing to refine the spatial and temporal dynamics of coastal nitrogen input into model. A modelled shelf-scale nutrient budget is in preparation.

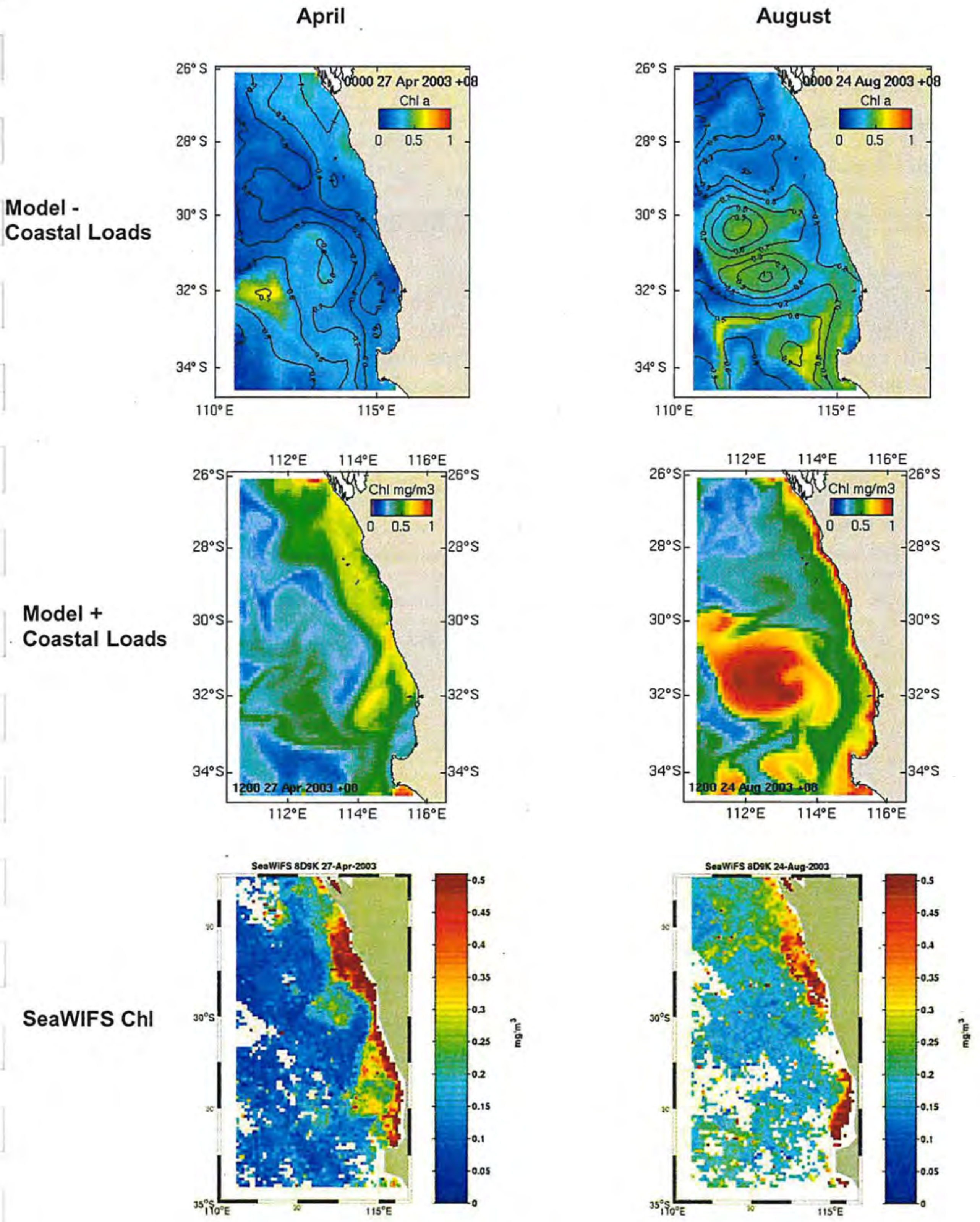

Figure 65. Comparison of modelled surface chlorophyll without coastal nutrient source (left), with coastal nutrient source (centre) and SeaWiFS sea surface chlorophyll observation.

Milestone 1.2.3: Analyse remote-sensed chlorophyll patterns - spatial and temporal variability

Original Forecast Finish Date: 30/06/08

Revised Forecast Finish Date: 30/06/08

This section unchanged from previous Biannual Report

Summary of Activities Undertaken, Outputs Produced:
Remotely-sensed chlorophyll patterns along the WA coast have been analysed at a range of different temporal and spatial scales. A strong relationship between seasonal and interannual changes in the strength of the Leeuwin Current and remotely-sensed chlorophyll biomass in offshore waters south of Abrolhos Islands (29-33^{0}S) has been observed (Figure 66). This mirrors a similar annual trend in the settlement of larvae of Western Rock Lobster at Alkimos, north of Perth (de Lestang and Melville-Smith, 2006), and offers a possible explanation for the long observed climate variability in breeding success of this important fishery in the area.

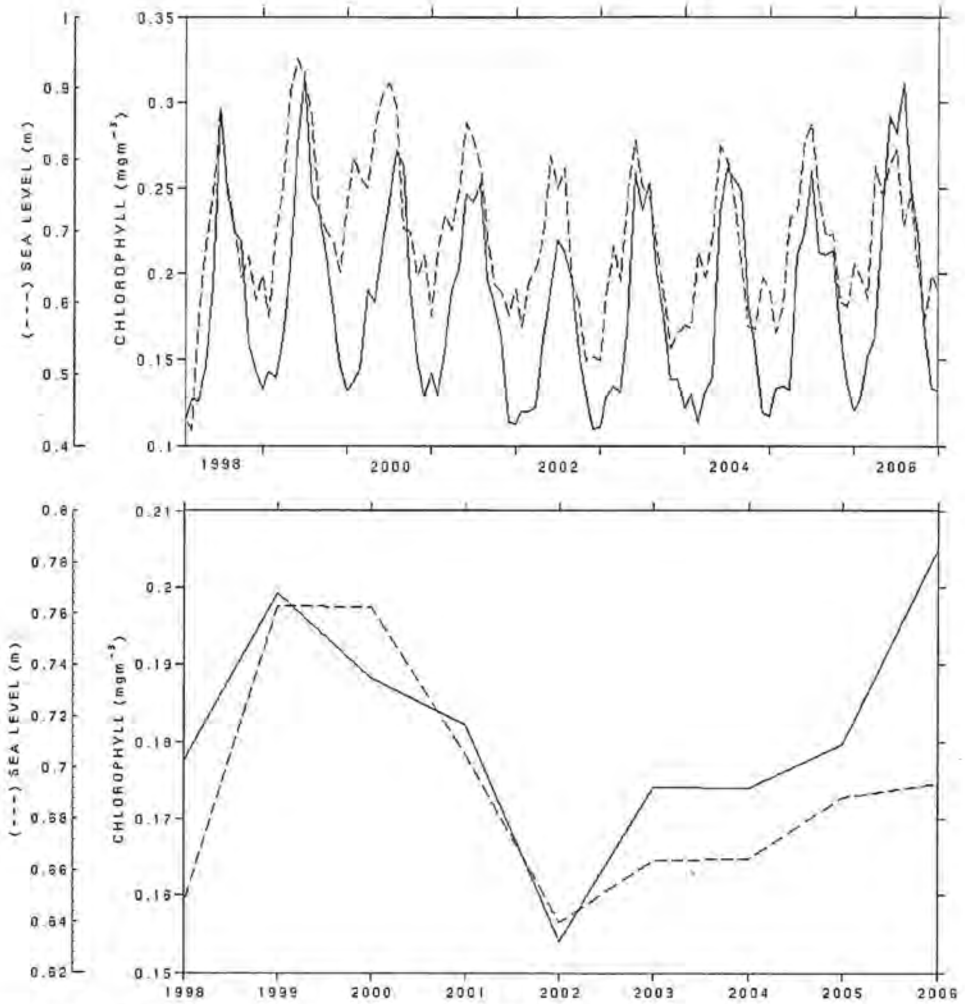

Figure 66. Comparison of monthly (upper panel), and annual (lower panel) averages of remotely-sensed chlorophyll in offshore waters with the variation in the strength of the Leeuwin Current (indicated by Fremantle sea level) between 1998 and 2006.

Similar plots of chlorophyll biomass on the inner continental shelf appear to be subtly different from the offshore signal suggesting a more complex mechanism might be involved. One particularly striking feature in the satellite data for the on-shelf distribution of chlorophyll is a positive gradient in biomass across the shelf that increases sharply close to the coast (Figure 67). This pattern has recently been confirmed from shipboard measurements of chlorophyll (Figure 68), alleviating previous doubts as to the validity of this satellite result.

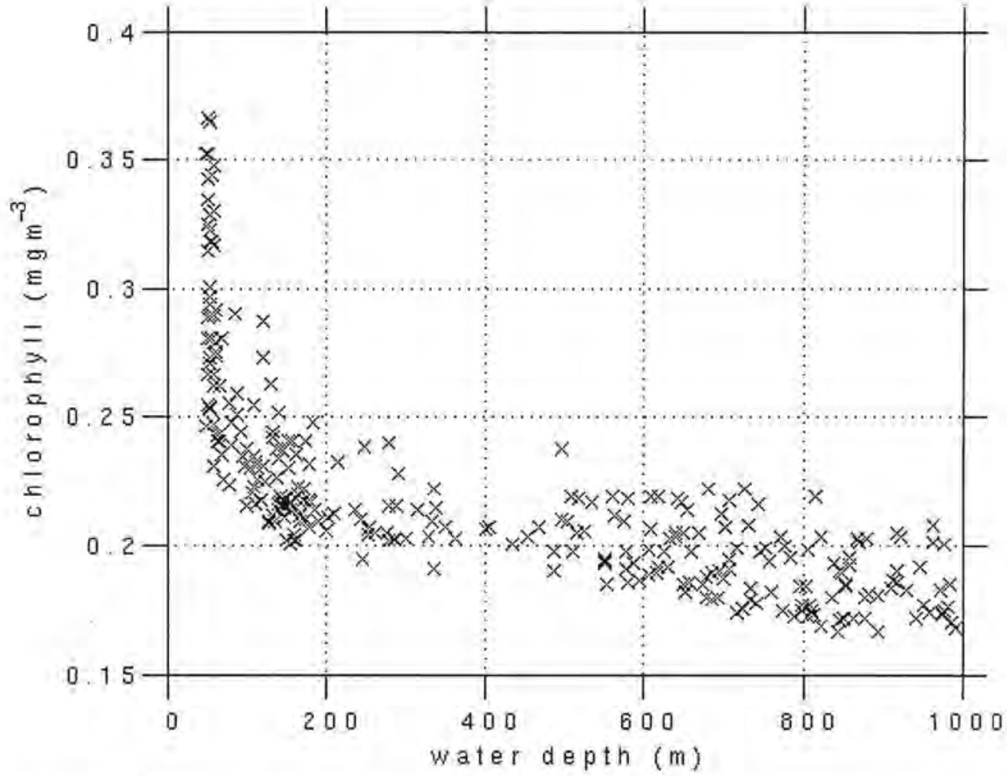

Figure 67. Increase in satellite derived surface chlorophyll biomass with decreasing depth of seabed on the continental shelf. Each point represents the 10-year mean of chlorophyll biomass recorded by the SeaWiFs satellite on a 9km grid between 29.5 and 31.5 degrees south.

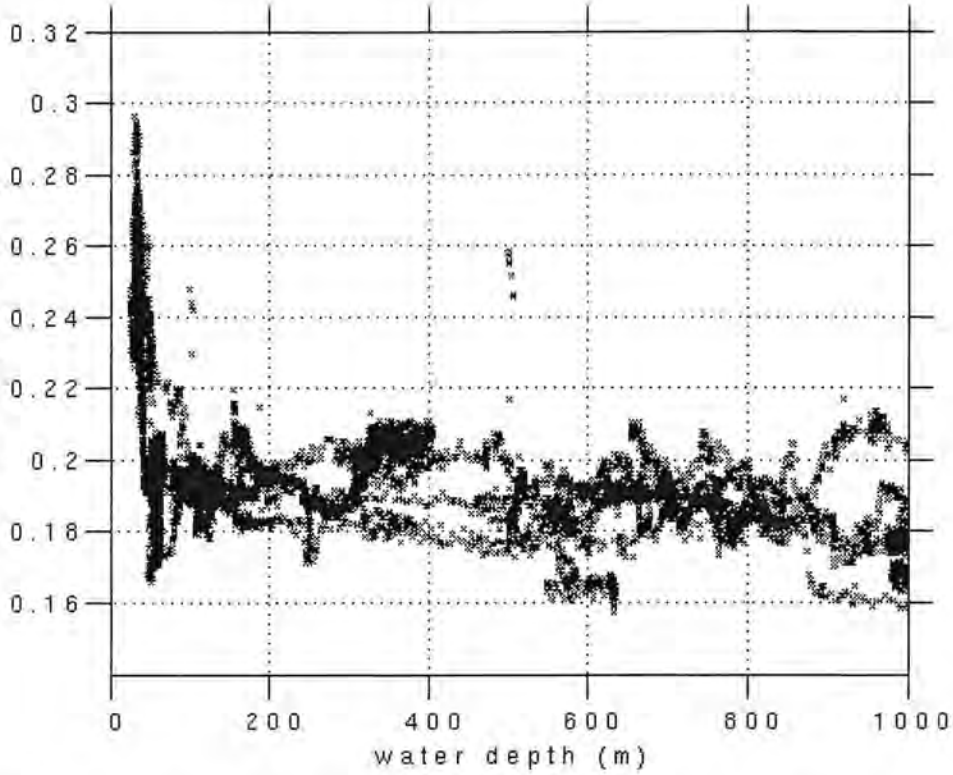

Figure 68. Increase in chlorophyll biomass with decreasing depth of seabed measured between 30 and 32 degrees south on board the Southern Surveyor by fluorometry during the autumn of 2007.

Most of the increase in coastal chlorophyll is seen to occur during the wintertime and detailed analysis of remotely-sensed chlorophyll on the inner shelf suggests that the influence of surface gravity waves in shallow water may offer a partial explanation (Figure 69).

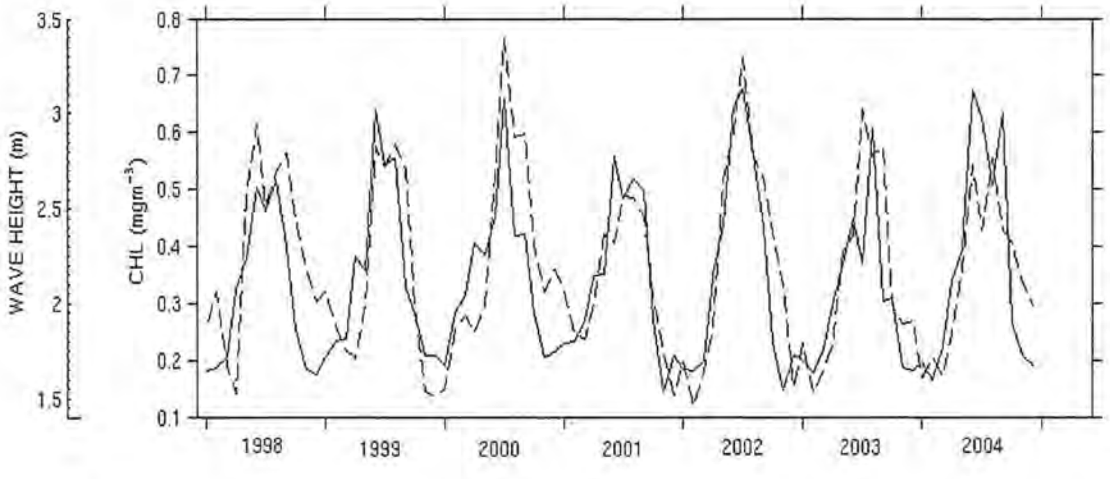

Figure 69. Comparison of the monthly averages in remotely-sensed chlorophyll on the inner shelf (solid line) with significant wave height (broken line).

Inter annual variation in mean annual chlorophyll *a* concentrations (from SeaWIFs) show considerable spatial variation along the coast of WA (Figure 71). It has already been established that between 29°S and 33°S they are highly correlated (Figure 66) with the Southern Oscillation Index (SOI) but outside of this range they are not responding to SOI (Figure 71). Over the range from ~ 50 meters water depth to ~ 2000 m water depth along the WA coast (Figure 71) the annual mean anomaly was a maximum of 10% (0.07 µg chlorophyll *a*.l^{-1}) reached during 2004 and 2005 off the Ningaloo Reef area. This large anomaly in the vicinity of Ningaloo Reef is currently under further investigation.

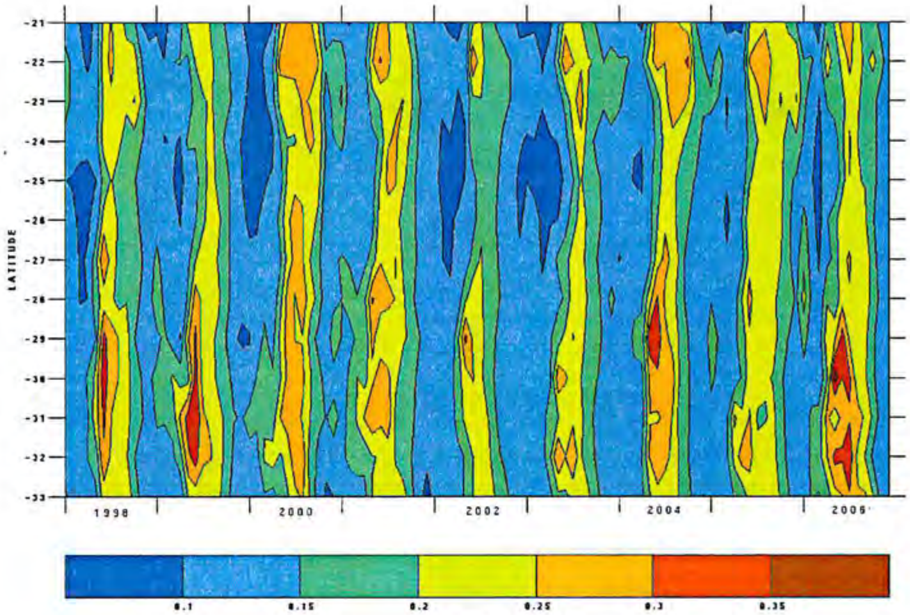

Figure 70. Variation in seasonal pattern of chlorophyll between 21 and 33 degrees south.

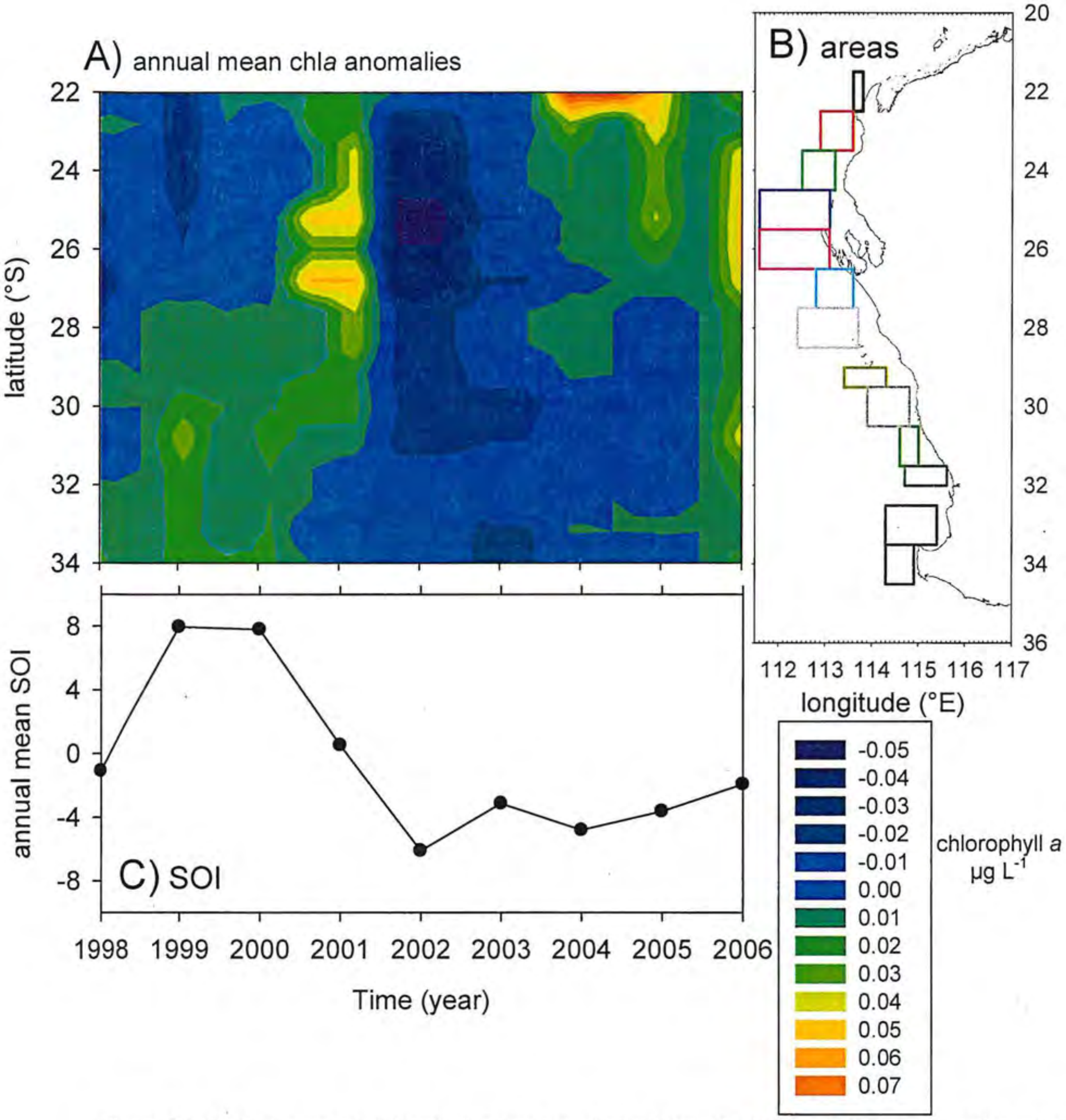

Figure 71. A) Annual mean chlorophyll anomalies, derived from SeaWIFs, plotted as a function of latitude (from 22 to 34 degS) and time (from 1998 to 2006); B) Geographic boxes used to calculate chlorophyll mean values; C) Annual-averaged Southern Oscillation Index from 1998 to 2006.

References

de Lestang, S. and Melville-Smith, R. (2006) West coast rock lobster managed fishery status report. In: *State of the fisheries report 2005/06*. WA Department of Fisheries. pp 14-63.

Milestone 1.2.4: Begin incorporating lagoon and shelf scale C& N flux into BGC models

Original Forecast Finish Date: 30/06/09

Revised Forecast Finish Date: 30/06/09

This section updated from previous Biannual Report

Summary of Activities Undertaken, Outputs Produced:

First, a nitrogen box-model is described, that identifies the major fluxes of nitrogen on the West Australian continental shelf. This is followed by results from several BGC models, of varying complexity, that incorporate different carbon and nitrogen fluxes.

Nitrogen budget on the continental shelf off the west coast of Western Australia

This section describes a mass-balance approach that has been used to help identify the major fluxes of nitrogen on the continental shelf.

The continental shelf between North West Cape and Cape Leeuwin off the west coast of WA is, on average, 66 km wide at the 200 m isobath. Due to the influence of the poleward flowing Leeuwin Current, the shelf and offshore waters off the WA coast are oligotrophic in nature and the water-column primary-production is generally low. In the Leeuwin Current off the southwest WA coast, autumn-winter phytoplankton blooms are observed from satellite and in-situ measurements, likely due to nutrient injections by enhanced horizontal advection of the Leeuwin Current and vertical mixing. Enhanced summer production is observed from the North West Cape to Shark Bay due to upwelling favourable winds which episodically overcome the large-scale pressure gradient.

The total nitrogen requirement for the primary production on the continental shelf off the west coast of WA is estimated to be 14.8 gN $m^{-2}y^{-1}$ in the water column, and 2.0 gN $m^{-2}y^{-1}$ in the benthic community, which equates to a total primary production of 111.3 gC $m^{-2}y^{-1}$, or 1.1×10^7 tonne C y^{-1} over the whole shelf. Preliminary estimates indicate that, of the new nitrogen required to support this annual production, 8% is derived from advection by the LC and its eddy field, and 7% from seasonal upwelling. Terrestrial and atmospheric contribution of nitrogen to the shelf accounts for less than 1% of the primary production. Although the direct offshore nutrient inputs may be small, they may still be important in driving the annual cycles in the marine ecosystem on the shelf.

It is estimated that 84% of the primary production is recycled on the shelf, both within the pelagic system and through the pelagic-benthic coupling. Thus, despite the uncertainties in the offshore input estimates, the continental shelf off the west coast of WA must be primarily a recycling system, more typical of wider shelf regions. Improved quantification of benthic-pelagic coupling on the shelf will lead to a better understanding of the marine ecosystem.

Of the total primary production, 7% is estimated to be exported offshore by the LC advection, Ekman transport, and eddy-driven offshore fluxes. This could be an underestimate. The upper limit of the offshore transport could be assumed to balance the onshore nitrogen fluxes (15% of the total production), which equates to a carbon flux of 17.2

gC $m^{-2}y^{-1}$, or 1.7×10^6 tonneC y^{-1} integrated over the whole shelf. Assuming an export flux of 30%, then 5.2 gC $m^{-2}y^{-1}$ or 5.1×10^5 tonneC y^{-1} integrated over the whole shelf, is transported from the shelf to the deep ocean, which equates to 5% of the total shelf primary production.

This work is to be published as follows:

Feng, M & K. Wild-Allen (2008). Productivity and nitrogen fluxes along the downwelling coast off Western Australia. In: *Carbon and Nutrient Fluxes in Continental Margins: A Global Synthesis.* Editors: Kon-Kee Liu, L. Atkinson, R. Quinones, L. Talaue-McManus (in press)

The following figure (Figure 72), from the paper, is a schematic of the nutrient budget.

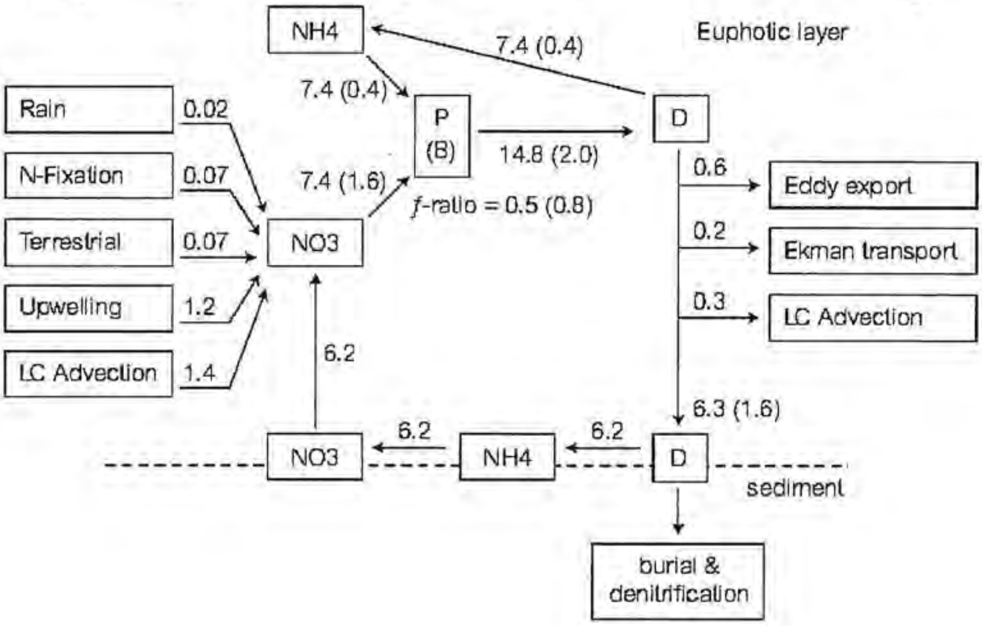

Figure 72. Preliminary shelf nitrogen budget (unit: gN $m^{-2}y^{-1}$). P denotes pelagic production and the contributions from benthic production (B) are given in brackets. D denotes organic detritus.

A 3D Biogeochemical Model of the WA Shelf

The 3D biogeochemical model developed during the SRFME program is being used to quantify a modelled nutrient budget for the region (see Milestone 1.2.2). The model has a 10km spatial resolution and simulates the cycling of carbon and nitrogen through organic and inorganic dissolved and particulate phases including phytoplankton, zooplankton, detritus, nutrient and benthic macrophyte pools. The model simulates a coupled pelagic and benthic system including deposition, remineralisation and resuspension of material.

To date the model has been used to simulate a seasonal cycle of Leeuwin Current activity and biogeochemical cycling along the shelf. Coastal nutrient sources have been shown to play a key role in the simulation of shelf phytoplankton biomass and are essential for the reproduction of near shore elevated chlorophyll concentrations as seen in remotely sensed images and reported from field campaigns (see Milestone 1.2.2).

To compute a modelled nutrient budget for the WA shelf, fluxes of all nutrient components of the biogeochemical model are computed along sections parallel to the shelf break. As the shelf has a convoluted shape this is a non-trivial task and requires the estimation of fluxes along a multitude of short east-west and north-south sections which are then summed to produce a net budget. The budget sums are repeated for each day of simulation and summed for seasonal and annual budget descriptions. Initial results show the cross shelf fluxes to be considerably smaller than along shelf water movements. This suggests the shelf waters are hydrodynamically isolated from offshore waters with cross-shelf exchange dominated by event scale Leeuwin Current meanders and eddy transport. These findings are supportive of the earlier estimates of cross-shelf transport (see above), and the general accumulative knowledge of the system dynamics. Work is ongoing to finalise the modelled budget calculations by the end of June and complete a manuscript for publication.

For consistency with the lagoonal modelling (Milestone 1.1.8), and with modelling in other Nodes of WAMSI, we are also implementing the coupled ROMS hydrodynamics and biogeochemistry at shelf scale.

Incorporating seasonal chlorophyll a dynamics into a BGC model

The phytoplankton pigment, chlorophyll a, is a good proxy for phytoplankton carbon (and nitrogen) content, and relatively easy to measure. It is therefore an important quantity to include in BGC models.

The dynamics of the seasonal evolution of chlorophyll a at the continental shelf break around 32 degrees south has been investigated using a numerical BGC model. The results show that a combination of vertical mixing associated with the Leeuwin Current and surface cooling during the winter months is responsible for the wintertime increase in chlorophyll a concentration. Variation in the timing and magnitude of the winter increase is shown to relate to the strength of the Leeuwin Current. The findings have been published as:
Greenwood, J. & K Soetaert (2008) Interannual variability in the seasonal cycle of chlorophyll within the Leeuwin Current off the southwest Western Australian coast. Journal of Marine Research, 66 (3), pp. 373-390

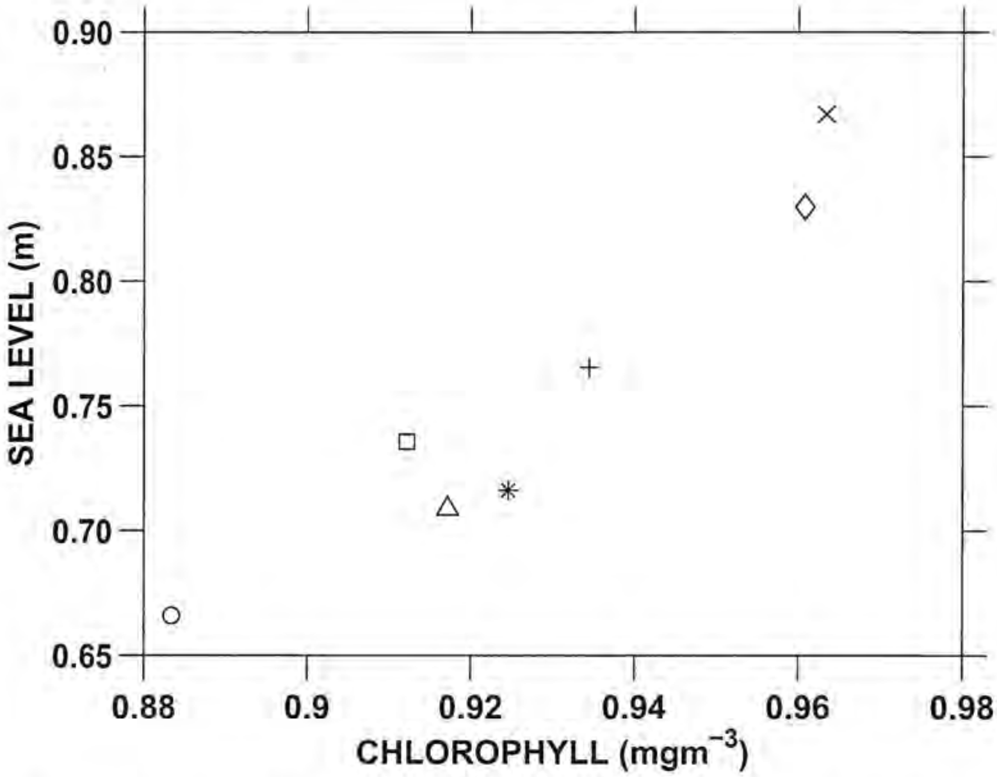

Figure 73. Increase in the magnitude of the autumn chlorophyll a signal in the Leeuwin Current at 32S between 1998 and 2005. Reproduced from Greenwood, J. and Soetaert K. (2008) JMR.

Incorporating regional chlorophyll a dynamics into a BGC model

The regional distribution of chlorophyll on the continental shelf has been investigated using a steady-state phytoplankton growth model. Using the model, chlorophyll a concentration is calculated for any location on the continental shelf by assuming a balance between growth (which is assumed to be light and nitrogen limited) and mortality (which is assumed to be constant). In a depth integrated sense the model is able to predict the cross shelf variation that is observed in chlorophyll a on the SW WA continental shelf (Figure 74).

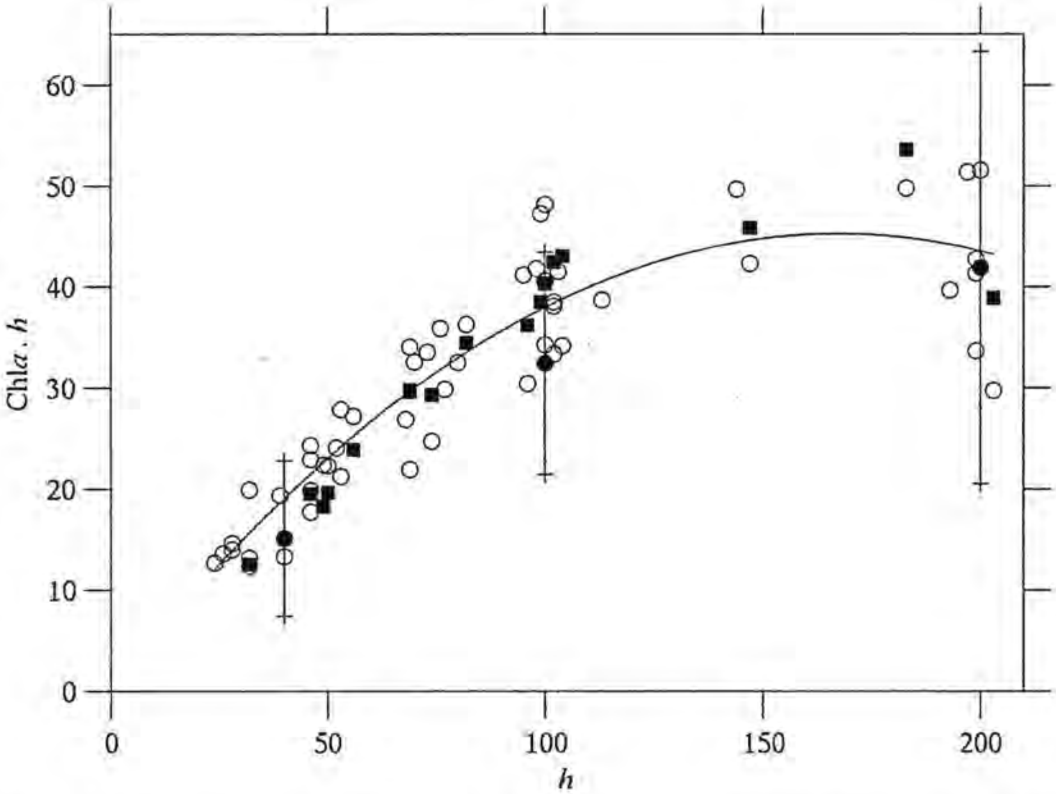

Figure 74. Observations (circles) between 22S and 34S, and model prediction (squares) of the depth integrated chlorophyll a concentration as it varies with shelf depth, h, between the 25 and 200m depth contours.

Incorporating **benthic nitrogen fluxes into a BGC model**

The estimate, reported above, that approximately 40% of the nitrogen production on the shelf could be recycled via the sediment (see Figure 72) has important implications for the modelling tasks that will follow in this project. As a minimum, it requires that some detail of the sediment biogeochemistry must be included in any realistic simulation of the shelf. Coupling between marine sediments and overlying water can be added to a BGC model in different ways. To help make an informed choice of how best to represent the sediment biogeochemistry for the lagoon and shelf scale models, a number of simplified numerical experiments have been conducted to examine likely interactions between the water column and the sediment.

The response of pelagic production to changes in the sediment nutrient flux has been investigated using a coupled pelagic-benthic model configured at different water depths. Model results have shown that variations in this flux within the range of field measurements can account for observed seasonal variations in surface chlorophyll. This flux could be affected by hydrodynamics. As an example of this, the benthic nitrogen flux has been linked to the surface wave field in a 1-D BGC model (following the completion of milestone 1.2.3). The model is able to provide a good simulation of chlorophyll a biomass for at least six years of observations at a 40m station on the inner shelf (Figure 75).

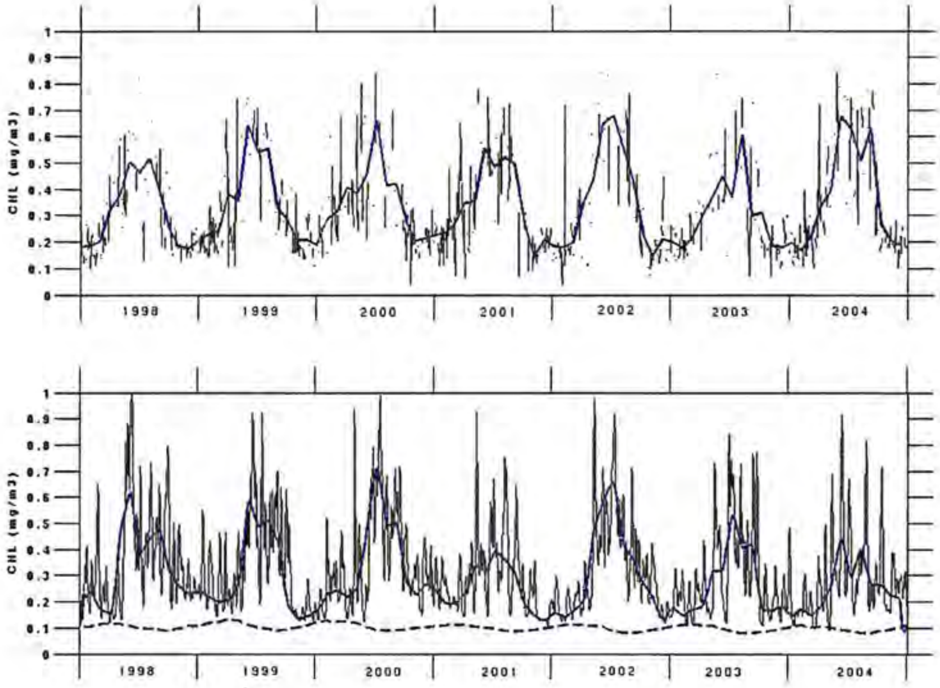

Figure 75

Agreement between model simulation of the seasonal variation in surface chlorophyll (lower panel) and satellite observations (upper panel) between 1998 and 2004. In each panel the black line represents daily values, and the blue line is the monthly mean. For comparison, in the lower panel the broken blue line is the monthly mean chlorophyll simulated by the model when wave forcing is removed.

A similar 1-D BGC model has been used to investigate how fluxes between the water column and sediment are modified by the presence or absence of key benthic biota. Results show that benthic production tends to dominate over pelagic production when the system is closed (i.e. no external nutrient sources). This pelagic-benthic balance has been shown in model simulations of a 20m water column and underlying sediment to be sensitive to changes in water column mixing rate (Figure 76) and benthic grazing (Figure 77), with strong vertical mixing and high levels of benthic grazing seen to cause important changes to the vertical distribution of chlorophyll in the water column.

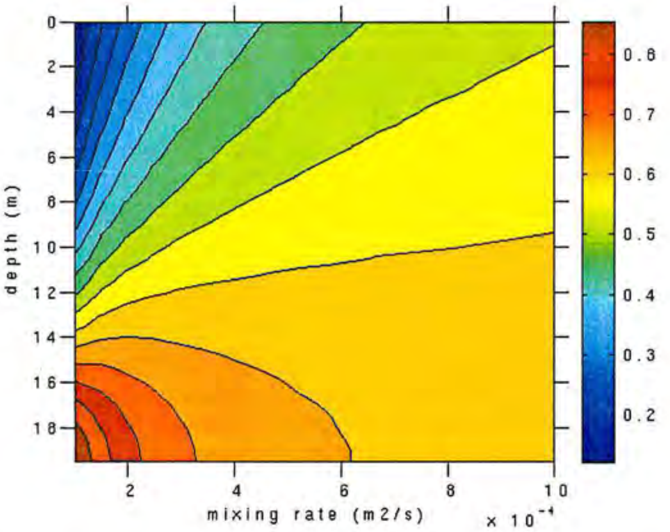

Figure 76
Variation in the steady-state simulated water column distribution of chlorophyll (mg m^{-3}) with changes in the vertical mixing rate

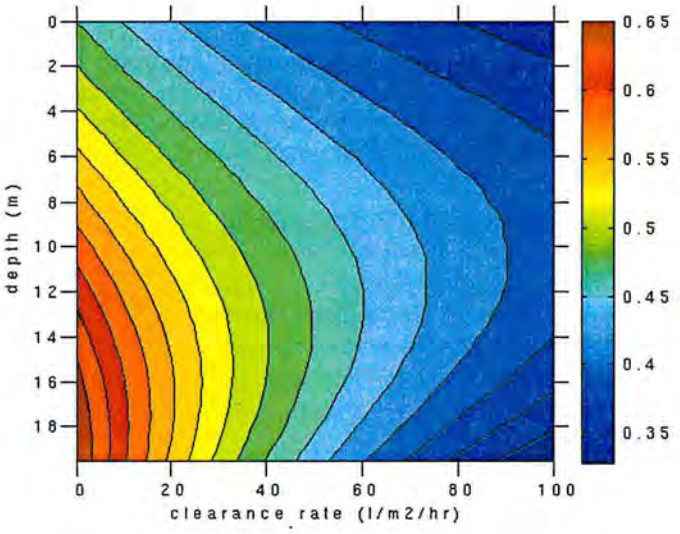

Figure 77
Variation in the steady-state water column distribution of chlorophyll (mg m^{-3}) with changes in the clearance rate of benthic filter feeders

Incorporating underwater light dynamics into a BGC model

The fixation of atmospheric carbon by autotrophic plankton is a major flux of carbon in biogeochemical ocean models, and is critically dependent on available sunlight. The attenuation of light with water depth is therefore an important parameterisation in BGC models, and warrants separate attention. This is especially true when benthic production is important, since the sea bed often receives very small amounts of light. Moreover, modelling underwater light can often be problematic in near-shore and shelf environments, where both inorganic and organic constituents can strongly affect the transparency of the water column.

In preparation for this challenge, of the underwater light field along the Western Australian coast has been analysed and modelled. Over 450 light profiles, collected from shelf depths between 10 and 500 m, have been compared with a light attenuation model to determine the rate of attenuation of the downward component of light. The result is that Light attenuation decreases exponentially with increasing shelf depth until it reaches a minimum of approximately 0.06 m^{-1} around the 100-150 depth contour (Figure 78). The increase in attenuation toward the coast appears to offset the effect of a shallowing seabed, so that there is little difference between the amount of light that reaches the seafloor inside the coastal lagoon and the amount that reaches the seafloor at mid-shelf depths (Figure 79).

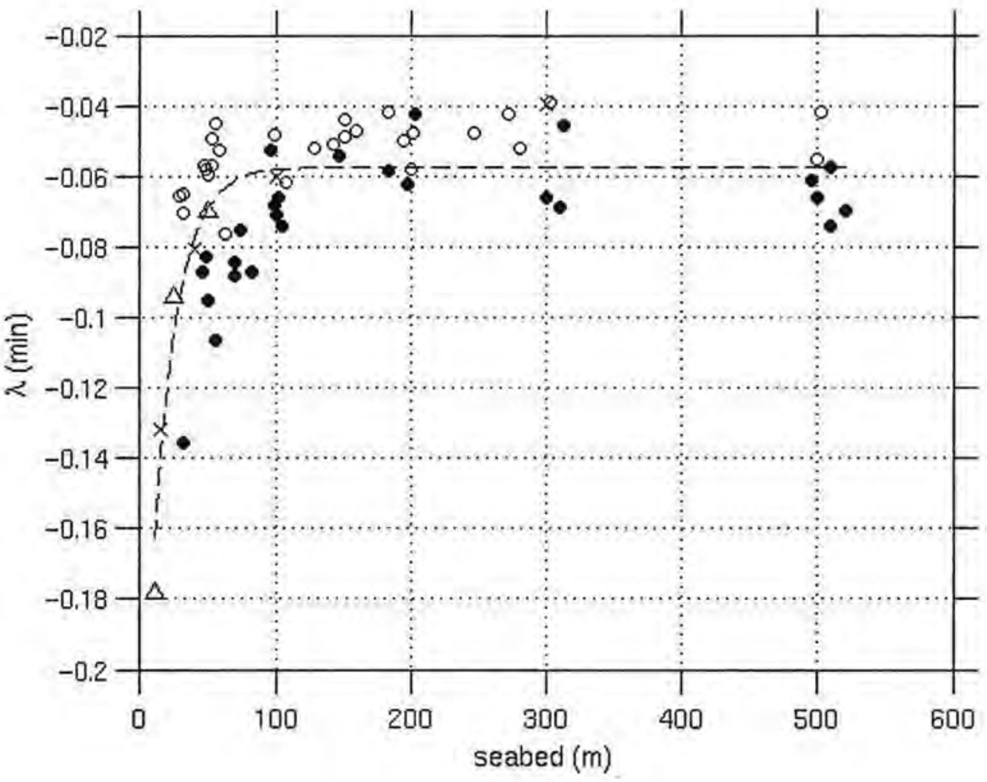

Figure 78

Variation in the diffuse daylight attenuation with depth of seabed calculated from light profiles measured along the WA coast between 2002 and 2007 (• SS 2007, o SS 2003, × Two Rocks transect, △ Marmion and Rottnest).

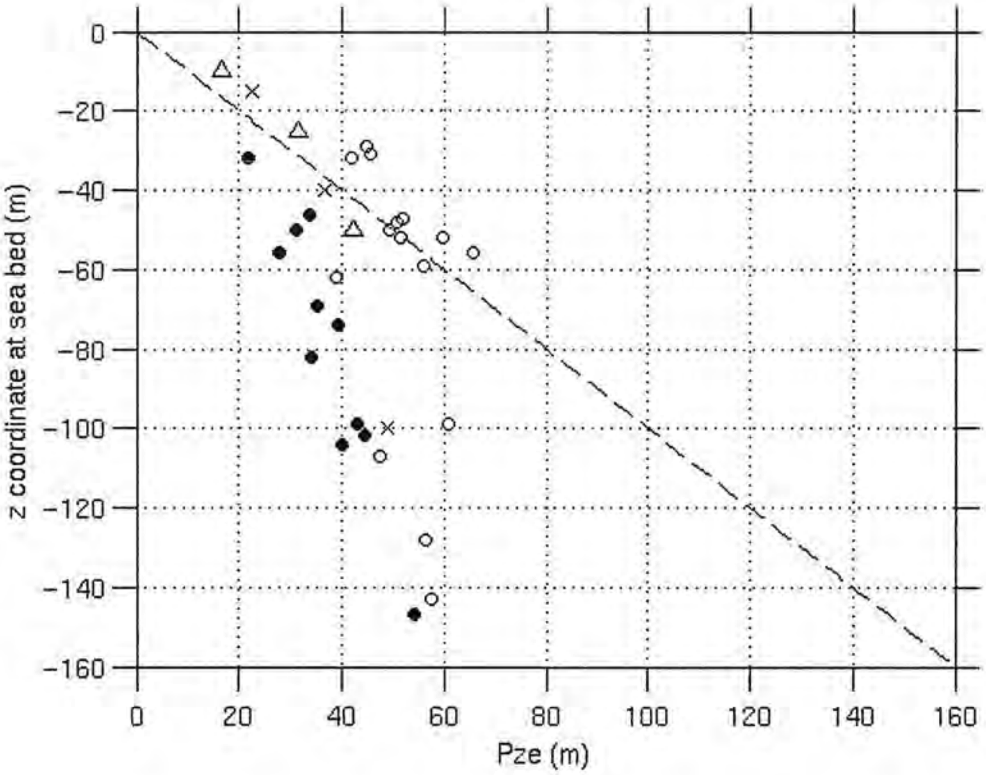

Figure 79
Potential euphotic depth (Pze) compared with total water column depth, for various shelf locations of differing water column transparency. Symbols are the same as used in Figure 78. The broken line shows the coincidence of the 1% light level with the sea floor. Points above this line indicate locations when more than 1% light reaches the seafloor, and points lying below the locations where less than 1% light reaches the seafloor.

3. Improved descriptions and conceptual biogeochemical models for shelf and lagoon waters incorporating seasonal and interannual variability and improved representation of benthic primary production and bentho-pelagic coupling.

Milestone 1.3.1: Complete Southern Surveyor "autumn bloom" cruise

Original Forecast Finish Date: 30/06/07

Revised Forecast Finish Date: 30/06/07

This section updated from previous Biannual Report

Summary of Activities Undertaken, Outputs Produced:

The cruise was hugely successful and we were fortunate enough to complete all the cruise objectives. The timing of the cruise was perfect, the Leeuwin Current was running very strongly and the entire continental shelf was experiencing a very large phytoplankton bloom. A brief summary of the voyage and several more detailed examples of the research undertaken are provided here and under milestone 1.3.4.

The May-June 2007 "autumn bloom cruise" on the National Marine Facility, *Southern Surveyor*, has been completed. With the departure of Tony Koslow the cruise was led by Peter Thompson. The voyage was conducted in three legs beginning in Fremantle on May 10 and concluding in Dampier on June 6. Researchers from WAMSI partners CSIRO, UWA, Murdoch Uni and the WA Museum, as well as Geosciences Australia, participated in the voyage.

The cruise plan which originally focused on the pelagic ecosystem productivity and dynamics off the west coast of Western Australia was revised to include a larger benthic and near-shore research component in light of recent findings described in the section above on "Nitrogen budget on the continental shelf off the west coast of Western Australia" which highlighted the importance of highly productive benthic habitats and nutrient recycling on the shelf.

The first leg of the voyage included a sampling regime designed to characterize benthic habitats and measure benthic biomass and primary productivity and sediment nutrient fluxes across the shelf between 30 and 150 m depths. Sampling across the domain shown in Figure 80 below included swath mapping, towed video, benthic sleds, sediment grabs and cores and CTD profiles. Detail from the first leg of the voyage relating to benthic work is included under milestone 1.3.4.

The Scientific Objectives for the 2nd and 3rd legs of the voyage relate to factors regulating the seasonal plankton cycle and it's inter annual variability, which remain poorly understood in this region. One of its most interesting features is the ~ ten-fold increase in chlorophyll, which coincides with the seasonal intensification of Leeuwin Current flow. Research conducted during the voyage was designed to examine:

- the regional extent of this bloom

- key drivers for primary production:
    - stratification
    - depth of the mixed layer
    - the influence of Leeuwin eddy dynamics
    - local wind-driven upwelling
    - alongshore and cross-shelf advection,
- plankton food web structure during the bloom
    - the relative importance of picoplankton and larger phytoplankton
    - micro- and meso-zooplankton
    - links with larval and juvenile fish in relation to onshore-offshore and north-south oceanographic features.
- If a suitable eddy had formed off the west coast between May 15th and May 20th we proposed to spend 1-3 days mapping the features of the eddy and sampling it. We were fortunate to encounter a large eddy forming at ~ 31°S. We took the opportunity to sample across the eddy providing additional data for comparison with eddies studied in 2003 and 2006. The data collected will be extensively used in David Holliday's PhD thesis.

The voyage plan was based on 13 CTD onshore-offshore transects undertaken every degree of latitude from Northwest Cape (22° S) to Capes Naturaliste and Leeuwin (34° S). Each transect extended from as near shore as is practicable (25 – 30 m depth) to 2000 m depth (Figure 80). Stations were undertaken at 25 (inshore), 50, 75, 100 (mid-shelf), 200 (shelf-break), 300, ~500 (Leeuwin core), 750, 1000, and 2000 (offshore) m water depths.

Each transect leg had a complimentary seasoar return leg to giving very high resolution vertical and horizontal X-sections of temperature, salinity and fluorescence. These have provided the best physical description of the Leeuwin Current ever obtained. They were also used to locate a station in the middle of the Leeuwin Current on each subsequent CTD transect. The SeaSoar mapping combined with current satellite images enabled us to place the 'Leeuwin' station within the core of the Leeuwin Current on each transect. CTD profiles were carried out at all stations to measure temperature, salinity, dissolved oxygen, PAR, and chlorophyll fluorescence. Water samples were taken at standard depths to measure salinity and nutrients (nitrate/nitrite, ammonia, dissolved organic nitrogen, particulate nitrogen, phosphate, silicate). Full biological sampling was carried out at the inshore (25 m), Leeuwin Current (200 - 500 m) stations, and offshore (2000 m), incorporating: replicate oblique bongo tows to 150 m maximum; the light profile to 50 m using a hyperspectral radiometer; water samples for phytoplankton pigment (HPLC) analysis and species composition from near-surface and chlorophyll maximum depths; measurement of size-fractionated primary productivity (^{14}C incubation method and PAM measurements from standard sampling depths); nitrogen uptake from labelled nitrate, ammonia, and N_2; sampling of stable C and N isotopes in the size-fractionated phytoplankton and in selected zooplankton and ichthyoplankton species to examine food web pathways; microzooplankton grazing based on the dilution method (Landry and Hassett, 1982); total alkalinity & DIC (to assess pH); and secondary production estimates based on egg production and a biochemical (aminoacyl-tRNA synthetase (Yebra and Hernandez-Leon, 2004)) assay. Zooplankton acoustic backscatter (using the 6-frequency Trachor

Acoustic Profiling System, TAPS) was measured through the water column to a depth of 200 m. Net tows for zooplankton were split, with part retained in ethyl alcohol to examine selected larval fish otoliths for growth to be related to oceanographic conditions. Neuston sampling was also carried out at each production station. The voyage track is shown in Figure 80.

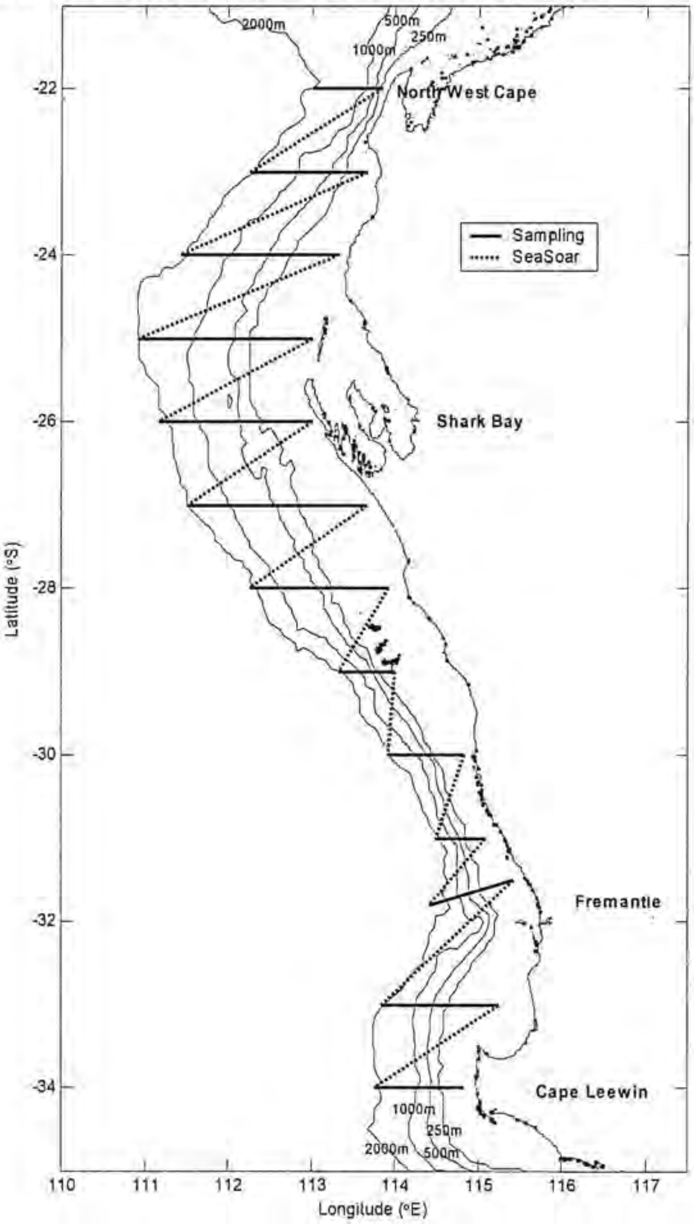

Figure 80. Southern Surveyor voyage track fro May/June "autumn bloom" cruise.

Mesozooplankton sampling during the Southern Surveyor cruise included collecting replicate Bongo tows using 355 and 100 µm mesh nets at 25, 50, 100, 300 and 100 m stations to 150 m depth for species composition and biomass on the 13 transects. Sampling was conducted during both the day and night. Grazing experiments to quantify mesozooplankton grazing on microzooplankton and phytoplankton were conducted at 4 transects (once at every geographic region) at 3 stations situated nearshore of Leeuwin Current, in Leeuwin Current and offshore of Leeuwin Current. Secondary production samples for Aminoacyl-tRNA synthetases (AARS) activity were collected. Female copepods were collected to measure the DNA/RNA ratio. The mesozooplankton portion of the project involves collaboration with AIMS where Felipe Gusmao is testing new techniques of estimating secondary production of zooplankton. In addition standard techniques of estimating secondary production: egg production and artificial cohort incubation will be run at 3 stations on all transects.

A large number of scientists, students and support staff were involved in the cruise. A summary of those involved and their roles is provided below.

Leg 1: May 10th to May 15th

PERSON	ORGANIZATION	ROLE
Peter Thompson	CSIRO	Chief Scientist
John Keesing	CSIRO	Benthic sampling
Martin Lourey	CSIRO	Primary production nutrient efflux
Bruce Barker	CSIRO	Camera operation
Jeff Cordell	CSIRO	Camera operation
Mark Lewis	CSIRO	Gear/camera operations
Karen Gowlett-Holmes	CSIRO	Invertebrate analysis
Andrea Cortese	GA	benthic (swath) mapping
Rick Smith	CSIRO	Swath support
Mark Salotti	WA Museum	Invertebrate analysis
Julia Phillips	CSIRO	Benthic plant physiology
Ron Plaschke	MNF	Voyage Manager
Pamela Brodie	MNF	Computing support
Drew Mills	MNF	Electronics support
Mark Rayner	MNF	Hydrochemistry

Leg 2. May 15th to May 21st

Peter Thompson	CSIRO	Chief Scientist
James McLaughlin	CSIRO	C14 uptake
Joanna Strzelecki	CSIRO	Zooplankton grazing
Pru Bonham	CSIRO	Pigments
Cecile Rousseaux	UWA	Microzooplankton grazing
Nugzar Margvelashvili	CSIRO	Zooplankton acoustics
Harriet Patterson	UWA	Flow cytometry
David Holliday	Murdoch Uni	Larval fish
Lynnath Beckley	Murdoch Uni	Larval fish
Martin Lourey	CSIRO	N15 uptake
Lindsay Pender	MNF	Seasoar operations
Pamela Brodie	MNF	Voyage Manager & Computing
Stephen Thomas	MNF	Electronics support
Dave Terhell	MNF	Hydrochemistry
Mark Rayner	MNF	Hydrochemistry

Leg 3. May 21st to June 6th

Peter Thompson	CSIRO	Chief Scientist
James McLaughlin	CSIRO	C14 uptake
Joanna Strzelecki	CSIRO	Zooplankton grazing
Pru Bonham	CSIRO	Pigments
Cecile Rousseaux	UWA	Microzooplankton grazing
Nugzar Margvelashvili	CSIRO	Zooplankton acoustics

Harriet Patterson	UWA	Flow cytometry
David Holliday	Murdoch Uni	Larval fish
Lynnath Beckley	Murdoch Uni	Larval fish
Martin Lourey	CSIRO	N15 uptake
Karen Wild-Allen	CSIRO	ocean optics
Pamela Brodie	MNF	Voyage Manager & Computing
Stephen Thomas	MNF	Electronics support
Dave Terhell	MNF	Hydrochemistry
Mark Rayner	MNF	Hydrochemistry

Much of the data collected during the research voyage has been fully processed since the voyage was completed and is currently undergoing interpretation. Examples include CTD data (available in August 2007) and ADCP data (available in December 2007). In some cases samples are still undergoing analysis (e.g. stable isotopes). Some samples have been analyzed but are still undergoing quality control checks (e.g. nutrients). As a consequence of the variable status of the data from this cruise different components of the interpretation are at different stages. Several examples of the cruise outputs are presented below. These are only representative, sometimes only partly completed and are meant to be indicative. A symposium based on the early results from the cruise was conducted in February 2008.

Nutrients

New in-situ observations of nitrate with very high vertical resolution have been obtained during the SS0407 cruise. For the first time in Australia an in-situ profiling underwater spectrophotometer was deployed with the capability to resolve nitrate concentrations at 2 m depth resolution. The preliminary calibration shows significant sub-bottle scale structure in nitrate profiles consistent with temperature and salinity structure, particularly in the vicinity of the Leeuwin Current fronts and mesoscale eddies. Figure 81 shows examples of this nitrate data.

This work was presented at the WAMSI symposium as: Wild-Allen 'Nutrient Sources for Phytoplankton in the Leeuwin Current'.

Full calibration of the instrument is now in progress.

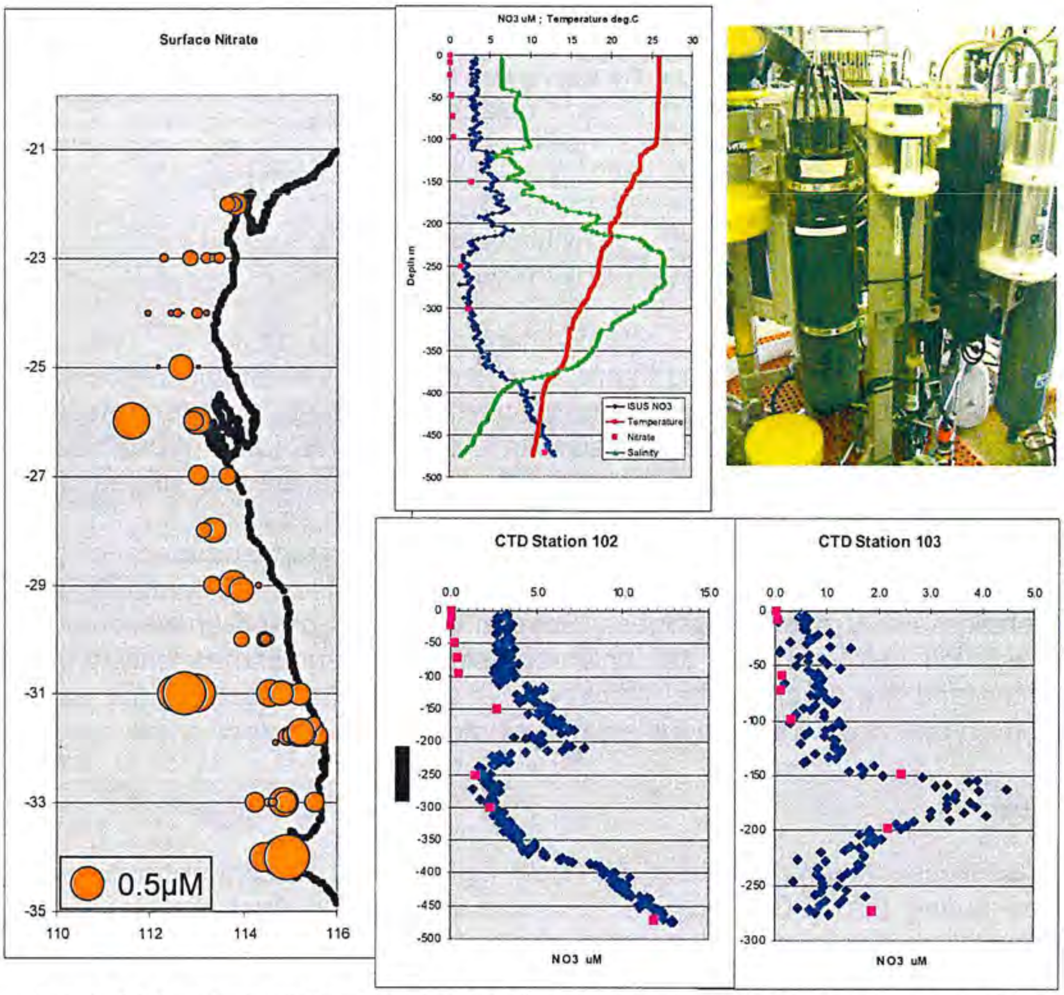

Figure 81. Example nitrate data from the SS0407 cruise. Preliminary in-situ nitrate sensor calibration suggests significant spatial and sub-bottle scale variation in nitrate concentration.

Benthic Microalgae

One outcome from SRFME has been an increased emphasis upon shelf processes on the cycling of nutrients. Portions of the WA coast have a relatively wide continental shelf with a large area of soft bottom sediments capable of supporting communities of benthic microalgae (BMA). The BMA in these sediments contribute to food webs, and play an important role in the nutrient cycling of coastal ecosystems worldwide but the role of BMA in nutrient cycling and primary production for the west coast of Australia is largely unknown. Worldwide there have only been ~ 85 studies of BMA and none of these have ever determined the depth at which BMA primary production reaches zero (Cahoon 1999). In fact only a handful of measurements exist at depths > 60 m.

The research voyage (SS04/2007) departed Fremantle, WA at 1600hrs, Thursday, 10 May 2007. The first 5 days of scientific investigation were a benthic survey of the shallow (30 – 150 m) bottom habitats off Perth (Figure 82). The benthic survey included high resolution 'swath' mapping, underwater video surveys of the bottom, benthic sampling by sledges and grabs with 12 ctd casts and associated water column sampling. The remaining 23 days of the research voyage involved mostly water column sampling from 34°S to 22°S with benthic grabs on the inshore legs of most transects (Figure 82).

BMA samples were collected using a Smith MacIntyre grab at depths from 28 to 140 m. Samples were only used if a visual inspection indicated a largely intact sample had been collected. The grab allowed some of the overlying water to escape during recovery and may have dislodged any unattached cells on the surface (e.g. sedimented phytoplankton). Once on deck the grab sample was cored by hand. Cores for flux incubations were sealed at the bottom with overlying water retained on top. At each site a conductivity, temperature and depth (CTD) cast using a Seabird SBE 911 dual conductivity (practical salinity units = PSU), temperature (°C), fluorescence was measured with a Chelsea Aquatracka™ fluorometer and a Licor LI-192SA sensor was used for photosynthetically active radiation (PAR) while multiple depths sampled for nutrients. Continuous underway data included PAR collected by a Licor LI-192SA sensor attached to the mast head. Samples were analysed for nitrate, nitrite, silicate and phosphate concentrations using Quick-Chem™ methods on a flow injection LACHAT® instrument as per the following protocols for nitrate and/or nitrite (Quik-Chem™ Method 31-107-04-1-A; detection limit ~0.03 µM; adapted from Wood et al. 1967), silicon (Quik-Chem™ Method 31-114-27-1-D; detection limit ~0.05 µM; adapted from Murphy and Riley 1962) and phosphate (Quik-Chem™ Method 31-115-01-1-G; detection limit ~0.02 µM; adapted from Armstrong 1951). Samples were analysed for ammonium on the LACHAT® instrument using the technique of Kerouel and Aminot (1997) adapted for flow injection by Watson et al. (2004), detect limit ~ 0.05 µM.

Material for pigment analysis was taken from the same grab samples used for nutrient, oxygen fluxes and PAM measurements. The top 4mm of the sediment surface was removed for pigment analysis by HPLC analysis. These were immediately preserved in liquid nitrogen. The top 20 mm was removed for pigment analysis by fluorometry. These samples were immediately extracted in 100% acetone in the dark at 4°C ~ 24 h before analysis on the calibrated Turner Designs model 10AU™ fluorometer. For HPLC analysis sediments were extracted twice in 100% acetone at 4°C, firstly for 18 hours and then for 4 hours. Following extraction, water was added to give a ratio of 9:1 acetone:water by volume, and filtered (0.2µm membrane filter; Whatman Anatop, Whatman plc, Brentford, UK) before analysis by HPLC. The analysis was by a Waters high performance liquid chromatography (Waters Corporation, Milford MA, USA), comprising a model 600 controller, 717 plus refrigerated auto-sampler, and a 996 photodiode array detector. Pigments were separated as described by (Wright, Jeffrey et al. 1991), detected at 436 nm, and identified against standard spectra. Concentrations of chlorophyll *a* (chl*a*), chlorophyll *b* (chl*b*), β,β carotene, and β,ε carotene in sample chromatograms were determined from standards, and all other pigment concentrations were determined from standards of purified pigments isolated from algal cultures. Information for the assignment of microalgal marker pigments was drawn from Jeffrey et al. (1997).

Fluorescence parameters of BMA communities were measured in cores with a Phyto PAM multi-channel fluorometer (Heinz Walz GmbH, Effeltrich, Germany) fitted with a Phyto-EDF fibre-optic attachment, designed for use on biofilms. After collection cores were allowed to re-equilibrate for several hours at in situ temperatures and in the dark prior to measuring photosynthetic parameters using the PAM. Microalgal cultures from the CSIRO Collection of Living Microalgae were used to calibrate the taxonomic discrimination of the measuring software (Phyto Win v1.46, Heinz Walz GmbH, J. Kolbowski). The cultures used were- brown: *Navicula jeffreyi* (CS-46), green: *Dunaliella* sp. (CS-353), blue-green: *Oscillatoria* sp. (CS-52). Given the reference spectra used in the Phyto PAM, "browns" are approximately equivalent to any species with chlorophyll c (referred to hereafter as browns) greens would contain chlorophyll b (= "greens") and cyanobacteria would contain zeaxanthin ("blue-greens"). F_o (the initial minimal fluorescence yield) was measured at 25 Hz; all fluorescence terminology is consistent with Buchel and Wilhelm (1993). Saturating irradiance pulses were applied and then a series of pulsed illuminations provided estimates of relative electron transport rates which were used to construct rapid light curves and fit to the model of Eilers and Peeters (1988) to estimate photosynthetic parameters I_k, ETR_{max} (maximum electron transport rate) and alpha (α = initial slope of irradiance vs ETR curve). The parameter ΔF is defined as the difference between the fluorescence yield from a saturating pulse (maximum yield, F_m) and the yield (F) from the measuring level of irradiance i.e.:

$$\Delta F = (F_m - F)$$

Visual inspection suggested the sampled cores ranged from undisturbed to moderately mixed. We therefore suggest that greater than normal variability may be present in the data with a possible negative bias in the results for BMA biomass and production. Pigment biomass (0 – 20mm) was a negative exponential function of depth (Figure 83) but with considerable scatter. Work is underway to include a greater range of near shore data from SRFME into these analyses with the hope reducing the variability. Small scale variability, however, is a well know feature of BMA and a well estimated mean value is likely to be the most useful parameter for biogeochemical modelling.

Estimated concentrations of chlorophyll *a* at zero depth (shore) were ~ 54 mg m^{-2}, somewhat below those values observed in Cockburn Sound (Forehead 2006). BMA samples over 0 – 4 mm and analysed by HPLC tended to have less pigment than those from 0 – 20 mm (Figure 83). Both 0 – 20 and 0 – 4 mm samples declined exponentially with depth reaching very low concentrations ~ 95m. The irradiance also declined exponentially with depth reaching ~ 0.9 µmoles photons m^{-2} s^{-1} at 95 meters (Figure 83). We suggest 95 meters and ~ 0.9 µmoles photons m^{-2} s^{-1} represent the maximum depth of net positive growth for BMA if using light as the sole energy source.

Conclusion: The results suggest that BMA biomass may be modelled as a simple exponential decay function of depth or as a linear function of bottom irradiance.

In the middle portion of the continental shelf (30 – 60m) diatoms comprised about 80% of the BMA biomass (Figure 84). This result is consistent with many other studies on the community composition of BMA, albeit most published studies have sampled at much shallower depths. Only at depths > 60m did other pigments increase their proportional contribution in a major way. At ~ 90m chlorophyll *b* increased as a proportion of chlorophyll *a* suggesting relatively more chlorophytes (possibly macrophyte debris or seagrass debris, Figure 84). At 138m alloxanthin and zeaxanthin were relatively high. The increase in alloxanthin may represent more cryptophytes or longer retention of this pigment by zooplankton. Even though alloxanthin and zeaxanthin both increased at 138 m they remained minor pigments found primarily in relatively deep waters where the BMA biomass was very low and BMA are unlikely to play a significant role in the active nutrient cycling. They may represent the accumulation of phytoplankton cells sinking out of the water column above and thus represent a vertically important flux but their role as active primary producers is likely to be insignificant (see later). They may also have a role in seeding phytoplankton back into the water column during times of strong vertical mixing. In particular the cryptophytes are known to produce a range of cysts for this purpose. They are also notoriously difficult to detect in samples preserved for microscopic examination due to their tendency to decompose.

Conclusion: Diatoms dominate the BMA community.

A range of photosynthetic parameters were measured using pulse amplitude modulated (PAM) fluorometry. The data all suggest that at depths > 100m the BMA are not photosynthetically active as both ΔF and active chlorophyll *a* declined to near zero as depths exceed 100 m (Figure 85). At shallow depths fluorescence parameters suggest primary production was an exponential function of irradiance. The rate of primary production is proportional to the electron transport rate (ETR) and can be modelled as:

$ETR = ETR_{max} (1\text{-}e^{aE})$

where ETR = electron transport rate, ETR_{max} is the maximum rate, *a* is a constant and E is irradiance. The observed data fit the model well as shown in the example (Figure 85) where $r^2 = 0.98$. The model output gives estimates of:

1. alpha (α) the initial slope of the primary production versus irradiance slope,
2. ETR_{max}, the maximum rate of electron transport
3. I_k the irradiance which half saturates primary production.

All three of these parameters varied with depth (Figure 85), all declining with increasing depth. In particular ETR_{max} was a negative exponential function of depth with a very high correlation ($r^2 = 0.94$) indicating that BMA primary production can be modelled from depth or an estimate of irradiance on the bottom.

Conclusion: BMA primary production can be modelled from depth or an estimate of irradiance on the bottom.

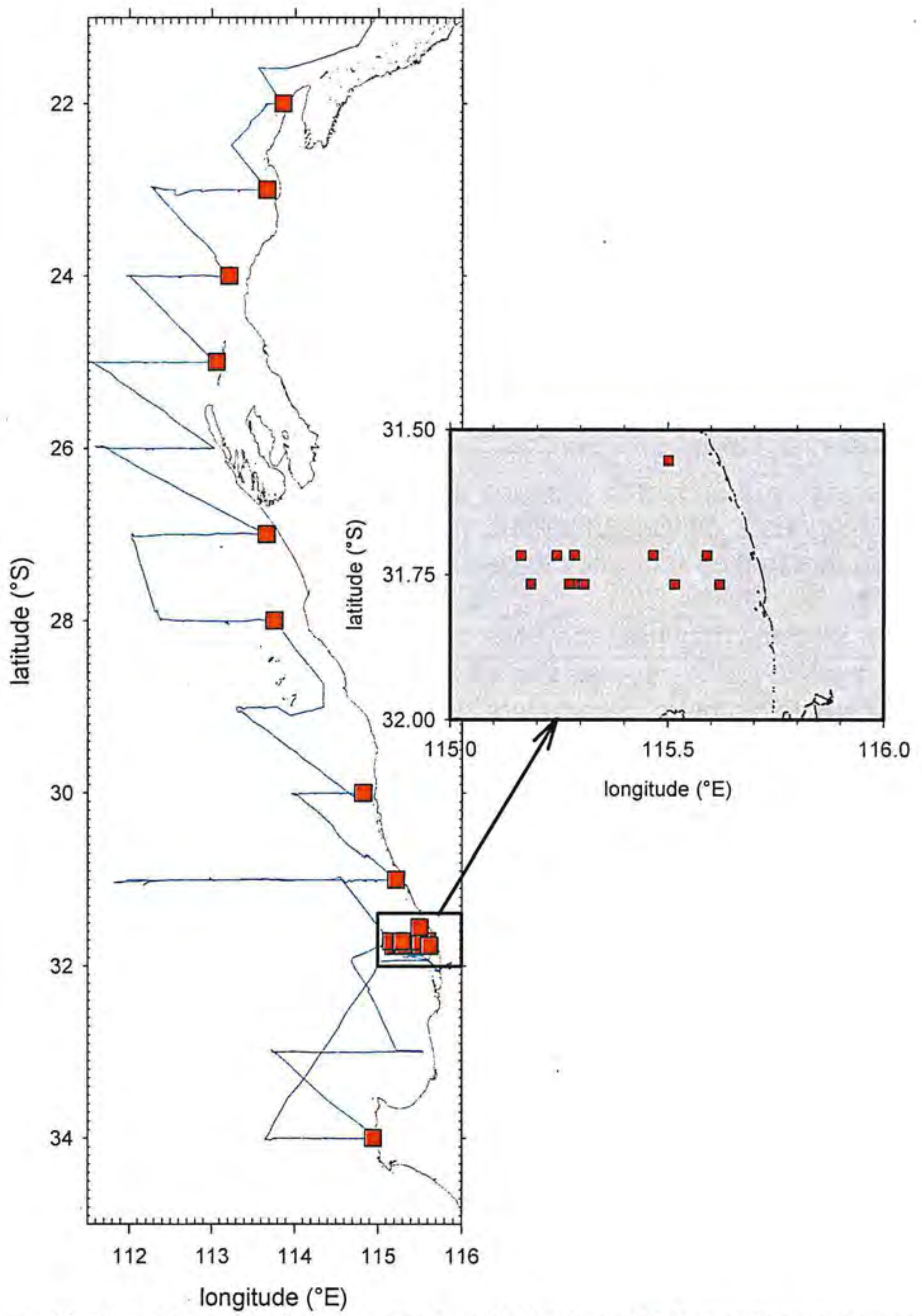

Figure 82. Map showing cruise track and sample locations (🟥) for benthic microalgae.

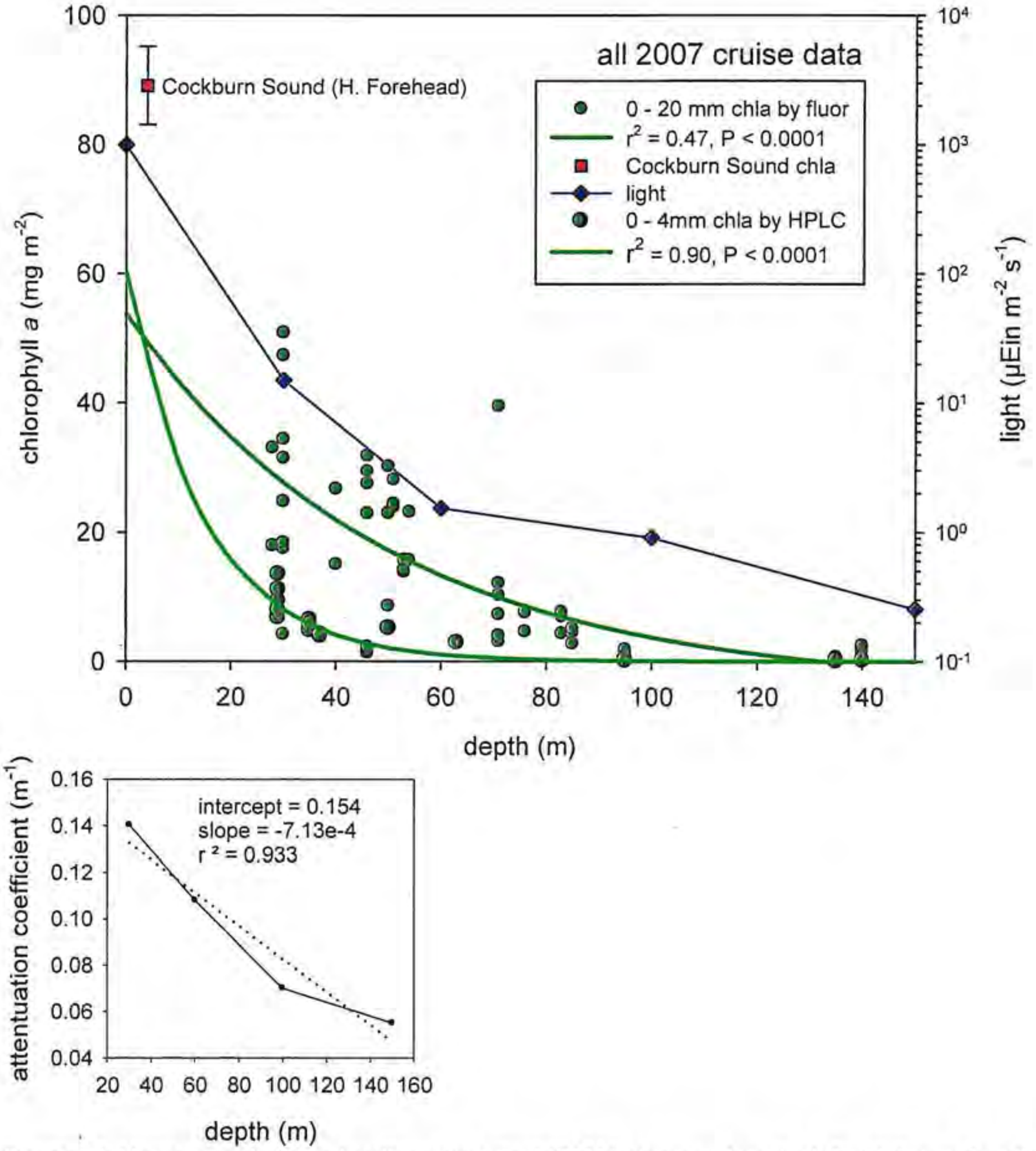

Figure 83. Upper panel shows benthic microalgal (BMA) biomass (y-axis, left side) as a function of water depth for 0 – 20 mm cores measured by fluorometry and 0 – 4mm cores measured by HPLC. Both data sets are fit to exponential decay curves:

$$y_d = y_0 e^{-bd}$$

where y_d = BMA biomass at depth (d), y_0 = BMA biomass at zero depth, *b* is a constant and *d* is depth. From the light versus depth data collected during CTD casts in this region the attenuation coefficients were calculated:

$$E_d = E_0 e^{-kd}$$

where E_d = light at depth (d), E_0 = light just below the surface, *k* = the attenuation coefficient and *d* = depth. Attenuation coefficients ranged from 0.14 to 0.055 m^{-1}.

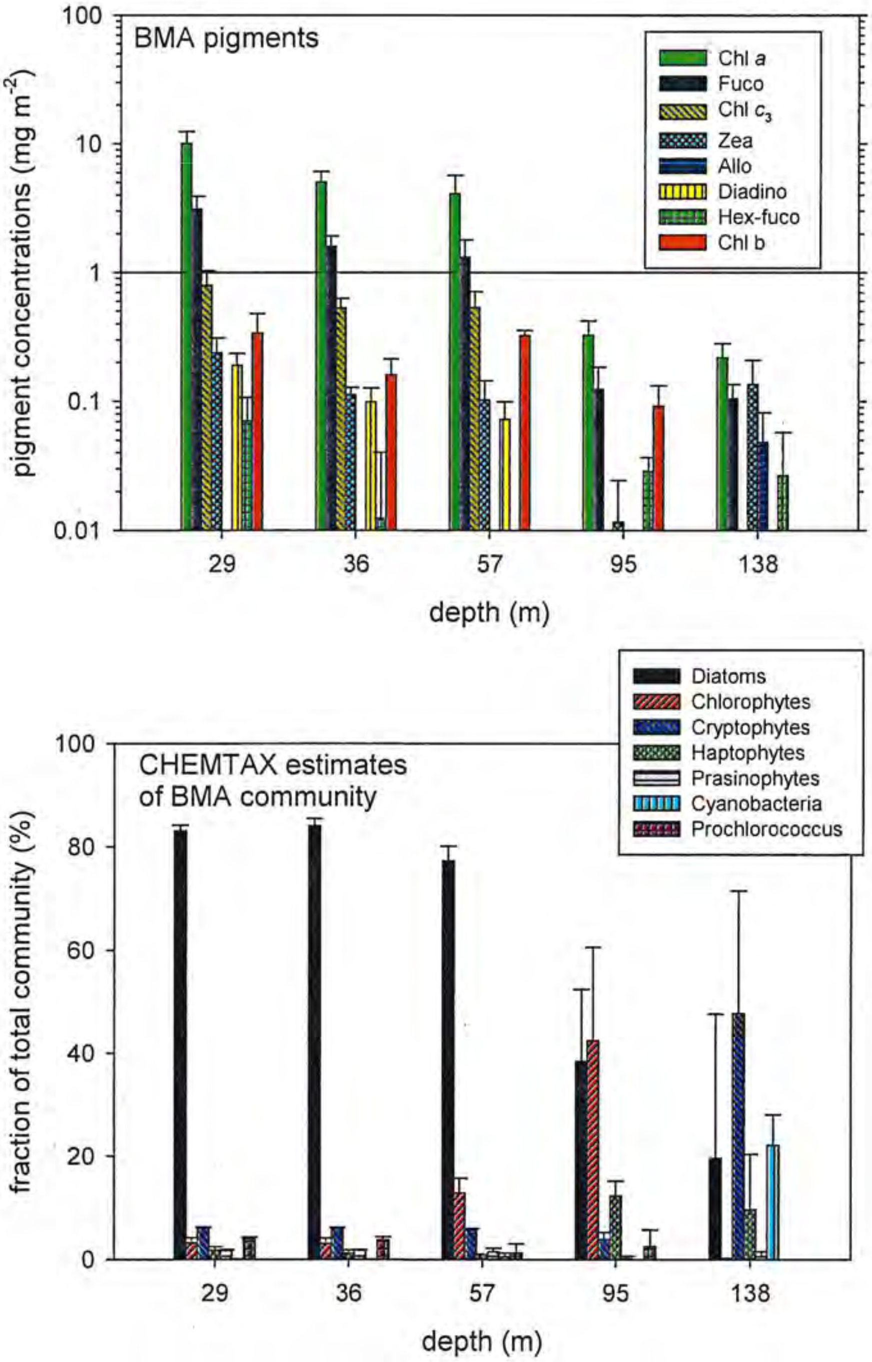

Figure 84. Pigment data for 0 – 4 mm cores obtained from benthic grabs at different depths at sites off Perth (see inset Figure 82). Samples were analysed by HPLC and data processed through CHEMTAX (Mackay et al. 1996) to estimate community composition of the BMA.

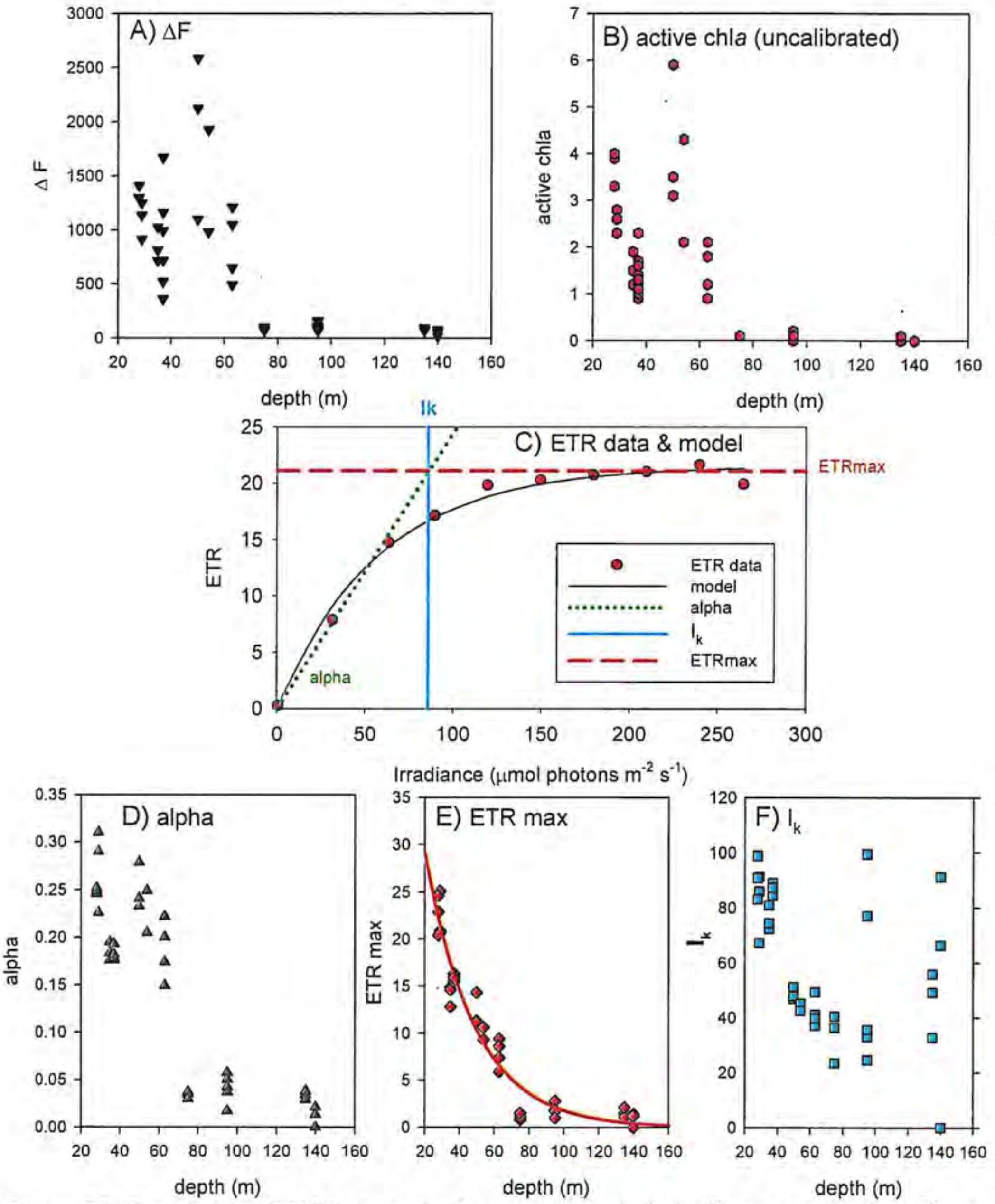

Figure 85. Results from PAM fluorometry for cores collected at different depths (see Figure 82 for locations).

Long term analysis of biological oceanography

In conjunction with colleagues in NSW we have analysed the long term records obtained from 4 coastal stations around Australia. The comparison provides unexpected insights into regional differences in oceanography and climate change. There were significant differences in the magnitude and timing of seasonal dynamics in temperature, salinity, nutrients, chlorophyll *a* and stratification (Figure 86A-E). All stations showed positive long term (> 10 year) linear trends in temperature, salinity, nitrate, and phosphate concentrations (Table 8). All stations showed a long term increase in depth-averaged salinity of ~ 0.003 ± 0.0008 y^{-1}. The fastest warming was in the western Tasman Sea; where it averaged 0.0202°C y^{-1} for more than 60 years. Warming trends were not intra-annually uniform with some months showing strong long term trends while there was no evidence of any warming in midwinter (July) at any station. A pronounced decline in the concentration of silicate was evident at the 3 east coast stations with depth-averaged concentrations falling by as much as 0.058 µM y^{-1} over the last ~ 30 y. A large region of the ocean off the southern west coast had positive chlorophyll *a* anomalies strongly associated with La Nina conditions. Although the phytoplankton data sets were much less comprehensive; diatoms tended to dominate, especially during periods of low stratification. In conclusion, changes in ocean circulation associated with climate variability appear to have pronounced effects on temperate zone biological oceanography, some effects that are not readily generalized from existing conceptual models.

Rottnest Island. Surface nitrate concentrations at Rottnest Island tended to be variable with near zero values recorded in every month of the year (Figure 87A). In spite of the high temporal variability there was a significant seasonal trend and fitting the data to a Gaussian curve showed a significant ($r^2 = 0.111$, $P < 0.0001$, $n = 462$) rise to ~ 0.7 µM in June peaking at day 172 ± 4.8 ($P < 0.001$). Silicate concentrations showed less seasonal variation than nitrate (data not shown) and no inter annual trend (Table 8) or correlation with SOI (data not shown). Over the 31 years between 1971 and 2002, silicate concentrations over 0 to 50 m averaged 2.28 µM while the mean nitrate concentration (0 – 50 m) was 0.59 µM giving an average NO_3:Si molar ratio of 0.26. The seasonal peak in surface nitrate was consistent with the minimum in stratification which also occurred in June. The seasonal dynamics of both nitrate concentration and stratification were extremely similar to those for chlorophyll *a* (Figure 87A, C) with a June maximum. Thus Rottnest Island was the station with the smallest temporal offset between the seasonal minimum in stratification and annual maximum in chlorophyll *a*. Over the period 1997 to 2007 the temporal variation in chlorophyll *a* was well described by a Gaussian curve ($r^2 = 0.743$, $P < 0.001$) with a peak on day 185 ± 1.5. The annual anomalies in chlorophyll *a* were a positive linear function of the annual mean southern oscillation index (SOI) across most of the southern west coast of Australia (28° to 34° by 114°E to shore). For example, in the region from 31° - 33°S by 114°E to 115°E, annual chlorophyll *a* anomalies were correlated with SOI ($P < 0.027$). Mean monthly chlorophyll *a* anomalies were also significantly ($P < 0.001$) correlated with mean monthly SOI values. Positive SOI years (1999, 2000) showed greater than normal chlorophyll *a* during late summer and early autumn across 2 areas 29 31°S [=S] and 31 to 33°S [=N] between 115 to 114°E (Figure 87C). Early 2001 was also SOI positive and showed greater than average chlorophyll *a* in the first half of the year. There are no long term records of phytoplankton at Rottnest Island but ~ 25 km away the mouth of the Swan River Estuary is fully marine during late summer. Depth integrated, monthly mean $\log_{10}$ diatom abundance in February (weekly samples) showed a strong relationship ($P = 0.034$) with annual mean SOI (Figure 87D). Similarly weekly samples from January to April ($n = 224$) also showed a significant ($P = 0.012$) relationship between $\log_{10}$ diatom abundance and monthly mean SOI.

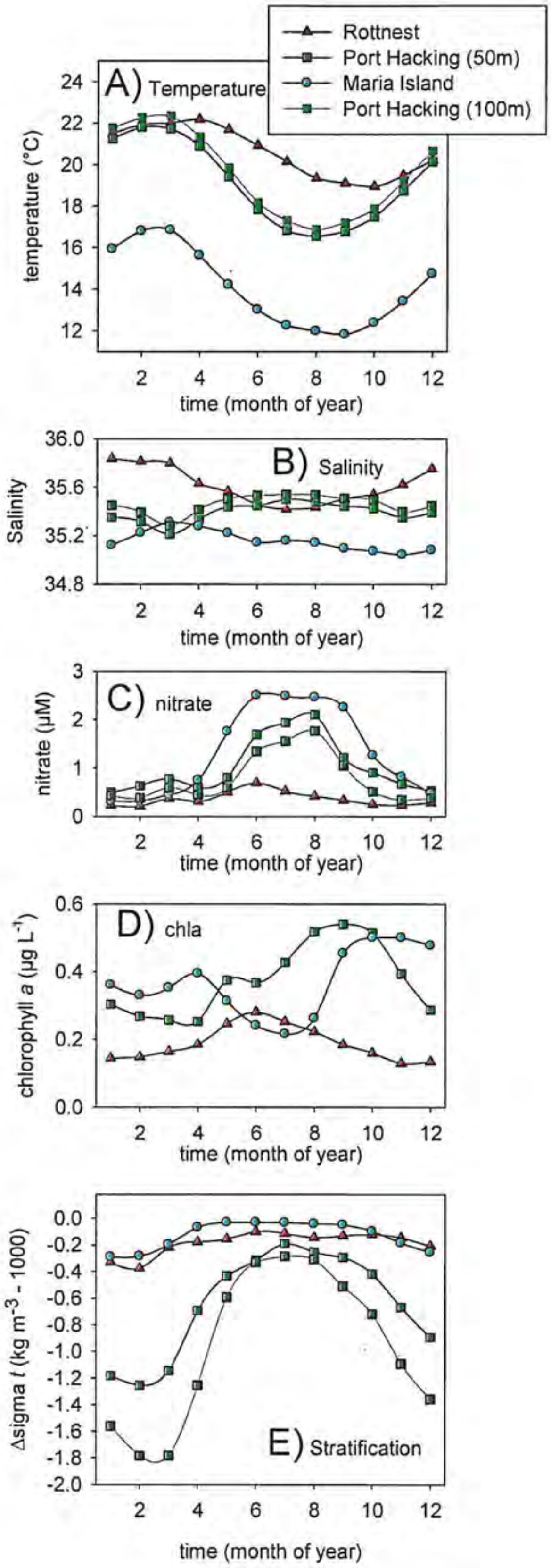
Rottnest
Port Hacking (50m)
Maria Island
Port Hacking (100m)
A) Temperature
temperature (°C)
24
22
20
18
16
14
12
2
4
6
8
10
12
time (month of year)
36.0
B) Salinity
Salinity
35.6
35.2
34.8
2
4
6
8
10
12
time (month of year)
3
C) nitrate
nitrate (μM)
2
1
0
2
4
6
8
10
12
time (month of year)
0.6
D) chla
chlorophyll a (μg L-1)
0.4
0.2
0.0
2
4
6
8
10
12
time (month of year)
0.0
-0.2
-0.4
-0.6
-0.8
-1.0
-1.2
-1.4
-1.6
-1.8
-2.0
Δsigma t (kg m-3 - 1000)
E) Stratification
2
4
6
8
10
12
time (month of year)

Figure 86

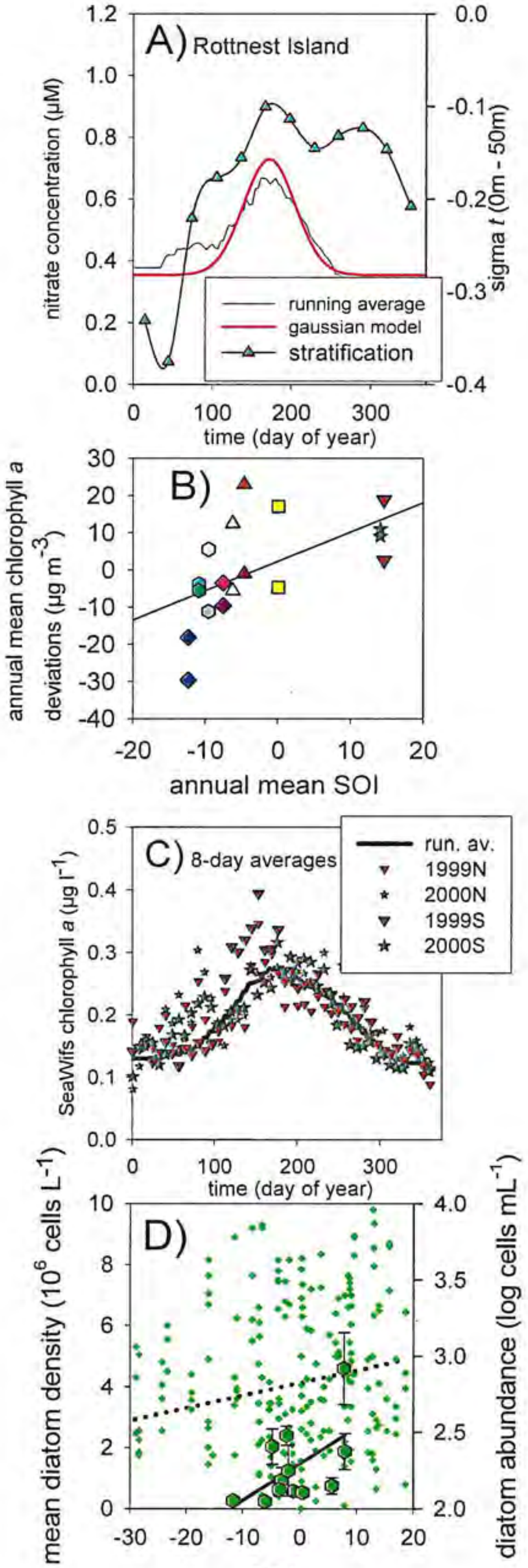
A) Rottnest Island
running average
gaussian model
stratification
nitrate concentration (μM)
sigma t (0m - 50m)
time (day of year)
B)
annual mean chlorophyll a deviations (μg m-3)
annual mean SOI
C) 8-day averages
run. av.
1999N
2000N
1999S
2000S
SeaWifs chlorophyll a (μg l-1)
time (day of year)
D)
mean diatom density (10^6 cells L-1)
diatom abundance (log cells mL-1)
SOI

Figure 87

Table 8 Long term (> 10 y) linear trends in surface parameters after seasonally detrending by removing monthly means. (Probabilities for all trends < 0.001 except nitrate where P < 0.008). Blank cells indicate non-significant result.

	Maria Island	Port Hacking (100 m)	Port Hacking (50 m)	Rottnest Island
Span (years analysed)	1944-2005	1953-2005	1944-2004	1969-2001
Maximum total # observations*	3273	9263	9882	2736
Temperature (°C/century)	2.02		0.744	1.23
Salinity (psu/century)	0.346	0.232	0.269	0.407
Nitrate (μM/century)		0.556		0.400
Phosphate (μM/century)	0.530		0.611	0.313
Silicate (μM/century)	-5.84	-1.97	-2.30	
dissolved oxygen (μM/century)			-12.9	-49.1

* for any parameter

A manuscript based on these results in nearing completion and further investigation into the new discovery that *La Nina* years are more productive in summer and autumn is anticipated.

Phytoplankton

Using samples from the cruise (SS04/2007) a new analysis of the phytoplankton community composition, its temporal and spatial patterns has been commenced. While the most recent cruise gives an unparalleled semi-synoptic data set, previous cruises expand the geographic range and pooling the data provides more opportunity for the analyses of seasonal and inter annual variability. Much of the data has never been published and there has not been a review of WA phytoplankton since the 1960s. In addition since the early research relied exclusively on net samples more than 95% of the phytoplankton biomass was ignored.

Samples for this analysis are drawn from the following

Phytoplankton taxonomic samples:

1. FR05 1995
2. FR10 2000
3. SS08 2003
4. SS04 2006
5. SS05 2005
6. SS07 2006
7. SS04 2007

Pigment samples analysed by HPLC are from (Figure 88) :

1. FR10 2000
2. SS08 2003

3. SS04 2006
4. SS05 2005
5. SS07 2006
6. SS04 2007

Grazing rate experiments are from:

1. SS05 2005
2. SS07 2006
3. SS04 2007

The complete data set for this analysis is still being constructed as we are adding environmental data to allow assessment of the underlying mechanisms that may influence distribution and abundance.

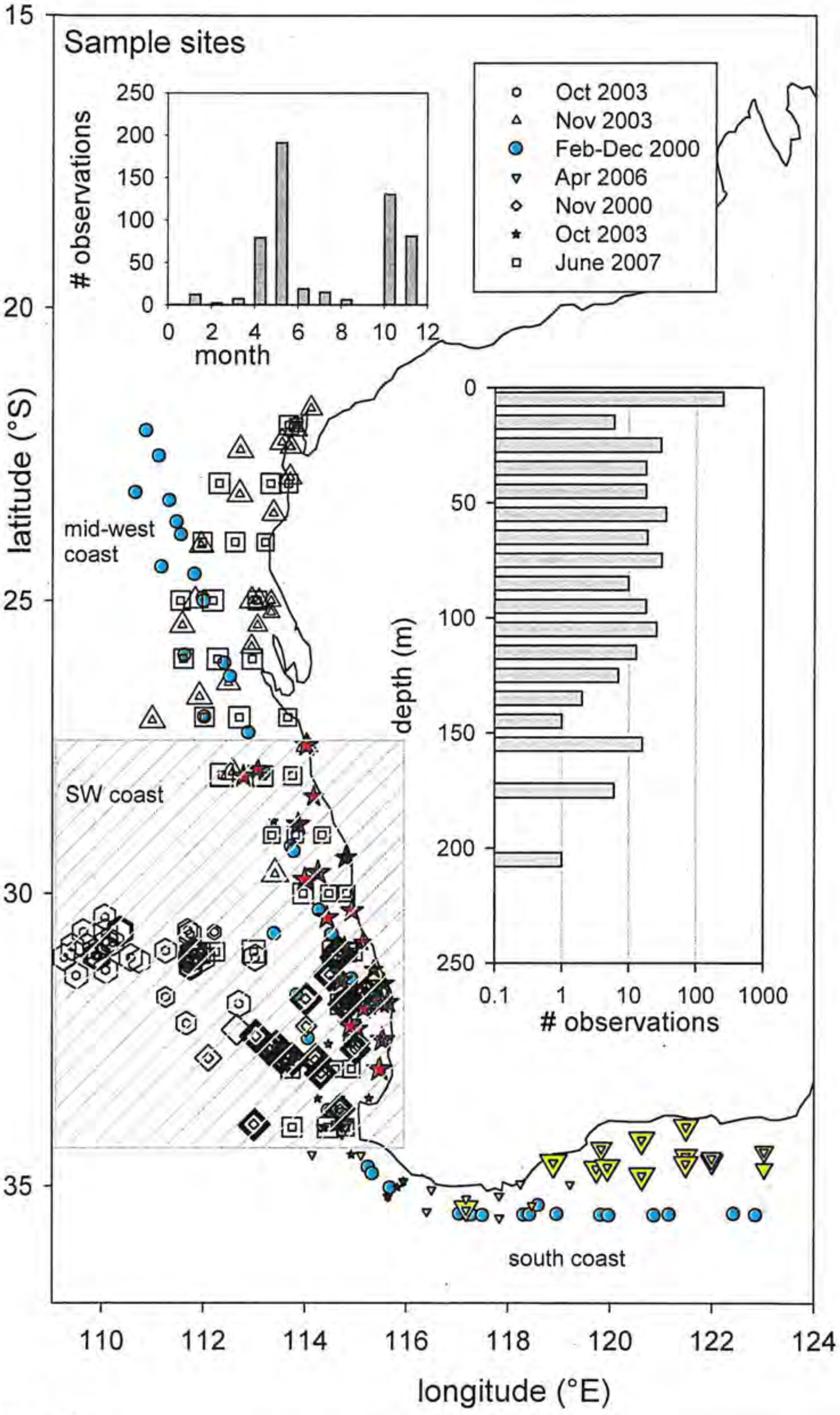

Figure 88
Map of sites with samples analysed by HPLC allowing chemotaxonomic phytoplankton assessment. Larger symbols are from greater depths.

Zooplankton

Mesozooplankton biomass from leg 2 and 3 of Southern Surveyor cruise was measured for 5 most northern transects (parallel 22 to 27). Net plankton samples especially from shallower waters contained considerable amount of ash (from 35% ±20% of dry weight inshore to 18% ± 7 % and 23% ± 4 % in LC and offshore respectively) caused by contamination of inorganic materials from re-suspension of sediments and phytoplankton originated detritus. Therefore ash-free dry weight was adopted to determine the biomass. Total sample collected from each station was sieved through a series of sieves to create size fractions to indicate any trends in size structure of the zooplankton.

The preliminary results show that in all transects inshore stations had the highest biomass (Figure 89). These analyses do not account for day and night sampling regime. Typically night tows would contain higher zooplankton biomass especially in deeper stations where large copepods migrate from deeper waters to feed. Diurnal factor will be included in final analyses of full data set. However, it probably will not change inshore-offshore trend.

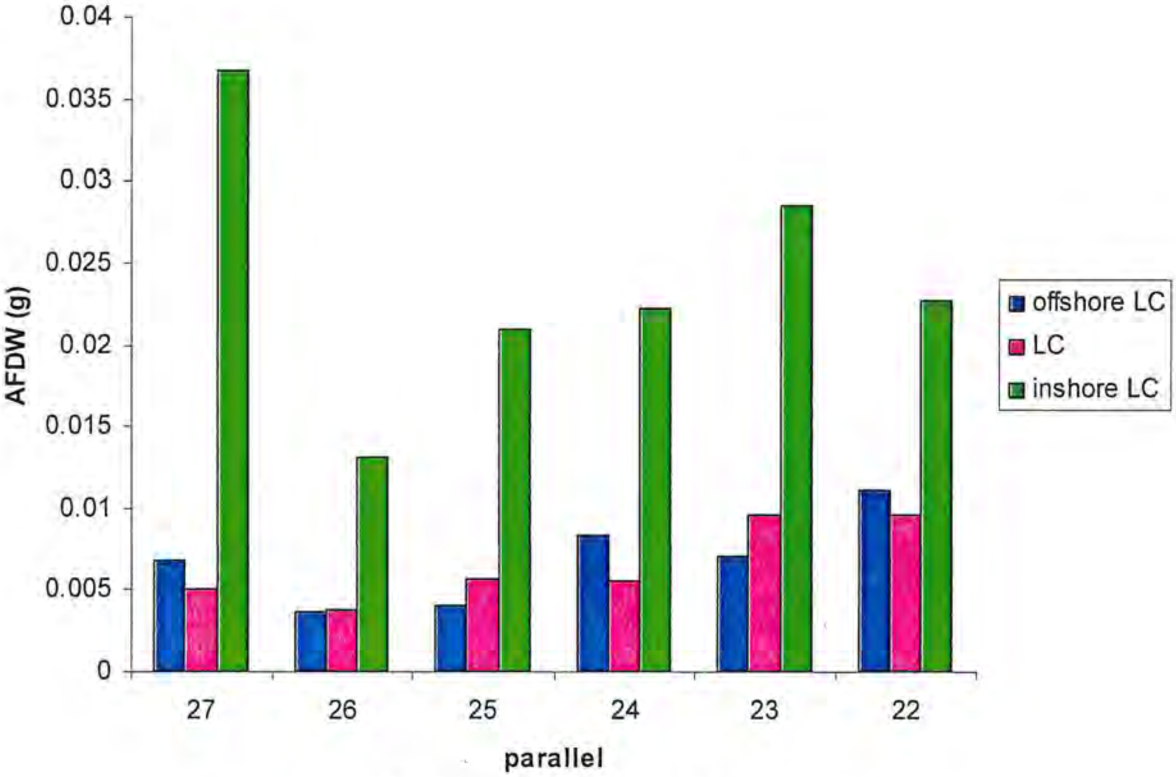

Figure 89. Total biomass of zooplankton.

Preliminary size fractionated analyses reveal some consistent trends i.e. 1000 to 355 µm organisms are important in terms of biomass at all stations (Figure 90). Nearshore, at parallel 23 and 24 large organisms dominated (Figure 91).

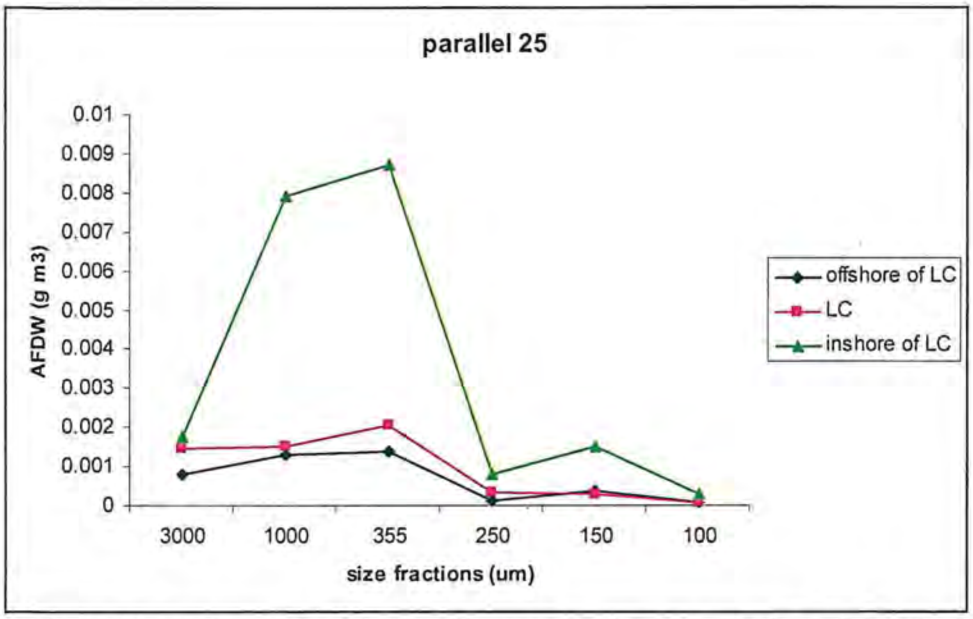

Figure 90. Fractionated zooplankton biomass showing typical pattern of size dominance.

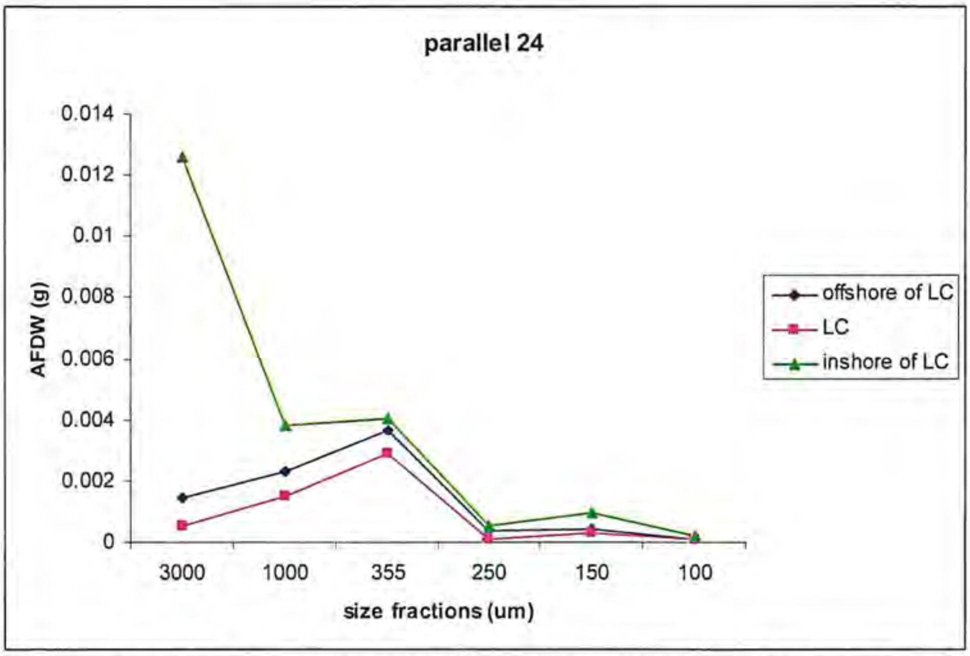

Figure 91. Size fractionated biomass (parallel 23 shows the same pattern).

Size fractionated zooplankton samples were also analysed for secondary production by measuring Aminoacyl-tRNA synthetases (AARS). The laboratory work has been completed however data has yet to be analysed.

Measurements of mesozooplankton biomass from leg 2 and 3 of Southern Surveyor cruise (Figure 92) was completed for all transects and all stations.

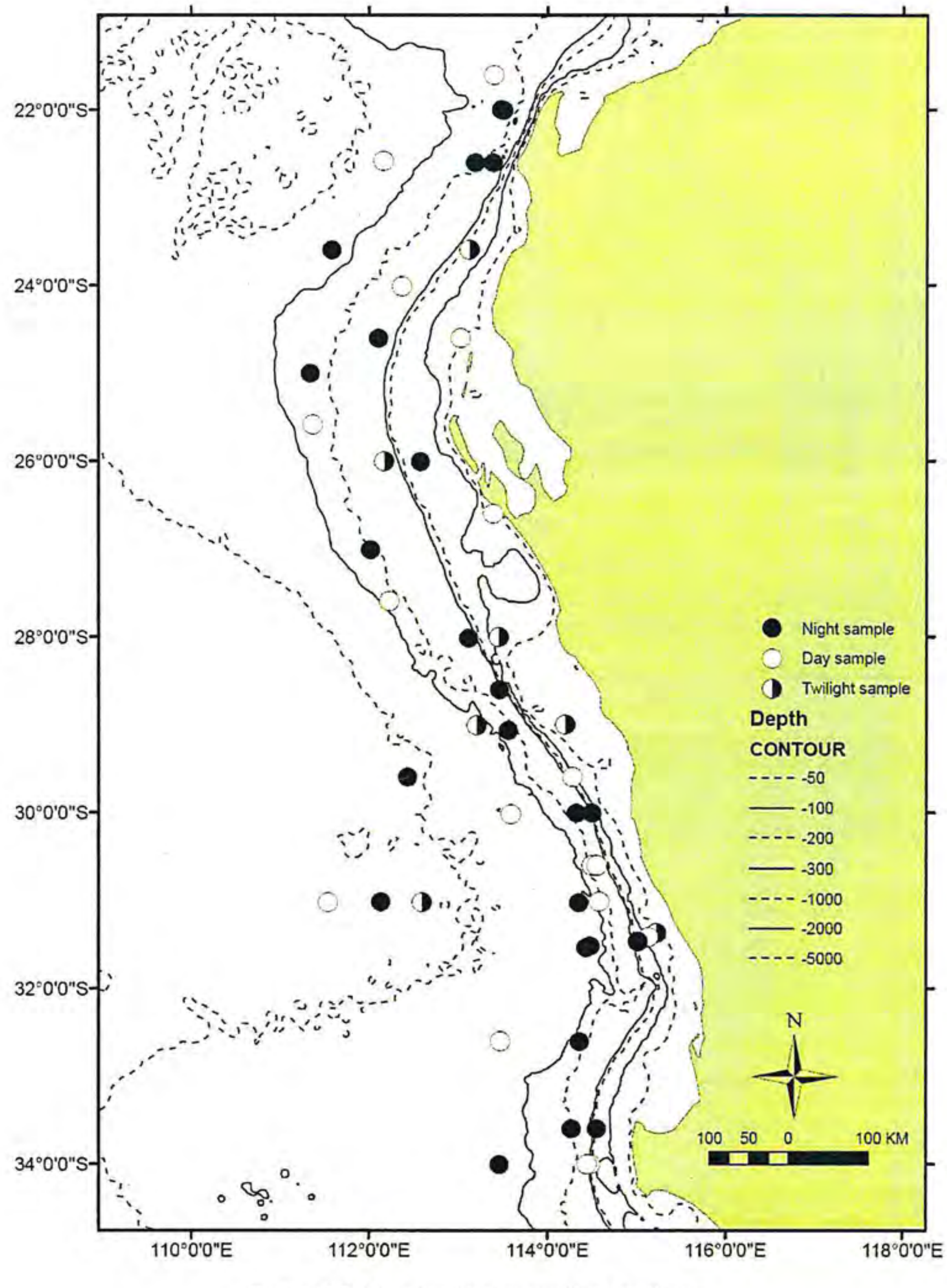

Figure 92. Zooplankton sampling stations.

Total and size fractionated biomass showed strong pattern following water masses. Biomass was higher inshore than in Leeuwin Current (LC) and offshore waters (Figure 93). From 34 to 29°S biomass offshore was lower than in LC waters but the difference disappeared north of 29 parallel. There was a clear South-North pattern in LC and offshore waters showing bimodal distribution with higher values between 33 and 29 °S and again between 24 and 22 °S and low of around .005 g AFDW m^{-3} between 28 and 27 °S. Inshore samples showed no geographic trend on the scale of sampling (every degree) implying possible smaller scale pattern or spatial autocorrelation.

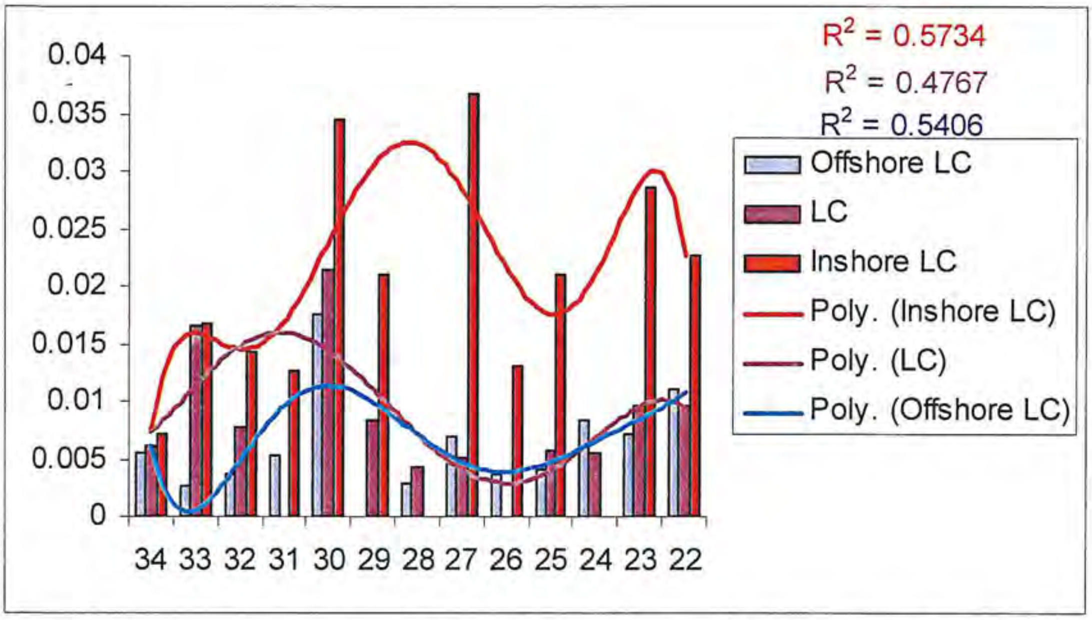

Figure 93. Biomass of zooplankton inshore, in Leeuwin current (LC) and offshore from 34 to 22 °S.

Larger size fraction (355 to 1000 µm) was a major contribution to total biomass in most stations (Figure 93). This size fraction consists mainly of larger copepods, smaller chaetognaths and siphonophores. In general inshore largest organisms (1000 µm +) were more important than offshore and in LC.

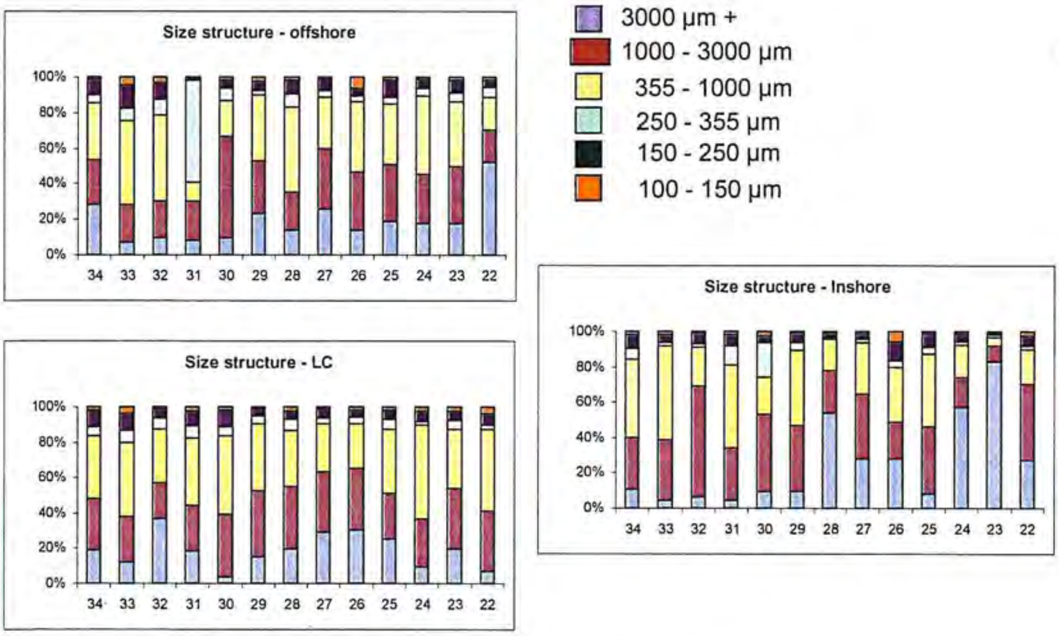

Figure 94. Size fractionated biomass of zooplankton.

Size fractionated zooplankton biomass followed total biomass pattern. LC and offshore samples clearly separated from inshore ones (Figure 95).

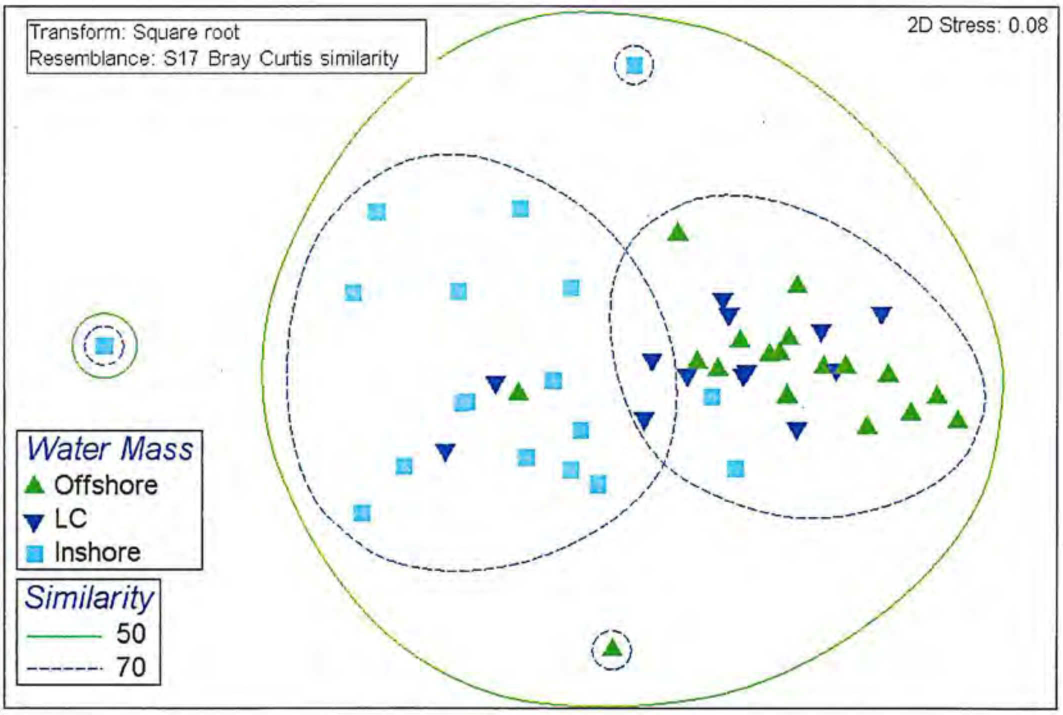

Figure 95. Size fractionated biomass: offshore-inshore gradient.

Preliminary investigations of process behind the pattern indicated that fluorescence was an important environmental variable best explaining the biomass pattern with Spearman rank correlation Rho = .479 (Figure 96).

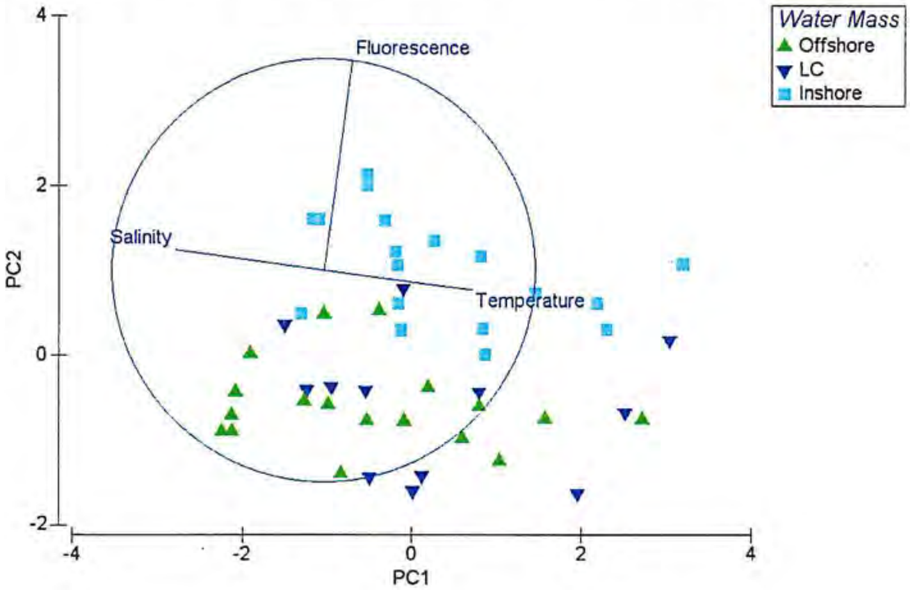

Figure 96. Linking biomass to environmental patterns.

Mesozooplankton from SS0407 cruise was analysed for fatty acid composition. Mesozooplankton forms a key trophic link in marine ecosystem and an important mediator of carbon flux. Mesozooplankton uses a wide range of prey including phytoplankton, microzooplankton, bacteria and marine snow. The analysis of fatty acid composition has been applied to reveal dietary components of marine organisms. The use of fatty acid trophic markers is based on the premise that phytoplankton, microzooplankton and bacteria all produce taxon-specific fatty acids which are retained by their predators and which can be used to quantitatively assess the relative trophic position and dietary quality. The time it takes for copepods (which usually form the bulk of mesozooplankton) to display changes in the fatty acid signatures of their diets varies considerably across genera and also depends on physiological condition but biomarkers integrate the trophic information over a longer time scale of several weeks while traditional approaches like gut content analysis provide information only on recent feeding. Fatty acids can be used to infer trophic relations in copepods because copepods acquire many of the fatty acids required for their growth and reproduction from their diets. Experimental studies have confirmed the trophic biomarker approach. Clear changes in fatty acid compositions could be induced by different phytoplankton diets. However, there are limitations in using fatty acids: no single fatty acid can be assigned uniquely to any one species. Fatty acids are not necessarily metabolically stable and turnover rate can be species specific and depends on metabolic condition of the organisms. Consequently fatty acids have been so far used as quantitative food web markers.

The aim of the project was to examine the variability in mesozooplankton feeding from south to north off Western Australia in three water masses: inshore of Leeuwin Current, in Leeuwin Current and offshore of Leeuwin Current. We hypothesized that mesozooplankton from coastal waters that tend to be more productive would have higher proportion of fatty acids associated with diatoms e.g. 16:1 n-7 and 20:5 n-3 and mesozooplankton from oceanic waters would have more fatty acids associated with small phytoplankton e. g. 18:3 n-3 and 18:4 n-3 and more omnivory or carnivory markers e.g. 18:1(n-9)/18:1(n-7), the proportion of PUFA to saturated fatty acids or ratio of DHA/EPA from microzooplankton prey. The inclusion of biochemical indices of zooplankton can add valuable information about the potential of food quality to higher trophic levels like fish.

Mesozooplankton for fatty acid analysis was size fractionated on board and frozen immediately after collection. Therefore fatty acids are a mixture of fatty acids from the food in the guts and fatty acids assimilated into the mesozooplankton body tissues. Size dependent patterns are important in marine ecosystems because invertebrates and planktivorous fish are size selective predators. Pelagic food webs can be microbial, when small phytoplankton dominates or herbivorous when large phytoplankton dominates. Protozoea (i.e. flagellates and ciliates) feeds on small algae and bacteria. Metazoans graze phytoplankton, flagellates and ciliates ≥ 5 μm. In oligotrophic waters main trophic links to the metazoan is via protozoa. Herbivorous food web is usually dominated by large diatoms and is characterized by efficient transfer of energy to higher trophic levels. Microbial food wed is based in flagellates. Diatoms vs dinoflagellates food web can be differentiated by 16:1 n-7/16:0 ≥ 1, high proportion of 20:5 n-3, high ratio of $\sum$C16 to $\sum$C18 and high ratio of EPA (20:5 n-3) to DHA (22:6 n-3).

The fatty acids were examined to reveal main food web patterns in mesozooplankton from different water masses. 16:1 n-7/16:0 and EPA/DHA ratios exemplify a high degree of correlation of diatom vs dianoflagellate markers (Figure 97).

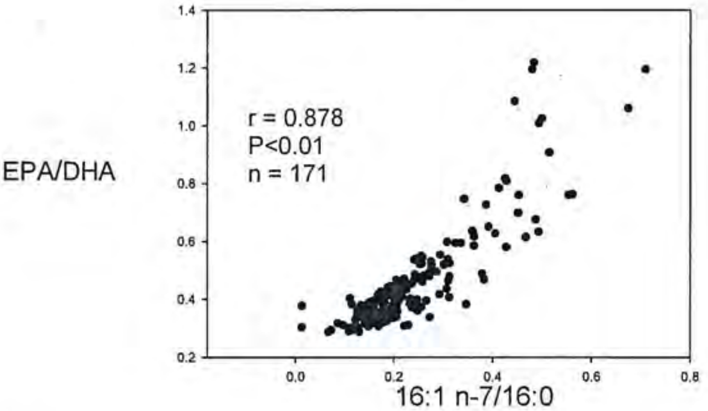

Figure 97
Degree correlation r = Pearson's product movement correlation coefficient between diatoms and dinoflagellates markers.

There was no difference between inshore and offshore or Leeuwin current water masses in diatom food web markers in zooplankton (Mann Whitney P = 0.9). Dinoflagellate food web dominated of the coast of Western Australia in May/June 2007. Eddy Edge bordering Leeuwin Current had the highest diatom to flagellate ratio however it was still below 1 (a cut off point for diatom dominance) (Figure 98).

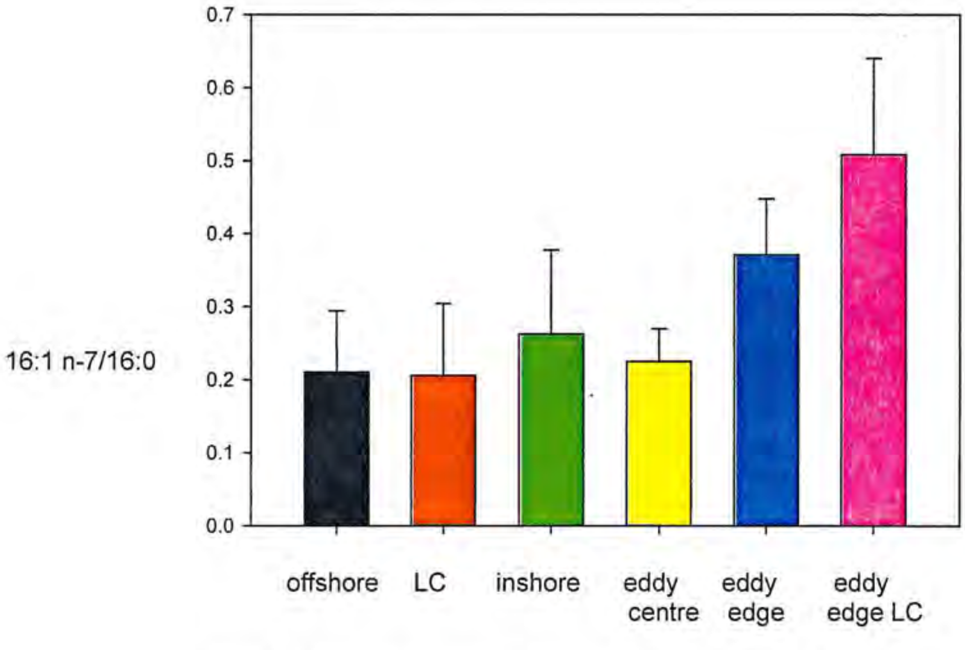

Figure 98. Herbivorous (Diatom) vs microbial dinoflagellate food web.

Microbial food web often leads to increase in omnivory where zooplankton selects microzooplankton over phytoplankton. Omnivorous diet is characterised by high 18:1 n-9/18:1 n-7 and high DHA to EPA ratios. There was a high degree of correlation between omnivory markers (Figure 99).

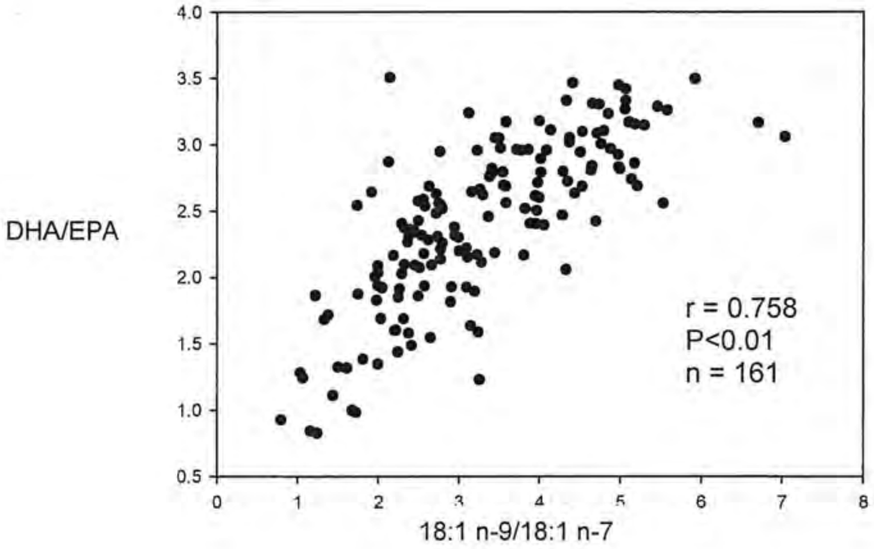

Figure 99
Degree of correlation r = Pearson's product movement correlation coefficient between omnivory markers.

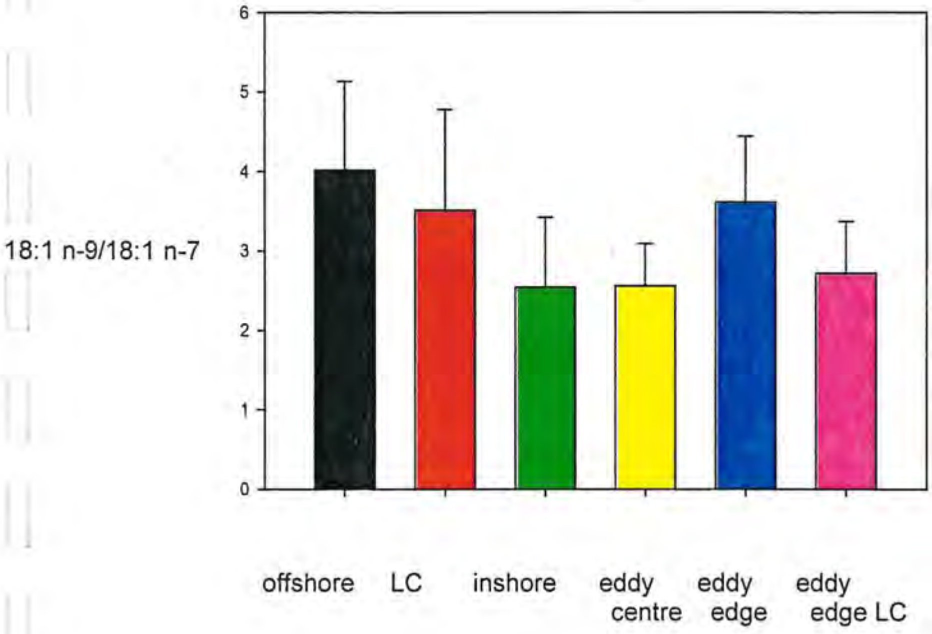

Figure 100
Degree of omnivory

We examined the quality of food for planktivorous fish and fish larvae. Long chain n-3 PUFA are important for fish since they can not convert short chain fatty acids into EPA or DHA. Lack of these essential fatty acids results in low growth and failed recruitment. Fish have higher demand for DHA than EPA. High dietary DHA to EPA ratios are correlated to enhanced growth and survival. High DHA to EPA is critical for growth and neural and eye development of larval and juvenile fish. All water masses had similar levels of EPA and DHA and there were no significant differences in DHA/EPA ratios from offshore to inshore (Kruskal-Wallis, $p = 0.8$) (Figure 109 & Figure 110).

However to know if there is a sufficient amount of needed PUFA generated in the phytoplankton and transmitted through the zooplankton to maintain a population of larval fish it is essential to consider fatty acids not only in terms pf percentage of individual fatty acids but to consider total pools of individual fatty acids and these analyses are pending.

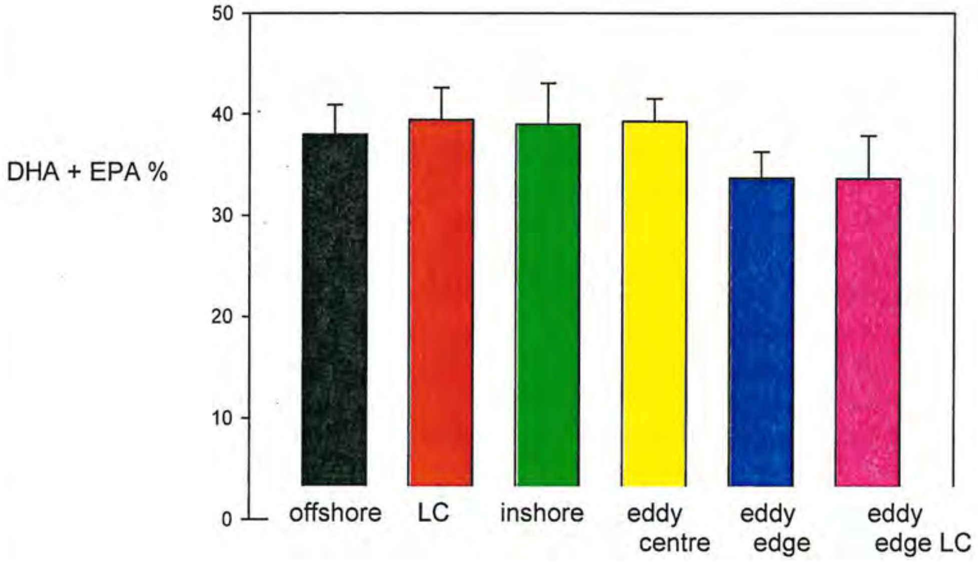

Figure 101
Proportion of long chain n-3 fatty acids in zooplankton

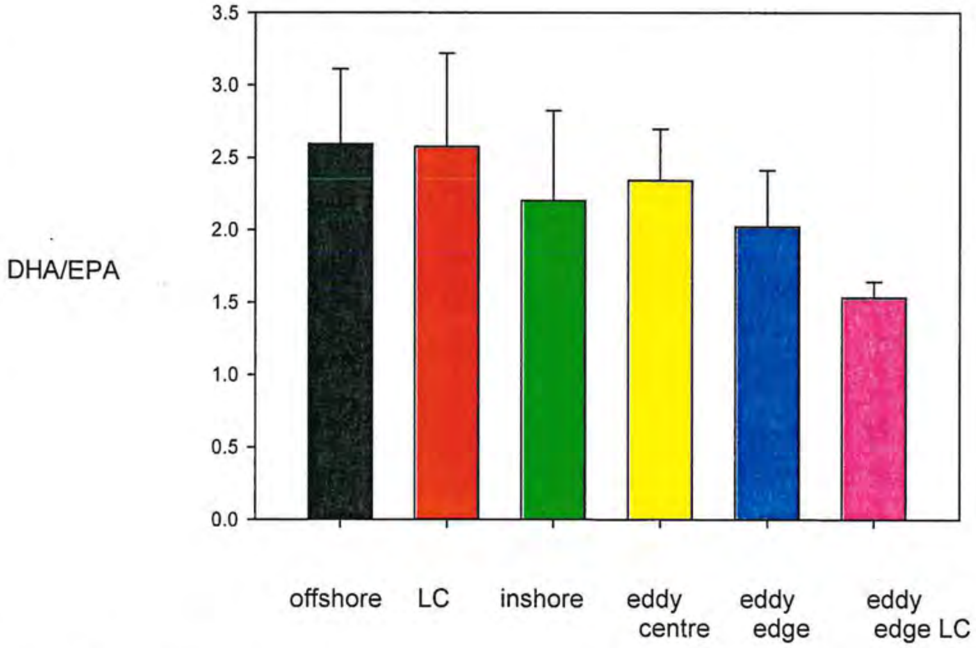

Figure 102
ratio of DHA to EPA in zooplankton

Using samples from the cruise (SS04/2007) analysis of the size fractionated zooplankton secondary production and its spatial patterns has been commenced. In conjunction with colleagues from AIMS we assessed the use of the enzymes aminoacyl-tRNA synthetases (AARS) as a proxy of growth of zooplankton. Samples were collected from 22°S to 34°S in the coastal zone, the Leeuwin current (LC) and oceanic environments (station depths of 50m, 300m and 1000-2000m respectively), and in an offshore anticyclonic eddy. Mesozooplankton was sampled with a 100µm mesh net from the bottom (coast) or from 150m depth (LC and oceanic stations) to the surface. The samples was size fractioned through 150µm, 250µm and 355µm meshes and frozen in liquid nitrogen for later enzymatic analysis. Preliminary analysis indicate that AARS activity was higher in coastal than in oceanic stations, with intermediate values in the LC (Figure 103). In all three regions, the largest size fraction contributed the most to biomass and total AARS activity. Biomass specific AARS activity was relatively homogeneous amongst the various fractions, especially in the LC, with some variation in the coastal and oceanic stations. Higher biomass and AARS activities, both in the total and in each size fraction, were also observed in the LC and oceanic stations between 29°S and 31°S. A preliminary estimation of secondary production ($mgC \times m^{-3} \times day^{-1}$) resulted in an average value of 0.39 for coastal areas, 0.11 in the LC and oceanic environments, 0.07 in the eddy centre, and 0.07—1.18 in the eddy edges. Our results indicate that zooplankton secondary production in coastal waters and anticyclonic eddies forming from the LC is higher than in oceanic waters.

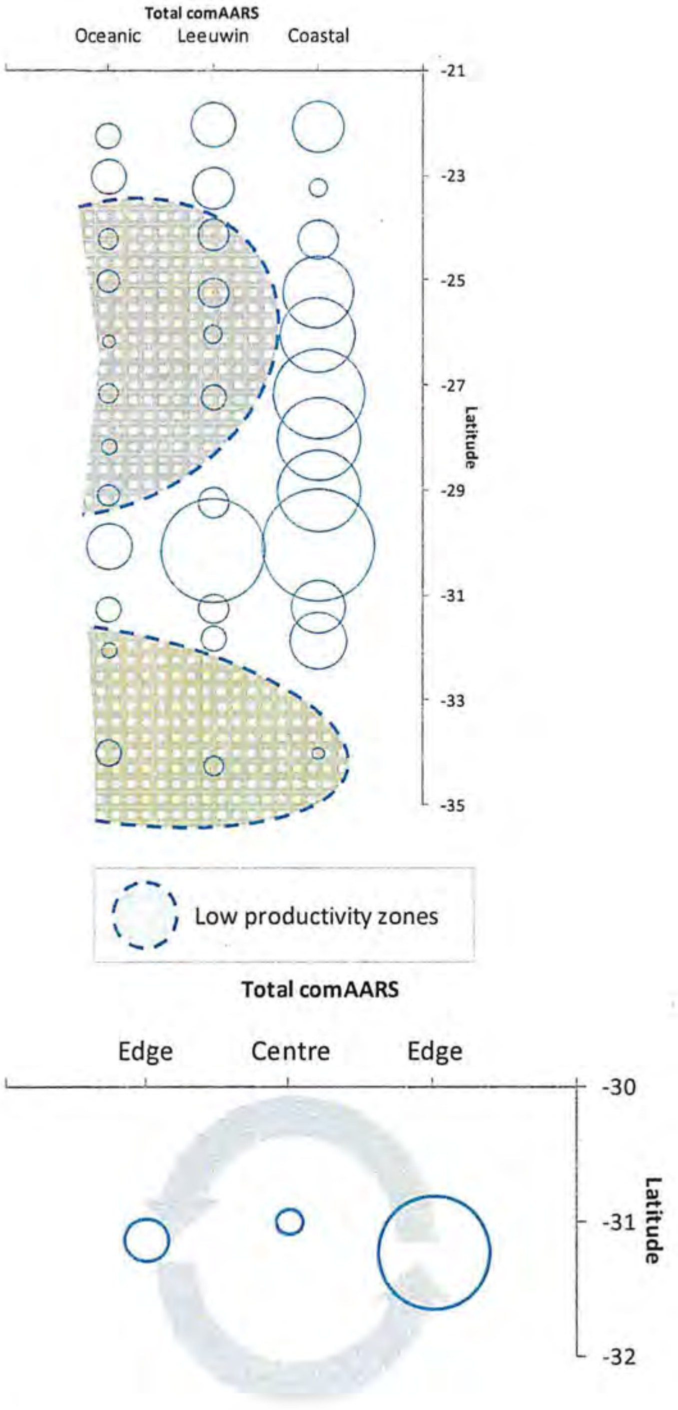

Figure 103
Secondary production of total zooplankton from 34 ° S to 22 ° S and in anticyclonic eddy.

Remotely sensed ocean colour (SeaWiFS chlorophyll a concentration as indication of phytoplankton biomass) generated by NASA (Giovanni.gsfc.nasa.gov) from April to May 2007 was used to correlate phytoplankton with zooplankton biomass from June-May 2007 cruise. Historical data was used in preference to phytoplankton data collected during the cruise because there is an observed time lag of about 10 weeks between phytoplankton and zooplankton biomass. There was a significant correlation (Spearman rank correlation P = 0.00) between zooplankton and phytoplankton biomass (Figure 104) indicating that zooplankton was feeding directly or indirectly (by consuming protozoa that were feeding on phytoplankton) on phytoplankton (Figure 104). Note that 4 data points with high biomass were removed from the second (b) analyses. It is not possible to estimate contribution of large zooplankton to total biomass from satellite data however all the samples collected from waters off Western Australia coast indicate that small (< 5µm) phytoplankton dominates. Since there is a general relationship between chlorophyll and particulate organic carbon (POC) in the euphotic zone of the oceans POC can be estimated from chlorophyll a (Legendre and Michaud, 1999). In turn the concentration of suspended POC provides estimates of biogenic carbon that is a potential food by zooplankton. This correlation indicated that sampled zooplankton was feeding on phytoplankton indirectly by consuming protozoa

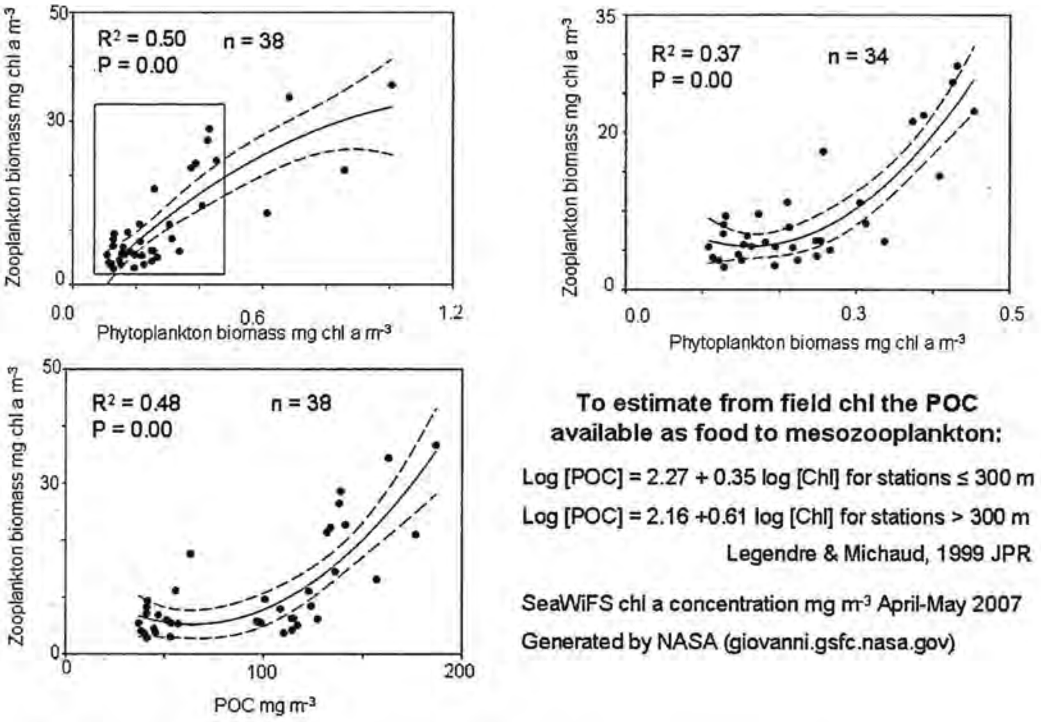

To estimate from field chl the POC available as food to mesozooplankton:

$\log [POC] = 2.27 + 0.35 \log [Chl]$ for stations ≤ 300 m

$\log [POC] = 2.16 + 0.61 \log [Chl]$ for stations > 300 m

Legendre & Michaud, 1999 JPR

SeaWiFS chl a concentration mg m^{-3} April-May 2007

Generated by NASA (giovanni.gsfc.nasa.gov)

Figure 104

Correlation of mesozooplankton biomass with biomass of potential food sources.

Milestone 1.3.2: Complete Yr 1 lagoon and biomass sampling and ecological process field work

Original Forecast Finish Date: 30/06/07

Revised Forecast Finish Date: 30/06/07

This section unchanged from previous Biannual Report

Summary of Activities Undertaken, Outputs Produced:

Pilot studies have commenced and detailed preparation and planning for this work, to take place during the summer field season, is ongoing. Joanna Strzelecki has trialled techniques for *in situ* assessment of sessile invertebrate filtration rates in Marmion lagoon. The summer field program investigating phytoplankton productivity and secondary production in Marmion Lagoon will commence in February. A series of local cruises will collect information on primary productivity and community dynamics of both pelagic and benthic phytoplankton communities as well as documenting the productivity and composition of the zooplankton community.

Samples to measure filtration rates and nutrition of sponges and ascidians were collected from 7 locations in Marmion Lagoon. The InEx technique (Yahel *et al.*, 2005) and suction sampling was used to sample *in situ* water inhaled and exhaled by organisms. Picoplankton populations from the samples were quantified with a Becton Dickson flow cytometer at the University of Western Australia. Picoplankton populations were identified to heterotrophic bacteria, *Prochlorococcus* sp and *Synechococcus* sp (collaboration with Christine Hanson, ECU). Samples were also collected to determine cell densities from inhalant and exhalent current on a Coulter Counter and FlowCam. Flow Cam will allow size measurements of plankton. An access to Flow Cam was negotiated with AIMS in Townsville where samples will be run in September.
Pumping rates of sponges and ascidians were measured using high definition video using dye-front speed technique. These measurements were based on three video recordings of the movement of a dye in a transparent tube located within the excurrent jet per organism. Previous studies (i.e. Lemmens et al, 1996 and Wiltshire, 1994) demonstrated the effects of water temperature on filter feeding. Therefore, the measurements will be repeated in Marmion Lagoon in winter.

During two cruises in February, zooplankton in Marmion Lagoon was sampled to determine species composition, biomass and secondary production. Zooplankton was sampled using Bongo nets with 355 and 100 µm mesh in two inshore and two offshore stations. Size fractionated samples were collected for secondary production to be analysed using Aminoacyl-tRNA synthetases (AARS) (Yebra and Hernandez-Leon, 2004). A visit to AIMS is planned in September to analyse these samples in collaboration with Felipe Gusmao. In addition, secondary production was measured using two standard methods;

artificial cohort incubations and egg production. AARS method is a new technique and standard methods need to be used to validate it.

Information on kelp density at varying depths was collected and analysed in conjunction with wave energy modelling results for Marmion Lagoon. Samples of kelp were also collected from numerous sites at varying depths and distances from shore for later C and N isotope analysis.

Rates of biomass production by kelp (*Ecklonia radiata*), a dominant canopy-forming species, were measured at four sites in Marmion Lagoon during warm summer months (February-March). Rates of biomass production by individual plants were in the order of 1-2 grams dry weight per day, but varied considerably among sites as well as among individual plants (Figure 105). One insight into the nature of this variability was uncovered in the discovery of a positive relationship between daily rates of extension, and the total length of an individual (Figure 106). This relationship implies that among-individual variation in extension rates leads to variation in morphology (longer thinner laminae), with potential implications for canopy structure and community structure, as well as for food webs.

References

Lemmens *et al.* (1996). The clearance rates of four ascidians from Marmion Lagoon, Western Australia. *Seagrass Biology: Proceedings of an international workshop.* Rottnest Island, Western Australia, 25-29 January 1996. pp 277-282

Wiltshire, K.H. (1994). Separating the physiological and mechanical effects of water temperature on the filtering feeding characteristics of the solitary ascidian *Herdmania momus* (Savigny). Honours Thesis, Flinders University, Adelaide, South Australia.

Yahel *et al.* (2005). Inex – a direct in situ method to measure filtration rates, nutrition, and metabolism of active suspension feeders. *Limnology and Oceanography methods*, 3 46-58.

Yebra L, Hernandez-Leon S (2004) Aminoacyl-tRNA synthetases activity as a growth index in zooplankton. *J Plankton Res* 26:351–356

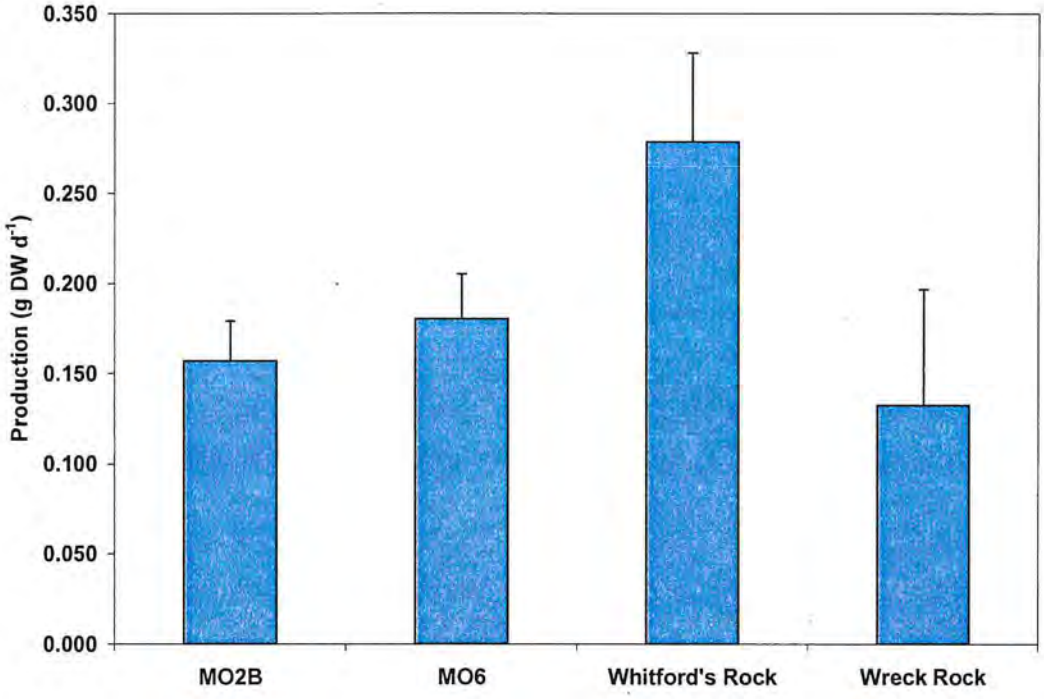

Figure 105. Kelp biomass production at Marmion Lagoon. Sites MO2B and MO6 are offshore sites, Whitfords Rock and Wreck Rock are inshore sites.

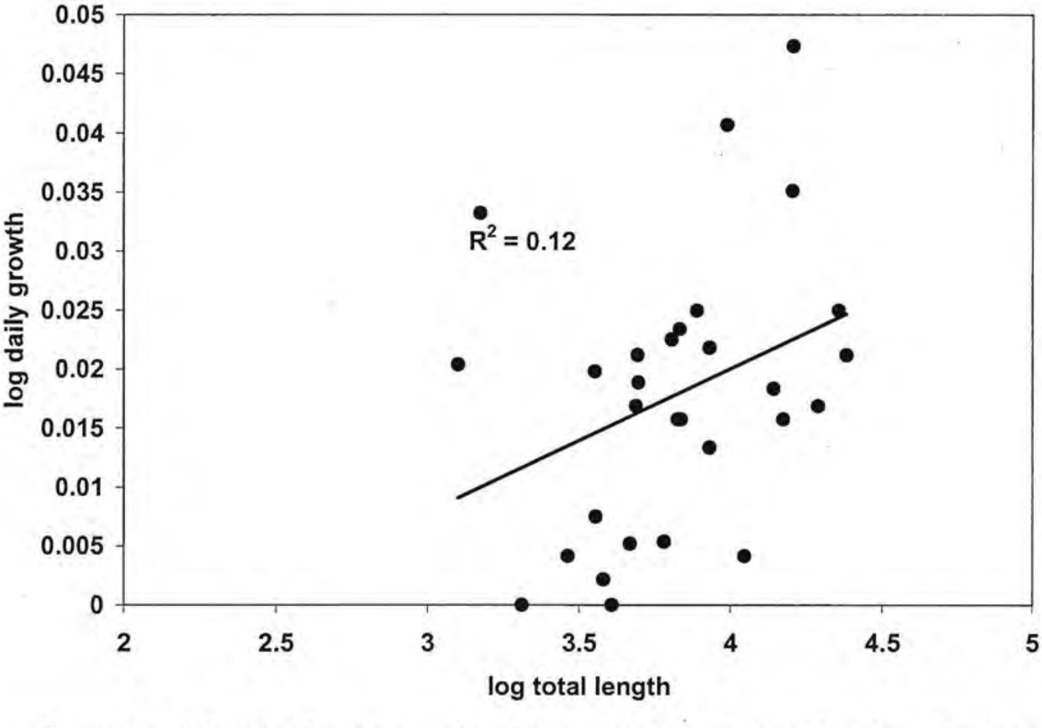

Figure 106. Kelp extension rate as a function of total plant length at Marmion. (Regression p=0.062)

Milestone 1.3.3: Complete Yr 2 lagoon biomass sampling and ecological process field work

Original Forecast Finish Date: 30/06/08

Revised Forecast Finish Date: 30/06/08

This section unchanged from previous Biannual Report

Summary of Activities Undertaken, Outputs Produced:

Data collection occurred during November-March 2008 focussing on measurements of predation (using mussels set up in aquaria: reported on under Milestone 2.2.2), surveys of soft sediment habitats (reported on under Milestone 1.4.2), and fine scale measurements of nutrients and particulates around filter feeders on reefs. Efforts continued on development of an Oracle database to house the large amounts of data of diverse kinds that are being collected. We concentrated efforts toward understanding secondary production on soft sediment habitats.

Preliminary analyses have yielded insights into among-habitat differences in biomass and important patterns of distribution of species within trophic groups. For example, reef and seagrass habitats – the two highly productive and spatially extensive benthic habitats in Marmion Lagoon – host very different assemblages of taxonomically and trophically similar species (see Figure 107 below for examples using assemblages of echinoids and asteroids).

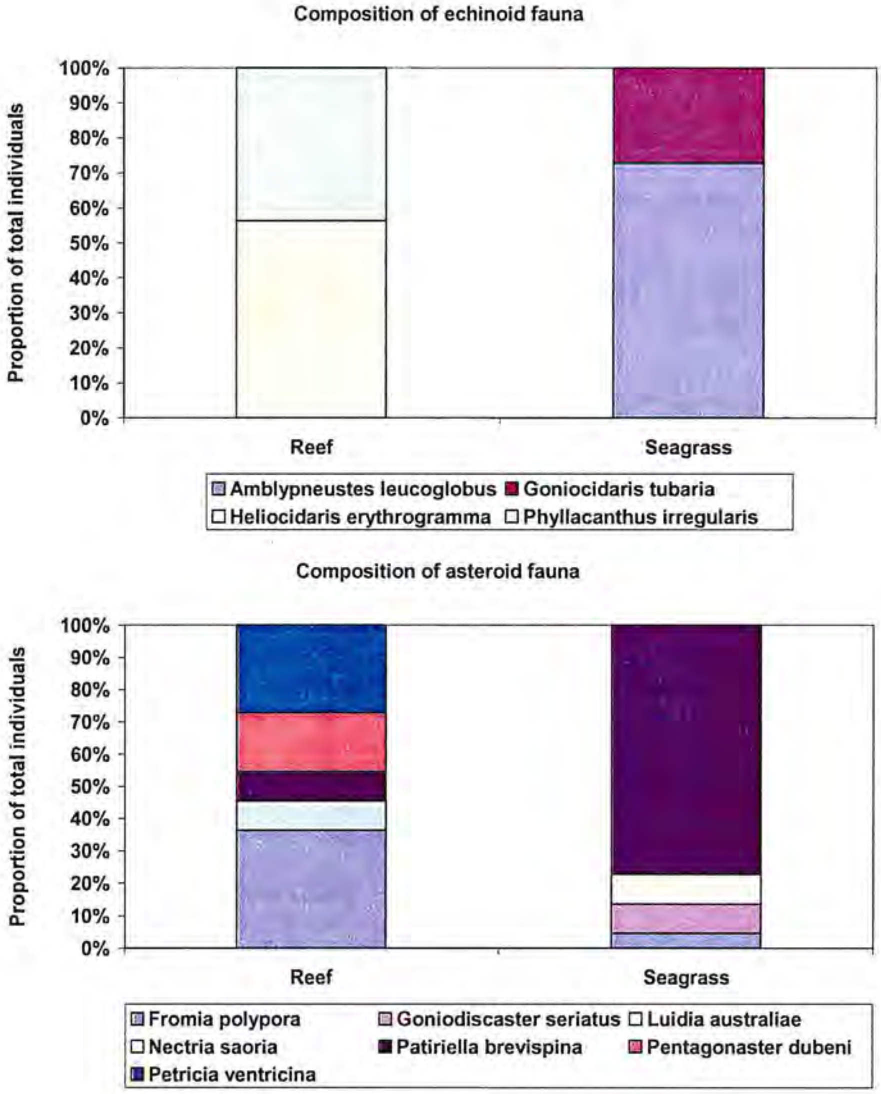

Figure 107. Taxonomic assemblages.

In addition, the *in situ* measurements of filtration rates of sponges and ascidians were continued from shallow reefs in Marmion Lagoon. Morphometric data including height, width and siphon diameter and number was collected *in situ*. A good correlation was obtained between filtration rates and diameter of exhalent siphons in ascidians and oscula in sponges (Figure 108). This would allow future estimation of community filtration rates based on measurements of excurrent siphons or oscula in field without the need for destructive sampling to obtain biomass.

Measured filtration rates per g of dry weight were higher in sponges than in ascidians: 1.31 (±0.35 st. dev.) L^{-1} hr^{-1} g DWt and 1.14 (±0.75 st.dev.) L^{-1} hr^{-1} g DWt respectively (Figure 109). However, these are preliminary results based on a subset of biomass data. The identification and biomass measurements are continuing. Three rates measured per animal were sometimes quite comparable and other times pretty variable. While sponges' rates were significantly less variable than ascidians' (t-test, P = 0.002) both animals were regulating their feeding rates.

All the samples for diet composition comparing the content of the water inhaled and exhaled by sponges and ascidians have been run on a flow cytometer at the University of Western Australia and the results are being analysed. The Flow Cam to measure larger size plankton (from nanoplankton up) has been purchased and delivery is scheduled for end of January 2008.

The preliminary results of this first attempt to measure active filter feeder rates *in situ* were presented at Connectivity Symposium Ecological Society of Australia conference in Perth, November, 2007.

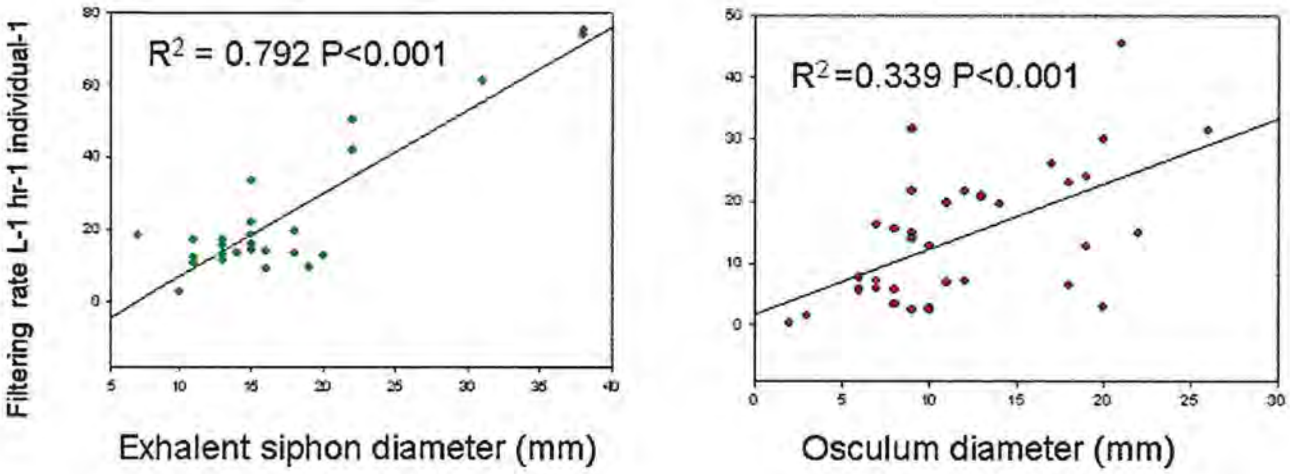

Figure 108. Relationship between siphon or osculum diameter and filtration rate.

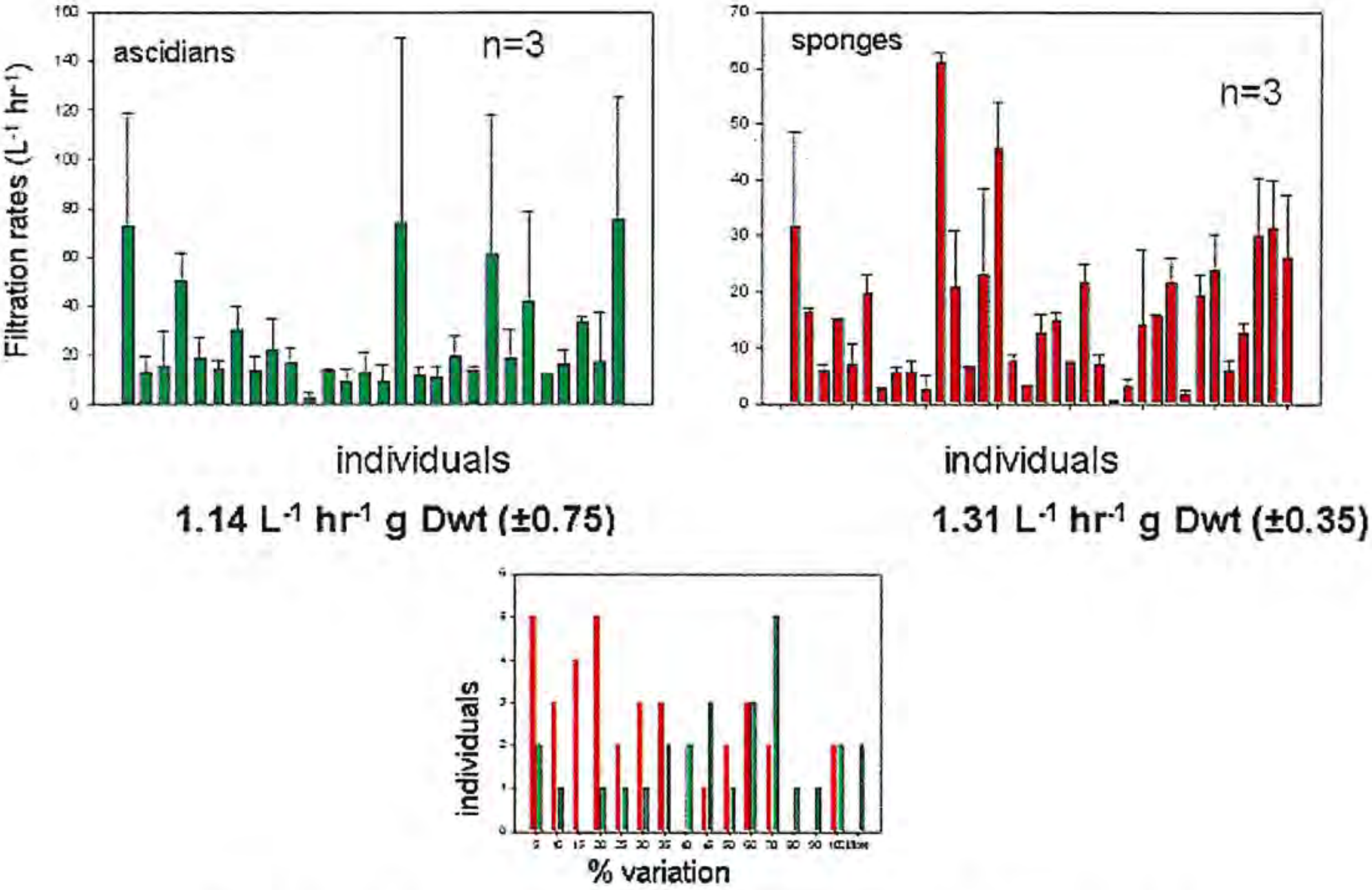

Figure 109. Filtration rates shown per individual and per g dry weight. Middle panel showing variability of rates in sponges (red bars) and ascidians (green bars).

Nutrient and phytoplankton samples were collected from 5 shallow reefs to determine the potential role of filter feeders as nutrient sources in Marmion Lagoon. 10 replicate samples were collected from each reef near the filter feeders and away from filter feeders. Nutrient samples were analysed for Nitrite/Nitrate, Phosphate and Silica. Phytoplankton samples were size fractionated to measure contribution of small phytoplankton to total biomass. Input and recycling of nutrients at the seabed and mixing into photic zone is an important part of benthic pelagic coupling and these measurements aim at providing insight into this process. Analysis showed an overall increased Nitrate/Nitrite near filter feeders ($P_{t\text{-}test}<.05$). Looking at 5 sites separately Wreck Rock showed no difference in concentration of Nitrate/Nitrite between filter feeders and way from filter feeders (Figure 110) At the time of sampling this site had a lot of detritus floating on top two meters of the water column. The source of detritus was not immediately obvious. All other sites showed increased Nitrate/Nitrite concentrations near filter feeders. Other nutrients were no different between near filter feeders and away. Both sponges and ascidians excrete ammonia as their waste product and can be an important nitrogen source on the reefs. The supply of nitrogen by filter feeders will be estimated once the analysis of biomass data is completed.

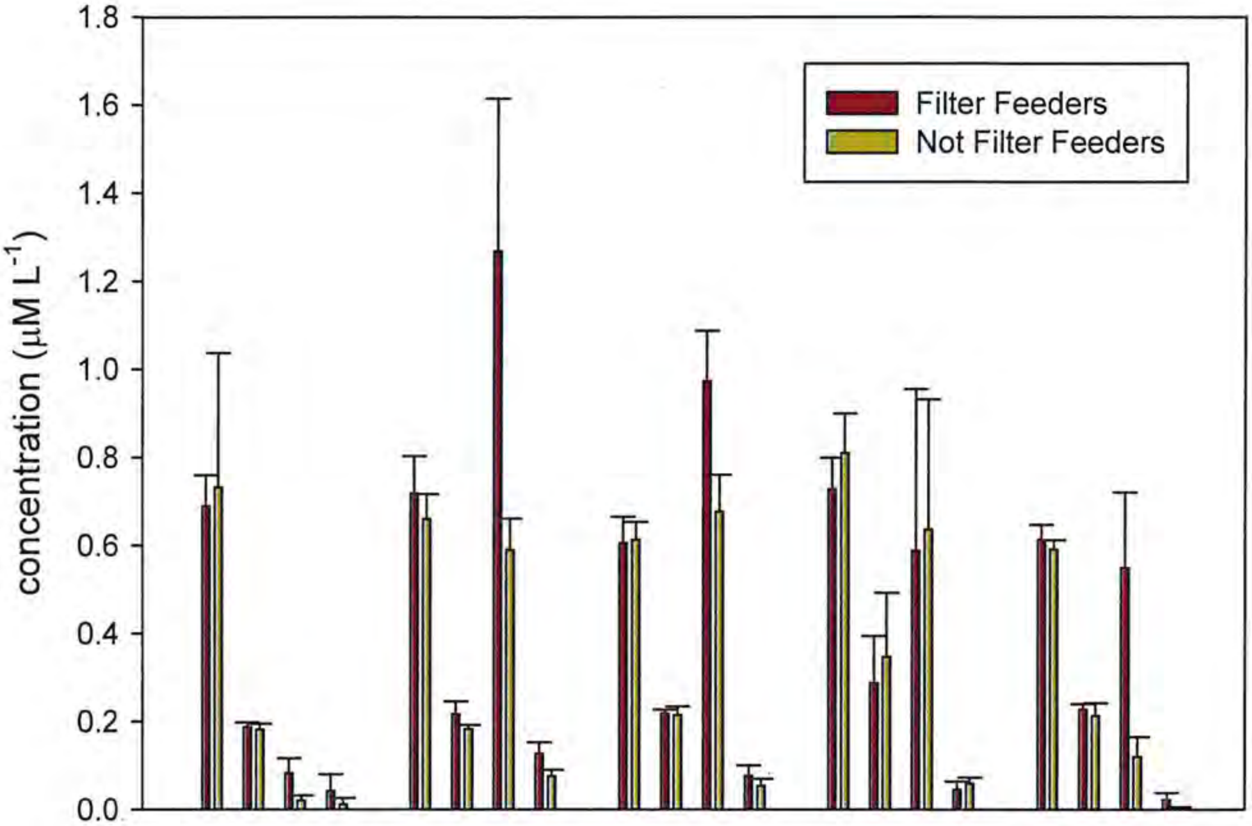

Figure 110.Nutrients next to filter feeders and away from filter feeders on 5 reefs in Marion Lagoon.

Analysis of cytograms are in progress and preliminary results show a high retention of small cells by sponges (Figure 111). Retention rate of total small particles (0.2 and 2 µm) varied between 37 and 94%. This is comparable to the data from other regions.

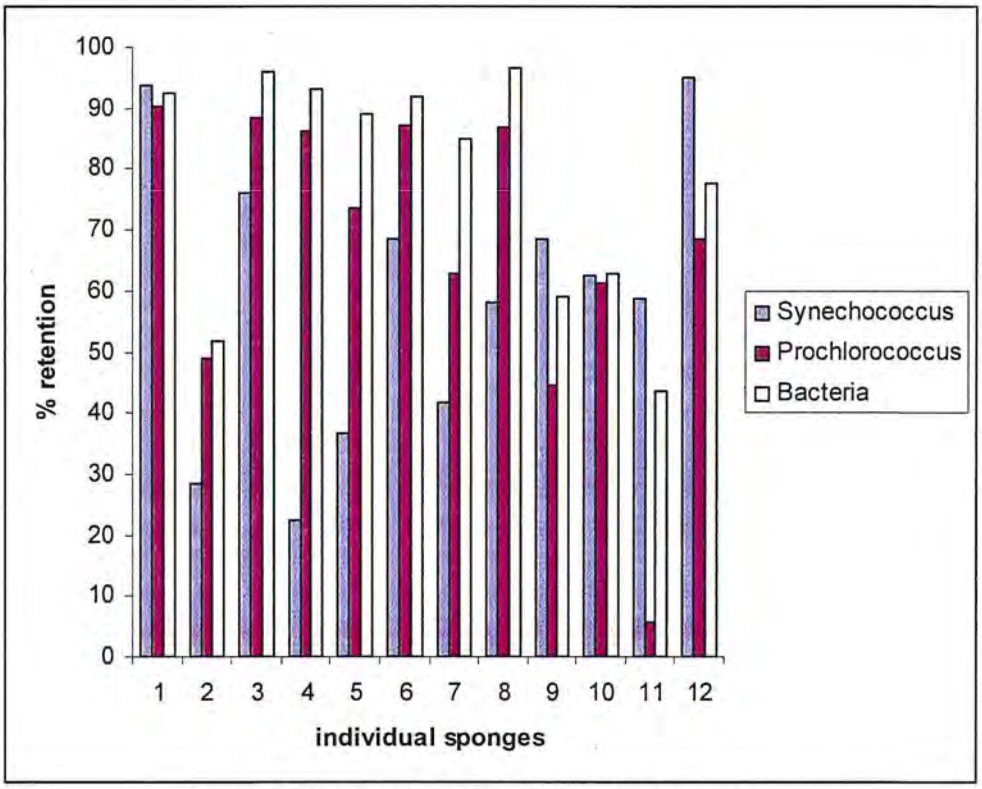

Figure 111. Retention rate of picoplankton by sponges

A first attempt was made to estimate grazing impact on small phytoplankton by pelagic (microzooplankton) and benthic (sponges and ascidians) grazers. Based on data collected in SRFME (Figure 112) it was estimated that microzooplankton graze 55% of primary production of small phytoplankton while ascidians and sponges 30%.

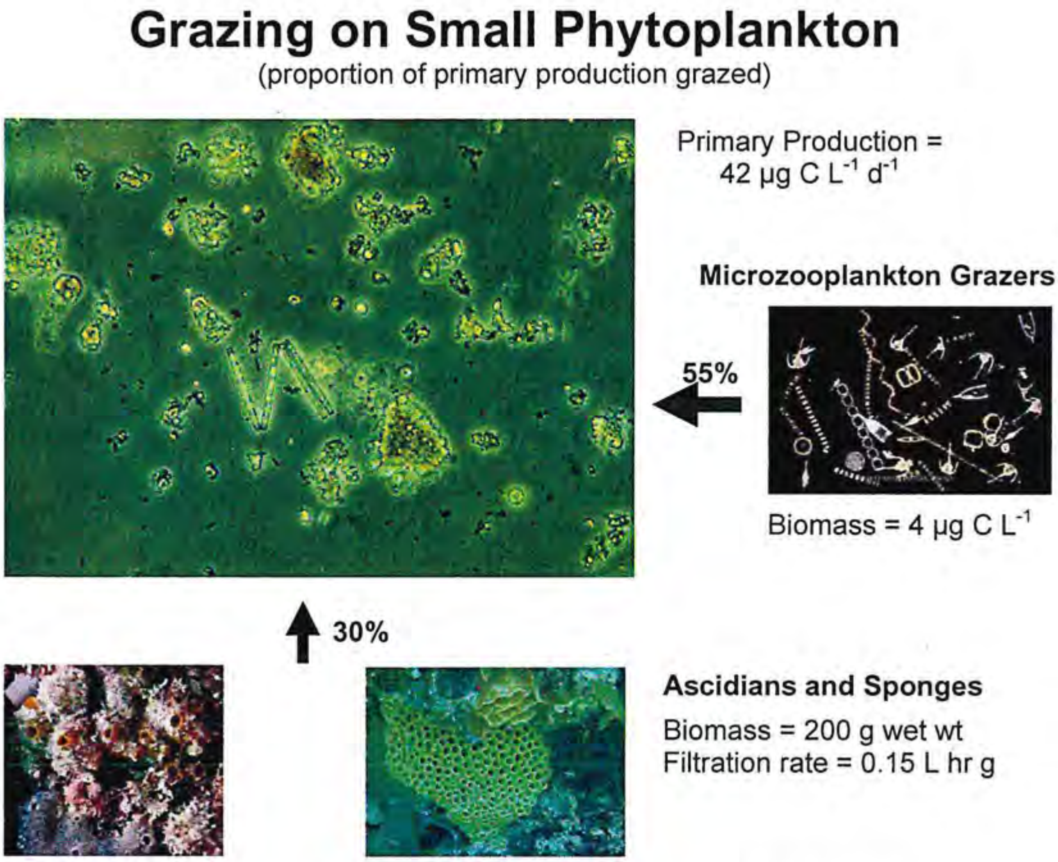

Figure 112. Impact of pelagic and benthic grazers on small phytoplankton

Benthic primary productivity

In Western Australian coastal waters abundant benthic plant communities (seagrass, macroalgae and microphytobenthos) may be more important primary producers than pelagic communities and are possibly a globally important carbon store. Macroalgae and seagrasses in particular are present at high biomass and while studies on biomass and assemblage composition are useful, direct measures of benthic productivity are likely to be most sensitive to anthropogenic or climate related stressors. At present there is little direct information on primary productivity at the assemblage level or for individual macroalgal species. Similarly, the WA coast has a wide shelf with large open areas of sand. Populations of benthic phytoplankton in these habitats may also make a substantial contribution to total primary productivity. These areas are dynamic and unstable, and while benthic algae are adaptive but disturbance, production is highly variable in space and time.

A factor that makes primary productivity difficult to quantify is the variable nature of the underwater light conditions. We have conducted incubations to determine the production of oxygen at a range of light intensities to develop productivity versus irradiance (P vs I) curves for benthic microalgal communities (Figure 113) and several key macroalgal species (*Ecklonia radiata, Sargassum sp. Hennedya* *sp.* and *Callophycus sp.*). The oxygen evolution versus light intensity relationship combined with high resolution *in situ* PAR measurements then yield sensitive temporal productivity estimates.

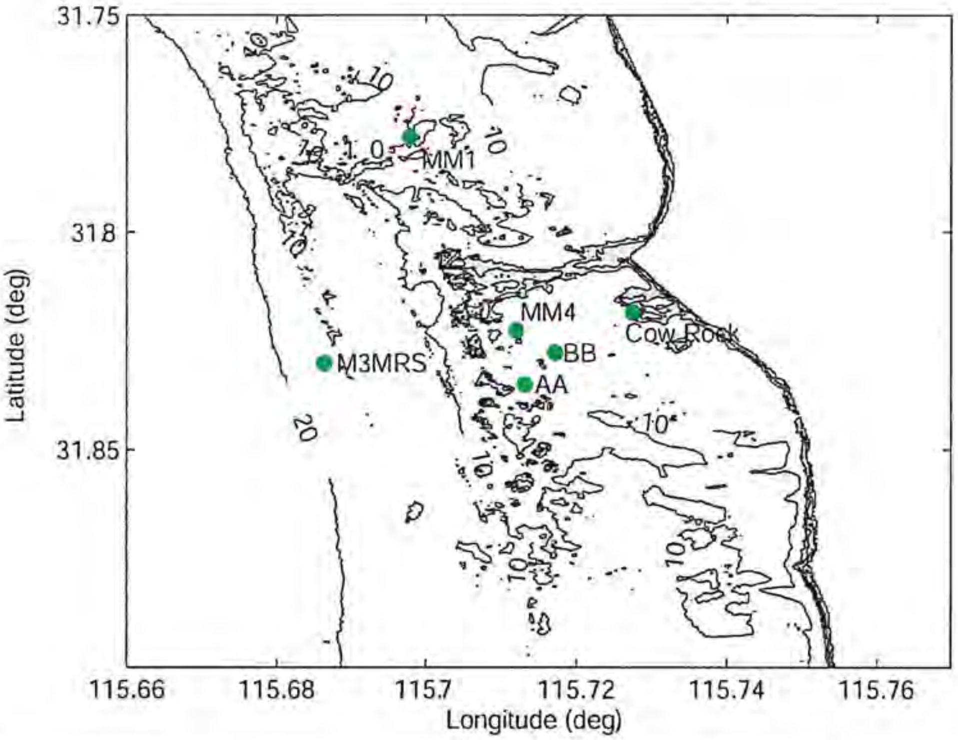

Figure 113 Map of the study area (see above for its location relative to the Australian mainland and within South-Western Australia. The opaque circles are the 6 stations where incubations for production by benthic microalgae were conducted.

Primary productivity in the macroalgae *Ecklonia radiata* as estimated by oxygen production is sensitive to variations in the incident radiation (Figure 114). Rates of primary productivity increased with increasing light exposure in a fashion typical of classic P vs I incubations. The correlation between oxygen production and light intensity is strong, over 90% of the variability in oxygen production can be explained by variations in the incubation light intensity. Preliminary incubations on benthic microalgal communities made during winter revealed a similar pattern (Figure 115) with some evidence for photoinhibition at the higher intensities.

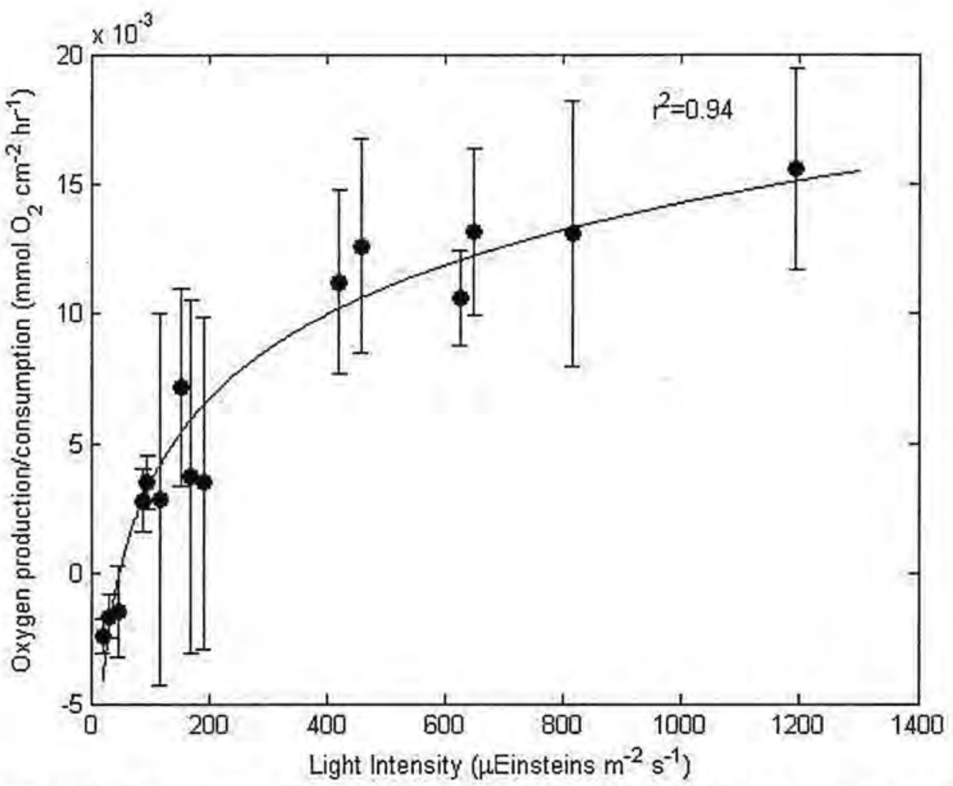

Figure 114 Preliminary estimate of oxygen evolution (consumption)by the macroalgae *Ecklonia radiata* measured in summer at a range of ambient light intensities.

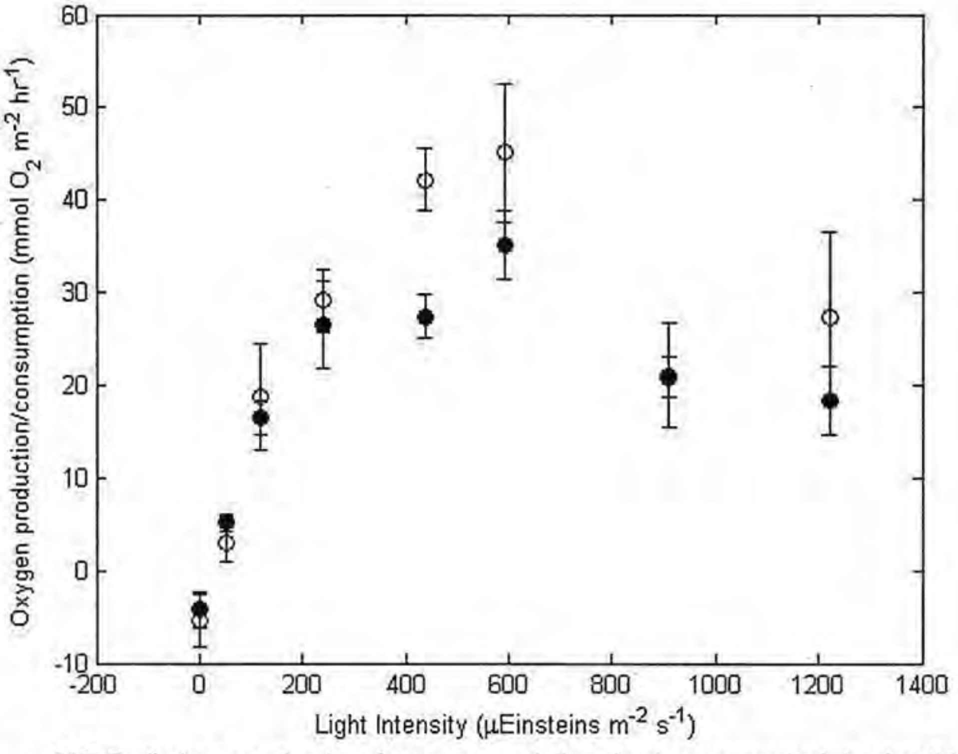

Figure 115 Preliminary estimate of oxygen evolution (and consumption) by benthic microalgae measured in winter from station AA at a range of ambient light intensities. Open and closed circles are the averages of samples (n=3) collected from THE SAME RIDGES AND TROUGHS, respectively.

As an example of how this P vs I relationship can be used to improve our understanding of the temporal variations in primary productivity we have used a 38 day record of shallow water PAR measurements collected by an *in situ* mooring in ~20m of water at Two Rocks which is located just to the north of our sampling area in Marmion Lagoon. Although the mooring was deployed in a different season to our P vs I curve, these data serve to demonstrate the potential for large variations in productivity between different days depending on the ambient light climate (Figure 116).

Here, we have used variations in oxygen evolution at various irradiance levels to demonstrate that benthic primary productivity is strongly dependent on light intensity. However, two factors presently limit the usefulness of this understanding. Firstly, variations in microalgal primary productivity need to be assessed relative to variations in the biomass present to determine whether spatial patterns are due variations in population size or differences in photosynthetic efficiency (possibly due to differences in nutrient availability and supply). Secondly the impact of these variations in primary productivity on sediment processes and nutrient release need to be quantified as an important improvement to our nutrient budgeting/modelling capability. The improvements to the analysis presented here will be made once nutrient and chlorophyll samples collected during incubations have been analysed. Continued significant delays outside our control in the processing of these nutrient samples and those to be collected this coming summer is anticipated and seems likely to result a failure not only to meet the June 2009 milestone but will have resource implications in 2009/2010 as a delay in receiving nutrient data will mean pushing out activity to 2009/2010 that was not budgeted for.

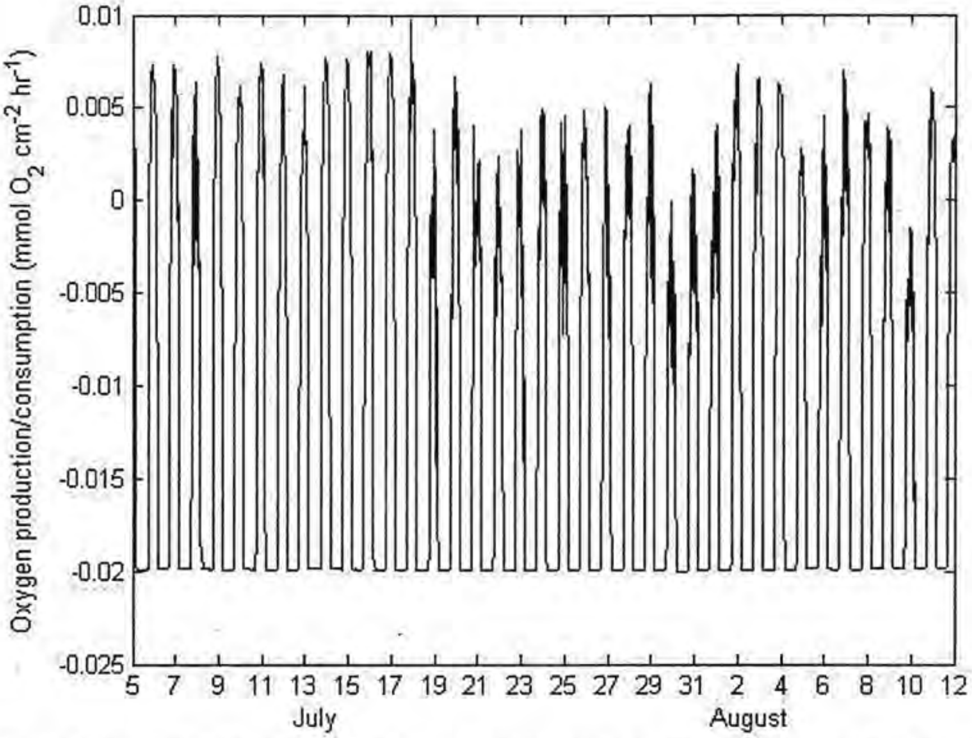

Figure 116. Daily oxygen evolution for the macroalgae Ecklonia radiata over a 38 day period (July – August) derived using the above relationship and measured PAR values.

Milestone 1.3.4: Complete shelf biomass sampling and ecological process field work

Original Forecast Finish Date: 30/06/08

Revised Forecast Finish Date: 30/06/08

This section unchanged from previous Biannual Report

Summary of Activities Undertaken, Outputs Produced:

A summary of the May/June 2007 Southern Surveyor voyage is provided under milestone 1.3.1. The component of the work to characterize structure, biomass and productivity profiles on benthic continental shelf habitats is described here. Analysis is still preliminary. Ultimately the data will be scaled up for a shelf scale representation of habitats, biomass distribution and productivity estimates and a conceptual model of benthic – pelagic coupling on the continental shelf.

Summary of Operations Performed
Benthic based operations were performed over two transects near Perth at 31.71°S and 31.76°S from 115.63°E to 115.15°E with stations at depths of 30,

40, 50, 75, 100 and 150m (Figure 117). Acoustic swath mapping of the sea-bed was conducted during the entire voyage; at each of the 12 study sites, benthic sled dredges, sediment grabs, benthic video and CTD casts were completed. Thirteen sleds comprised 6 over hard sediment (from 30-75m depth) and 7 over soft sediment (from 40-150m depth); 40 sediment grabs and thirteen CTD casts were executed. Thirteen videos were captured- 1 at each station of 30, 40 and 150m depth and 2 continuous tows from 50-100m depth. Extra videos were also performed between 35-50m depth to target a range of habitat heterogeneity identified from the swath imagery.

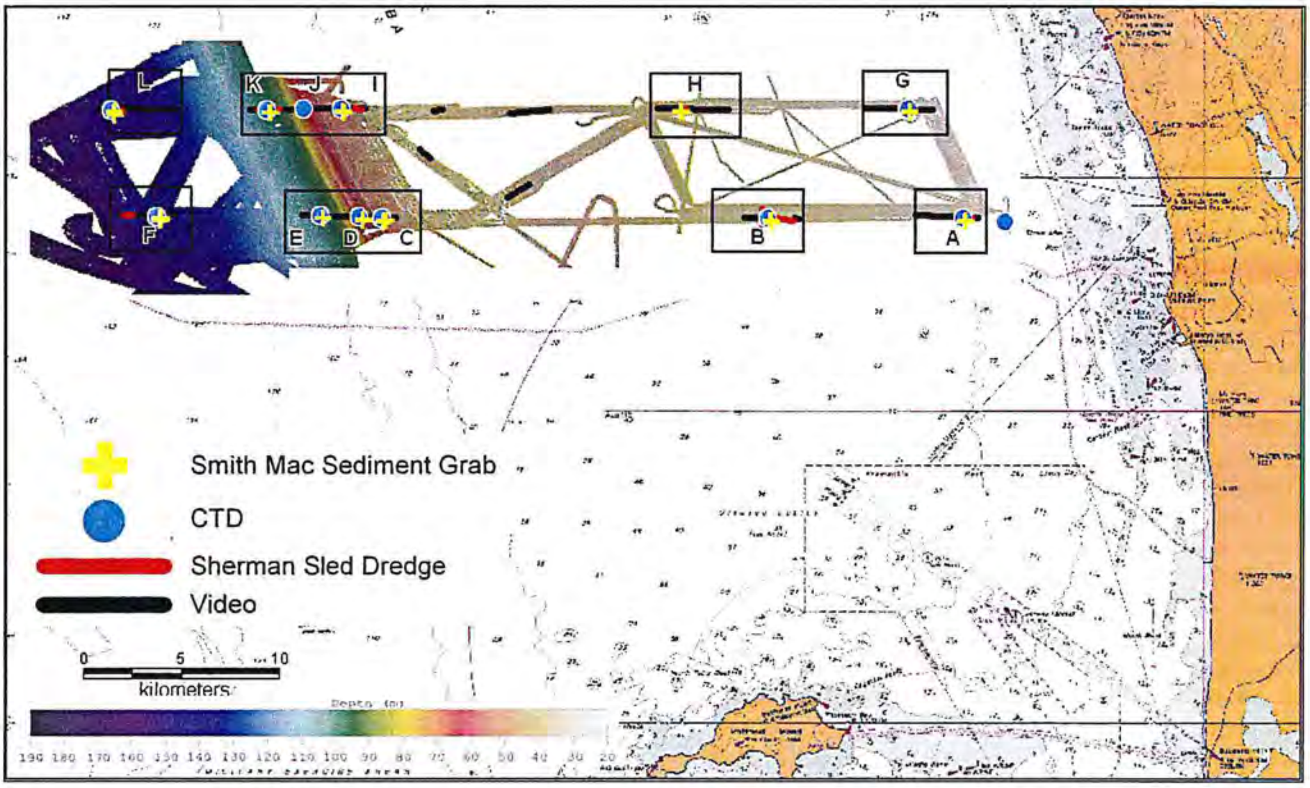

Figure 117. Sampling domain for the 1st leg of the May/June Southern Surveyor voyage.

Swath Mapping and Backscatter

Acoustic swath mapping during Leg 1 of the voyage covered a depth range of 30-180m (Figure 117). Results of the technique were used to aid the positioning of operations during the voyage and have been useful in GIS mapping of these operations, as seen in Figure 118.

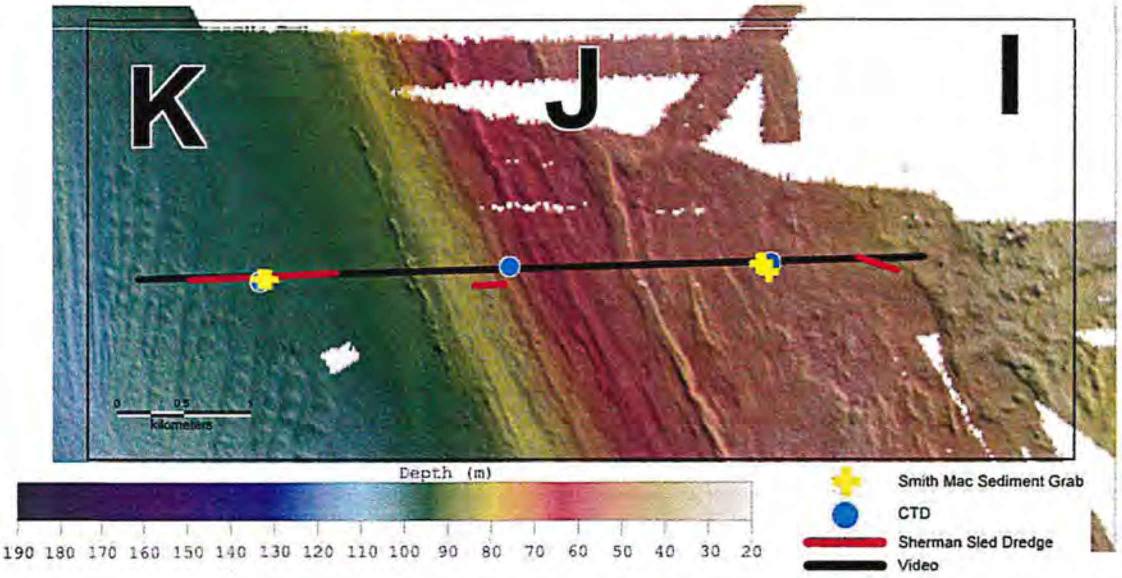

Figure 118. Example of GIS mapping of voyage operations over acoustic swath map image.

Continuous multibeam ping responses, or backscatter, collected during the voyage is being used to separate and identify sea-bed cover classes. Work is focusing on backscatter tracks with corresponding video operations to determine a correlation between backscatter data and sea-bed type as seen on video.

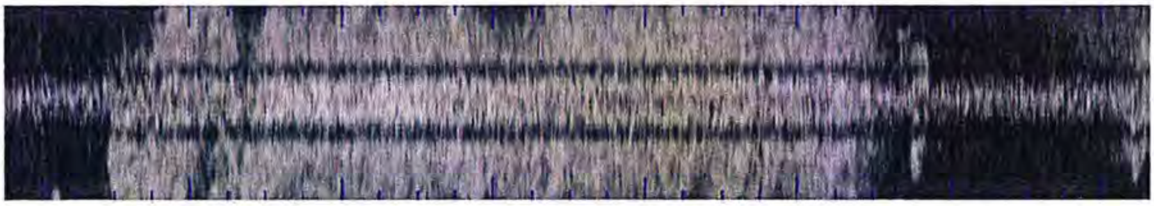

Figure 119. Example section of backscatter track showing contrasting light and dark sections.

One approach to examine the similarities and differences between the backscatter responses for the various seabed cover types is to identify contiguous segments which appear to be homogeneous in grey level and texture, as shown in Figure 119 above, as training classes. Canonical variate analysis is used to find linear combinations of the backscatter data at each angle which best separate the training classes, relative to the variation within each class. Figure 120 shows a plot of the training class means, the cluster of sites near (24.5,13.0) corresponds to the lighter regions in the backscatter track while those in a group on the right are the dark areas. The towed video of this same location (Figure 121) demonstrates that the dark backscatter areas tend to relate to sand and light areas to hard substrate types.

It is apparent that points on the left of the horizontal axis have dense cover and/or hard substrate while those on the right on the graph are sandy sites. For points on the left, the vertical axis shows sites with dense cover having low scores, and sites with hard bottoms and sparser vegetation cover having high scores. For the sandy sites, the vertical axis shows sites with long, strong ripples having low scores, and sites with more fine ripples having high scores. Such interpretation has been shown to hold true over a number of tracks examined thus far.

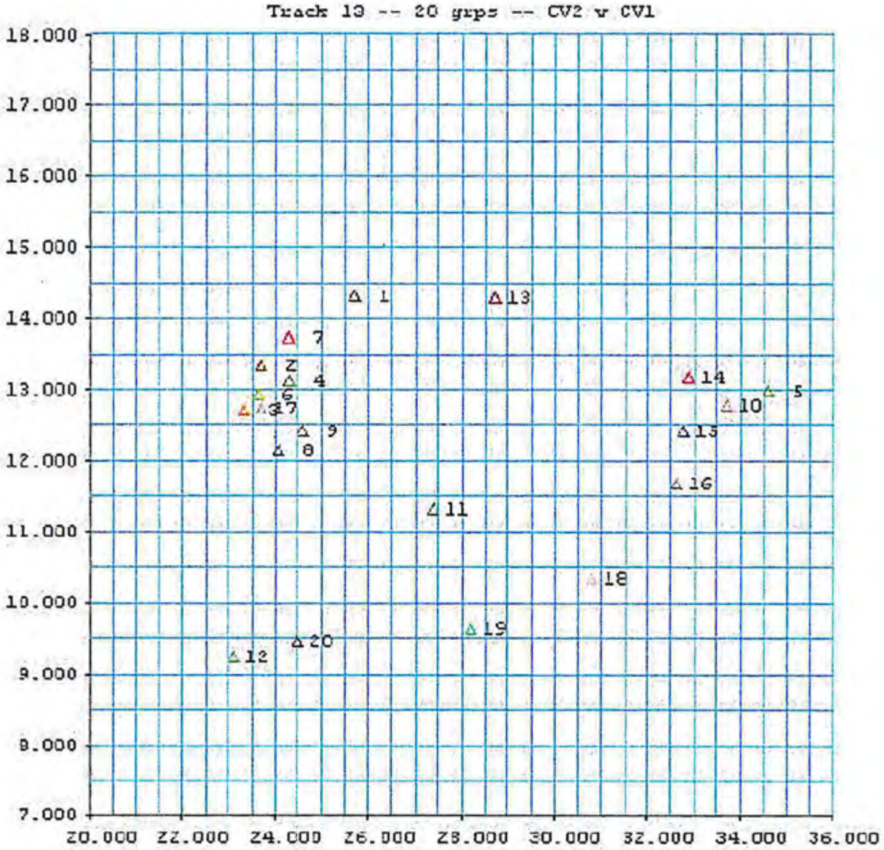

Figure 120. Canonical variate means for 20 training classes of a backscatter track.

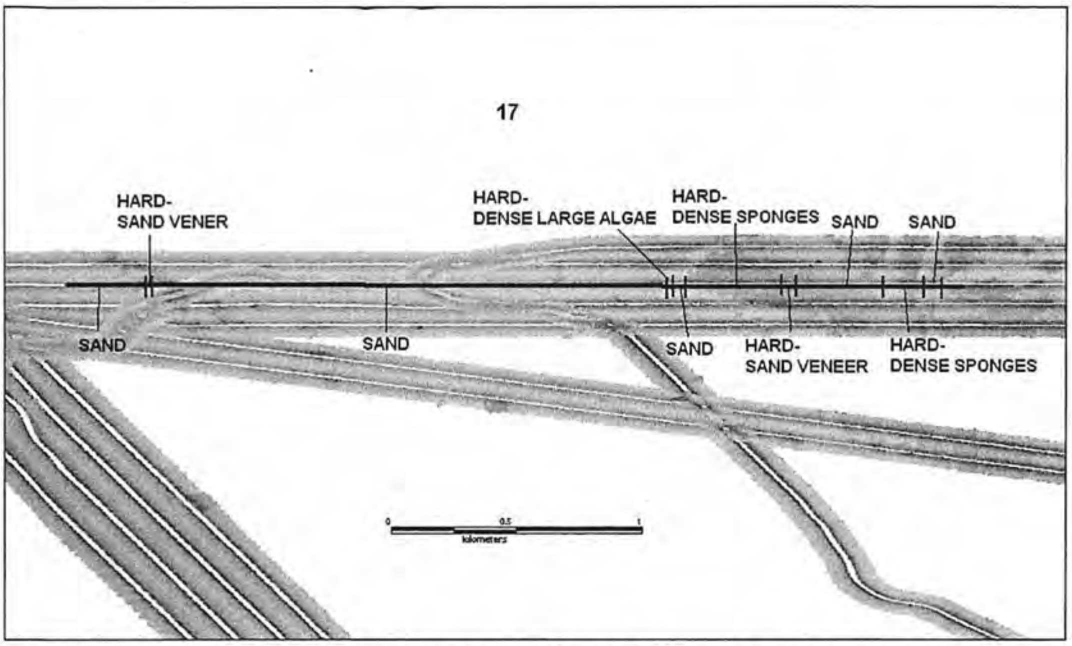

Figure 121. Descriptions applied to a video track (black line) overlaid on backscatter information.

Towed Benthic Videos and Habitat Structure

The series of towed videos ranged from a distance of 470m to 5.9km, with a total distance of 32.5km of benthic footage, Figure 122 demonstrates the depths of video captured. The footage was manually described into 15 categories based on sea-bed type and associated plants and animals and their densities. Analysis revealed a great variety of habitat types between the depths of 30-110m while the benthos at 150m was constant and remained as its own sea-bed category due to different features to shallower depths. For simplicity these 15 categories were pooled into 9 broad categories (Table 9).

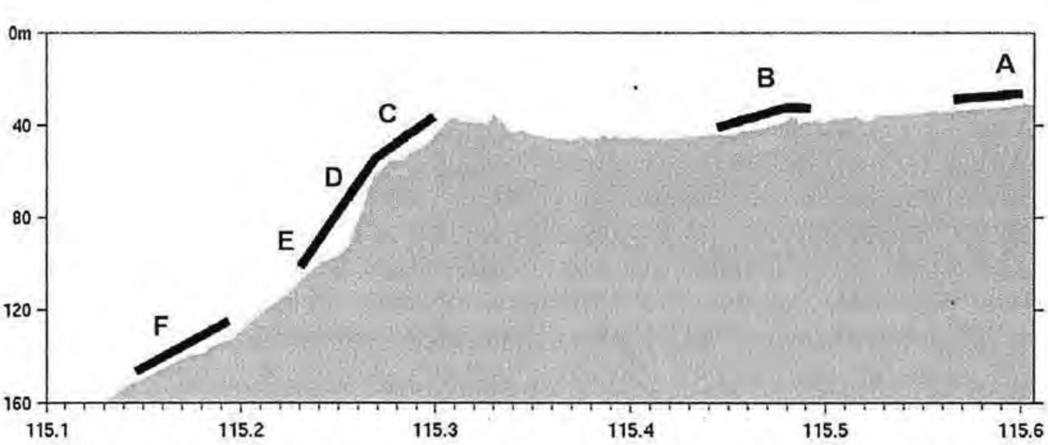

Figure 122. Bathymetry cross section of voyage transect and approximate depths of towed benthic videos.

Table 9 displays the broad habitat categories observed on videos. These broad categories can be further pooled into sand, reef and patchy habitat types, with the latter referring to areas where both sand and hard substrate are present in very small alternating areas. Analysis has revealed an overall estimate of 51% sand, 31% reef and 18% patchy substrate between 30-110m depth. Perhaps if we make the large assumption that these highly patchy areas are 50% sand and 50% reef then we have overall estimates of 60% sand and 40% reef.

Table 9 . Percentage of Habitat Types Present on Towed Videos (averaged across depth ranges).

Depth (m)	**Bare Sand ± Sparse Algae**	**Seagrass**	**Flat Fine Sediment, Sparse Filter Feeders**	**Bare Hard Substrate ± Sparse Algae**	**Patchy Sand & Hard Substrate (Varying Size Algae ± Filter Feeders)**	**Hard Substrate, Low-Med Density Low Algae, Low-Med Density Filter Feeders**	**Hard Substrate, High Density Low Algae**	**Hard Substrate, Med- High Density Large Algae (primarily *Ecklonia*)**	**Hard Substrate, Dense Sponges**
30-39	47.9	1.6	-	-	48.7	1.4	-	-	0.4
40-49	57.0	-	-	3.1	9.6	0.5	3.6	9.6	16.6
50-74	13.9	-	-	36.8	3.1	6.3	-	30.2	9.8
75-99	20.6	-	-	14.9	10.1	7.7	9.8	5.7	31.2
100-110	93.4	-	-	-	4.7	-	-	-	1.9
140-150	-	-	100.0	-	-	-	-	-	-

Figure 123 illustrates the importance of determining the benthos of the area covered by the Southern Surveyor voyage. While we know the habitat from the coast to 30m depth which falls within Marmion Marine Park, this is only 13% of the area to 100m depth. The towed video work allows us to fill in habitat of the areas at deeper depths.

Combination of this habitat characterisation with chlorophyll *a* measurements discussed in milestone 1.3.1 and algal biomass outlined below, suggests the importance of characterising the areas for which little is know. The sand habitats in 30-50m depth have biomass six times higher as in 0-30m depth, and reef habitats in 30-50m depth have about the same tonnage of algae as in shallower depths. This highlights the significance of this mid-depth region of 30-50m off Perth, which is as important as shallower areas in terms of benthic primary producer biomass.

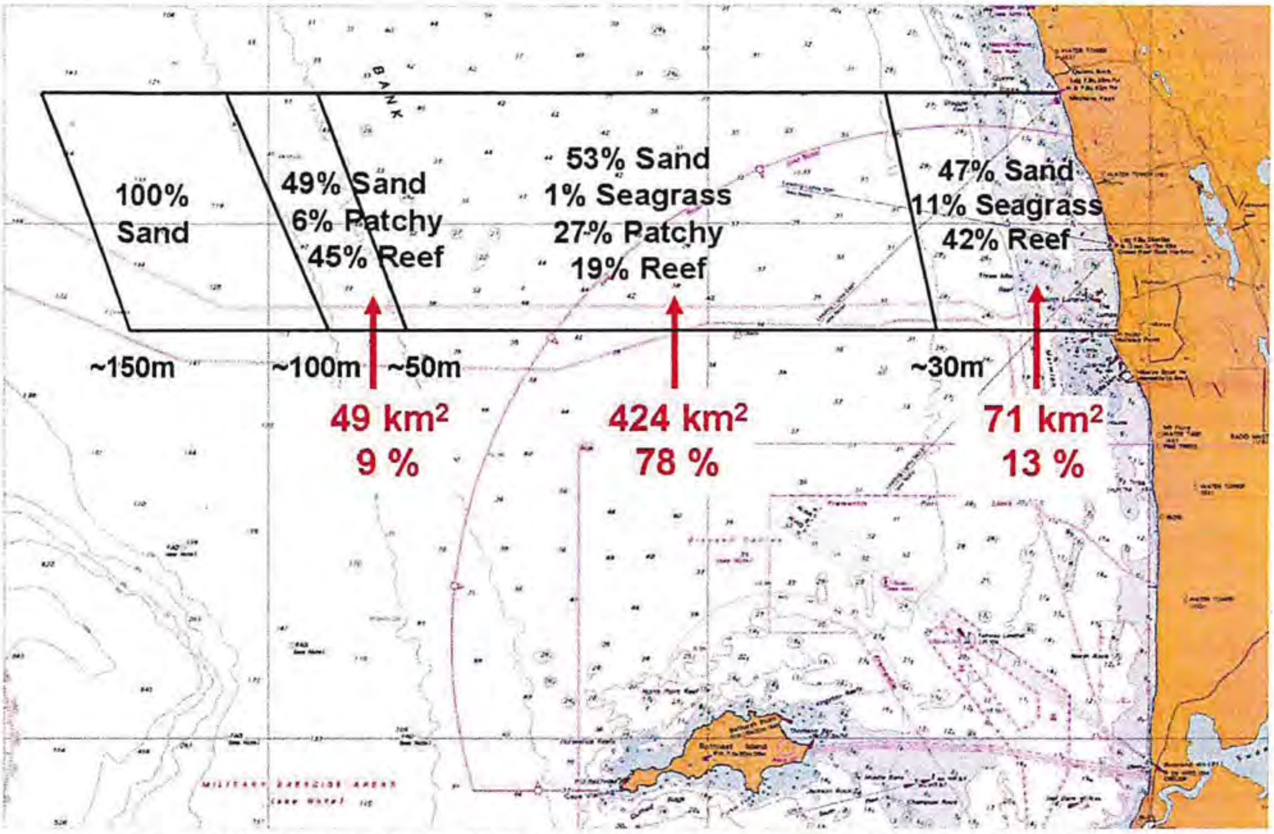

Figure 123. Marmion shelf scale domain illustrating proportions of shelf area (in red) and proportions of benthic type in each depth range (in black). Benthic type to 30m depth calculated from Marmion Marine Park Habitat Map, CALM (2002).

Benthic Biomass Estimates

In order to characterise the plant and animal communities of shelf-scale benthic habitats, a large heavy epibenthic sled, 1.2m wide, was used to dredge the sea-bed at each of the stations; retrieved samples were photographed, identified, catalogued, counted and weighed.

Animals

The average densities of animals at each depth recovered by sled dredge are given in Figure 124. The overall average animal density for hard bottom habitats was $0.55.m^{-2}$ and for soft substrata was $1.02.m^{-2}$. The density at 150m is attributed to one sled with large numbers of very small sponges. This sled is also responsible for the increased density of sponges average for all sled dredges (Figure 125). Excluding this sample, the average density of sponges for the other 6 sleds on soft sediment was $0.041.m^{-2}$. The densities of all animals captured by the sled dredge remain low (Figure 125). Those animals grouped as "other", consisted largely of echinoderms, molluscs, polycheaetes and crustaceans.

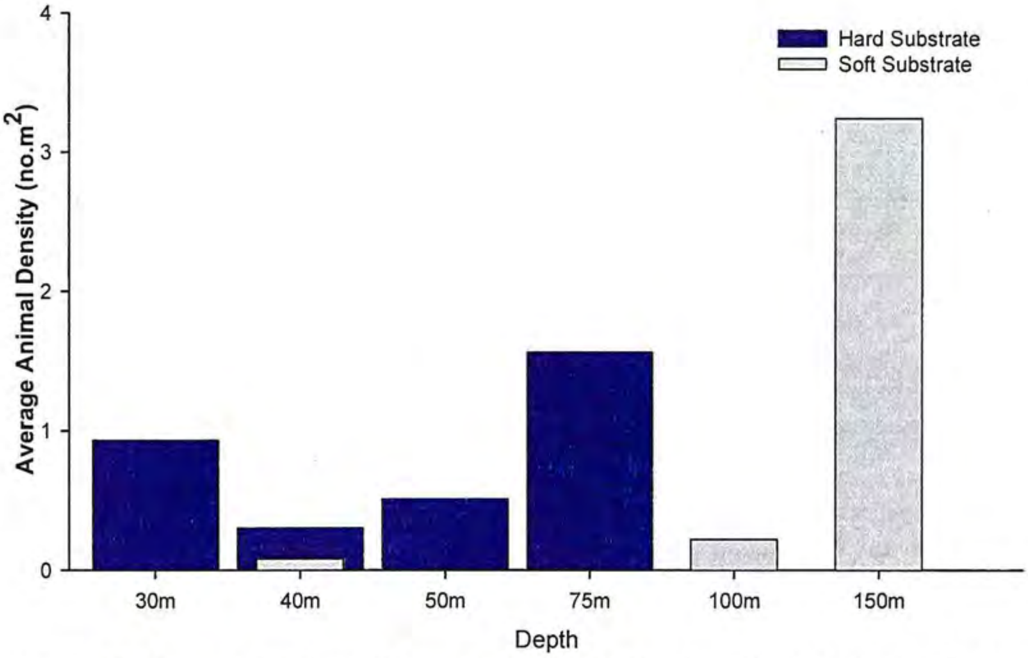

Figure 124. Average total animal densities for sled dredges from leg 1 of Southern Surveyor 2007-04.

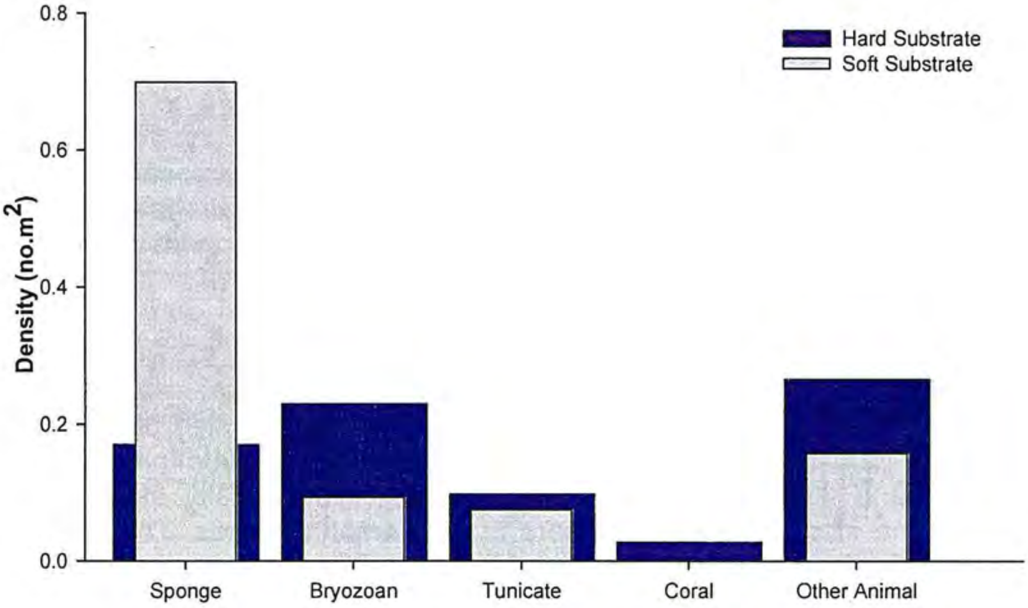

Figure 125. Average density of animal types recovered by sled dredge.

Average total animal biomass is shown in Figure 126 for sled dredges over hard and soft sediment at specific depths. The overall average for hard sea-bed areas from 30-75m was 121.0g.m^{-2}, for soft sediment at 40 and 100m was 0.8 g.m^{-2} and for the deeper 150m sites was 43.9 g.m^{-2}.

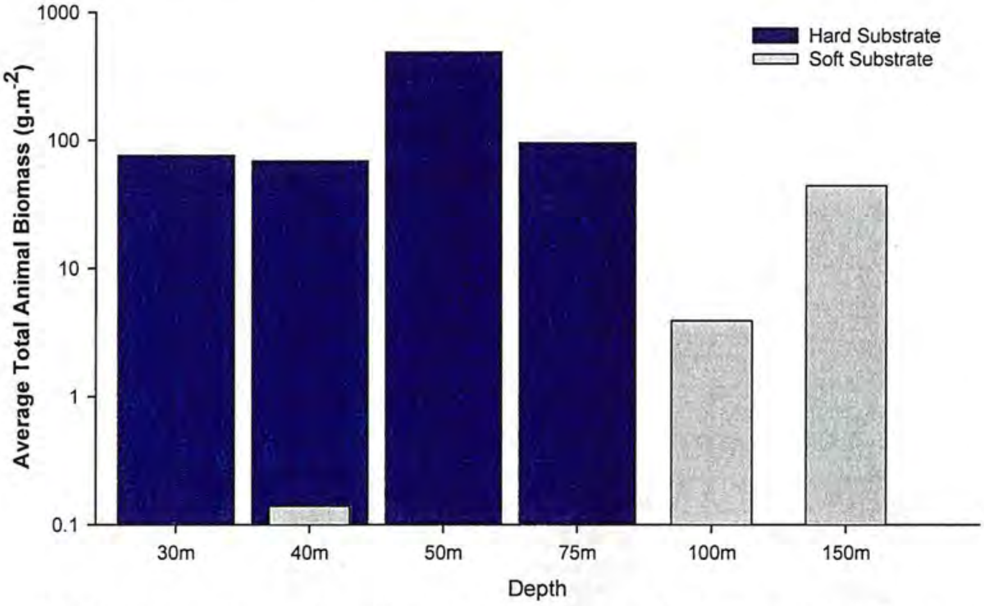

Figure 126. Average total animal biomass for sled dredges from leg 1 of Southern Surveyor 2007-04.

Sponges were the dominant biomass of sled samples over both hard and soft sediment, and the biomass of all animal types was greater for hard sea-bed habitats (Figure 127).

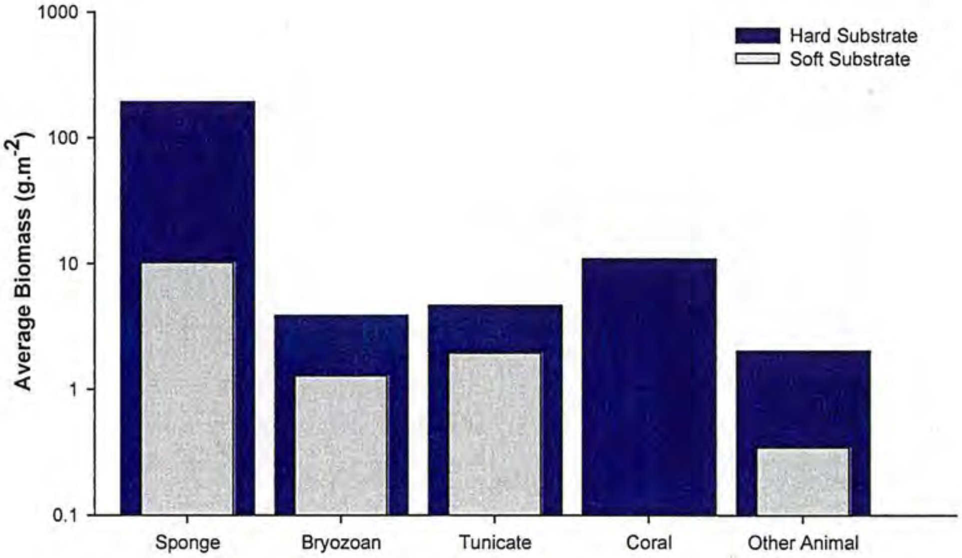

Figure 127. Average biomass of animal types recovered by sled dredge.

Plants

Average total plant biomass is given in Figure 128 for sled dredges over hard and soft sediment at specific depths, not shown on the figure are the sled over hard substrate at 75m and two over soft sediment at 150m, all of which had no plant material. The overall average for hard sea-bed areas from 30-75m was 152.1g.m^{-2}, for soft sediment at 40 and 100m was 0.03g.m^{-2} and for the deep 150m sites was 0g.m^{-2}.

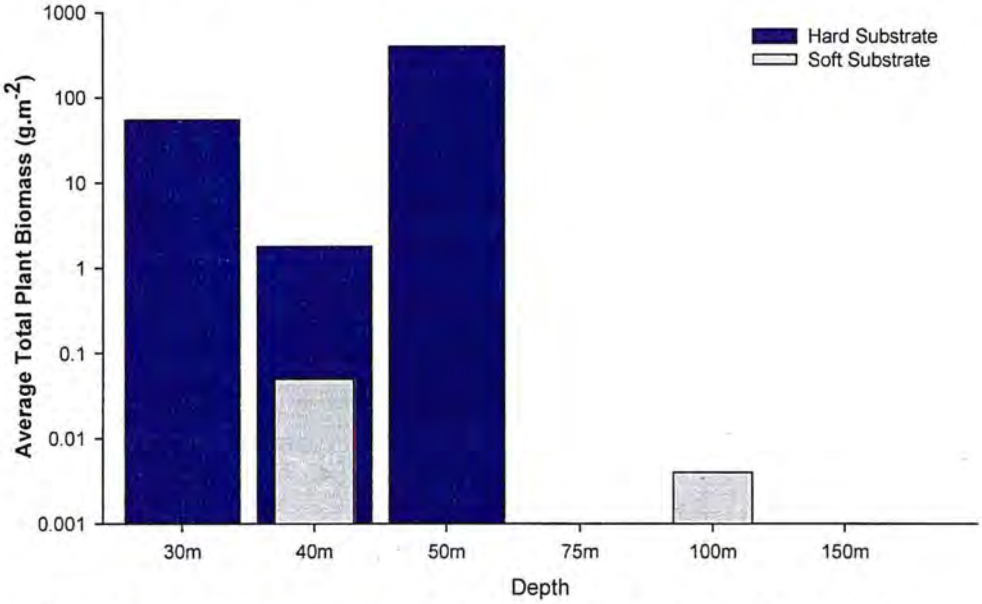

Figure 128. Average total plant biomass for sled dredges from leg 1 of Southern Surveyor 2007-04.

The kelp *Ecklonia* dominated hard substrate sled samples by an order of magnitude, this was due to the large biomass retrieved on both sleds at 50m depth (Figure 129).

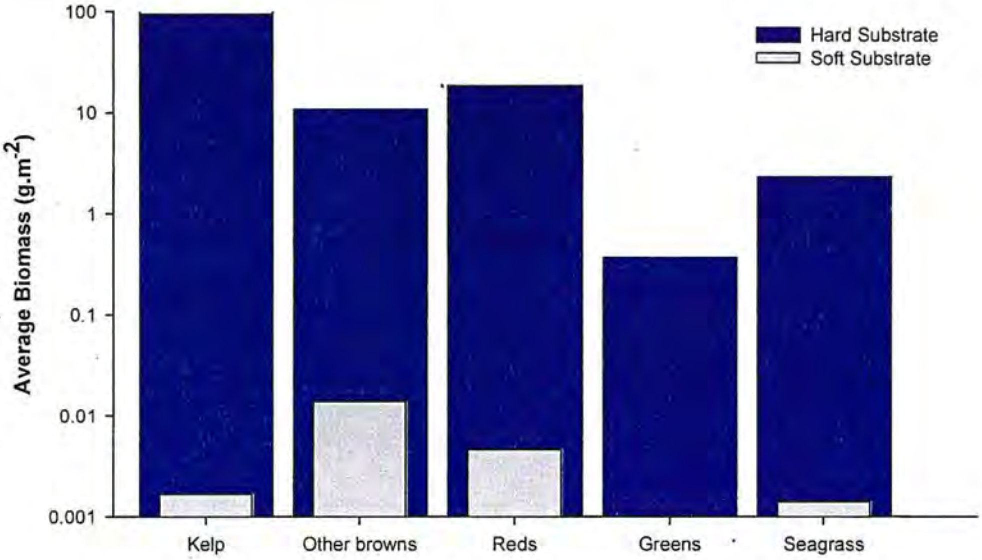

Figure 129. Average biomass of plant categories recovered by sled dredge.

Benthic Microalgae

Refer to milestone 1.3.1

Photosynthetic Performance

Benthic microalgae

Refer to milestone 1.3.1

Macroalgae

Productivity measurements were conducted on a number of abundant macroalgal species collected from 40 – 60 m depths during the cruise. Additionally, the diversity and biomass of all species collected was recorded, to allow for estimation of benthic plant biomass and productivity in depths >40 m. Samples were also collected for a number of algal bioassays (e.g. isotopic composition, nutrient status, pigment concentration) that will allow comparison between deep- and shallow-water benthic plants of Marmion Lagoon.

Measurements of the photosynthetic performance of a number of abundant macroalgal species, collected from 33 – 55 m depths, were conducted by Julia Phillips during the cruise. Additionally, the diversity and biomass of all species collected was recorded, to allow for estimation of benthic plant biomass and productivity in depths >40 m. Samples were also collected for a number of algal bioassays (e.g. isotopic composition, nutrient status, pigment concentration) that will allow comparison between deep- and shallow-water benthic plants of Marmion Lagoon.

The photosynthetic performance of 4 brown and 3 red algal deep-water species was measured in terms of potential quantum yield (Fv/Fm, which indicates 'health' status of photosystem II) and electron transport rates (ETR). Brown algae (Phaeophyta) had significantly higher yield values compared to red algae (Rhodophyta) (see Table 10 below). The kelp, *Ecklonia radiata*, had the highest F_v/F_m of 0.80 ± 0.00 (mean ± SE) and highest ETR_{max} of 12.6 µmol electron m^{-2} s^{-1}. ETR_{max} and F_v/F_m related to depth ($r^2 = 0.03$ and $r^2 = 0.01$ respectively).

Table 10 . Algal species, functional form and depth collected, F_v/F_m (mean ± SE), ETRmax (μmol electron m^{-2} s^{-1}), I_k (μmol quanta m^{-2} s^{-1}), absorptance factor (AF), maximum noon irradiance at depth (μmol quanta m^{-2} s^{-1}) and percent surface irradiance.

Species	Functional form	Depth (m)	AF*	F_v/F_m	ETR_{max}	I_k	maximum irradiance at depth	% surface irradiance
Phaeophyta								
Sargassum peronii	corticated foliose	33	0.78	0.76 ± 0.00^{A}	8.9 ± 0.6^{a}	$29.9 \pm 1.8_{A}$	92	4.6
Dictyopteris muelleri	foliose	33	-	0.74 ± 0.01^{A}	-	-	92	4.6
Myriodesma quercifolium	corticated foliose	40	0.78	0.74 ± 0.01^{A}	5.3 ± 0.1^{b}	$16.9 \pm 0.3_{AB}$	48	2.4
Scytothalia dorycarpa	leathery	50	0.84	0.74 ± 0.01^{A}	6.7 ± 0.3^{c}	$22.1 \pm 1.3_{AB}$	19	1.0
Ecklonia radiata	leathery	50	0.84	0.80 ± 0.00^{B}	12.6 ± 0.2^{d}	$37.0 \pm 1.2_{AB}$	19	1.0
Rhodophyta								
Osmundaria prolifera	leathery	33	0.84	0.46 ± 0.02^{C}	3.0 ± 0.2^{e}	$38.0 \pm 6.2_{AB}$	92	4.6
Hennedya crispa	corticated foliose	55	0.57	0.56 ± 0.01^{D}	1.7 ± 0.1^{f}	$45.5 \pm 9.6_{B}$	12	0.6
Callophycus costatus	corticated foliose	55	0.57	0.56 ± 0.02^{D}	1.2 ± 0.1^{f}	$35.5 \pm 6.8_{B}$	12	0.6

** estimated from Markager (1993), Franklin and Badger (2001), Figueroa et al (2003), Beer and Axelsson (2004)*

Letters indicate significant differences among species

Although it is commonly thought that red algal species fare better under low light conditions and are more productive than brown or green species (Gail 1922, Larkum et al. 1967, Dring 1981), the higher F_v/F_m and ETR_{max} of the brown species in this study suggests that in well-mixed oligotrophic waters of Western Australia this is not the case. The biomass of reds and browns was, on average, similar across depths 33 to 55 m, while greens had significantly lower biomass than both reds and browns (data not shown here). High F_v/F_m, prolific standing stock and high biomass at low light intensities (<5% of surface irradiance) indicate an efficient utilisation of available light energy (Littler et al. 1986). The high photosynthetic rates of the brown algae may also be due to greater availability of nutrients in the well-mixed waters, or reduced levels of herbivory and grazing, which allowed greater standing stocks to develop.

This work represents the first measurements of photosynthetic performance of deep-water algae from Western Australia, and is currently being prepared as a manuscript for submission to an international journal.

Isotopic composition:
Samples for isotopic composition were collected from 16 algal and 1 seagrass species, from 33 – 55 m depths. Where possible, matching samples were collected from shallow water plants. Samples have recently been analysed for %C, %N, $\delta^{15}N$ and $\delta^{13}C$ by the School of Natural Sciences Stable Isotope Laboratory at Edith Cowan University, but have yet to be analysed.

Nutrient status of macroalgae:
The nutrient status of 7 red and brown macroalgal species was determined by extraction of soluble tissue nitrogen (N) pools from the algal tissue. Samples were collected from deep waters (40 – 55 m) during the cruise, and additional shallow water (4 – 15 m) samples were collected immediately after the cruise. Soluble tissue N pools are a useful bioindicator of a plant's recent, short-term exposure to N availability, and as such can be used to supplement data on ambient seawater N levels that were collected during the cruise (Figure 130).

Some species examined, such as the brown alga *Sctyothalia dorycarpa* and the red alga *Hennedya crispa*, exhibited increased soluble tissue N pools with increasing water depth, while others such as the brown algae *Ecklonia radiata* and *Dictyopteris muelleri* showed no trend with depth. These differences may be due to localised nutrient availability or to physiological differences in the N requirements among species. These investigations are ongoing.

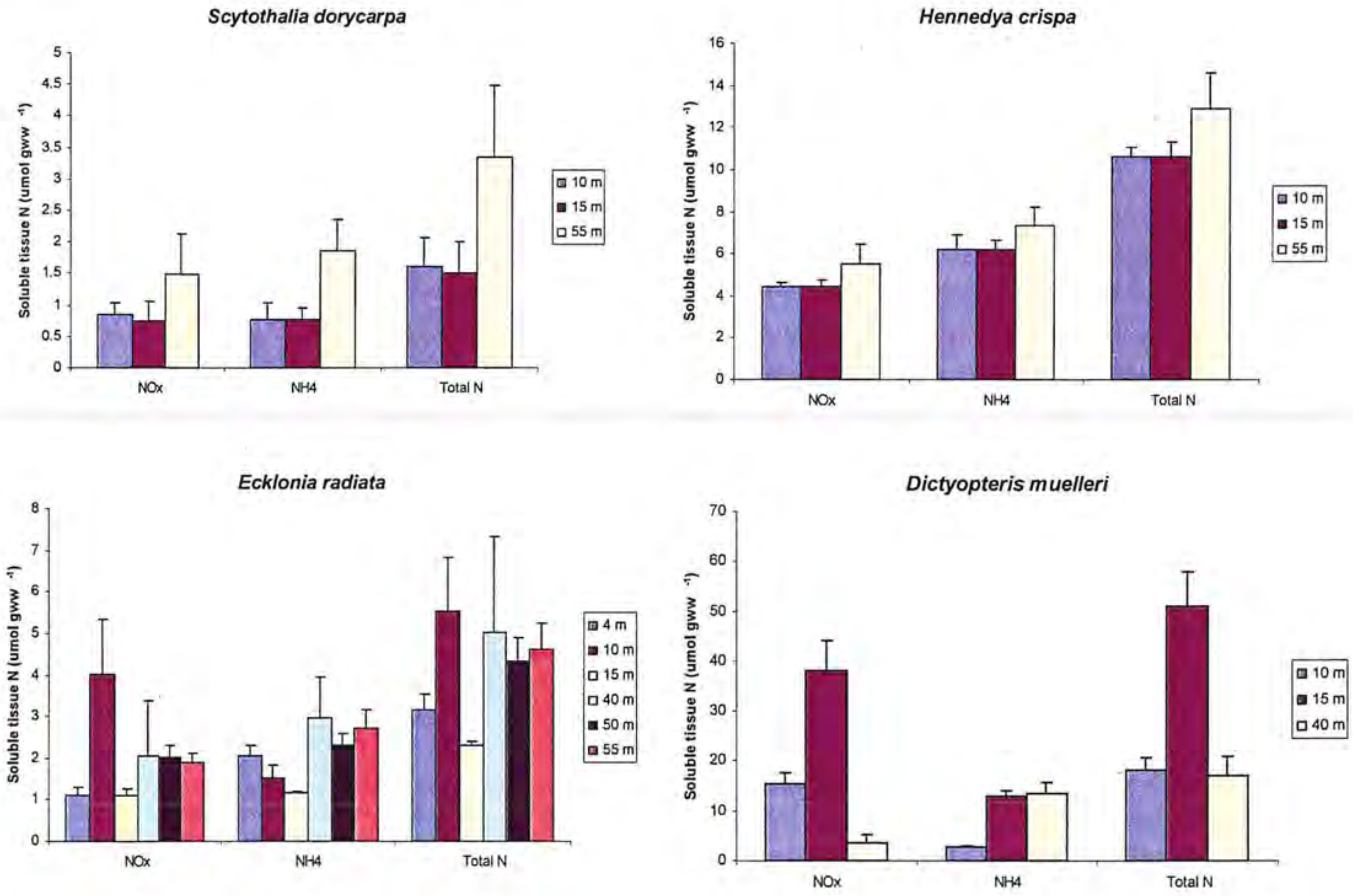

Figure 130. Soluble tissue nitrogen pools extracted from macroalgae growing at different depths.

Pigment composition and concentration:
Samples for pigment composition and concentration were collected from 9 algal and 1 seagrass species, from 33 – 55 m depths. As with the isotopic analyses, where possible, matching samples were collected from shallow water plants. Samples have recently been analysed for pigments and preliminary results only are available at this stage.

Results from pigment analyses varied among species. Some species showed increased pigment concentration with depth, as would be expected in algae that are compensating for lower light availability. Conversely, other species showed either no change, or decreased pigment concentrations with increasing depth. This may result from light levels not falling below critical levels, or from the acclimation of individual species to reduced light availability. This work is ongoing and additional samples may be collected in May 2008 to supplement existing data if necessary.

Role of benthic filter feeders

Deeper areas of Marmion lagoon provide a habitat for a considerable biomass of filter feeders. Biomass of sponges and ascidians in sled samples varied from less that 1 g of wet weight to a high of 850 g.m^2 (Figure 131).

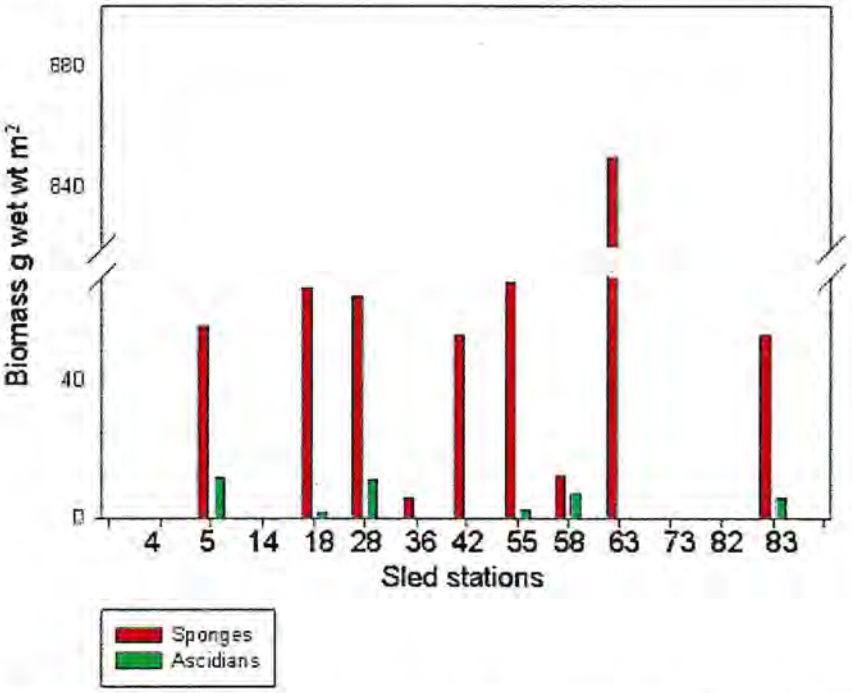

Figure 131. Biomass of sponges and ascidians in Marmion Lagoon 30 to 150 m stations.

Comparison of biomass of all invertebrate phyla dredged revealed that sponges and ascidians were present in all stations that were located on hard substrate and sponges dominated in terms of biomass in most of them (Figure 132). Ascidians were important in stations 5, 28, 58 and 83.

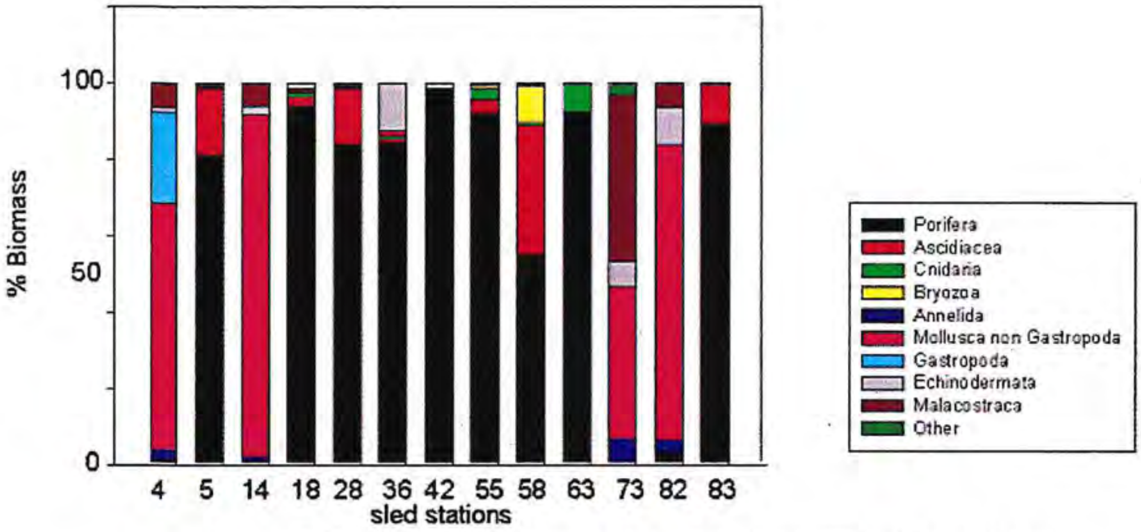

Figure 132. Proportion of biomass of invertebrates in 30 to 150 m stations.

Filtration rates measured *in situ* in shallow reefs were applied to biomass obtained from sled material to estimate the clearance rates of sponges and ascidians. Figure 133 below shows rates shown per day based on 12 hours activity (standard assumption in calculating rates).

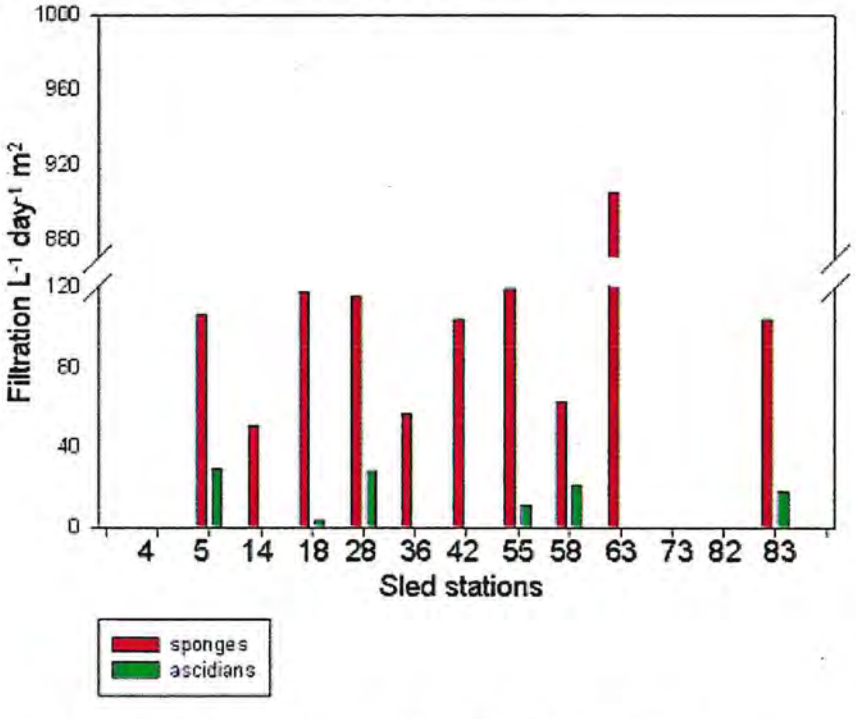

Figure 133. Daily filtration rates in 30m to 150 m stations.

Milestone 1.3.5: Data report on shelf and lagoon biomass & ecological sampling

Original Forecast Finish Date: 30/06/09

Revised Forecast Finish Date: 30/06/09

This section updated from previous Biannual Report

Summary of Activities Undertaken, Outputs Produced:

To date the analysis and reporting of data has been embedded in the progress reports (see milestones 1.3.1 – 1.3.4 above). A data report that contains summaries of data that has been collected as part of the shelf and lagoon benthic ecology research (see milestones 1.3.1 – 1.3.4 above including biomass and abundance of key functional groups, production of kelp, growth of mussels, measurements of sources of production with stable isotopes, measurements of grazing and predation, measurements of filter feeder grazing rates) has been completed and is provided separate to this Biannual Report.

4. Develop simple models for assessing and predicting impacts of physical forcing factors, primarily nutrients, on key benthic functional groups/habitats informed by experiments and observations conducted across a range of naturally varying and anthropogenically altered gradients related to nutrient enrichment.

Milestone 1.4.1: Complete Nutrient enrichment pilot study

Original Forecast Finish Date: 30/06/09

Revised Forecast Finish Date: 30/06/09

This section unchanged from previous Biannual Report

Summary of Activities Undertaken, Outputs Produced:

In November – December 2007 we conducted a pilot study to test a system for the delivery of nutrients to primary producer communities in reef and seagrass meadow habitats. Once perfected, the system will be used to investigate the long term effects of elevated nutrient concentrations on these communities. Eighteen sachets, each containing 500 g of slow release fertiliser, were anchored in nine places to form a grid over a 2 m x 2 m plot in each habitat. The sachets were anchored to the reef using10 lb weights and tent pegs in the seagrass. Control plots were established in the same fashion using sachets of clean gravel with a similar grain size to the fertiliser. The slow release fertiliser was chosen for its N:P ratio and because it is readily available in large quantities. We monitored the photosynthetic efficiency (quantum yield and electron transport rates) of 4 algal and 3 seagrass species found in both plots weekly over a 2 week period. Samples for bioassays (isotopic composition, soluble tissue nitrogen pools, TN, TP) were collected, along with samples for ambient seawater nutrient concentration.

Total nitrogen content in two macroalgal species was significantly higher in the experimental plot than the control plot at the second and third sampling periods (see Figure 134 and Table 11) suggesting that the fertilisation treatment has had some influence on the plants internal nitrogen pools. However, the difference between the treatments was accompanied by a reduction in the tissue nitrogen content of both the control and experimental plants over the course of the experiment (Figure 134). This reduction in tissue nitrogen content (from 1.4% to 0.8% in the control plot) over the three weeks was greater than the difference between the control and experimental plots at day 3 (0.2%). As such, it is not possible to definitively attribute differences in tissue nitrogen content to the nutrient treatments over spatial variations in the magnitude of the temporal decrease in the background levels. Variations between species and the sampling day notwithstanding, there were no significant differences in tissue nitrogen content between the control and experimental treatments in the seagrass experiment (Table 12). It is possible that the slow release fertiliser did not dissolve as readily due to the reduced water movement in seagrass meadows compared to the higher energy reef areas and as a result nutrient delivery was less efficient

Table 11. Analysis of variance table examining the tissue nitrogen content in two species of macroalgae (Species), surveyed on 3 occasions separated by one week (Day) and including control and experimental plots (Treat).

Analysis of Variance

Effect	*Sum Sq.*	*d.f.*	*F*	*p*
Species	*0.66*	*1*	*19.51*	*<0.001*
Day	*2.23*	*2*	*33.7*	*<0.001*
Treat	*0.27*	*1*	*8.05*	*0.007*
Species x Day	*0.04*	*2*	*0.66*	*0.522*
Species x Treat	*<0.001*	*1*	*0*	*0.971*
Day x Treat	*0.08*	*2*	*1.15*	*0.3244*
Error	*1.66*	*50*		

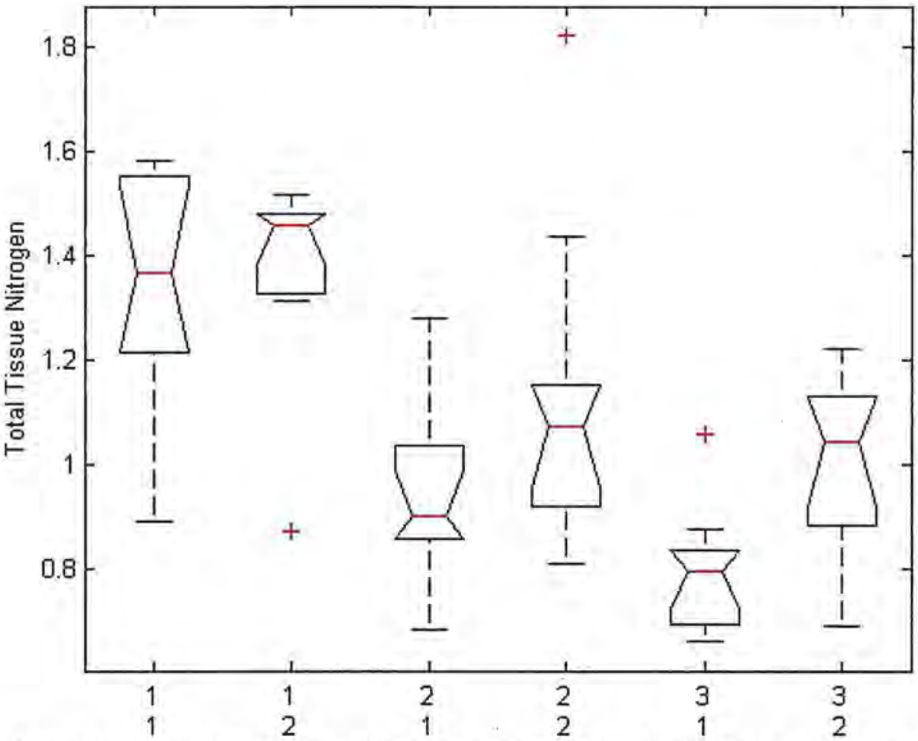

Figure 134. Box plots comparing the total nitrogen concentrations of two species of macroalgae (%), surveyed at 3 weekly intervals (top line of x axis) and collected from control and experimental treatment plots (bottom line of x axis). The centre line of each box is the median. The notched area is the uncertainty about the medians for box-to-box comparison (boxes whose notches do not overlap indicate that the medians of the two groups differ at the 5% significance level). The top and bottom of the box represent the 25th and 75th percentiles (the distance between the upper and lower percentiles is the interquartile range). The error bars bound the rest of the data except for outliers (red crosses which are data that is more than 1.5 times the interquartile range outside the 25th or 75th percentiles).

Table 12. Analysis of variance table examining the tissue nitrogen content in two species of seagrass (species), surveyed on 3 occasions separated by one week (Day) and including control and experimental plots (Treat).

Analysis of Variance

Effect	*Sum Sq.*	*F*	*p*
Species	*0.69*	*28.78*	*<0.001*
Day	*0.64*	*13.4*	*<0.001*
Treat	*0.02*	*0.76*	*0.389*
Species x Day	*0.18*	*3.72*	*0.031*
Species x Treat	*0.07*	*2.77*	*0.102*
Day x Treat	*<0.001*	*0*	*0.997*
Error	*1.21*		

While there are some promising aspects to this nutrient delivery system, questions still remain over the efficiency of the delivery.

Milestone 1.4.2 Complete Nutrient enrichment experiment across natural and anthropogenic gradients

Original Forecast Finish Date: 31/12/10

Revised Forecast Finish Date: 31/12/10

This section updated from previous Biannual Report

Summary of Activities Undertaken, Outputs Produced:

This milestone has two components. Firstly, we are carrying out a comparison of environmental and biotic attributes of pre-existing sediment nutrient gradients at a range of sites with a gradient of anthropogenic impacts. We can use these measurements to develop simple models which estimate ecosystem to increased sediment nutrient load. Following discussions with DEC we have added Northern Harbour in Cockburn Sound and the Whitfords sewage outfall site to an expanded set of 29 sites for this work. Secondly we have planned to follow up the above pilot experiment (see milestone 1.4.1 above) with a more extensive manipulative experiment which would look at the seasonal response of reef and soft sediment habitats to artificially induced nutrient enrichment. We have decided to suspend this latter component of the work for reasons outlined in the second of the two sections below.

Influence of gradients of sediment nutrient load on soft bottom community macroinvertebrate assemblages

One way of assessing ecosystem response to anthropogenic change is to compare biological features across existing gradients of one or more variables of interest. By sampling across natural and anthropogenic gradients, inter-reefal soft bottom communities in the Perth and mid-west region are being assessed to examine spatial differences in benthic plants and animals and relate any differences to the environmental conditions. It represents a portion of our research into assessing impacts of physical forcing factors on key benthic habitats by observations across naturally varying and anthropogenically altered gradients relating to physical dynamics and nutrients. Our goal is to develop a predictive capacity that will improve our capability to manage these coastal environments.

Physical parameters, primary production and characteristics of the sediment infauna and macroinvertebrate populations are being described and quantified. 2007/08 fieldwork has been completed collecting samples to determine species composition, distribution, abundance, biomass and secondary production of infauna and macro-invertebrates, and how these are affected by benthic microalgae biomass, sediment grain size, organic content or water column chlorophyll *a*. The methodology utilised is adapted from Edgar (1990) and Edgar and Shaw (1993) and is compatible with other work being undertaken on reefs and seagrass areas in Marmion and elsewhere as part of WAMSI.

Twenty-nine sites have been surveyed as shown in Figure 135: 13 in Marmion Marine Park (one near the sewage outfall and the remaining forming transects across a depth gradient with 4 inner, 4 mid and 4 outer, see Figure 136), 6 in Cockburn Sound (5 forming a transect along an anthropogenic stress gradient at the northern end and 1 at the southern end), 2 localities between these regions at City Beach and Hall Bank, 1 within the Swan River and 7 at Jurien Bay to the north. Some of these sites are considered replicates of a region and have been pooled for analyses while other sites although occurring in proximity to one another are considered individual sites due to differences in natural and anthropogenic stresses. The seven Jurien sites (JV007, Favourite, Dry Lumps, South Bay, Fishermans, Essex and Boullanger North) have been pooled as the Jurien region. Similarly, South Lumps, Whitford Rock, Wreck Rock and Cow Rock make up the Marmion Inner region; MM1, MM2, MM3 and MM4 comprise Marmion Mid; and MM_11, MOF2, M3MRS and M3MRN are Marmion Outer.

At each site, physical factors of bottom water temperature, depth, and water column light attenuation and the structure of sediment such as presence of ripples, depth of anaerobic sand and compactness were recorded. In addition, a water column integrated sample was collected for chlorophyll *a* quantification.

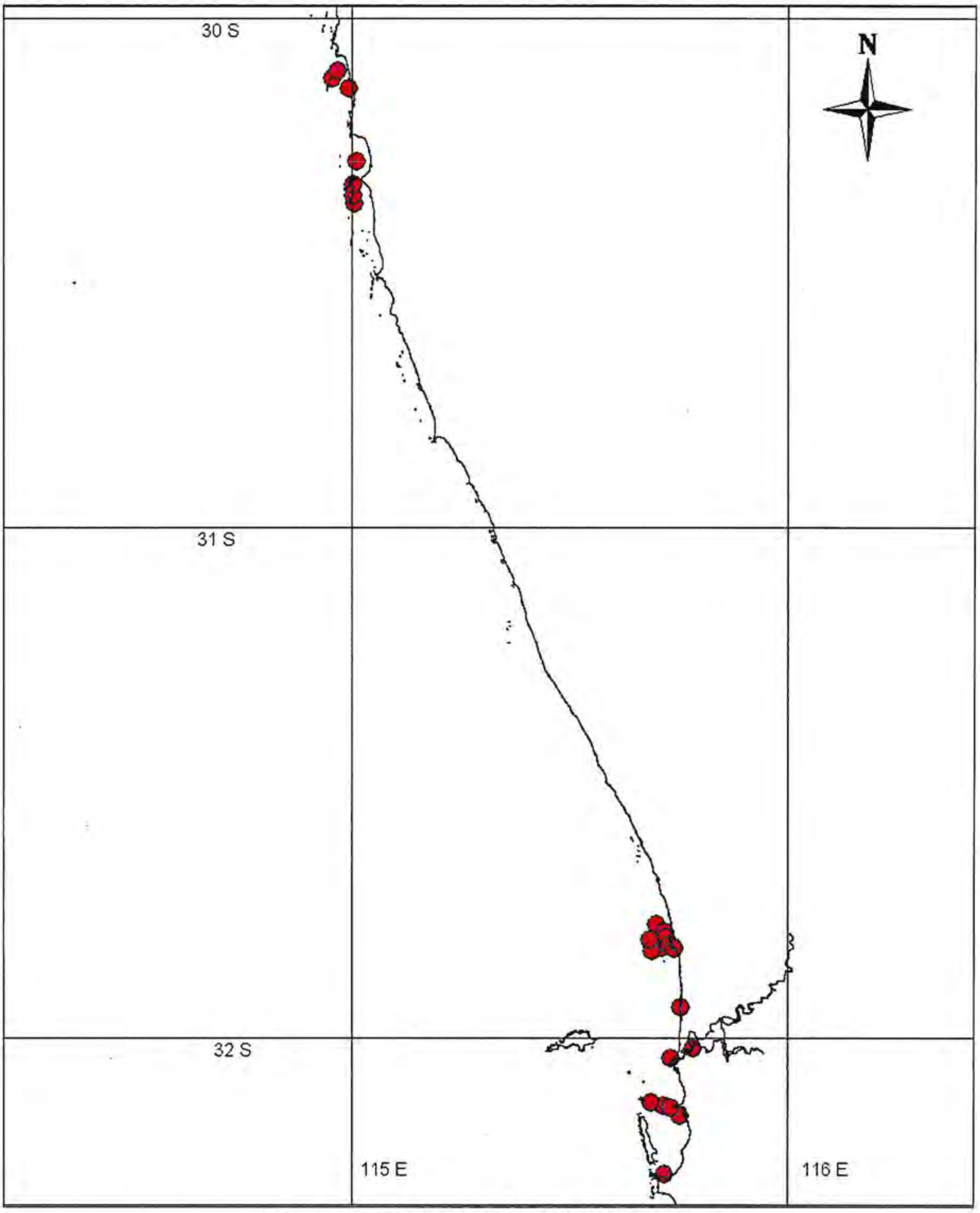

Figure 135. Site locations for soft sediment survey.

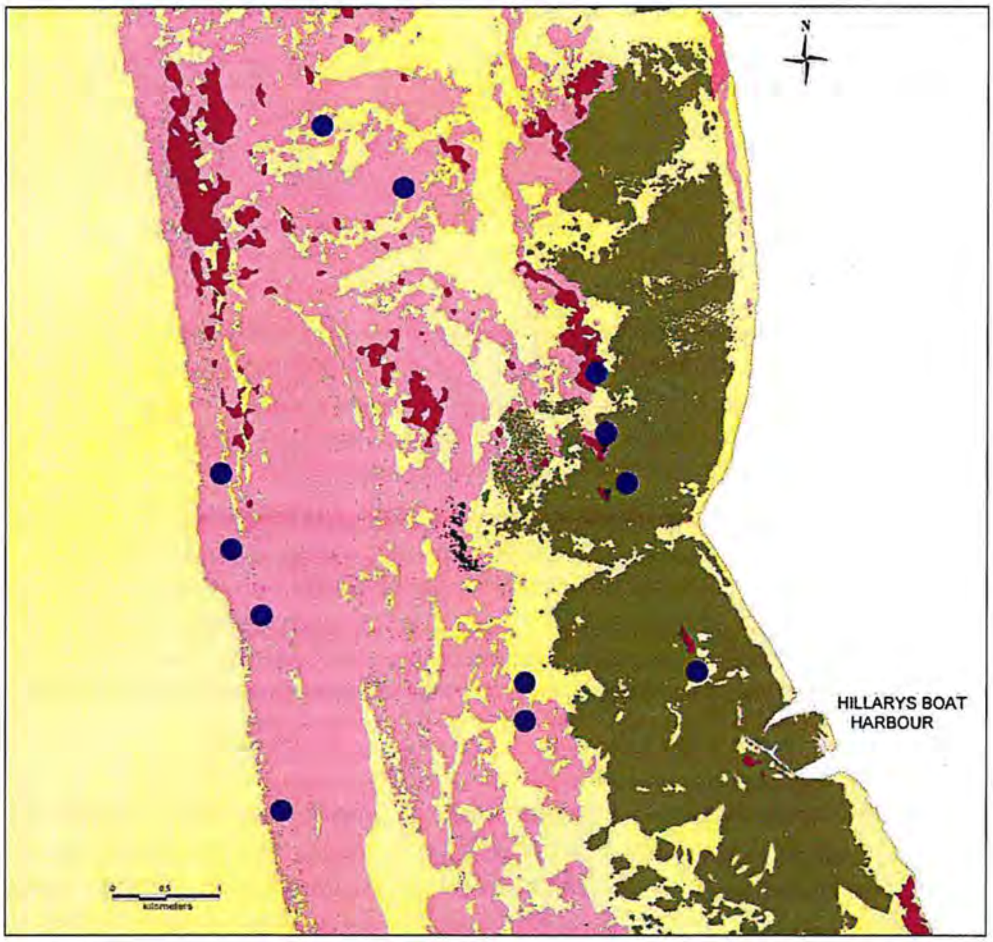

Figure 136. Site locations (blue circles) in Marmion Marine Park, shown on Habitat Map (DEC, 2002).

The sampling strategy was designed to reduce small scale (< 10 m) horizontal variability and focus on larger scale (> 100 m) patterns. Five transects of 5x1m were established, 10 x 30mm diameter cores to 50mm depth and 3 x 150mm diameter cores to 100mm depth were randomly collected within the transect, and all macrofauna collected using a small rake to search the sediment.

The small cores of each transect were sectioned into 0-2cm and 2-5cm depths and the size fractions from all 10 relating to 1 transect pooled and mixed to homogeneity. Four 20ml subsamples were collected for 0-2cm depth and two for 2-5cm. One of each size fraction is being analysed for carbon, from a second set chlorophyll *a* has been determined and the final 2 samples from 0-2cm will be analysed for identification of phytoplankton if found necessary.

One of the large cores was dry sieved through a set of 15 sieves from 0.063 to 8.0 mm pore size to determine proportions of grain size. One of the remaining cores was washed through 9 sieves from 8.0 to 0.5mm and biomass of infauna of each size class determined to allow for calculation of daily secondary production as per Edgar (1990).

Field work and sediment grain size analysis calculation of infauna secondary production of infauna, chlorophyll *a* analysis of benthic microalgae, identification and biomass of macrofauna and water column chlorophyll *a* analysis have been completed. Analysis of total organic carbon, total nitrogen and isotopic analysis of carbon and nitrogen are currently underway.

Sediment Grain Size

Size fractionation has been completed for all transects at all sites, see Figure 137. Sediments at all sites were dominated by particles in the range of 125µm to 500µm sieve size classes (Table 13). At sites within Cockburn Sound and the Swan River sediments were dominated by 250µm grain size class, while at sites in the outer Marmion Marine Park (Marmion Offshore) and in the Fremantle and City beach locations sediments were dominated by larger particles in the 500µm sieve size class. Figure 137 indicates that samples of the Fremantle/City beach region were composed of more particles at least 8.0mm in size compared to other localities, with a mean of 12% of the overall sample weight. This proportion is a result of the Fremantle samples only, which comprised large rocks (comprising limestone, shell rubble and corral rubble)not found anywhere else.

The size distribution of particles was more heterogeneous at sites in Jurien Bay, and the inner and mid areas of Marmion Marine Park. At the shallower inner Marmion sites sediments were dominated by both 125 and 250µm size classes, while at sites in the mid Marmion region overall had slightly larger overall size with modes of 250 and 355µm. Jurien Bay sediment had the greatest heterogeneity with multimodal distribution across the 125µm to 50 µm size classes.

Results from all transects at all sites had an obviously lack of particles in the 180 µm sieve size class. Post-analysis of the equipment revealed that wear of the sieve had resulted in hole sizes approximately 220 µm, thus only capturing particles between 220-250 µm. As a result, data from the faulty 180 µm size were added to the next smallest size class (125 µm) and the 180 µm class removed.

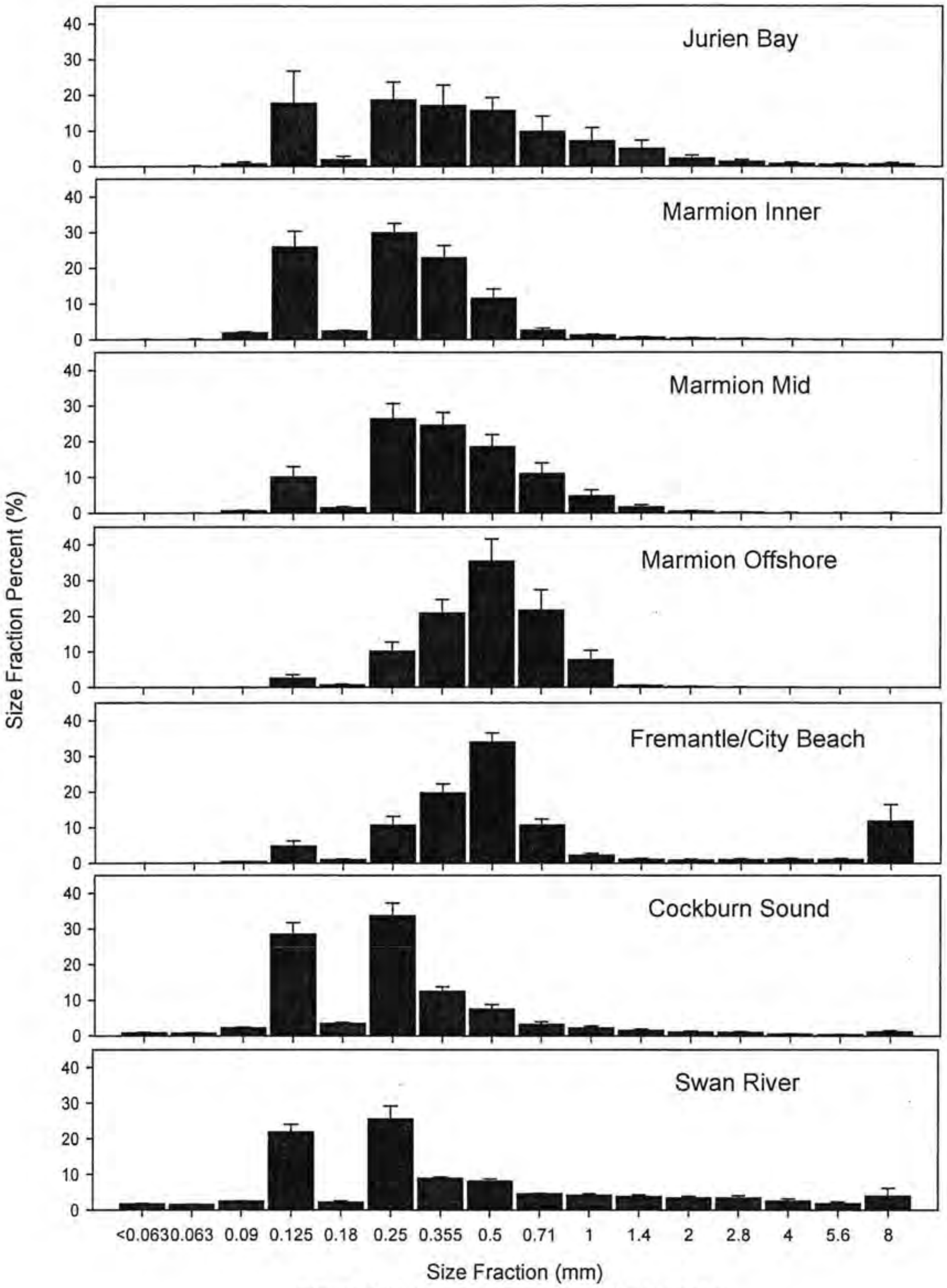

Figure 137. Sediment grain size fractionation

Table 13. Modes and medians of sediment grain size fractionation

	Mode(s)	Median
Jurien Bay	0.125, 0.25, 0.355, 0.50	0.355
Marmion Inner	0.125, 0.25	0.25
Marmion Mid	0.25, 0.355	0.25
Marmion Offshore	0.50	0.50
Fremantle/City Beach	0.50	0.50
Cockburn Sound	0.25	0.25
Swan River	0.25	0.25

Infauna biomass and secondary production

Secondary production has to been calculated for each transect at each site using the total ash-free dry weight (AFDW) biomass of infauna retained by sieves of differing mesh size and formula established in Edgar (1990). At the time of writing, methods to determine biomass have been tested and determined, and 78 of 108 sediment samples have been sieved successfully to quantify infauna.

The biomass of animals in the various sieve size classes used in secondary production calculations can be measured directly, or by a formula given in Edgar (1990) based on the number of individuals and the sieve size they are contained in; the latter saving time and effort. All transects at two Marmion Marine Park sites and two Cockburn Sound sites were employed to conduct a pilot study to establish which of these methodologies was most applicable to this study.

Edgar's (1990) work discerned equations for each phyla separately, concluding that there was no statistical difference between the equations, with the exception of caprellid amphipods due to their elongate morphology. A combined equation for all fauna unless dominated by long thin animals was established as an accurate and rapid method of determining biomass for each sieve size.

The equations established by Edgar (1990) are as such:

mean biomass of animals in a particular sieve size is calculated as:

$\log B = a + b*\log S$ Eqn 1

(where B = mean AFDW (mg); S = sieve size (mm))

this is then used to calculate total biomass of animals as:

$B = \Sigma n_i * B_i$ Eqn 2

(where n_i = abundance of animals in sieve size i; B_i = mean biomass of animals in sieve size i (as calculated from above regression equation)

Table 14 shows the coefficients in Equation 1 for both Edgar (1990) and those calculated from the actual measured AFDW biomass in this study. The work of Edgar (1990) showed strong correlation between sieve size and AFDW in all phyla and when pooling all fauna, as shown by high r^2 values. As mentioned, the combined equation adequately estimates total biomass of all fauna, thus the formula of log B = -1.01 + 2.64*logS can be used. In contrast, with the exception of platyhelminthes (which comprised only a small sample size) none of the regressions in this study were strong (as shown by very minimal r^2 in Table 14). Thus, neither the equations for individual phyla or the combined equation can be accurately used to measure mean biomass for a sieve size class.

Table 14. Coefficients and regression strengths for Eqn 1, comparing results of Edgar (1990) and this study.

	Edgar (1990)				**This Study**			
	a	b	r^2	n	a	b	r^2	n
Mollusc	-1.02	2.76	0.99	17	-0.15	0.47	0.13	24
Echinoderm	-	-	-	-	-0.54	0.48	0.09	3
Crustacean	-1.04	2.67	0.99	16	-0.95	-0.13	0.01	7
Polychaete	-0.99	2.49	0.98	18	-0.85	-0.19	0.01	22
Platyhelminth	-0.96	2.64	0.98	12	-1.74	2.96	0.99	4
Caprellids	-1.21	1.90	0.98	14	-	-	-	-
Foramifera	-	-	-	-	-0.19	0.87	0.28	11
Combined	-1.01	2.64	0.98	63	-0.55	0.43	0.04	71

Without being able to calculate mean biomass in this way, abundance data can be converted to biomass data using equation 2 as in Edgar (1990). As a result, biomass can only be measured directly as AFDW, the difference between the dried (80°C for 48 hr) and ashed (500 °C for 2 hr) weights of the fauna retained by each sieve. . This direct measurement method was applied to all cores in order to determine infaunal biomass present.

AFDW biomass of infauna is shown in Figure 138. Blackwall Reach in the Swan River had the greatest infaunal biomass. This is attributed to the presence of hermit crabs, polychaetes and molluscs all in high numbers and in a range of sizes. In addition, 3 hermit crabs greater than 8mm contributed 0.21g AFDW in one core and 1 hermit crab and 2 molluscs > 8mm in another core contributed 0.14g AFDW. Hall Bank, Jervoise Bay and Southern Flats all had significantly greater infaunal biomass than other marine sites. At Hall Bank this was simply the result of one large mollusc weighing 0.23g AFDW, hence the large standard error associated with this mean. At Jervoise Bay, the large AFDW was the result of 2 large molluscs (>8mm) in one core with a total weight of 0.10g and a large number of polychaetes found in all size fractions up to 5.6mm. At Southern Flats, also in Cockburn Sound, the biomass was not the result of a small number of individuals but rather large numbers of molluscs (3607 - 4540 per core in 3 of 5 transects) and forams (8443 – 10875 per core in the same 3 of 5 transects) found in a range of size, with smaller ones more abundant than larger.

Within Marmion Marine Park, the outer sites contained less biomass (0.17 ± 0.03 $g.m^{-2}$) than the inner (0.49 ± 0.07 $g.m^{-2}$, excluding the Marmion Outfall site) and mid sites (0.66 ± 0.21 $g.m^{-2}$).

The sites that might been predicted to be most heavily impacted, Marmion Outfall and Northern Harbour show infaunal biomass within the range of other sites in a similar location.

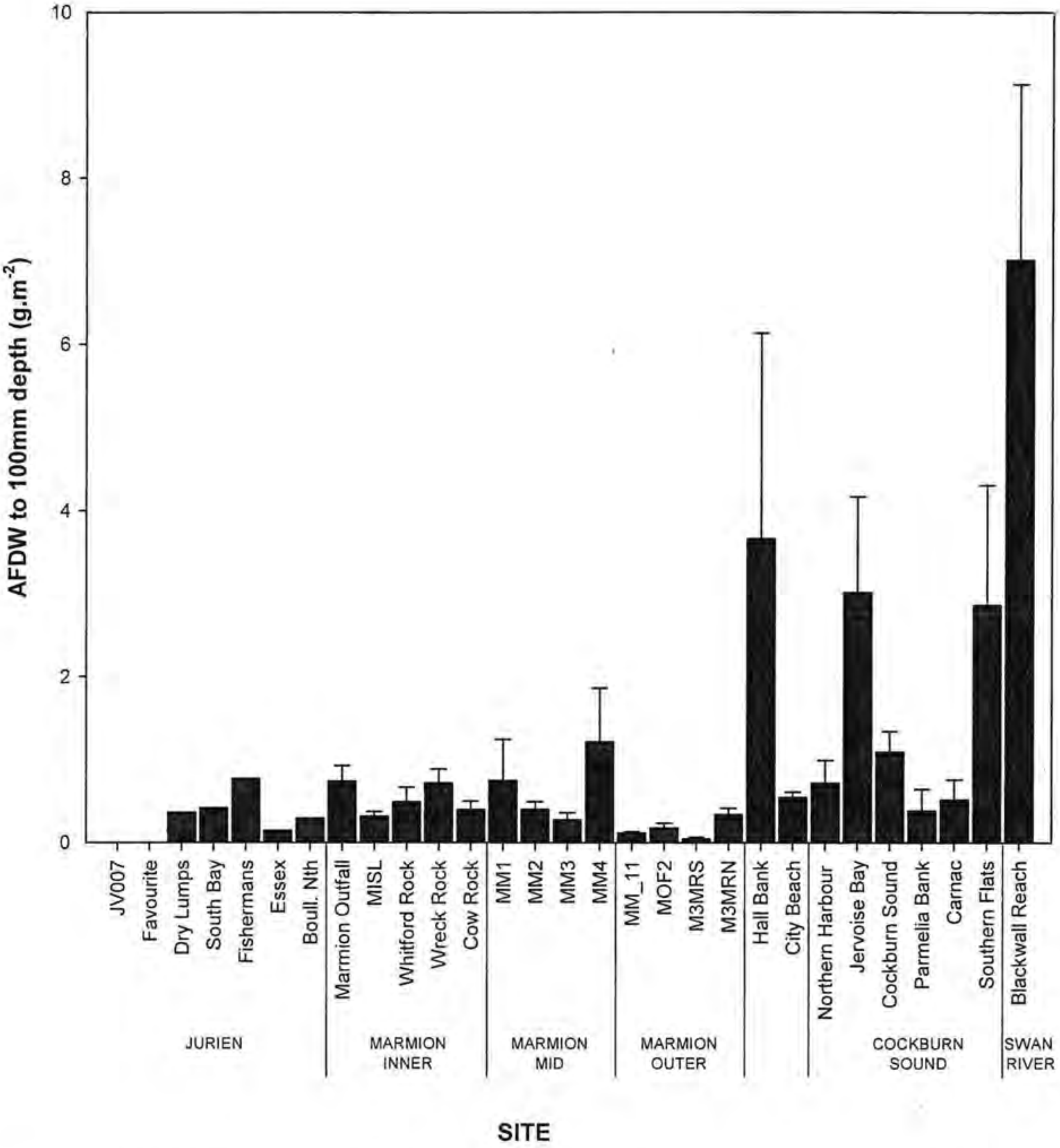

Figure 138. AFDW biomass of infauna to 100mm depth at each site (mean ± S.E., except Jurien sites where only one core per site was sampled)

Secondary production was calculated from infaunal biomass as described by Edgar (1990) with the following equation:

$$\text{Production } (\mu\text{g.day}^{-1}) = 0.0049 \times B^{0.80} \times T^{0.89}$$

where B = AFDW biomass (µg)

T = mean monthly water temperature (°C)

Preliminary secondary production values have been calculated with available temperature information from Pearce *et al.* (1999) for marine sites and from Water Corporation (pers. comm.) for the Swan River (Table 15). It is hoped that more accurate temperature values will be obtained and these production values will be revised.

Table 15. AFDW biomass, temperature and secondary production values of soft sediment sites or regions.

Region/Site	Mean AFDW Biomass ± SE ($g.m^{-2}$)	Mean Annual Temperature (°C)	Production ± SE ($g.m^{-2}.yr^{-1}$)
Jurien Bay	0.28 ± 0.10	20.4	1.25 ± 0.41
Marmion Outfall	0.74 ± 0.18	19.4	2.74 ± 0.62
Marmion Inner	0.49 ± 0.07	19.4	1.97 ± 0.23
Marmion Mid	0.66 ± 0.21	19.4	2.31 ± 0.58
Marmion Outer	0.17 ± 0.03	19.4	0.81 ± 0.14
City Beach	0.54 ± 0.06	19.4	2.20 ± 0.21
Hall Bank	3.66 ± 2.47	19.4	9.03 ± 5.01
Northern Harbour	0.72 ± 0.27	19.3	2.63 ± 0.82
Jervoise Bay	3.02 ± 1.15	19.3	8.25 ± 2.60
Cockburn Sound	1.09 ± 0.25	19.3	3.80 ± 0.69
Parmelia Bank	0.38 ± 0.26	19.3	1.46 ± 0.83
Carnac	0.52 ± 0.24	19.3	1.97 ± 0.76
Southern Flats	2.86 ± 1.44	19.3	7.79 ± 3.09
Swan River	7.02 ± 2.11	19.1	16.35 ± 4.04

Secondary production was almost twice as high in the Swan River compared to the next highest value. Hall Bank, Jervoise Bay and Southern Flats had the greatest production of the marine sites. As temperature values did not vary much between sites or regions, secondary production is tightly linked to AFDW biomass.

Macrofauna biomass

At present, all macrofauna has been sorted, identified or processed for identification by the Western Australian Museum and total wet weights of each species measured. Additionally, for the abundant large fauna *Archaster angulatus, Ammotropus arachnoides, Peronella lesueuri,* and a red holothurian yet to be identified each individual was wet weighed and size measured (diameter of sand dollars, arm length of starfish and total length of holothurians). For these species a subsample of individuals encompassing the size range of the species were used to measure ash free dry weight (AFDW) as the difference between the dried (70°C) and ashed (500°C) weights of the individuals and a regression to wet weight and size performed. Regression showed in all cases the better estimate of AFDW was wet weight rather than length/diameter, with r^2 values ranging 0.83 to 0.97. Hence, the wet weight of individuals of these species will be used to calculate biomass.

The mean number of individuals, species and total wet weights are given in Table 16. Figure 139 demonstrates the animals which contribute to each site and Figure 140 the animals which contribute to biomass. The greatest density of animals was found in the Swan River, where hermit crabs were measured at 7.04 ± 2.45 individuals per m^2 and ophiuroids at 3.16 ± 2.67 individuals per m^2 (Figure 139). This site also had the greatest species diversity, with a range of species encompassing all animal groups found in the study except for Crinoidea and Cephalopoda. In addition to having greatest quantities of infauna biomass of the marine sites, Hall Bank, Jervoise Bay and Southern Flats had some of the largest densities of macrofauna, with City Beach also having high numbers. With the exception of Southern Flats, these sites also had some of the highest species diversities.

Fewer individuals, fewer species and less biomass were found in the deeper outer region of Marmion Marine Park than the inner and mid regions (Table 16). The heavily impacted site of Marmion Outfall had animal densities, diversity and biomass similar to other sites in the area. However, the other heavily impacted site of Northern Harbour had less individuals, species and biomass compared to its nearby sites.

The greatest biomass was found at Jervoise Bay and Southern Flats (Table 16), at both sites this was the result of echinoids (Figure 140)- *Peronella lesueuri* and *Ammotropus arachnoides* at Jervoise Bay and *Peronella lesueuri* at Southern Flats. Similarly, the biomass in the Swan River and Cockburn Sound was also due to *Peronella lesueuri*. At Hall Bank and Marmion Inner sites, biomass was composed mainly of the seastar *Archaster angulatus*. All other sites had less than 6g wet biomass per m^2 (Figure 140).

Table 16. Characteristics of macrofauna assemblage at soft sediment sites or regions (mean ± SE).

Region/ Site	**Density (no. indiv. per m^2)**	**Species Diversity (no. per m^2)**	**Wet Wt Biomass (g per m^2)**
Jurien	0.43 ± 0.12	0.19 ± 0.03	2.36 ± 0.85
Marmion Outfall	1.88 ± 0.77	0.72 ± 0.08	5.79 ± 3.84
Marmion Inner	1.60 ± 0.25	0.86 ± 0.10	43.52 ± 9.15
Marmion Mid	1.88 ± 0.31	0.86 ± 0.12	3.35 ± 1.08
Marmion Outer	0.30 ± 0.08	0.22 ± 0.06	0.18 ± 0.06
Hall Bank	3.44 ± 0.51	1.52 ± 0.37	47.92 ± 10.03
City Beach	4.36 ± 1.14	1.48 ± 0.22	6.01 ± 1.43
Northern Harbour	0.64 ± 0.22	0.32 ± 0.05	0.58 ± 0.20
Jervoise Bay	5.08 ± 0.60	1.56 ± 0.44	231.69 ± 19.88
Cockburn Sound	2.04 ± 0.94	0.56 ± 0.23	96.69 ± 27.46
Parmelia Bank	0.20 ± 0.09	0.12 ± 0.05	0.16 ± 0.13
Carnac	0.76 ± 0.17	0.72 ± 0.15	5.44 ± 3.42
Southern Flats	3.44 ± 1.26	0.48 ± 0.08	252.49 ± 87.15
Swan River	14.72 ± 3.34	2.36 ± 0.39	130.46 ± 25.41

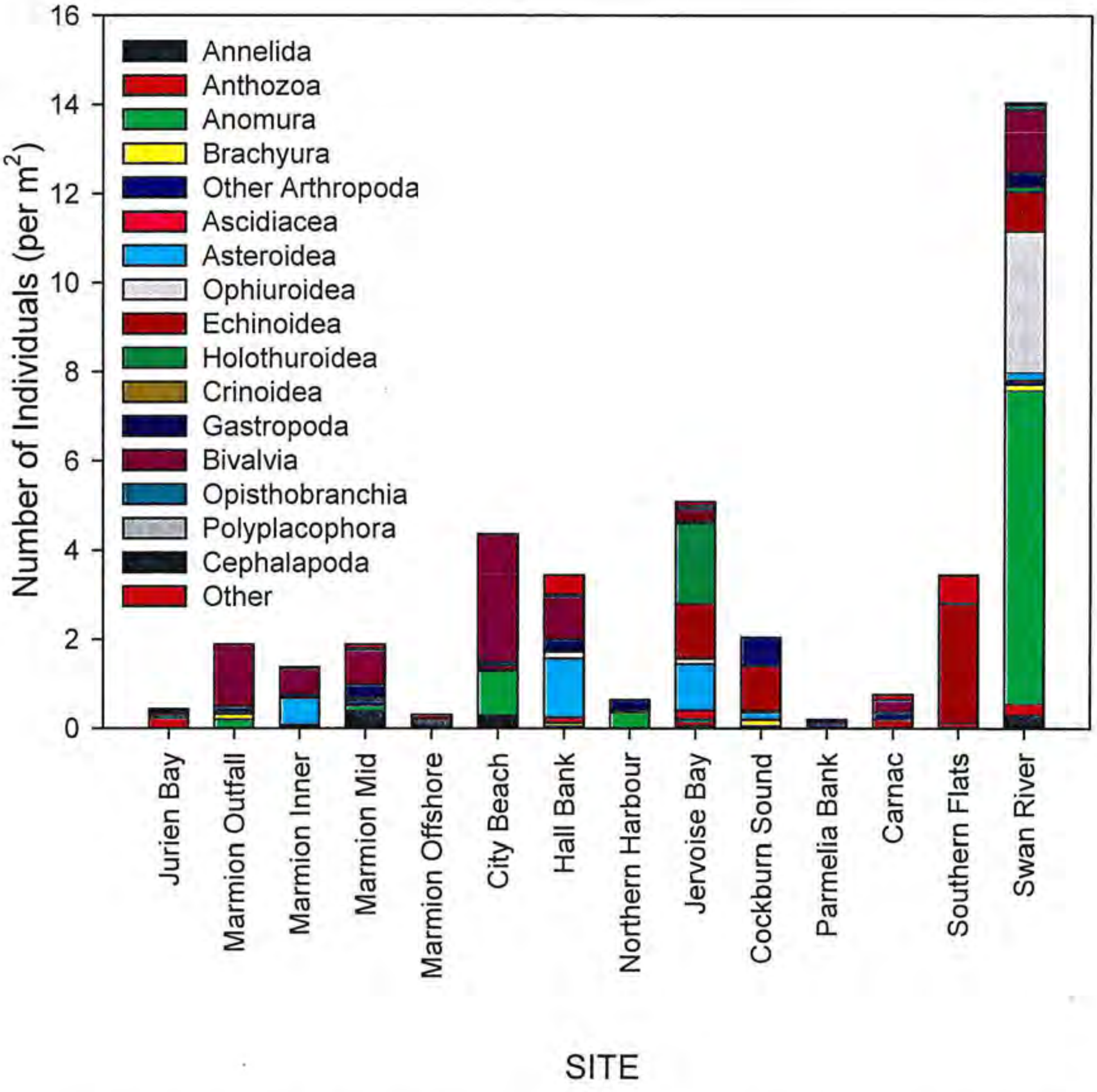

Figure 139. Number of individuals of various phylum and classes present in soft sediment sites and regions

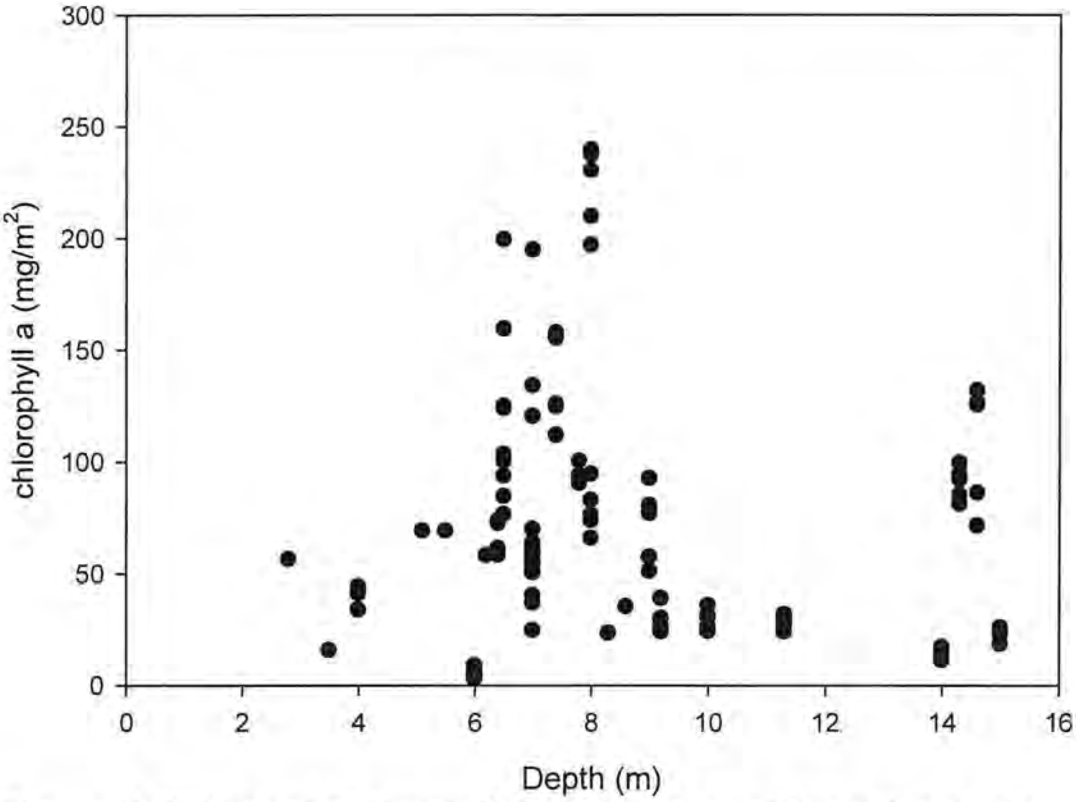

Figure 143. Chlorophyll *a* biomass (0-5 cm sediment depth) as a function of water column depth.

Water Column Chlorophyll *a*

Results of chlorophyll *a* and phaeopigments for water column integrated samples are given in Figure 144. Northern Harbour had significantly greater concentrations of both compared to all other sites examined. All regions of Marmion Marine Park had similar pigment concentrations (Table 17). Variability in concentrations within the mid region were due to variability between all samples, whereas the variability in chl. *a* in the outer region was the result of one site with a much larger concentration. Further analysis of these results and what they signify is yet to be explored.

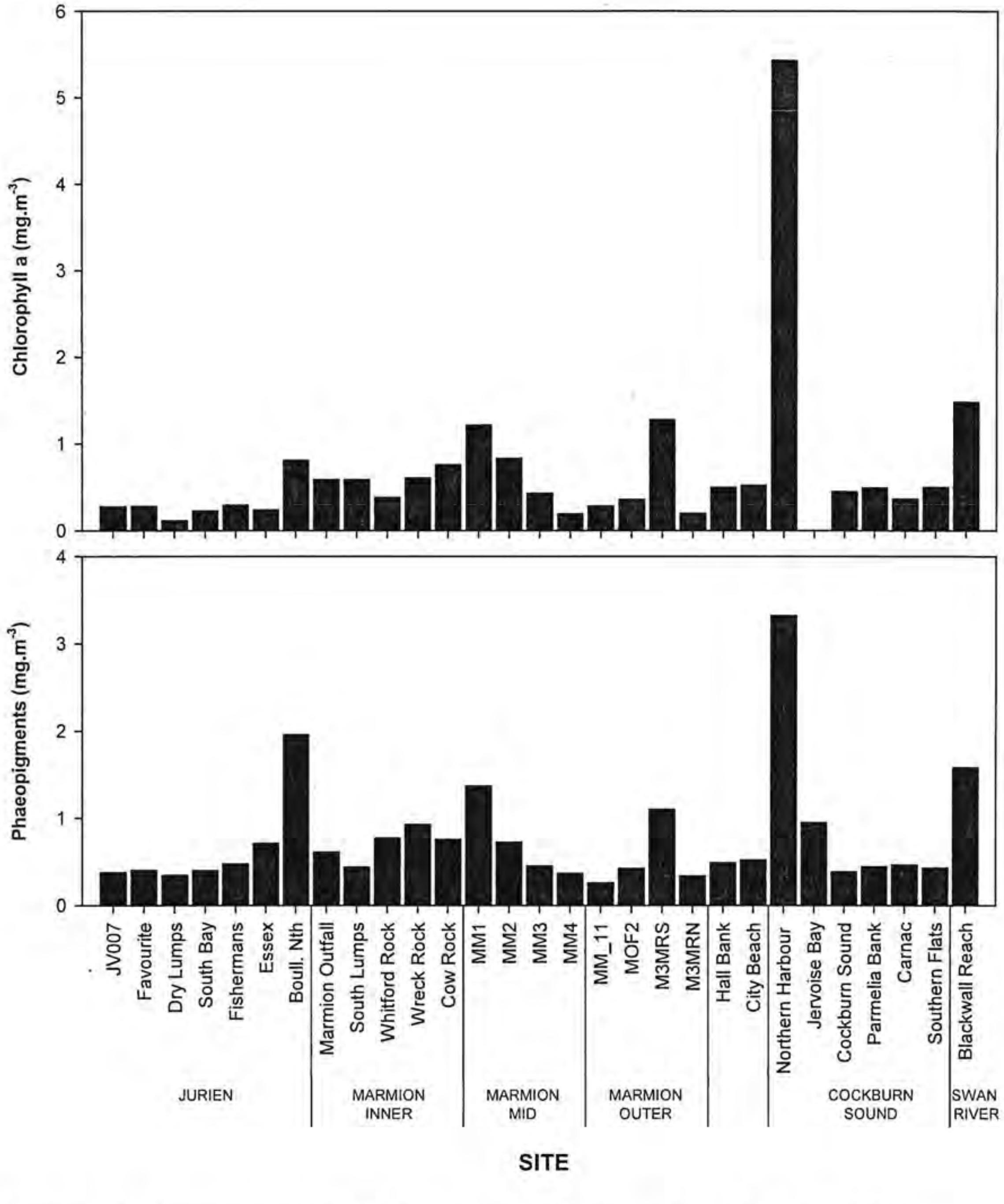

Figure 144. Concentrations of chlorophyll *a* and phaeopigments from water column integrated samples.

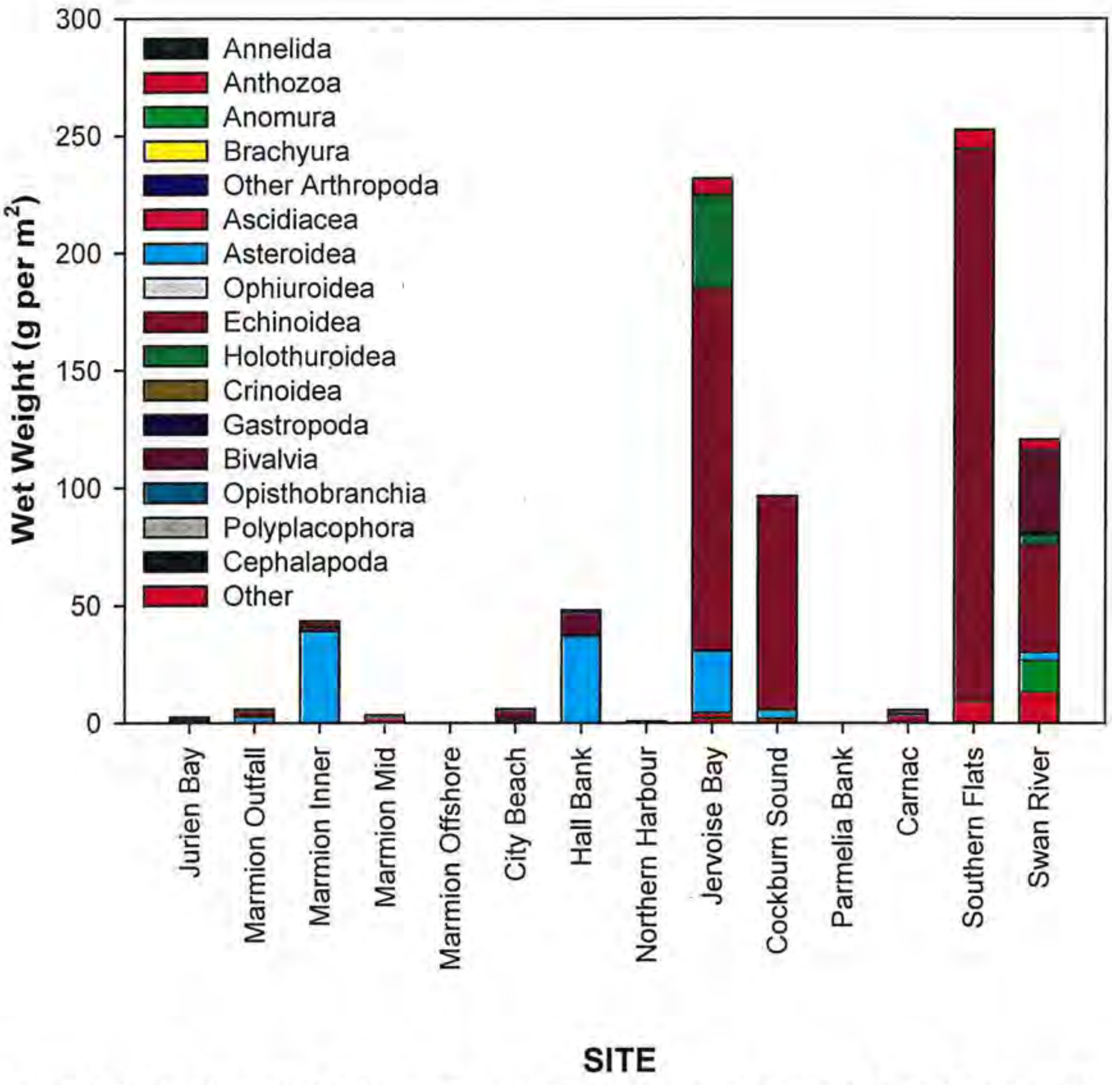

Figure 140. Wet weight of various phylum and classes present in soft sediment sites and regions

Benthic Microalgae

The chlorophyll *a* content for all but two sites has been determined, as shown in Figure 141 and Figure 142. The mean chlorophyll *a* concentrations in the surface 0-2 cm deep samples ranged from 4 $mg.m^{-2}$ to 126 $mg.m^{-2}$, while in the lower 2-5cm deep samples ranged from 1 $mg.m^{-2}$ to 97 $mg.m^{-2}$. Of the 107 samples analysed, most had more chlorophyll *a* in the surface layer, however this trend was reversed in 27 of the samples.

Results demonstrate most of the variability in cholorophyll *a* biomass is not associated with water column depth (Figure 143). Further analyses of these results and what they signify is yet to be explored.

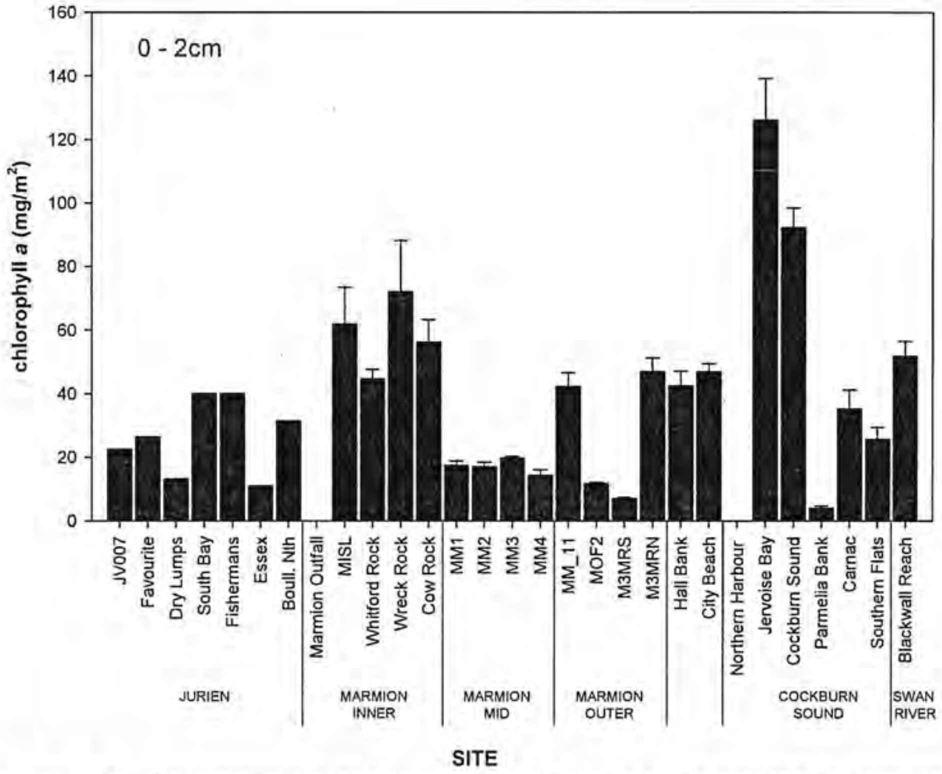

Figure 141. Chlorophyll *a* concentration of sediment samples 0-2cm depth (mean ± S.E.).

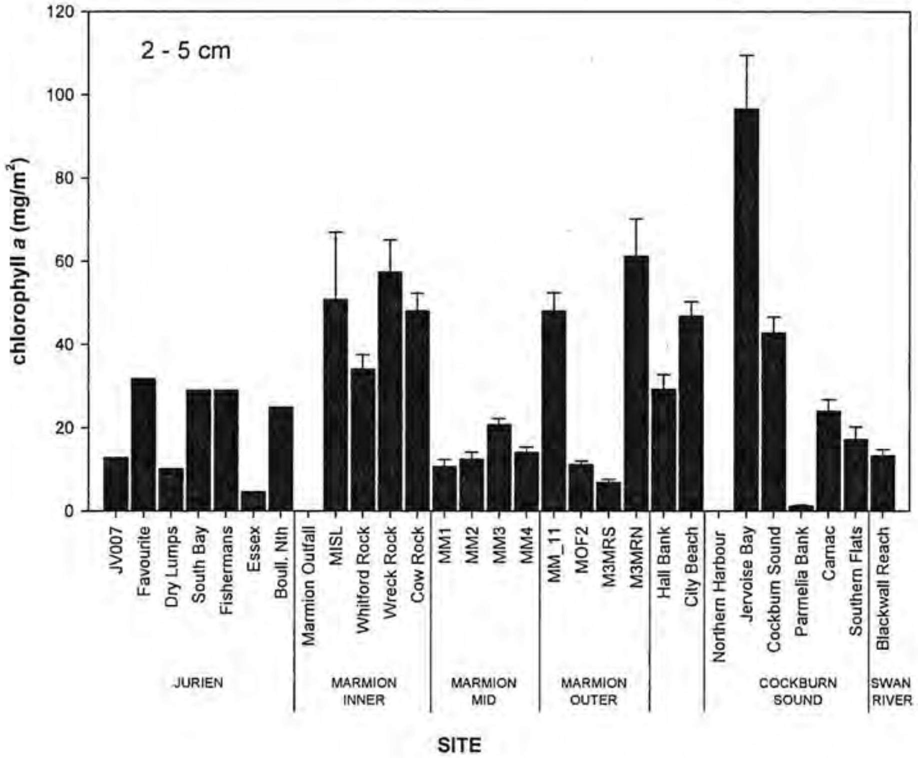

Figure 142. Chlorophyll *a* concentration of sediment samples 2-5cm depth (mean ± S.E.).

Table 17. Pigment concentrations within Marmion Marine Park regions (mean ± S.E.) .

	Chlorophyll a (*mg.m*$^{-3}$)	*Phaeopigments* (*mg.m*$^{-3}$)
Marmion inner	*0.58 ± 0.08*	*0.72 ± 0.10*
Marmion mid	*0.67 ± 0.23*	*0.73 ± 0.23*
Marmion outer	*0.53 ± 0.25*	*0.53 ± 0.19*

Where to from here

A number of processes need to be completed:

- organic carbon and nitrogen analyses from sediment samples
- quantification of BMA from sediment samples of final two sites
- statistical analyses of data

Once all the above data is collected, conclusions will be made about the relationship between all of these biotic and abiotic factors, with emphasis on the spatial differences relating to the nutrient gradients.

Large scale manipulative experiment enriching nutrients on reef and soft sediment habitats

Following the equivocal results achieved in the pilot study (see Milestone 1.4.1) we have applied to WAMSI drop this price of work from the work plan. We still expect to deliver on this milestone but just for one habitat type based on the work described examining the response of soft sediment communities to gradients of nutrient enrichment. The following challenges have influenced our decision not to proceed with plans to conduct targeted nutrient enrichment manipulations as a part of milestone 1.4.2:

- Firstly, the results obtained from the pilot study (milestone 1.4.1) have not been promising and suggest that nutrient delivery from slow release fertilizer may be temperature dependent which would cast some doubt over winter dosing regimes. An extensive period of (largely unpublishable) testing and validation would be required to repeat aspects of the pilot study, settle on the most appropriate fertiliser type and gain confidence in the delivery system. We do not believe such cost and allocation of staff time is the most effective use of resources and given the delays in other parts of the project resulting from a backlog of nutrient samples, could jeopardise timely completion of other parts of the project.

- Secondly, we have also experienced considerable delays in the delivery of nutrient data to a number of components of WAMSI Node 1 Project 1 as a result of decisions taken by CSIRO affecting our ability to have nutrient samples analysed. This problem is outside the control of any of the project scientists and was reported on in our last progress report. As a result there is a considerable sample backlog of about 3000 nutrient samples accumulated. A strategy is been developed by CSIRO in Hobart to address the sample backlog, but it will take some time to clear and for results to be reported. The nutrient enrichment manipulations to take place as part of milestone 1.4.2 would require significant nutrient samples in addition to the backlog already existing. Adding a further nutrient sample load to this existing backlog is not in the best interests of overall project delivery in a timely fashion.

There are two positives mitigating the decision to drop the nutrient manipulations. Firstly, additional effort has instead been put into comparing environmental and biotic attributes of pre-existing sediment nutrient gradients at a range of sites with a gradient of anthropogenic impacts (see above section). Following discussions with DEC we have added Northern Harbour in Cockburn Sound and the Whitfords sewage outfall site to an expanded set of sites for this work on Marmion, Cockburn Sound and the Swan River, This work has been successful and will contribute greatly to the development of models envisaged for Output 4. Secondly as part of Node 1, we have developed a CSIRO Flagship Collaboration Fund (FCF) postdoc project: "*The role of herbivory and hydrodynamics in ameliorating the effects of nutrient enrichment in marine ecosystems*" with Edith Cowan University. This project will also contribute greatly to the outcomes of Output 4. CSIRO will contribute $184,000 to this project and ECU about $500,000.

References

Edgar, G.J. (1990). The use of the size structure of benthic macrofaunal communities to estimate fauna1 biomass and secondary production. *J. Exp. Mar. Biol. Ecol.*, 137: 195-214.

Edgar, G.J. and C. Shaw (1993). Inter-relationships between sediments, seagrasses, benthic invertebrates and fishes in shallow marine habitats off south-western Australia. In: F.E. Wells, D.I. Walker, H. Kirkman and R. Lethbridge (Eds.) *The marine flora and fauna of Rottnest Island, Western Australia.* Western Australian Museum, Perth. pp. 429–442.

Pearce, A.F., M.Rossbach, M.Tait and R.Brown (1999). *Sea temperature variability off Western Australia 1990 to 1994.* Fisheries WA Research Report 111. 45pp.